

Investigation of Crosstalk Between GSK3 and the
MAPK Pathway in ^{V600E}*BRAF*-Driven Colorectal
Cancer

Thesis submitted for the degree of
Doctor of Philosophy
at the University of Leicester

Pooyeh Farahmand M.Sc. (University of Leicester)
Department of Biochemistry/Molecular and Cell
Biology

University of Leicester

June 2018

Abstract

Investigation of Crosstalk Between GSK3 and the MAPK Pathway in V^{600E} BRAF-Driven Colorectal Cancer

Pooyeh Farahmand

Colorectal cancer (CRC) is the third most prevalent cancer in advanced countries which mostly falls within the traditional class involving APC mutation. However, a recently classified V^{600E} BRAF-driven class, sessile serrated CRCs (SSCRCs) was discovered to develop in the proximal colon. SSCRCs often evade detection because of their location and flat pale appearance. They have poor prognosis and are resistant to BRAF inhibition – necessitating the development of novel therapies for this devastating disease affecting ~3000 people in the UK each year.

A greater understanding of disease initiation and progression is needed for this purpose. A conditional, Cre-regulated, V^{600E} Braf ($Braf^{SL-V^{600E}/WT}; Villin-CreER^T$ (BVE/Cre)) knockin mouse model was therefore characterized. We show that initiation and progression of tumour development, from hyperplastic crypts to serrated adenomas and carcinomas, is similar to that reported in humans. A 3 day V^{600E} Braf expression results in the formation of hyperplastic crypts, which is surprisingly not associated with activation of the downstream MAPK pathway, and is not reversed by treating mice with MEK inhibitors. Instead, gene expression profiling shows upregulation of negative regulators of the MAPK pathway, a subset of Wnt pathway target genes, and genes involved in cholesterol biosynthesis and glycolysis, possibly accounting for the effect on crypt hyperplasia.

GSK3 phosphorylation role in V^{600E} BRAF effects were investigated by intercrossing BVE mice with $Gsk3\alpha/\beta$ S9A/S21A mice. The combined mutant showed increased early-stage crypt elongation – suggesting GSK3 phosphorylation suppresses V^{600E} BRAF-driven tumour initiation. Consistently, these mice demonstrated increased tumour burden at later stages, with no differences in tumour stage. Gene expression profiling shows this suppressive effect of GSK3 phosphorylation is most likely due to suppression of a subset of MAPK target genes.

Altogether, these results provide novel insight into the role of V^{600E} Braf at early stages of serrated CRC neoplasia.

Acknowledgements

I would like to thank my supervisor Professor Catrin Pritchard for her guidance during my PhD.

I would like to express my gratitude to my dearest mother and father, if it was not for their lifetime of unconditional love and support, especially through the very difficult periods of my life, none of my success would be possible today.

My sincerest appreciation goes to my dearest brother Nima and sister-in-law, Ladan, for their never-ending encouragement and love.

I would like to thank my dearest Adi for his wholehearted support during my hard PhD life.

A big thank you and hug to Karen kuchulu azizam for cheering me up with his cuteness. You melt my heart.

I would like to thank my grandmother and late grandfather for always being there for me. You are one of the reasons I am here today.

I would like to express my gratitude to Gayatri and Chandru for their support during past three years.

Finally, I would like to acknowledge Dr. Tamiharo Kamata, Dr. Fiona Hey, Susan Giblett, David Brown, Dr Sue Shakelton, Dr. Raj Patel and Dr. Kath Clark for their guidance.

Contents

Table of Titles

Abstract	ii
Table of Titles	iv
Table of Contents	iv
Table of Figures	x
Table of Tables	xv
Abbreviations	xvii

Table of Contents

Acknowledgements	iii
Contents	iv
Chapter 1. Introduction	1
1.1. Colorectal cancer	1
1.2. Classification of colorectal cancer	4
1.2.1. Molecular classification of CRC	4
1.2.2. Morphological classification of CRC	13
1.3. Signalling pathways associated with colorectal cancer	19
1.3.1. Canonical WNT pathway	19
1.3.2. MAPK-ERK signalling pathway	27
1.3.3. Senescence	39
1.3.4. Other signalling pathways involved in intestinal homeostasis	43
1.4. Inhibition of the RAF-MEK pathway	44
1.5. Mouse models of colorectal cancer	47
1.5.1. <i>Apc</i> mouse models	48

1.5.2. <i>Kras</i> mutant mouse model	53
1.5.3. ^{V600E} <i>Braf</i> mouse model	55
1.5.4. <i>Gsk3</i> knockin mice	63
1.6. Aims and objectives:	66
Chapter 2. Materials and methods	67
2.1. Molecular biology	68
2.1.1. Cell line culture	68
2.1.2. Infection with Adenoviral Cre	70
All of the following procedures were carried out in a Class II hood.	70
2.1.3. Freezing stock of the cells	70
2.1.4. Thawing stock of the cells	71
2.1.5. Inhibition of MAPK pathway and S6K	73
2.2. Biochemistry	75
2.2.1. Immunofluorescence staining of cells	75
2.2.2. Preparation of soluble protein lysates	77
2.2.3. SDS-polyacrylamide gel electrophoresis	80
2.2.4. Western-blot Semi-dry transfer	82
2.2.5. Immunostaining of western blots	82
2.2.6. Genotyping	85
2.3. Mouse breeding and Cre recombinase induction	89
2.3.1. Cre recombinase induction	90
2.3.2. Inhibitor treatment of mice	90
2.4. Histology	92
2.4.1. Mouse tissue harvesting	92
2.4.2. Tissue processing	93
2.4.3. Pre-treatment of glass slides (Subbing)	93
2.4.4. Sectioning of wax embedded tissue samples	93

2.4.5. Hematoxylin and Eosine (H&E) staining	94
2.4.6. Immunohistochemistry	94
2.4.7. Nuclear β -catenin IHC	95
2.5. Statistical Analysis	99
2.6. Microarray assay	100
2.6.1. Tissue preparation for RNA extraction	100
2.6.2. RNA extraction from tissue sections and Microarray	100
Chapter 3. Investigation of the crosstalk between the MAPK and GSK3 pathways in $V600E$ <i>BRAF</i> mutant cell lines	103
3.1. Introduction	103
3.1.1. Evidence of crosstalk in $V600E$ <i>Braf</i> mouse model (<i>in vivo</i>)	104
3.2. Aims	105
3.3. Results	106
3.3.1. No correlation between activation of the MAPK pathway and phosphorylation of GSK3 in $V600E$ <i>BRAF</i> mutant human CRC cell lines.	106
3.3.2. $V600E$ <i>BRAF</i> induced activation of the MAPK pathway increases nuclear β -catenin levels in RKO human CRC cells.	108
3.3.3. Investigation of crosstalk in $V600E$ <i>Braf</i> mouse embryonic fibroblasts (MEFs).	111
3.3.4. Crosstalk talk between MAPK and WNT pathways in lung and melanoma cell lines.	113
3.3.5. MEK inhibition in human lung and melanoma cells with $V600E$ <i>BRAF</i> mutation.	115
3.3.6. MEK inhibition in melanoma cells with $V600E$ <i>BRAF</i> mutation.	118
3.3.7. S6K inhibition in melanoma cells with $V600E$ <i>BRAF</i> mutation.	120
3.4. Conclusion	122
Chapter 4. Setting up the <i>Braf</i> ^{<i>L</i>SL-V600E/WT} / <i>Villin-CreER</i> ^{T0/WT} model of serrated CRC: short-term study	128

4.1. Introduction	128
4.2. Aims	130
4.3. Results	131
4.3.1. ^{V600E} BRaf mouse gut models	131
4.3.2. PCR analysis to determine mouse genotypes	133
4.3.3. Crosstalk between MAPK and GSK3 in the <i>Braf</i> ^{L^{SL}-V600E/WT} ; <i>AhCreER</i> ^{T0/WT} mouse model	136
4.3.4. Expression of MAPK and WNT pathway components using immunohistochemistry	138
4.3.5. Investigation of crosstalk in the <i>Villin-CreER</i> ^{T0/WT} mouse model	140
4.3.6. Crypt elongation in the small intestine as a result of the ^{V600E} <i>Braf</i> mutation	142
4.3.7. Increase in number of proliferative cells in the small intestinal crypts	145
4.3.8. Effect of MAPK pathway inhibition in the <i>Braf</i> ^{L^{SL}-V600E/WT} ; <i>Villin-CreER</i> ^{T0/WT} mouse model	148
4.3.9. Effect of PD184352 treatment on crypt hyperplasia	152
4.4. Conclusion	154
Chapter 5. Investigation of the role of GSK3 phosphorylation in ^{V600E} <i>Braf</i> -driven early changes in the gut	157
5.1. Introduction	157
5.2. Aims	158
5.3. Results	159
5.3.1. <i>Gsk3</i> knockin mouse model	159
5.3.2. Inter-crossing of <i>Gsk3</i> knockin mice with ^{V600E} <i>Braf</i> mice	161
5.3.3. Characterisation of intestinal tissue	166
5.3.4. Effect of <i>Gsk3</i> α/β knockin mutations on crypt hyperplasia following ^{V600E} BRaf induction	168

5.3.5. Effect of GSK3 phosphorylation on crypt cell proliferation	170
5.3.6. Gene expression analysis	173
5.3.7. Analysis of the impact of <i>Gsk3α/β</i> knockin mutations on gene expression	174
5.3.8. Molecular effect of ^{V600E} BRaf expression	176
5.3.9. Effect of <i>Gsk3</i> mutation on gene expression changes induced by ^{V600E} BRaf	184
5.3.10. Group 1 and Group 2 genes	186
Group 3: Additive effect of <i>Gsk3</i> mutation and ^{V600E} BRaf induction	189
5.3.11. Group 3a: <i>Gsk3</i> knockin mutation alters expression level of some common genes	194
5.3.12. Effect of ^{V600E} BRaf induction on the expression of AMP-activated protein kinase α	196
5.4. Conclusion	199
Chapter 6. Investigation of the role of GSK3 phosphorylation in ^{V600E} BRaf-induced tumour development: long-term study	205
6.1. Introduction	205
6.2. Aims	206
6.3. Results	207
6.3.1. Effect of <i>Gsk3</i> mutation on long-term survival following ^{V600E} BRaf induction	207
6.3.2. Effect of <i>Gsk3</i> mutation on tumour burden following ^{V600E} BRaf induction	209
6.3.3. Tumour burden in different regions of the intestine	216
6.3.4. Impact of <i>Gsk3</i> mutation on tumour grade	219
6.3.5. Conclusion	222
Chapter 7. Summary and Discussion	224
7.1. Background to the project	224

7.2. Summary of results	226
7.2.1. CRC cell lines as model system	226
7.2.2. <i>Villin-CreER^{T0/WT}; Braf^{LSL-V600E/WT}</i> (BVE/Cre) as a model of serrated CRC	229
7.2.3. MAPK-independent crypt hyperplasia in the BVE/Cre model	229
7.2.4. WNT pathway involvement in crypt hyperplasia	233
7.2.5. Cholesterol biosynthesis is induced by ^{V600E} BRaf	233
7.2.6. ^{V600E} BRaf induces components of glycolysis	237
7.2.7. Effect of GSK3 phosphorylation on crypt hyperplasia and tumour burden	238
7.2.8. Conclusion	241
Chapter 8. Appendix	242
Chapter 9. References	304

Table of Figures

Figure 1.1 Twenty most common cancers in the UK, 2014 (CancerReaserchUK, 2016b).	2
Figure 1.2 Twenty most common cancer deaths in the UK, 2014 (CancerReaserchUK, 2016c).	2
Figure 1.3 Colorectal cancer five-year survival by stage, in both sexes - 2002-2006 (CancerReaserchUK, 2016a).	3
Figure 1.4 Graph showing frequency of the 20 most common mutations detected in human colorectal carcinoma (Cosmic, 2019).	5
Figure 1.5 Fearon and Vogelstein model proposed in 1990 for colorectal cancer development and progression (Walther et al., 2009).	5
Figure 1.6 Schematic representation of traditional and sessile serrated pathways in colorectal carcinoma (Mäkinen, 2007).	7
Figure 1.7 Classification of CRC proposed by the international expert consortium (Guinney et al., 2015).	12
Figure 1.8 Comparison between the two-recent molecular classifications of the colorectal cancer (Müller et al., 2016).	12
Figure 1.9 Pathological features of conventional adenomas (Fleming et al., 2012).	14
Figure 1.10 Illustration of underlying processes responsible for different subtypes of serrated adenoma appearance (Snover, 2011).	17
Figure 1.11 Sessile serrated adenoma (Amersi et al., 2005).	18
Figure 1.12 Schematic representation of the WNT canonical pathway (Barker and Clevers, 2006).	22
Figure 1.13 Schematic diagram of GSK3 involvement in different signalling pathways (Kaidanovich-Beilin and Woodgett, 2011).	24
Figure 1.14 Schematic diagram of the two isoforms of Glycogen Synthase Kinase 3 (GSK3) (Doble and Woodgett, 2003).	24

Figure 1.15 Schematic diagram of GSK3 phosphorylation inhibition mechanism (Cohen and Frame, 2001).	26
Figure 1.16 Schematic diagram of 4 major MAPK pathways in mammalian cells (Roberts and Der, 2007).	28
Figure 1.17 Simplified schematic diagram of the ERK-MAPK signalling pathway (Lavoie and Therrien, 2015).	32
Figure 1.18 Schematic diagram of RAF family protein kinases domain structure (Roskoski, 2010).	34
Figure 1.19 Structure of BRAF kinase domain in humans (Roskoski, 2010).	36
Figure 1.20 BRAF mutations in human cancers.	38
Figure 1.21 Schematic diagram of molecular pathways involved in cellular senescence (Ben-Porath and Weinberg, 2005).	42
Figure 1.22 Schematic diagram of the 2843 amino acids structure of APC protein (McCart et al., 2008).	49
Figure 1.23 Conditional knockin allele for ^{V600E} Braf in GEMMs (Pritchard et al., 2007).	56
Figure 1.24 Control of Cre activity using the AhCreER ^T system.	59
Figure 1.25 Timeline of ^{V600E} BRaf induced small intestine hyperplasia followed by senescence and ultimately tumour development.	59
Figure 1.26 Evidence of crosstalk between MAPK/ERK and the WNT pathway in a ^{V600E} Braf mouse model at various time points (Carragher et al., 2010).	60
Figure 1.27 Formation of lung and stomach hyperplasia in $\text{Braf}^{+/LSL-V600E}; \text{AhCreER}^{T+/o}$ (Carragher et al., 2010).	62
Figure 1.28 Pathological characteristics of the $\text{Braf}^{+/LSL-V600E}; \text{Villin-Cre}$ Mouse model (Rad et al., 2013).	
Figure 3.1 Western blot analysis of human CRC cell lines RKO.	107
Figure 3.2 Immunostaining of RKO cell lines for subcellular localisation of β -catenin.	109

Figure 3.3 Immunostaining of the parental RKO cell line treated with U0126 (MEK inhibitor) for 16 or 24 hours.	110
Figure 3.4 Western blot analysis of MEFs with conditional Cre regulated $V600E$ Braf.	112
Figure 3.5 Western blot analysis of human cancer cell lines with the $V600E$ BRAF mutation.	114
Figure 3.6 Analysis of protein and phospho-protein expression levels associated with the two pathways by western blot in human HCC364 lung and melanoma A375P cell lines treated with U0126 (MEK) inhibitor or DMSO for control cells.	116
Figure 3.7 Western blot analysis of MEK inhibitor (PD184352) treated human melanoma (A375P) cells.	119
Figure 3.8 Western blot analysis of A375P melanoma cells treated with rapamycin for 5 or 24 hours.	121
Figure 3.9 Schematic diagram of the RAF/MEK/ERK pathway and GSK3 crosstalk.	123
Figure 3.10 Schematic diagram of proposed autocrine/paracrine mechanism of crosstalk.	132
Figure 4.2 PCR genotyping to determine the genotype of the offspring as well as Cre-mediated recombination.	134
Figure 4.3 Schematic diagram showing treatment regime for AhCreER ^{T0/WT} and Villin-CreER ^{T0/WT} mouse models.	135
Figure 4.4 Western blot analysis of the Braf ^{LSL-V600E/WT} ; AhcreER ^{T0/WT} gut tissue at different times p.i. after animals were injected with β -NF and TM.	137
Figure 4.5 A) Immunohistochemical analysis of 3 days p.i. tissue samples taken from Braf ^{LSL-V600E/WT} ; AhCreER ^{T0/WT} mice. Adjacent sections from the same piece of tissue were stained for phospho-ERK and β -catenin.	139
Figure 4.6 Analysis of BVE/Cre tissue following 3 days of induction of $V600E$ BRAF.	141

Figure 4.7 Schematic diagram of mouse small intestine (Carragher et al., 2010).	143
Figure 4.8 Crypt hyperplasia in $\text{Braf}^{\text{LSL-V600E/WT}}$; $\text{Villin-CreER}^{\text{T0/WT}}$ mice following TM induction at 3 days p.i.	144
Figure 4.9 Immunohistochemical analysis of 3 days p.i. tissue for BrdU incorporation.	146
Figure 4.10 Immunohistochemical analysis of, 3 days p.i., tissue for phospho-H3.	147
Figure 4.11 PD184352 treatment regime.	149
Figure 4.12 Western blot analysis of PD184352 treated, 3 days p.i., mouse tissue.	151
Figure 5.1 PCR genotyping to determine the genotype of Gsk3 offspring.	160
Figure 5.2 Western blot analysis of gut tissue from $\text{Braf}^{\text{LSL-V600E/WT}}$; $\text{Villin-CreER}^{\text{T0/WT}}$ (BVE/Cre), $\text{Gsk3}\alpha^{\text{S21A/S21A}}$, $\text{Gsk3}\beta^{\text{S9A/S9A}}$, $\text{Braf}^{\text{LSL-V600E/WT}}$; $\text{Villin-CreER}^{\text{T0/WT}}$ (BVE/Cre/Ki/Ki), $\text{Villin-CreER}^{\text{T0/WT}}$ (WT/Cre), and WT mice.	167
Figure 5.3 Examination of crypt length is observed following V^{600E} BRaf expression.	169
Figure 5.4 Immunohistochemical analysis for BrdU incorporation.	171
Figure 5.5 Immunohistochemical analysis for phospho-histone H3.	172
Figure 5.8 Venn diagram indicating number of genes with minimum of 2-fold change following V^{600E} BRaf induction or Gsk3 mutation.	185
Figure 5.9 Schematic diagram of the proposed model on the effect of Gsk3 mutation on gene expression changes induced by V^{600E} BRaf.	185
Figure 5.11 Expression and phosphorylation of AMPK- α protein kinase following V^{600E} BRaf induction with or without Gsk3 α/β mutations.	198
Figure 6.1 Effect of the genotype on mouse survival.	208
Figure 6.2 Appearance of macroscopic and microscopic tumours in mouse gut tissue.	210

Figure 6.3 Analysis of number of macroscopic tumours in ^{V600E} BRaf mice small intestine, with or without Gsk3 α/β knockin mutations, over time.	212
Figure 6.4 Analysis of the number of microscopic tumours in ^{V600E} Braf mice small intestine with or without Gsk3 α/β knockin mutations, over time.	213
Figure 6.5 Impact of Gsk3 α/β mutations on macroscopic and microscopic tumour burden in ^{V600E} BRaf mice small intestine.	215
Figure 6.6 Impact of the genotype on the number of macroscopic tumours in different sections of the small intestine.	217
Figure 6.7 Impact of genotype on the number of microscopic tumours in each section of the small intestine.	218
Figure 6.8 H&E staining of mouse gut tissue containing tumours at different stages. On the left-hand panel, is an example of a low-grade dysplastic tissue.	220
Figure 6.9 Impact of Gsk3 α/β knockin mutations on tumour grade.	221
Figure 7.1 Schematic diagram of the potential effect of activated ^{H1047R} PI3K on AKT and GSK3 phosphorylation in RKO cells.	228
Figure 7.2 Schematic diagram of the proposed model on the effect of dietary fat on tumour growth in ^{V600E} BRAF-induced melanoma (Xia et al., 2017).	232
Figure 7.3 Simplified schematic diagram of cholesterol biosynthesis and ketogenesis pathways showing some of the important enzymes involved in the pathways deregulated by ^{V600E} BRaf (in red).	235
Figure 7.4 Schematic diagram of the proposed model of the mechanism involved in interaction between ^{V600E} BRAF and HMGCS1 in early stages of serrated CRC.	236
Figure 7.5 Schematic diagram of proposed model on the effect of MAPK target genes on crypt hyperplasia.	240

Table of Tables

Table 1.1 Molecular characteristics of CRC as described by The Cancer Genome Atlas Network (Müller et al., 2016).	9
Table 1.2 List of different Apc mutant mice (McCart et al., 2008).	52
Table 1.3 List of different models of Gsk3 mouse (Kaidanovich-Beilin and Woodgett, 2011).	64
Table 2.1 List of the reagents used in cell culture procedures.	72
Table 2.2 List of inhibitors used to treat cells.	74
Table 2.3 List of the chemicals and reagents used in the immunofluorescence staining of cells.	76
Table 2.4 List of the chemicals and reagents used in preparation of protein lysate and estimation of protein concentration.	79
Table 2.5 Detailed formulation of the SDS-PAGE gels used in the experiments.	81
Table 2.6 List of primary antibodies used for immunoblotting.	84
Table 2.7 List of secondary antibodies used for immunoblotting.	84
Table 2.8 List of the chemicals and reagents used for SDS-polyacrylamide gel electrophoresis.	85
Table 2.9 List of primers used for genotyping.	89
Table 2.10 List of the chemicals and reagents used in genotyping.	89
Table 2.11 Inhibitor name and concentration used in animal study.	91
Table 2.12 List of the reagents used in <i>in vivo</i> studies.	92
Table 2.13 Details of primary antibodies used for immunohistochemistry.	97
Table 2.14 List of secondary antibodies used for immunohistochemistry.	98
Table 2.15 List of the chemicals and reagents used in histology.	99
Table 5.1 Mating 1 and Mating 2 strategies conducted in parallel and genotypes of the offspring.	162
Table 5.2 Mating 3 strategy and genotypes of offspring. Genotypes shown in red were used in Mating 4.	163
Table 5.3 Mating strategy used to maintain the colony population used in this study.	165

Table 5.4 WIKI pathway enrichment analysis indicating top pathways whose components change in expression following ^{V600E} BRaf induction.	177
Table 5.5 WIKI pathway enrichment analysis indicating top pathways whose components change in expression as a result of additive effect of Gsk3 α/β mutations and ^{V600E} BRaf induction.	190

Abbreviations

A375P	Human malignant melanoma cells
AA	Acetoacetate
Ad β -gal	Adenoviral beta galactosidase
AdCre	Adenovirus carrying Cre recombinase
AKT	Protein kinase B
AMPK	AMP-activated protein kinase
APC	Adenomatous polyposis coli
ATM	Ataxia telangiectasia mutated
ATP	Adenosine triphosphate
ATR	ATM and Rad3-related
β -gal	β -galactosidase
β -NF	β -naphthoflavone
BMP	Bone morphogenetic protein
BrdU	5-bromo-2'-deoxyuridine
BSA	Bovine serum albumin
BVE/Cre	<i>Villin-CreER^{T0/WT}</i> ; <i>Braf^{fLSL-V600E/WT}</i>
BVE/Cre	<i>Braf^{fLSL-V600E/WT}</i> ; <i>Villin-CreER^{T0/WT}</i>
BVE/Cre/Ki/Ki	<i>GSK3α^{S21A/S21A}</i> ; <i>GSK3β^{S9A/S9A}</i> ; <i>Braf^{fLSL-V600E/WT}</i> ; <i>Villin-CreER^{T0/WT}</i>
cAMP	Cyclic adenosine monophosphate
CBP	CREB-binding protein
CDK	Cyclin dependent kinase
CDKI	Cyclin dependent kinase inhibitor
CGAN	Cancer genome atlas network
Chk2	Check point kinase 2
CIMP	CpG island promoter methylation
CIN	Chromosomal instability
CK1	Casein kinase 1
CMSs	Consensus molecular subtypes of colorectal cancer
CRC	Colorectal cancer
CRD	Cysteine-rich domain
Cre	<i>Villin-CreER^{T0/WT}</i>
DAG	Diacylglycerol
DDR	DNA damage response
DFG	Asp/Phe/Gly sequence
DKK	Dickkopf
DMEM	Dublecco's modified Eagle Medium
dMMR	DNA mismatch repair genes
dMMR	DNA mismatch-repair
DMSO	Dimethyl sulfoxide
DNA	Deoxynucleic acid

Dvl	Dishevelled
EDTA	Ethylenediaminetetraacetic acid
EGF	Epidermal growth factors
EGFR	Epidermal growth factor receptor
EGTA	Ethylene glycol-bis(β -aminoethyl ether)-N,N,N',N'-tetraacetic acid
EMEA	European medicine evaluation agency
EMT	Epithelial to mesenchymal transition
ENU	N-ethyl-N-nitrosourea
ERK1/2	Extracellular signal regulated kinases 1/2
ES	Embryonic stem cells
FAP	Familial adenomatous polyposis
FBS	Foetal Bovine Serum
FDA	Food and drug administration
FGF4	Fibroblast growth factor
Fz	Frizzled
GCPR	G protein-coupled receptor
GDP	Guanosine diphosphate
GEF	Guanine nucleotide exchange factor
GEM	Genetically engineered model
GEMMs	Genetically modified mouse models
GF	Growth factor
GI	Gastrointestinal
GRB2	Growth factor receptor-bound protein 2
GS	Glycogen synthase
GSK3	Glycogen synthase kinase 3
GTP	Guanosine triphosphate
H&E	Hematoxylin and Eosine staining
HCC364	Human lung non-small cell carcinoma
HCC364	Human lung adenocarcinoma cells
HCL	Hydrochloric acid
HGD	High grade dysplasia
Hh	Hedgehog
HMGCL	3-hydroxy-3-methylglutaryl-CoA
Hox	Homeobox genes
HPs	Hyperplastic polyps
Hsp90	Heat shock protein 90
IgG1	Immunoglobulin G1
IL 6/8	Interleukin 6/8
IRS1/2	Insulin receptor substrate1/2
ISC	Intestinal stem cells
kDa	Kilo Dalton
KI	Knock-in
KO	Knock-out

Lct	Lactase
LEF	Lymphoid enhancing factor-1
LGD	Low grade dysplasia
LRP5/6	LDL-receptor-related proteins 5 and 6
LS	Lynch syndrome
LSL	Lox-STOP-Lox
mAbs	Monoclonal antibodies
MAP	Microtubules-associated protein
MAPK	Mitogen-activated protein kinase
MEFs	Mouse embryonic fibroblasts
MEK1/2	MAPK-ERK kinase 1/2
Min	Multiple intestinal neoplasia
Mom	Modifiers of Min
mRNA	Messenger ribonucleic acid
MSI	Microsatellite instable
MSI-immune	Microsatellite instable immune
MSS	Microsatellite stable
mTOR	Mammalian target of rapamycin
NaCl	Sodium chloride
neoR	Neomycin resistance
NSCLC	Non-small cell lung cancer
O.D.	Optical density
OIS	Oncogene-induced senescence
p.i.	Post injection
p38MAPK	p38 mitogen-activated protein kinases
p70S6K/p85S6K	p70/p85 ribosomal S6 kinase
p90RSK	p90 ribosomal S6 kinase
PBS	Phosphate buffer saline
PCR	Polymerase chain reaction
PDAC	Pancreatic ductal Adeno-carcinomas
PDGF	Platelet-derived growth factors
PDK	Phosphoinositide-dependent kinase
PFA	Paraformaldehyde
pH	Potential of hydrogen
pH3	phospho-Histone3
PI3K	Phosphatidylinositol 3' kinase
PKA	Protein kinase A
PKB	Protein kinase B
PKC	Protein kinase C
PLC	Phospholipase C
PLX4032	Vemurafenib
POLE	Polymerase E
PP2A	Protein phosphatase 2

PRF	Pre-clinical research facility
RAF	Rapidly accelerated fibrosarcoma
RAS	Rat sarcoma
Rb	Retinoblastoma protein
RBD	RAS-binding domain
Rheb	Ras homology enriched in brain
RIPA	Radioimmunoprecipitation assay buffer
RKO	Human CRC cell line
RNA	Ribonucleic acid
RSK1	Ribosomal s6 kinase
RTK	Receptor tyrosine kinases
RTKs	Receptor tyrosine kinases
SA- β -gal	Senescence-associated β -galactosidase
SASP	Senescence -associated secretory phenotype
SCNAs	DNA somatic copy number alteration
SD	Standard deviation
SDF	Senescence associated DNA damage foci
SDS	Sodium dodecyl sulfate
SH2	Src homology 2 domain
Si	Sucrose isomaltase
SOS	Son of Sevenless
SSA/P	Sessile serrated adenoma/polyps
TA	Transit amplifying cells
TA	Tarnsit amplifying cells
TBST	Tris buffer saline
TCF	T cell factor
TCGA	Cancer genoma atlas network
TEMED	Tetramethylethylenediamine
TM	Tamoxifen
TSA	Traditional serrated adenoma
TSC1/2	Tuberous sclerosis protein
v/v	volume/volume
V600E	^{V600E} BRAF mutation
VE	V600E
VEGF	Vascular endothelial growth factor
VEGF	Vascular-endothelial growth factor
w/v	weight/volume
WT	Wild type
WT/Cre	Villin-CreER ^{T0/WT}
WT/Cre/Ki/Ki	GSK3 α ^{S21A/S21A} ; GSK3 β ^{S9A/S9A} ; Villin-CreER ^{T0/WT}

Chapter 1. Introduction

1.1. Colorectal cancer

Colorectal cancer (CRC), also commonly known as large bowel cancer, is responsible for 9% of deaths caused by cancer worldwide. CRC is quite common in advanced countries such as Canada, United States, New Zealand and parts of western Europe such as the UK but not as common in the developing countries for instance China, India and parts of Africa (Hagggar and Boushey, 2009). Colorectal cancer is the third most common cancer, fourth most common cause of death globally, and it affects both men and women at an equal rate (Hagggar and Boushey, 2009, Marley and Nan, 2016, Amersi et al., 2005). In the UK, approximately 113 cases of colorectal cancer are diagnosed every day which makes it the third most common cancer after breast and lung (Figure 1.1). Almost half (46%) of cancer deaths in 2014 were caused by lung, bowel, and breast/prostate cancers. More than 8 out of 10 cases of bowel cancer happen in people aged 60 and over, with the peak rate between 85-89 years of age. Colorectal cancer (10%) is the second most common cause of cancer death after lung (22%) in the UK (Figure 1.2) (CancerReaserchUK, 2016a).

Survival rate for colorectal cancer depends on the stage of diagnosis. The Five-year survival rate rapidly decreases between stages 1 and 4. There is no significant difference between men and women survival rate. In men, the five-year survival rate drops from 95% at stage 1 to 7% at stage 4, whereas in women it changes from 100% at stage 1 to 8% at stage 4 (CancerReaserchUK, 2016c, Amersi et al., 2005). The bowel cancer survival rate more than doubled in the UK in last 40 years (Figure 1.3) (CancerReaserchUK, 2016c).

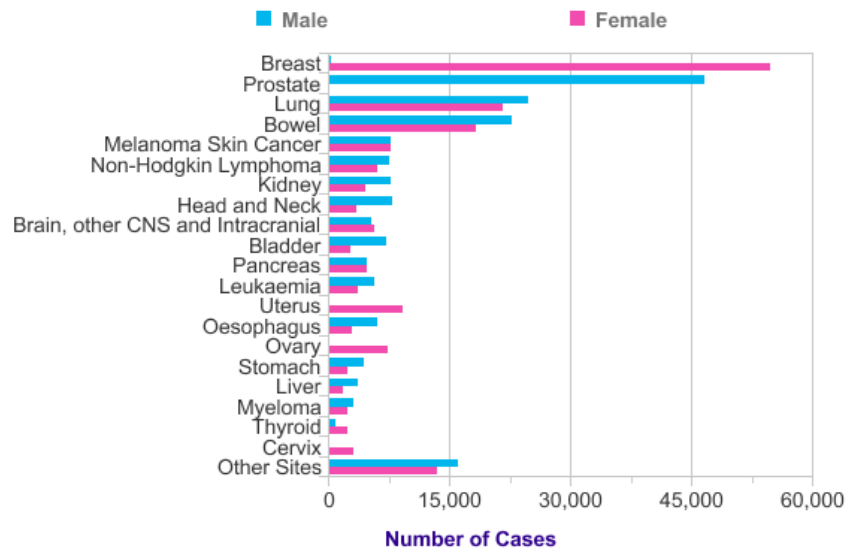


Figure 1.1 Twenty most common cancers in the UK, 2014 (CancerResearchUK, 2016b). Colorectal (Bowel) cancer is the third most common cancer after breast/prostate and lung in the United Kingdom.

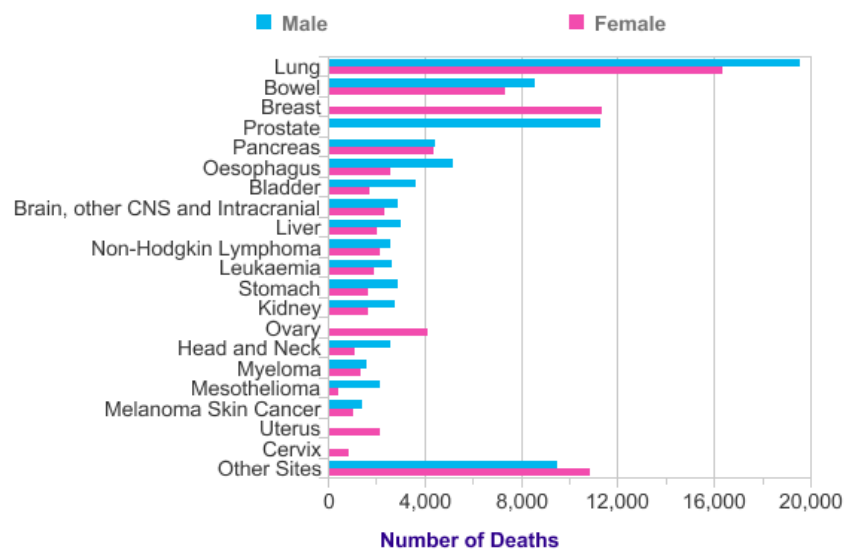


Figure 1.2 Twenty most common cancer deaths in the UK, 2014 (CancerResearchUK, 2016c). The graph shows number of deaths regardless of the age per year. Colorectal (bowel) cancer is the second most common death after lung.

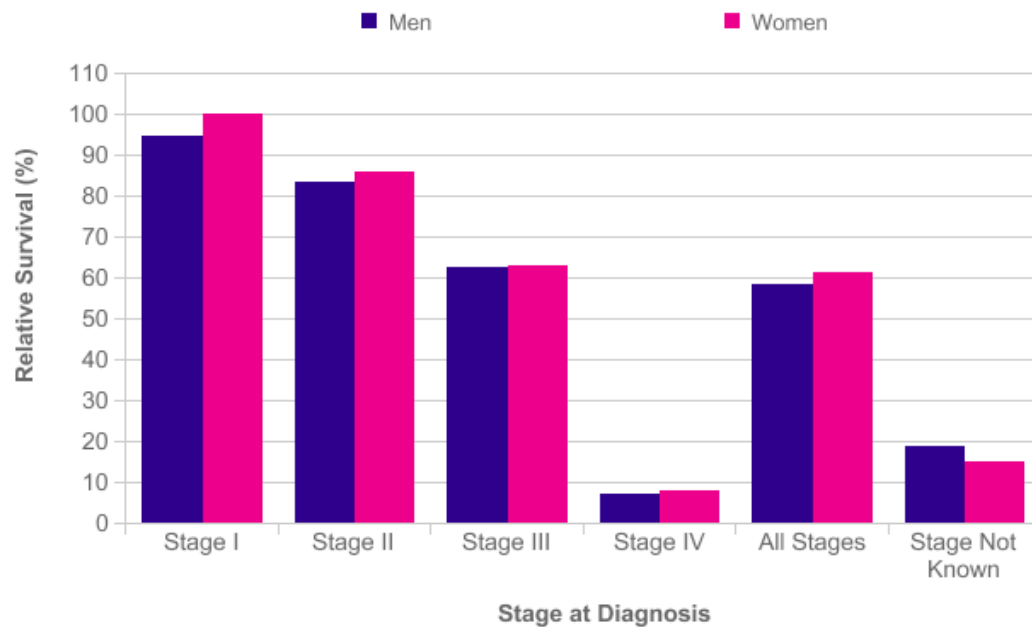


Figure 1.3 Colorectal cancer five-year survival by stage, in both sexes - 2002-2006 (CancerResearchUK, 2016a). Five-year survival rate does not show any significant difference between male and female patients, but it decreases significantly between stage 1 and stage 4. Therefore, the survival rate is significantly higher at earlier stages of diagnosis.

1.2. Classification of colorectal cancer

Colorectal cancer is a deadly disease with heterogeneous characteristics, making it a challenge in terms of diagnosis and treatment. Figure 1.4 shows the frequency of 20 most common mutations detected in human colorectal carcinoma (Cosmic, 2019). There is a need to have distinct molecular and morphological classification systems, to improve outcomes. Around 70-80% of CRC cases are sporadic, while between 20-30% are hereditary such as Lynch syndrome (LS) (3-4%) and familial adenomatous polyposis (FAP) (~1%). Mutation order seems to play a crucial role in cancer and development events (Pino and Chung, 2010). In the traditional adenoma-carcinoma model, activation through *APC* mutation serves as an initiating event which leads to adenoma formation, whereas *KRAS* mutation cannot initiate cancer formation *in vivo*; and the combination of these two events seems to promote tumour progression (Pino and Chung, 2010). Each of these mutations gives biological advantages which drive tumorigenesis (Jass, 2007). An additional factor is genetic instability, which leads to additional mutations that can drive the disease.

1.2.1. Molecular classification of CRC

The traditional colorectal carcinoma mode of progression was proposed by Fearon and Vogelstein in 1990. The model shows that conventional adenomas arise via inactivation of the *APC* gene followed by other changes with the most prevalent ones being *KRAS* mutation and inactivation of the *TP53* gene (Figure 1.5) (Jass, 2007, Fearon and Vogelstein, 1990, Fearon, 2011).

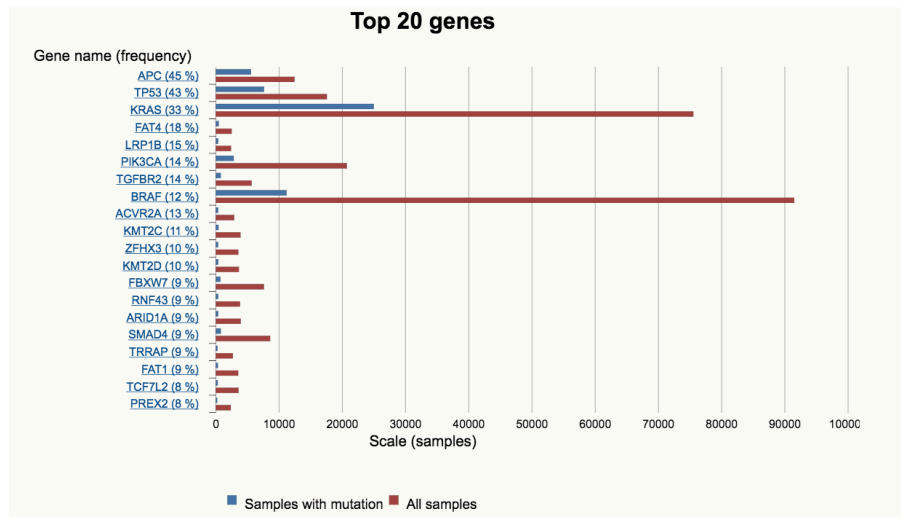


Figure 1.4 Graph showing frequency of the 20 most common mutations detected in human colorectal carcinoma (Cosmic, 2019). Both APC, TP53 and KRAS genes show the highest mutational frequency with 45%, 43% and 33% respectively. BRAF mutation is detected in 12% of the cases.

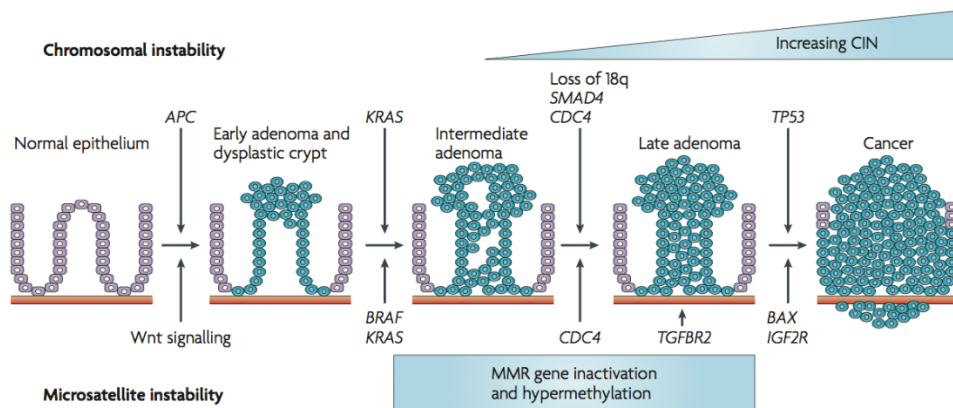


Figure 1.5 Fearon and Vogelstein model proposed in 1990 for colorectal cancer development and progression (Walther et al., 2009). The multi-hit model in cancer development shows more than one mutation in tumour suppressor genes and oncogenes are necessary for the development of metastatic cancer. Loss of the APC tumour suppressor gene is the first in a series of events which causes the formation of hyperplastic epithelium, followed by oncogenic mutation of KRAS and the last step is the loss of TP53 tumour suppressor gene, which leads to formation of carcinoma and invasive cancer.

The traditional class of colorectal cancer is the most common type of sporadic CRC accounting for 84% of reported cases. The most noticeable characteristic of this group is the association with chromosomal instability (CIN) which are changes in chromosome number and structure within cells, including: deletions, translocations, gains and other chromosomal rearrangements. These changes are often detectable as high frequency DNA somatic copy number alteration (SCNAs) (Müller et al., 2016, Guinney et al., 2015). An early key event in the CIN subtype is abnormalities in the WNT pathway i.e. APC inactivation. Around 80% of tumours show mutation in *APC* whereas ~5-10% harbour mutations or epigenetic changes in other components of the WNT signalling pathway for example *β-catenin* (Müller et al., 2016).

A less common and recently described class of CRC, known as serrated adenocarcinoma, accounts for ~20% of cases and has been described as having *BRAF* or *KRAS* mutations as the earliest alterations (Mäkinen, 2007). These two mutations are exclusive in serrated CRC which suggests that there are two major subtypes of serrated colorectal carcinomas in human (Ko et al., 2015) (Figure 1.6). The family of serrated polyps is subdivided into sessile serrated adenoma (SSA), traditional serrated adenoma (TSA) and hyperplastic polyps (HPs) (Ensari et al., 2010). SSAs develop via a series of alterations in the defective tissue that leads to formation of carcinoma with vast CpG island promoter methylation (CIMP) which can be linked to either microsatellite stable (MSS) or microsatellite instable (MSI) (Crockett et al., 2015, Snover, 2011).

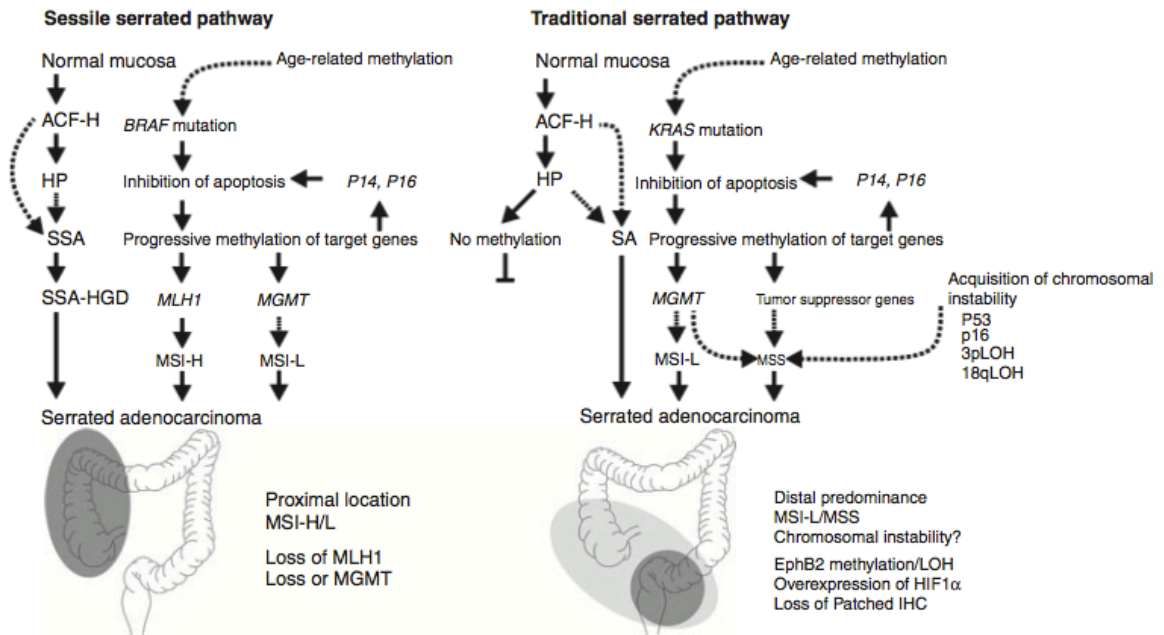


Figure 1.6 Schematic representation of traditional and sessile serrated pathways in colorectal carcinoma (Mäkinen, 2007). Molecular changes lead to development of two different subtypes of serrated colorectal carcinomas in human; the Sessile serrated pathway (SSA) involving BRAF mutation and the traditional serrated pathway (TSA) involving KRAS mutation. It is estimated that SSA/Ps represent 8-20% of serrated polyps with a preference for the right colon, whereas TSA are much less common and are mainly found in the left colon.

In 2012, the Cancer Genome Atlas Network (TCGA) proposed a new classification of CRC known as TCGA classification (CGAN, 2012). In this classification, it was proposed that CRC should be categorised into two different major categories; non-hypermuted and hypermutated. The hypermutated category was further divided into two sub-categories, ~13% of the hypermutated group showed defects in DNA mismatch repair genes (dMMR), high microsatellite instability usually with hypermethylation and MLH1 gene silencing, and a small group of ~3% had an extremely high mutation rate of somatic mismatch repair gene, and polymerase ϵ (POLE), DNA replicating enzyme mutation, which was named as the ultramutated subcategory (Table 1.1) (Müller et al., 2016).

Group	(1a) Ultramutated <i>POLE</i> mutant	(1b) Hypermutated dMMR/MSI	(2) CIN/SCNA-high, MSS
Mutation rate	++++	+++	+
Somatic copy number alterations	+/-	+	+++
Key molecular/genetic abnormality	<i>POLE</i> EDM proofreading mutation	Defective MMR/MLH1 promoter hypermethylation	Variety of mutated cancer genes; WNT pathway activation (mostly by APC mutation/inactivation)
Predominant histological type	Moderately differentiated adenocarcinoma	Mucinous, or signet ring, or poorly differentiated adenocarcinoma	Moderately differentiated adenocarcinoma
Proportion of all colorectal carcinomas	~3 %	~13 %	~84 %
Prognosis	Good (more data required)	Good/poor after relapse	Good-poor (depending on other characteristics)

CIN chromosomal instability, *POLE* DNA polymerase epsilon, *EDM* exonuclease domain mutant, *SCNA* somatic copy number alteration, *MMR* mismatch repair, *MSI* microsatellite instability

Table 1.1 Molecular characteristics of CRC as described by The Cancer Genome Atlas Network (Müller et al., 2016). The TCGA integrated molecular classification shows there is a major group which accounts for ~84% of reported cases and is described by having high level of chromosomal instability but with microsatellite stability. A smaller group which accounts for ~13% of the cases is known for having hypermutated DNA mismatch repair gene mutations and microsatellite instability, and a very small fraction of ~3% of cases is known to have ultra-mutated polymerase E (*POLE*) DNA replicating enzyme mutations.

In 2015, a new classification was reported by an international expert consortium as previous attempts of gene expression profiling by several groups showed very little agreement with each other (Müller et al., 2016, Guinney et al., 2015). The consensus molecular subtypes of colorectal cancer (CMSs) shows the interconnectivity between six independent classification systems (Guinney et al., 2015). The CMSs system divides CRC into 4 subcategories with distinguishing features: CMS1 which accounts for ~14% of reported cases is microsatellite instable immune (MSI-immune) which is characterised by having defective DNA mismatch repair with MSI and silencing of *MLH1* along with *BRAF* mutation and high rate of CpG islands methylator phenotype (CIMP-H) while having a low number of SCNAs (Guinney et al., 2015). CMS1 subgroup is similar to sporadic MSI CRC subgroup which is also known as the Sessile Serrated CRC. The CMS1 group shows a very strong immune response in the tissue, such as prominent infiltration of CD8+ cytotoxic T lymphocytes in tumour areas (Müller et al., 2016). CMS1 tumours are frequently observed in females with right sided lesions (Guinney et al., 2015).

CMS2-CMS4 groups are shown to have high levels of CIN and are therefore the subcategories of the, previously described, larger group of traditional adenoma-carcinoma CRC with CIN characteristics (Müller et al., 2016, Guinney et al., 2015). CMS2 (canonical, 37%) has the highest level of gain in oncogene copy number, and loss of tumour suppressor genes, in comparison to other subtypes (Guinney et al., 2015). CMS2 CRC display prominent WNT and MYC signalling activation of downstream pathways (Müller et al., 2016, Guinney et al., 2015). Furthermore, CMS2 tumours tend to be left sided with a higher proportion of long-term survival, whereas CMS1 patients show a very poor long-term survival rate (Guinney et al., 2015). CMS3 (metabolic), which accounts for ~13% of cases, have high frequency of *KRAS* mutation with fewer SCNAs and contain more hypermutated / MSI samples than CMS2 and CMS4 (Guinney et al., 2015). CMS4 CRC subtype (mesenchymal, 23%) shows an increase in epithelial-to-mesenchymal transition (EMT) gene expression, with expression of genes involved in stromal invasion, remodelling of cellular matrix, inflammation and angiogenesis pathway as well as a higher proportion of non-cancerous

cells. CMS4 tumours tend to be diagnosed at a more advance stage (III and IV) (Guinney et al., 2015) (Figure 1.7). There is a sub-group in the CMS system which accounts for ~13% of samples showing mixed features, possibly representing a transition phenotypic stage or intratumoral heterogeneity (Müller et al., 2016).

Comparison between the two recent major subtyping systems proposed by CGAN in 2012 and CMSs in 2015 (Figure 1.8) indicates that both classification systems are in agreement on the presence of dMMR/MSI with *BRAF* mutation in the CMS1 category that accounts for ~13%-14% of cases. The CIN subcategory (84%), proposed by CGAN, was subdivided into 3 categories CMS2-CMS4 by consensus molecular sequence classification (Figure 1.8) (Müller et al., 2016).

CMS1 MSI immune	CMS2 Canonical	CMS3 Metabolic	CMS4 Mesenchymal
14%	37%	13%	23%
MSI, CIMP high, hypermethylation	SCNA high	Mixed MSI status, SCNA low, CIMP low	SCNA high
<i>BRAF</i> mutations		<i>KRAS</i> mutations	
Immune infiltration and activation	WNT and MYC activation	Metabolic deregulation	Stromal infiltration, TGF- β activation, angiogenesis
Worse survival after relapse			Worse relapse-free and overall survival

Figure 1.7 Classification of CRC proposed by the international expert consortium (Guinney et al., 2015). The consensus molecular subtypes of colorectal cancer (CMSs) divides CRC into 4 subgroups: CMS1 (MSI-immune, 14%), CMS2 (canonical, 37%), CMS3 (metabolic, 13%) and CMS4 (mesenchymal, 23%).

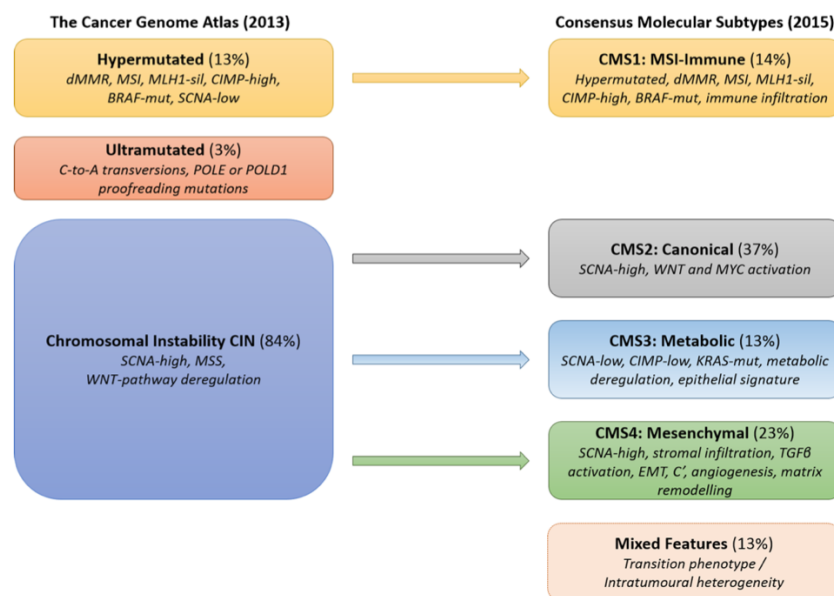


Figure 1.8 Comparison between the two-recent molecular classifications of the colorectal cancer (Müller et al., 2016). On the left, the classification proposed by The Cancer Genome Atlas Network (CGAN) in 2012 categorising CRC into three main categories in which ~84% of cases showed chromosomal instability (CIN) with deregulation in the WNT signalling pathway but are microsatellite stable (MSS). The hypermutated subcategory accounts for 13% of cases and has *BRAF* mutation along with microsatellite instability (MSI) and high levels of CpG island methylation. The third subcategory accounts for only ~3% of cases which has ultramutated polymerase E (*POLE*) DNA replication enzyme. On the right, The Consensus Molecular Subtypes (CMSs) are categorized into 4 subtypes. CMS1 (MSI-immune) accounts for ~14% of cases and are hypermutated with *BRAF* mutation along with defects in DNA mismatch repair genes (*dMMR*) and MSI. In this system CMS2 (Canonical, 37%), CMS3 (Metabolic, 13%), CMS4 (Mesenchymal, 23%) fall under the subcategory of chromosomal instability proposed by CGAN in 2012.

1.2.2. Morphological classification of CRC

Colorectal cancers are classified into two categories: hereditary and sporadic. The hereditary subclass itself divides into different types like Lynch Syndrome, which is detected in the proximal colon, and familial adenomatous polyposis (FAP) which develops on the left side of the colon (Fleming et al., 2012). Sporadic CRC is subcategorised into two major groups: conventional adenomas and serrated adenomas. The latter subdivides into three categories: traditional serrated adenoma, sessile serrated adenoma and hyperplastic polyps (Crockett et al., 2015). About 70-80% of sporadic colorectal cancer cases are categorized as conventional adenomas with CIN and, in the past, were considered to be the precursors of all sporadic cancer cases (Crockett et al., 2015). Conventional adenomas show distinct molecular and pathological features, and are specifically recognised by glandular formation (Fleming et al., 2012). Conventional adenoma-carcinomas are known to have necrotic debris, called dirty necrosis, (Figure 1.9B) as they progress into more advanced stages (Fleming et al., 2012) and can cause bowel obstruction and bleeding. This type tends to be dysplastic. A faecal screening test was developed based on the bleeding characteristic of the conventional adenomas. *BRAF* mutations are extremely rare in conventional adenomas (Crockett et al., 2015).

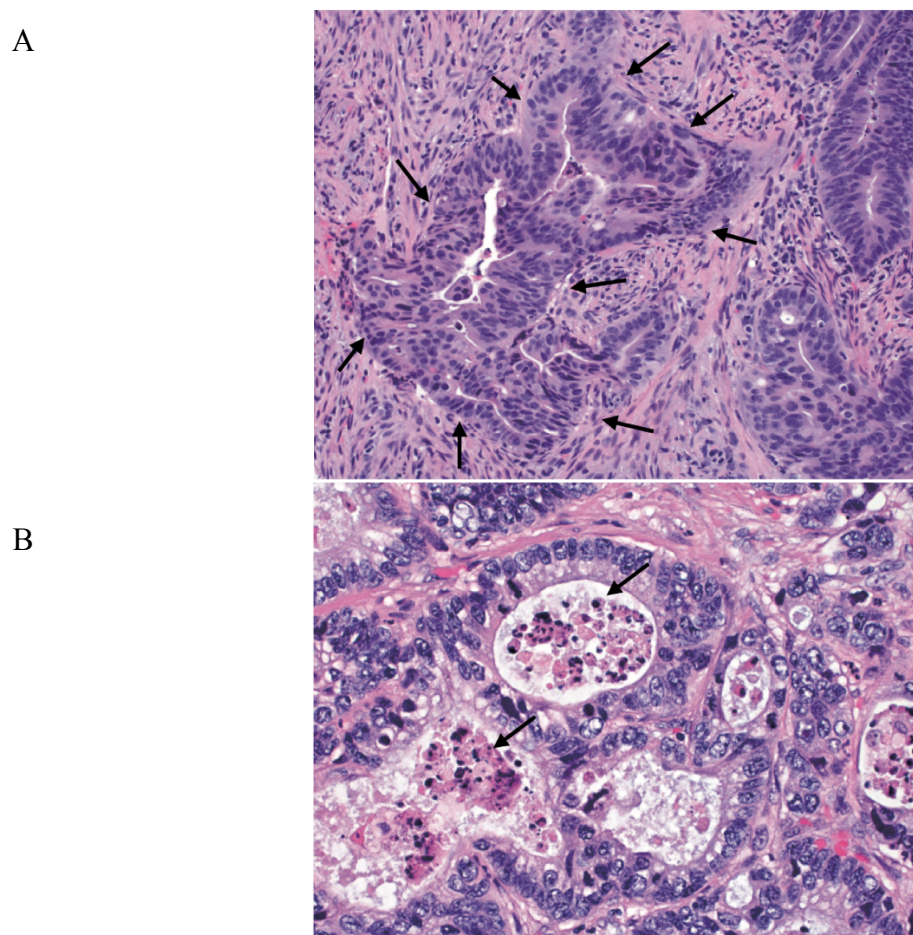


Figure 1.9 Pathological features of conventional adenomas (Fleming et al., 2012).

A) Glandular formation, with edges marked by black arrows, as a distinct characteristic of conventional adenomas used as a basis for pathological grading.

B) Presence of necrotic debris (dirty necrosis) in invasive colorectal carcinoma. Necrotic debris are shown by black arrows.

Serrated adenomas, a recently described class of sporadic CRC, are any type of polyp that shows serrated (sawtooth like or stellate) structures of the epithelium (Fleming et al., 2012). Serrated pathways rapidly progress in comparison to the conventional *APC*-mutated cancers (Snover, 2011). Predominant mutations in serrated adenomas are *BRAF* and *KRAS* (Rad et al., 2013). As was stated previously, serrated adenomas are a highly heterogeneous group of lesions with 3 subtypes:

- Hyperplastic polyps (HPs) are usually small in size and are located in the distal colon. They can be identified by their simple tubular architecture with straight and elongated crypts and luminal serration and mature appearance of the upper portion of the crypt (Fleming et al., 2012). The malignant potential of HPs is currently considered to be insignificant (Amersi et al., 2005). In HPs, the proliferation zone is limited to the basal area of the crypt, while maturation occurs towards the lumen area. A Sawtooth-like structure is the result of reduced apoptosis in the tissue (Figure 1.10A) (Fleming et al., 2012, Snover, 2011).
- Traditional serrated adenomas (TSA) are characterised by *KRAS* mutation as an early event with serrated tissue structure and are mostly detected in male patients (Ko et al., 2015). TSA accounts for 1% of colorectal polyps and can occur throughout the colon but they have a tendency to develop in the distal colon and rectum (Amersi et al., 2005). The traditional serrated pathway is reported to have two morphological subtypes: serrated dysplasia and conventional adenomatous dysplasia (Tsai et al., 2014). The morphological structure of the TSA is the result of relocation of the proliferation zone to the side of the crypt in which outward growth creates ectopic crypts (Figure 1.10C) (Snover, 2011). The focal presence of the ectopic crypts, which is the result of loss of anchoring of the crypt base to the muscle layer, is in fact a diagnostic criterion of TSA (Snover, 2011).
- Sessile serrated adenoma/polyps (SSA/P) harbour the ^{V600E}*BRAF* mutation and are mostly detected in females on the right side of the colon (proximal colon) with a flat appearance and relatively large size (Ko et al., 2015). SSA/Ps are structurally distorted because of abnormal

proliferation (Crockett et al., 2015, Fleming et al., 2012, Ko et al., 2015). Serrated adenomas are pale yellow in colour and capped with mucus, which must be removed to allow visualisation (Amersi et al., 2005). They also show rims of debris and bubble as well as distortion of the underlying mucosal vascular pattern (Amersi et al., 2005). As described recently, these lesions are very ill defined and pale. They are therefore very difficult to be recognised by colonoscopy at the time of screening and some of them fall between the folding of the colon which makes them even harder to detect (Figure 1.11) (Amersi et al., 2005). High levels of intracellular and luminal mucin are present in SSA. SSA/P appearance is like a dilated L, or an inverted T, which is the result of a movement of the proliferative zone to the side and bidirectional maturation with mature cells in the normal proliferative zone (Figure 1.10B) (Crockett et al., 2015, Snover, 2011, Amersi et al., 2005). The difference between TSA and SSA appearance is that in TSA the crypt remains attached and oriented to the muscle layer underneath (Snover, 2011).

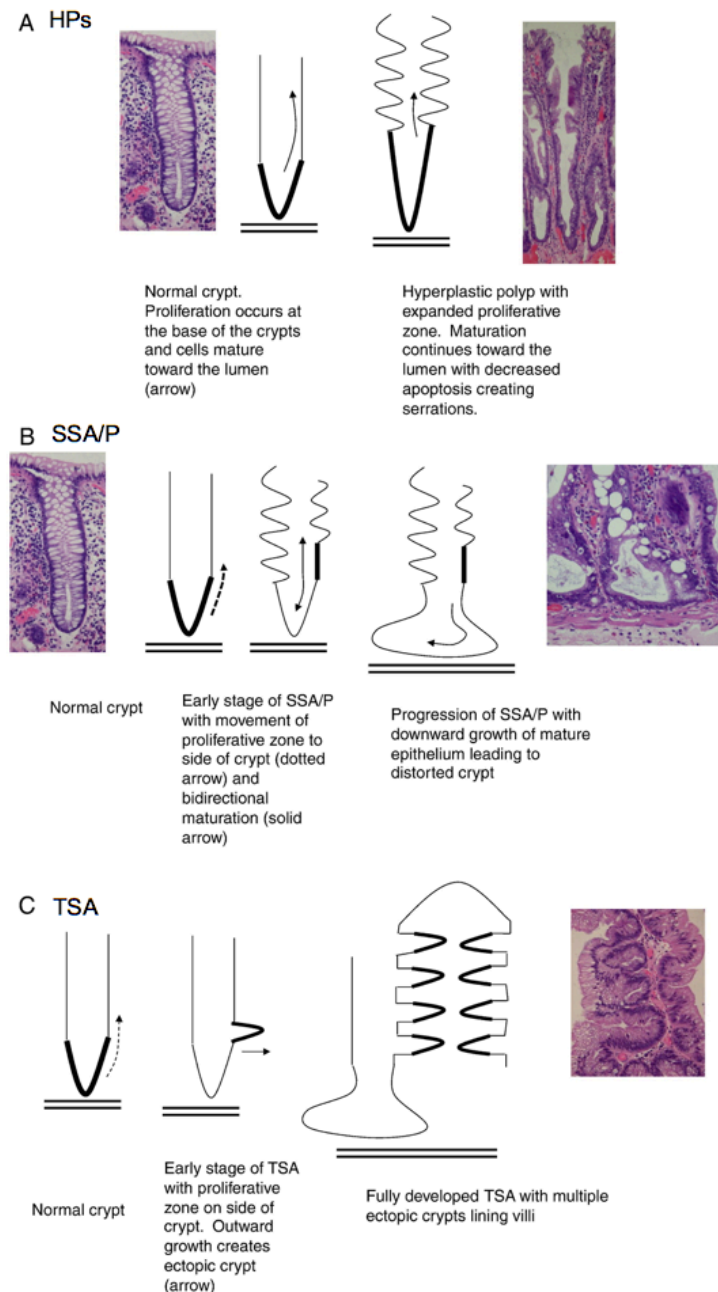


Figure 1.10 Illustration of underlying processes responsible for different subtypes of serrated adenoma appearance (Snover, 2011).

A) In HPs, the proliferative zone remains at the bottom of the crypt and proliferation direction remains toward the lumen area but, due to altered apoptotic rate, serrated structures appear.

B) In the case of SSA/P, the proliferative zone moves to the side of the crypt and because of bidirectional maturation and altered apoptosis rate, the formation of dilated L or inverted T structures occur.

C) In TSA, the proliferative zone moves to the side of the crypt, outward growth as well as muscle crypt detachment leads to formation of ectopic crypts.

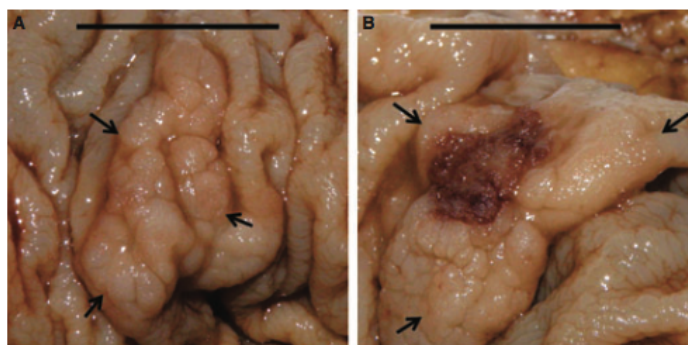


Figure 1.11 Sessile serrated adenoma (Amersi et al., 2005).

A) SSA showing pale and flat morphology, arrows are showing the edges of the lesion, which make it hard to detect in screening.

B) SSA showing early stage of carcinoma (dark brown). Arrows mark the edges of residual tumours.

1.3. Signalling pathways associated with colorectal cancer

1.3.1. Canonical WNT pathway

The WNT pathway is an evolutionarily conserved pathway involved in a wide range of crucial aspects of cell function, such as: cell fate determination, cell migration, organogenesis during embryonic development, and stem cell renewal (Komiya and Habas, 2008). Activation of the WNT pathway in homeostasis and renewal of the intestinal tissue is of utmost importance (Mah et al., 2016).

WNT signalling is subdivided into two subcategories: the canonical (β -catenin dependent) pathway and the non-canonical (β -catenin independent) pathway. The non-canonical pathway is further subdivided into the Planar Cell Polarity pathway and the WNT/ Ca^{2+} pathway (Komiya and Habas, 2008). WNT signalling deregulation is known to have catastrophic consequences for embryonic development and it is now known to be the cause of a number of human diseases such as cancer of the skin, breast, colon, skeletal muscle, ovary and human birth defects such as spina bifida (Komiya and Habas, 2008, Barker and Clevers, 2006). The canonical WNT pathway is known to be involved in colon cancer development. *APC* mutation in cancer was first described in 1991. It is a component of canonical WNT signalling and is altered in the human hereditary cancer Familial Adenomatous Polyposis (FAP). Most somatic colorectal cancer cases carry a homozygous mutation of *APC* which leads to stabilization of β -catenin and constant activation of its target genes (Clevers and Nusse, 2012). WNT proteins are 40kDa secreted cysteine-rich glycoproteins with many conserved cysteines, which are heavily modified prior to transport and comprised of 19 proteins in humans that act as short range ligands to locally activate receptor mediated signalling pathways (Komiya and Habas, 2008, Clevers and Nusse, 2012). The WNT canonical pathway is activated following interaction of WNT ligands with a heterodimeric receptor complex consisting of the Frizzled (Fz) and a single pass transmembrane LDL-receptor-related proteins 5 and 6 (LRP5/6), which leads to β -catenin stabilisation (Clevers and Nusse, 2012, Niehrs, 2012). The Fz family of seven pass transmembrane proteins are comprised of 10 members in humans and

contain an extracellular cysteine rich domain that interacts with WNT proteins (Niehrs, 2012, MacDonald et al., 2009). Following WNT protein interaction with the transmembrane receptor proteins, signal transduction leads to recruitment of the Dishevelled cytoplasmic proteins to the membrane. It is at this level that WNT signalling branches into three different sub-pathways mentioned below (Komiya and Habas, 2008).

1.3.1.1. WNT-Off state

In the absence of WNT, the cytoplasmic β -catenin protein is constantly degraded through a protein complex known as the β -catenin destruction complex (Axin complex), which is composed of several different proteins including scaffolding protein Axin, APC, casein kinase 1 (CK1) and glycogen synthase kinase 3 (GSK3) (MacDonald et al., 2009). CK1 phosphorylates β -catenin at serine 45 whereas GSK3 phosphorylates threonine 41, serine 37 and serine 33 at the N-terminal region (MacDonald et al., 2009, Beurel et al., 2015). Phosphorylated β -catenin is recognised by the Fbox/WD recognition site, of the β -Trcp subunit of the E3 ubiquitin ligase enzyme, which leads to β -catenin proteasome-mediated proteolytic degradation (MacDonald et al., 2009, Wu and Pan, 2010, Frame and Cohen, 2001, Clevers and Nusse, 2012). Proteosomal degradation of β -catenin prevents it from translocating into the nucleus (MacDonald et al., 2009, Zhan et al., 2017). In the absence of WNT signalling and subsequent lack of nuclear β -catenin, T cell factor (TCF) and Lymphoid Enhancing Factor -1 (LEF) transcription factors interact with repressor Grouchos - which in turn leads to repression of WNT target genes such as *c-Myc* and *cyclinD1* (Zhan et al., 2017, Klaus and Birchmeier, 2008) (Figure 1.12A).

There are two distinct groups of WNT antagonists; the Dickkopf (DKK) family and the Wise/SOST family in the extra-cellular matrix which inhibit WNTs through binding, preventing their interaction with Fz or LRP5/6 receptors (Komiya and Habas, 2008, MacDonald et al., 2009). DKKs are known to be the

specific antagonist of the WNT- β -catenin signalling pathway (MacDonald et al., 2009).

1.3.1.2. WNT-On state

Following WNT protein binding, to the Fz extracellular cysteine rich domain and co-receptor LRP5/6, hyper-phosphorylation of the Dishevelled (Dvl) proteins occurs. The cytoplasmic tail of Fz interacts with Dvl proteins. LRP5/6 phosphorylation as well as the formation of Dvl polymer serves as a trigger for the translocation of Axin to the plasma membrane (Klaus and Birchmeier, 2008). The LRP5/6 cytoplasmic association is through the phosphorylation of the LRP cytoplasmic domain by GSK3 and CK1 (Clevers and Nusse, 2012, Klaus and Birchmeier, 2008). Regulation of GSK3 by the WNT pathway does not occur through inhibitory phosphorylation of Serine 21/9 (Hey et al., 2016). Three theories are being considered as possible mechanisms of WNT pathway inhibition of GSK3. One is through spatial separation of GSK3 and β -catenin by uptake of GSK3 into multivesicular bodies. The second is that the phosphorylated cytoplasmic tail of LRP acts as a pseudosubstrate in the GSK3 catalytic pocket. Another mechanism is through formation of the destruction complex (Hey et al., 2016). These events lead to inactivation of the destruction complex (APC, Axin, GSK3 and CK1), allowing cytoplasmic accumulation and stabilization of β -catenin (Klaus and Birchmeier, 2008). Stabilized β -catenin enters the nucleus through an unknown mechanism. In the nucleus, β -catenin forms a transcriptionally active complex with two transcription factors, LEF and TCF, by replacing Grouchos. The activity of this complex depends on simultaneous interactions with other co-activators such as Pygopus, CREB-binding protein (CBP), BC19 and mediator (Klaus and Birchmeier, 2008, MacDonald et al., 2009). Many genes are named as downstream targets of the WNT pathway such as *E-cadherin*, *c-Myc*, *cyclinD1*, fibroblast growth factor (*FGF4*), vascular endothelial growth factor (*VEGF*) and many more (Klaus and Birchmeier, 2008) (Figure 1.12B).

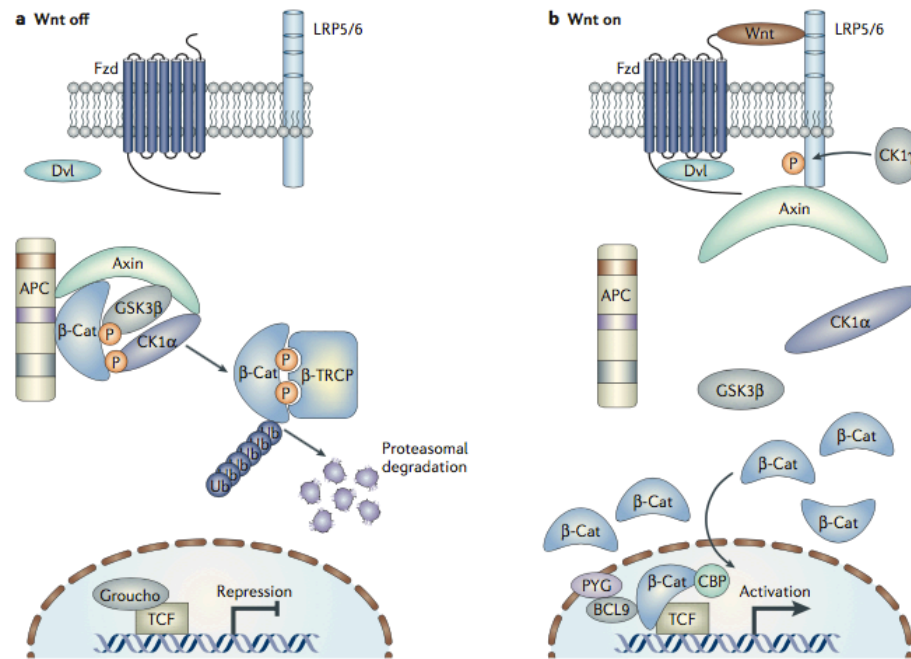


Figure 1.12 Schematic representation of the WNT canonical pathway (Barker and Clevers, 2006). There are two pools of β -catenin present in the cell; one is associated with cadherins in cell junction and the other is involved in the WNT signalling pathway.

A) In the absence of WNT ligands, the β -catenin destruction complex, composed of APC, Axin, GSK3 and CK1, phosphorylates β -catenin on several residues on the N-terminal tail which makes it a target for proteasomal degradation. Therefore β -catenin levels remain low.

B) In the presence of WNT ligands, binding of WNT proteins to Fz and LRP5/6 transmembrane proteins lead to inactivation of the destruction complex as a result of Axin, GSK3 and CK1 binding to the LRP5/6 cytoplasmic tail. Therefore β -catenin translocates into the nucleus through an unknown mechanism and replaces repressor proteins, Grouchos which are otherwise associated with TCF/LEF transcription factors. β -catenin binds TCF/LEF through its central arm repeat and at the same time binds other transcriptional co-activators such as BCL9, through its amino terminal arm repeat, Pygopus, mediator and CBP through its carboxyl terminal region. This association with other proteins leads to upregulation of its target genes such as *cyclinD1* and *c-Myc*.

1.3.1.3. Glycogen synthase kinase 3

Glycogen synthase kinase 3 also known as GSK3 was discovered in 1980 as a kinase which activates the ATP–Mg-dependent form of type-1 protein phosphatase “Factor A” and to phosphorylate the key metabolic enzyme in the last step of glycogen synthesis, glycogen synthase (GS) (Kaidanovich-Beilin and Woodgett, 2011, Takahashi-Yanaga, 2013). GSK3 is a highly conserved serine/threonine protein kinase encoded by two genes in human/mouse and is involved in many disorders such as inflammatory conditions, neurological disorders (Alzheimer’s disease, schizophrenia, mood disorder, bipolar disorder, Parkinson’s), cancer (gastrointestinal, liver, pancreatic and glioblastomas) and metabolic disorders (diabetes, atherosclerosis) through its involvement in multiple signalling pathways (Medina and Wandosell, 2011, McCubrey et al., 2014). GSK3 is known to participate in multiple signalling pathways such as WNT, Notch, Hedgehog (Hh), insulin and phosphatidylinositol 3’ kinase (PI3K) pathways (Figure 1.13) (Kaidanovich-Beilin and Woodgett, 2011). Two GSK3 isoforms are reported in mammals, a 51kDa variant called GSK3 α (483 amino acid in human) and a 47kDa variant known as GSK3 β (433 amino acid) (Figure 1.14). Expression of the two isoforms is universal and the kinase is expressed at high level in all types of brain cells (Perez-Costas et al., 2010). In certain type of brain cells, alternative splicing of the exon 8 and 9 of the GSK3 β generates a 13 amino acid extension insert within the catalytic domain of the kinase known as GSK3 β 2 (Hanks and Hunter, 1995). GSK3 α has a glycine-rich extension at its N-terminal end which is proposed to act as a pseudo-substrate (Dajani et al., 2001). Both isoforms share 85% overall homology which includes a 98% amino acid similarity in their kinase domain. Despite all the similarities, products of the genes just show 36% identity at their C-terminal end (Doble and Woodgett, 2003). The two isoforms do not have identical functions as embryonic loss of GSK3 β is proven to be fatal due to a high level of hepatic apoptosis and GSK3 α cannot compensate for β isoform loss (Doble and Woodgett, 2003).

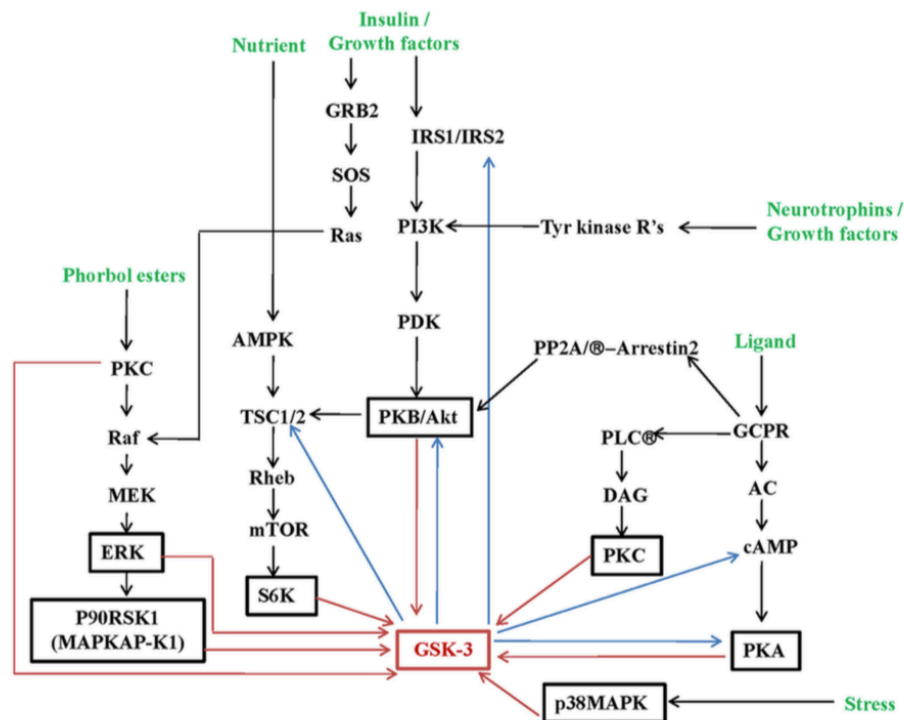


Figure 1.13 Schematic diagram of GSK3 involvement in different signalling pathways (Kaidanovich-Beilin and Woodgett, 2011). The above diagram shows the overall picture of GSK3's involvement in different cellular functions. Signalling pathways (black colour) are involved in regulation of GSK3 in response to various stimuli (green). Red arrows indicate proteins that can regulate GSK3 either by activation of protein kinases that can act on the N-terminal domain of GSK3 or through phosphatase-1 regulators. Studies have indicated that GSK3 can affect expression of some proteins through a feedback regulation mechanism shown in blue arrows. Pathways shown in black colour are the ones involved Dysregulation of GSK3 is reported to be the cause of many human pathological conditions.

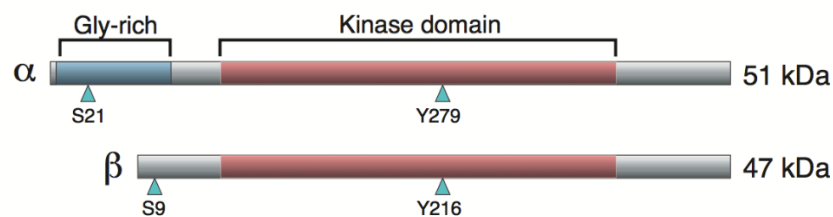


Figure 1.14 Schematic diagram of the two isoforms of Glycogen Synthase Kinase 3 (GSK3) (Doble and Woodgett, 2003). GSK3 α/β isoforms show 98% similarity in the kinase domains but have just 36% homology in their C-terminal ends. GSK3 α is a 51kDa protein whereas GSK3 β is 47kDa. The size difference is due to the presence of a glycine-rich stretch in the N-terminal end of the α isoform.

The regulation mechanism of GSK3 is very complex and not fully understood but it appears to be a combination of phosphorylation, sequestration and sub-cellular localization (Medina and Wandosell, 2011). Phosphorylation inactivation of GSK3 occurs following phosphorylation of serine and 21 residues of the N terminus of GSK3 α and GSK3 β respectively (Beurel et al., 2015). In the insulin pathway, insulin activates glycogen synthase through dephosphorylation of the C-terminal residues (Ser641, Ser645, Ser649, and Ser651) which is otherwise phosphorylated by GSK3. In muscle tissue, insulin inactivates GSK3 by phosphorylation of Ser21/9 of GSK3 α/β with the help of AKT (PKB) (McManus et al., 2005). GSK3 substrates need to be primed to be able to bind to and get phosphorylated by the kinase. Primed substrate is defined as a substrate which is previously phosphorylated by another protein kinase at its serine/threonine residue (Cohen and Frame, 2001). Phosphorylated substrates that have the priming phosphate then bind to the priming phosphate site on GSK3. GSK3 can then phosphorylate serine/threonine residues located four residues on N-terminal side of the priming phosphate (active form of GSK3). In the inactive state, GSK3 phosphorylated serine 21/9 acts as a pseudo-substrate (Beurel et al., 2015). The phosphate group at serine 21/9 on the N-terminal tail of the GSK3 α/β isoform occupies the priming phosphate site of GSK3 following N-terminal tail folding. Therefore the substrate cannot bind to GSK3 (Cohen and Frame, 2001).

A number of kinases have been identified to be involved in phosphorylation of serine 9 of GSK3 β such as AKT, p90 ribosomal S6 kinase (p90^{RSK}), p70/p85 ribosomal S6 kinase (p70^{S6K}/p85^{S6K}) and protein kinase B (PKB) (Figure 1.15) (McCubrey et al., 2014). Additionally, GSK3 α and GSK3 β activities can be controlled by phosphorylation of tyrosine (Y) 279 and Y216 respectively which was suggested to be an auto-phosphorylation event which increases the kinase catalytic activity (McCubrey et al., 2014, COLE et al., 2004, Pandey and DeGrado, 2016). GSK3 has been found in the mitochondria, cytoplasm and nucleus. In the nucleus, it is involved in regulation of its substrates such as cyclin-D1, β -catenin and HSF1, with possible involvement in alternative splicing (Cohen and Frame, 2001, Medina and Wandosell, 2011).

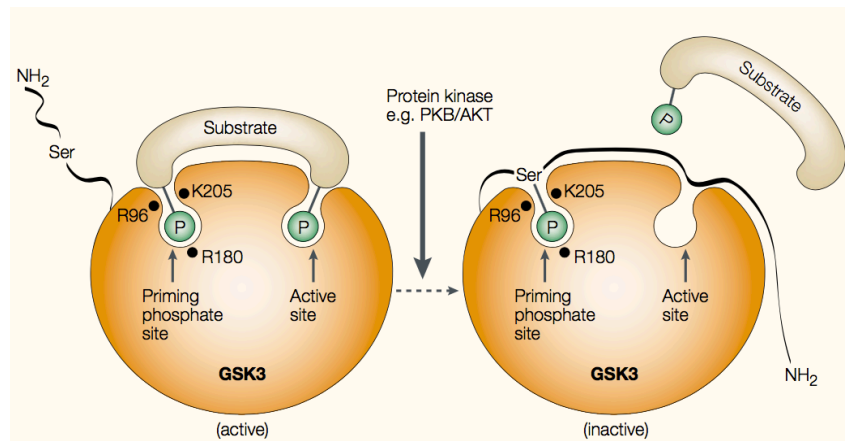


Figure 1.15 Schematic diagram of GSK3 phosphorylation inhibition mechanism (Cohen and Frame, 2001). In the active state, primed substrate binds to the priming phosphate site and then it can be phosphorylated by the active site of GSK3. In the inactive state, the phosphorylated N terminal tail of GSK3 α/β (serine 21/9) folds back and occupies the priming phosphate site. Therefore, primed substrate cannot bind to GSK3 preoccupied priming phosphate site.

1.3.2. MAPK-ERK signalling pathway

Mitogen-activated protein kinase (MAPK) pathways are sophisticated evolutionarily conserved pathways which receive extracellular signals and translate them into a wide range of cellular responses, including: cell proliferation, differentiation, survival, motility, metabolism and apoptosis (Roberts and Der, 2007, Dhillon et al., 2007). MAPK pathways all consist of three-tiered kinases; MAPKKK, MAPKK, MAPK (Dhillon et al., 2007). There are four major MAPK pathways; the ERK5, p38 and JNK pathways are activated in response to cellular stress condition such as osmotic shock and radiation, whereas the ERK pathway activation is in response to growth factors (Figure 1.16) (Zhang and Liu, 2002, Roberts and Der, 2007). The ERK pathway is subjected to the most intensive studies and is reported to be deregulated in one-third of human cancer cases (Dhillon et al., 2007). The first genetic alterations are reported to occur in serrated colorectal cancers are *KRAS* or *BRAF* which are upstream regulators of the ERK signalling pathway (Mäkinen, 2007).

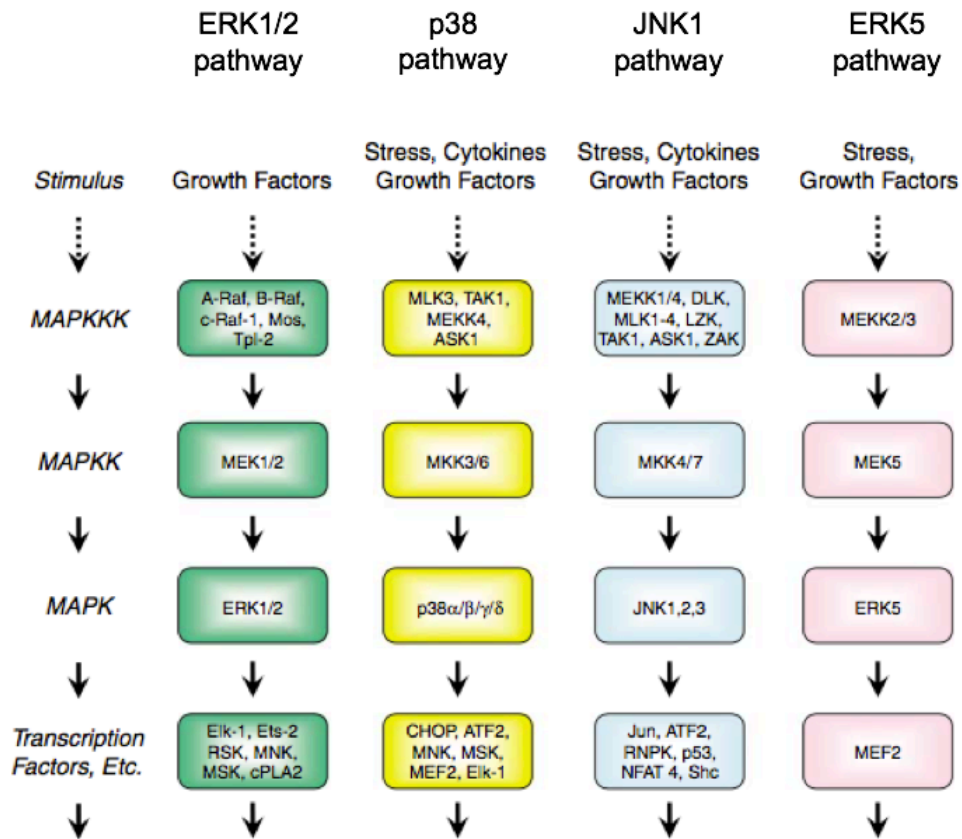


Figure 1.16 Schematic diagram of 4 major MAPK pathways in mammalian cells (Roberts and Der, 2007). The most advanced studies of MAPK pathways have been undertaken for the ERK pathway, which is activated as the result of growth factor stimulation on recipient cells whereas the P38, JNK, and ERK5 pathways respond to cellular stress conditions such as radiation, osmotic shock, inflammation, etc. Each MAPK pathway is comprised of 3 groups of kinases; MAPKKKs which are activated upon engagement of growth factors and the cell surface receptors. Once activated, it phosphorylates the downstream kinase known as MAPKK which is activated and in turn phosphorylates its downstream kinase MAPK. Phosphorylated MAPK transfers into the nucleus generating a cellular response(s).

The ERK pathway is activated once extracellular growth factor (GF) binds to its cognate receptor tyrosine kinases (RTK) on the cell surface. Different types of growth factors can bind and activate RTKs, such as epidermal growth factors (EGF), insulin, and platelet-derived growth factors (PDGF) (Margolis and Skolnik, 1994). GF binding to RTK leads to autophosphorylation of multiple tyrosine sites on the receptor cytoplasmic domain (Zhang and Liu, 2002, Pearson et al., 2001, Margolis and Skolnik, 1994). Signalling proteins, with Src homology 2 domain (SH2), then bind to phosphorylated tyrosine residues on the receptor cytosolic site; one of which is the GRB2 protein which is in complex with the Son of Sevenless (SOS) protein. The GRB2 and SOS protein complex translocates to the cell membrane following the activation of RTKs and only then can activate inactive RAS-GDP bound protein by catalysing its GDP exchange with GTP (Margolis and Skolnik, 1994). The SOS protein is a guanine nucleotide exchange factor (GEF) that can facilitate RAS activation once located in the proximity of the RAS-GDP protein by relocating it to the cell membrane (Margolis and Skolnik, 1994, Pearson et al., 2001).

RAS proteins are reported to exist in three different isoforms in humans; N-RAS, H-RAS, and K-RAS (Dhillon et al., 2007, McCain, 2013). Some publications have categorised human RAS proteins into four categories: N-RAS, H-RAS, K-RASA, and K-RASB (Wellbrock et al., 2004, Mercer and Pritchard, 2003). RAS mutations are reported in ~15% of human cancer cases (Wellbrock et al., 2004).

Following conversion of RAS to RAS-GTP it can recruit the downstream serine/threonine protein kinase, RAF, to the plasma membrane where it is activated by phosphorylation (Dhillon et al., 2007, Roberts and Der, 2007). Under no-signalling conditions, RAF proteins usually are present in the cytosol. Once RAS is activated, RAF is recruited to the cell membrane by binding to the RAS-GTP protein complex (Dhillon et al., 2007). Active RAS-GTP can bind to the RAS-binding domain (RBD) of RAF at the N-terminus region and at the same time can also interact with the cysteine-rich domain (CRD) of the CR1 of RAF, and the latter is GTP independent. This association results in RAF

conformational change and its subsequent phosphorylation (Wellbrock et al., 2004). Two of the most important phosphorylation sites are T598 and S601 within the activation segment of the kinase domain of RAF (Wellbrock et al., 2004, Garnett and Marais, 2004). More recently, it has been proposed that upon activation of RAS, a network of interacting kinases consisting of members of RAF and KSR families forms, which is a key player in RAS-ERK signalling transduction. The RAF and KSR network complex are affected by activated RAS as well as protein-protein interactions and phosphorylation-dephosphorylation events (Lavoie and Therrien, 2015) (Figure 1.17).

There are three different isoforms of RAF proteins in human: A-RAF, B-RAF, and C-RAF (RAF-1) (Wellbrock et al., 2004, Garnett and Marais, 2004). RAF protein function is regulated by different types of proteins, such as HSP90 and a dimeric adaptor/scaffolding protein known as 14-3-3 (Roberts and Der, 2007, Pearson et al., 2001, McCubrey et al., 2007, Wellbrock et al., 2004). 14-3-3 binding to the CR2 region of RAF can be disrupted following phosphorylation of S259 by RAS-GTP (Wellbrock et al., 2004). The phosphorylated, active form of RAF, then activates the downstream dual specificity protein kinase, MEK1/2 by phosphorylation of the serines 218 and 222 in the activation loop of MEK (Roberts and Der, 2007, Dhillon et al., 2007). It has been reported that different RAF isoforms display different abilities for phosphorylation of MEK 1/2. A-RAF is known to be the weakest of the RAF proteins, but still can activate MEK1, whereas B-RAF is the strongest due to constant negative charge in the N region which then in turn phosphorylates both MEKs very strongly either directly or through its ability to activate C-RAF. C-RAF can activate both MEK proteins with similar efficiency (Dhillon et al., 2007, Wellbrock et al., 2004).

Once activated, MEK1/2s can phosphorylate and activate its downstream target MAPK, also known as extracellular signal regulated kinases 1/2 (ERK1/2), on threonine and tyrosine residues within their activation segments (Figure 1.17). ERK1 and ERK2 are proteins of 43 and 41 kDa size respectively showing ~85% homology (Pearson et al., 2001, Roberts and Der, 2007). p44 ERK1 and p42 ERK2 proteins can trigger a wide range of cellular responses with most substrates being in the nuclear region but also some are reported to be in the

cytoplasm (Roberts and Der, 2007). ERK1/2 can activate transcription factors, such as c-Jun, c-Myc, and Ets-1. They can also phosphorylate and activate cytoplasmic proteins such as 90kDa ribosomal S6 kinase protein (p90^{RSK}), microtubules-associated protein (MAP), and cytosolic phospholipase A2 (McCubrey et al., 2007, Dhillon et al., 2007, Pearson et al., 2001). RSK is reported to be associated with cell cycle regulation by triggering a series of events which leads to activation of the cyclin dependent kinase p34^{cdc2} (Dhillon et al., 2007). ERK substrate phosphorylation is known to be proline-directed, meaning that activated ERK phosphorylates serine and threonine residues on substrates when they are followed by a proline at the P1 position. In the case of ERK1/2 the presence of proline at the P2 position is also reported in some cases, with the consensus motif being PX(T/S)P (Pearson et al., 2001).

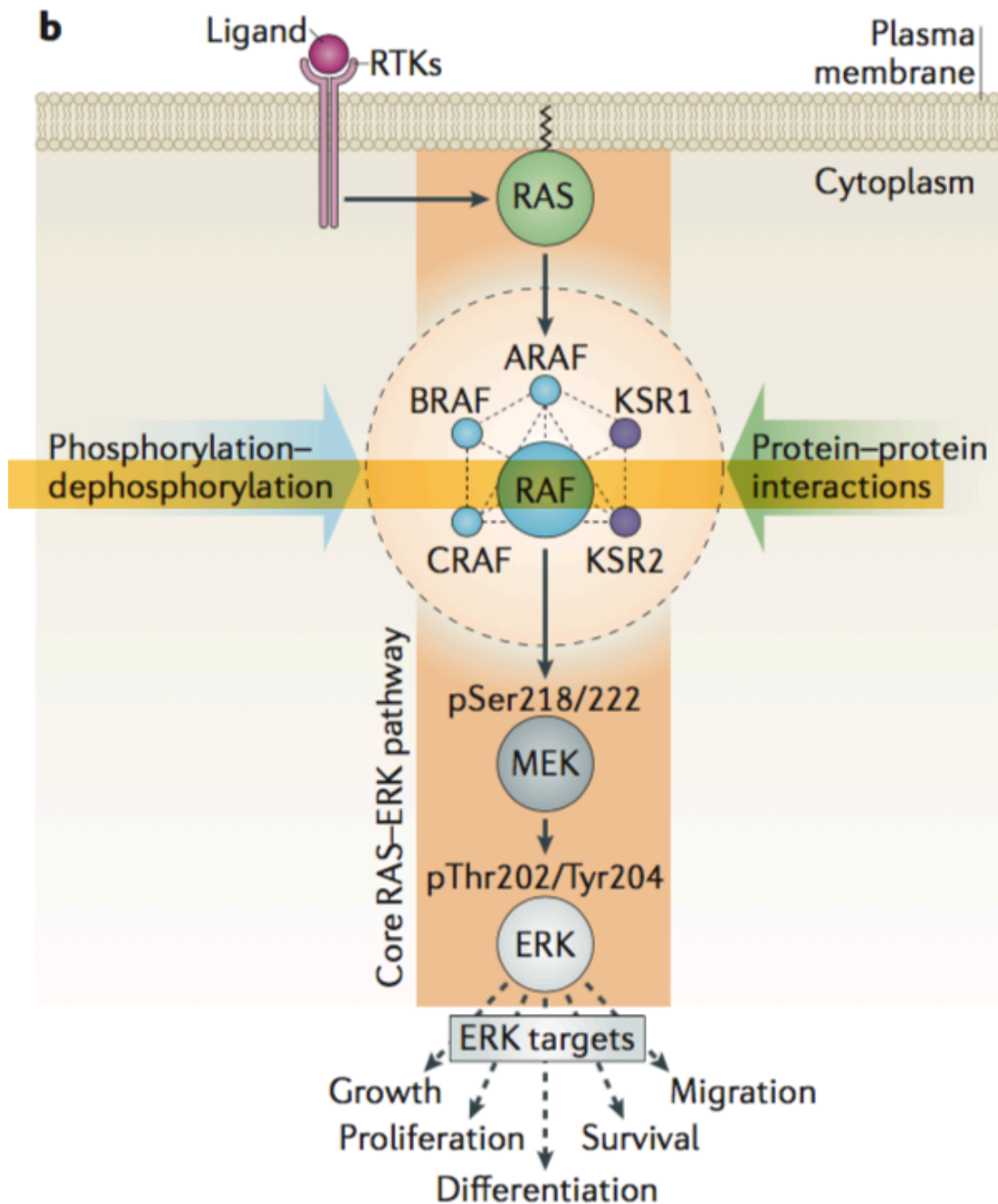


Figure 1.17 Simplified schematic diagram of the ERK-MAPK signalling pathway (Lavoie and Therrien, 2015). Growth factors bind to and activate receptor tyrosine kinases (RTKs) on the outer surface of the plasma membrane, which in turn activates RAS which is bound to the inner-plasma membrane through a series of events including adaptor proteins and activators. Activated RAS proteins in their GTP bound form bind to and recruit RAF proteins from the cytosol to the plasma membrane where they are activated. Activated membrane-bound RAF phosphorylates and activates MEK which in turn can again phosphorylate and activate ERKs. Activated ERKs can target cytosolic proteins and phosphorylate them as well as translocating into the nucleus where they can phosphorylate various transcription factors. Mutated forms of RTK, RAS, and RAF proteins are reported in human cancers.

1.3.2.1. RAF protein kinases and their roles in cancer

Raf genes were initially described as oncogenes in retrovirus that induced tumours in mice and chickens (Mercer et al., 2005, Mercer and Pritchard, 2003). As stated previously there are three human RAF isoforms, ARAF, BRAF and CRAF (RAF-1) (Wellbrock et al., 2004, Garnett and Marais, 2004). Structurally, RAF proteins share three conserved regions, CR1, CR2 which are regulatory regions in the N terminus, and CR3 which is the kinase domain in the C terminus (Garnett and Marais, 2004, Mercer and Pritchard, 2003, Wellbrock et al., 2004). CR1 carries two domains; the RAS binding domain (RBD) and cysteine-rich domain (CRD) that can bind two zinc ions and interacts with RAS-GTP as well as membrane phospholipids. CR2 is a serine/threonine rich region which contains a site that can bind to inhibitory protein 14-3-3 once phosphorylated (Roskoski, 2010, Wellbrock et al., 2004). CR3 is the kinase domain located near the C-terminus region (Figure 1.18) (Roskoski, 2010).

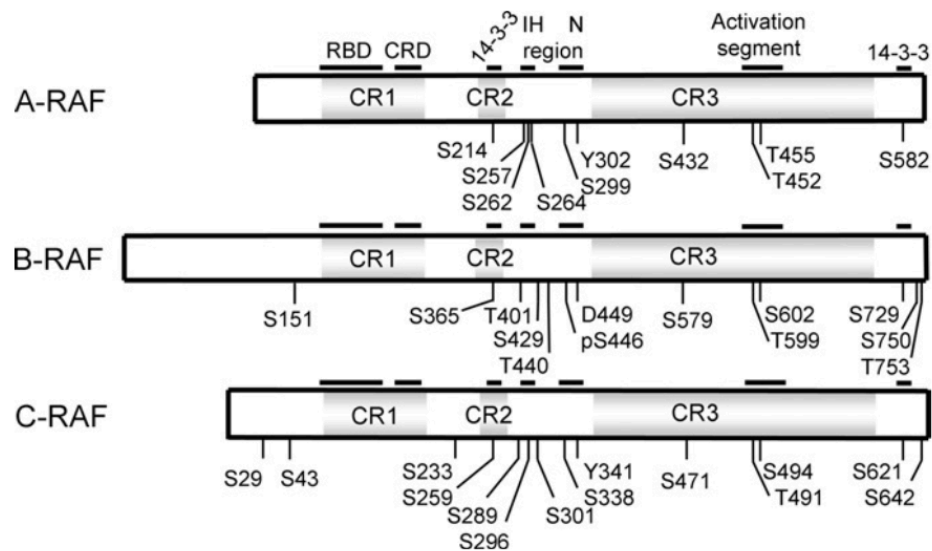


Figure 1.18 Schematic diagram of RAF family protein kinases domain structure (Roskoski, 2010). RAF protein kinases have three conserved regions; CR1, CR2, and CR3 but at the same time there are differences which make regulation of each of them a unique process. The CR1 region consists of the RAS binding domain (RBD) and cysteine-rich domain (CRD). The CR2 domain contains a site which binds 14-3-3 upon phosphorylation. There is an additional 14-3-3 binding site located after the kinase domain (CR3) near the C-terminus of the protein.

Despite their similarities, RAF kinases have parts which are unique to each one of them. RAF proteins are of different sizes, ARAF is the smallest of approximately 68kDa, C-RAF is ~72-74 kDa. BRAF, however, is the biggest of RAF kinases and is subjected to differential splicing. Therefore its size can vary between 75-100 kDa (Wellbrock et al., 2004). The *BRAF* gene is detected in 10 different isoforms which is the direct result of variable splicing of exons 8b and 10a (Barnier et al., 1995). Looking at the structure of RAF kinases they are composed of a small N-terminal lobe and a large C-terminal and a catalytic cleft (Roskoski, 2010, Garnett and Marais, 2004). The small lobe mostly consists of antiparallel β -sheets and contains an ATP-phosphate binding loop (P-loop). The large lobe is mostly α -helical and is responsible for MEK1/2 binding (Roskoski, 2010). The α -helix structure of the small lobe (N-lobe) is known as α C-helix and is responsible for side-to-side dimerization of the RAF protein kinases (Figure 1.19) (Lavoie and Therrien, 2015). It was shown that RAF dimerization is an important event in regulation of RAF activation. BRAF and CRAF form a heterodimer in which BRAF Arg509 plays a crucial role in the side-to-side hydrogen bond formation between the two kinases which in turn can trans-activate CRAF (Lavoie and Therrien, 2015). The activation segment, which is part of the C-lobe, starts with the Asp/Phe/Gly (DFG) sequence. In the inactive state, the Phe side chain engages the ATP binding site and the Asp side chain falls away from the active site. This phenomenon is called the “DFG Asp-Out” conformation (Lavoie and Therrien, 2015, Roskoski, 2010). The kinase active state is defined by the closed conformation in which the Phe side chain is moved out of the ATP binding site and Asp faces into the binding pocket for ATP. This is called the “DFG Asp-In” conformation (Roskoski, 2010).

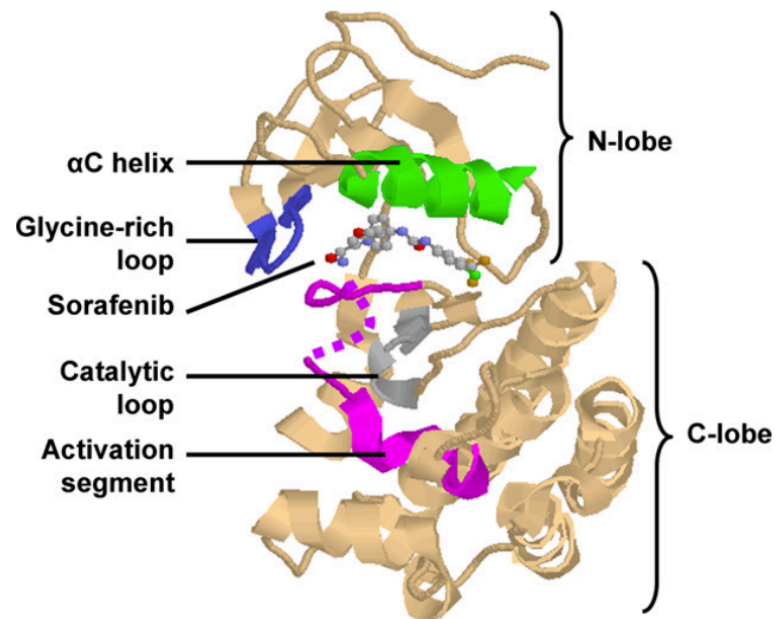


Figure 1.19 Structure of BRAF kinase domain in humans (Roskoski, 2010). The protein consists of the three main structures: the N-lobe which is the small lobe and mostly comprises antiparallel β -sheets, the C-lobe which is known as the large lobe and is mostly α -helical structures, and a catalytic lobe located in between the small and large lobes. The α C-helix, which is part of the N-lobe is crucial in kinase side-to-side dimerization.

Different *BRAF* mutations have been reported in human cancers whereas *ARAF* and *CRAF* mutations are very rare. An explanation for this is the 15-20 times higher levels of BRAF basal kinase activity compared to its CRAF counterpart (Mercer and Pritchard, 2003). *ARAF* and *CRAF* require phosphorylation, of some of the residues on their N-region by Src, in addition to binding with activated RAS for their activation; whereas in *BRAF*, RAS-GTP binding is enough for *BRAF* activation due to the constant phosphorylation of the serine 445 in its N region, which gives it a high level of negative charge (Rahman et al., 2013, Wellbrock et al., 2004). More than 65 missense mutations concerning 24 different codons, have been identified in the human *BRAF* gene in human cancers (Rahman et al., 2013). Most of the *BRAF* mutations have been detected in codons 11 and 15 of the catalytic kinase domain (Rahman et al., 2013). The highest frequency of *BRAF* mutation is reported in malignant melanoma (27-70%), papillary thyroid cancer (36-53%), colorectal cancer (5-22%), ~30% of ovarian cancer and 1-3% of other cancer cases at valine 600 of the protein (Garnett and Marais, 2004, Wellbrock et al., 2004). Human *BRAF* mutations that have been reported are detected within the activation loop, ATP-binding stretch of the kinase domain and some are detected outside of these two domains (Mercer and Pritchard, 2003). The most active mutant of *BRAF*, which accounts for ~90% of human *BRAF* mutations, is the substitution of valine to glutamic acid at the position 600 of the protein which represents a single nucleotide change (A-T) at position 1799 (exon 15) of the gene (Figure 1.20). This mutation increases the kinase activity of BRAF by 500 fold in comparison to the wild type gene (Wan et al., 2004). The V600E mutant of BRAF disrupts the interaction of the P-loop and activation loop, resulting in constant activation of the kinase which is resistant to dimer interface disruption. The ^{V600E}BRAF mutant forms a homodimer when its RAS binding is impaired (Cseh et al., 2014). In some of the *BRAF* mutations such as G466E, G466V and G596R, kinase activity is impaired. Therefore for mutated BRAF to be able to activate the MEK-ERK signalling pathway it is crucial to form a heterodimer with wild type CRAF protein - trans-activating it (Rahman et al., 2013).

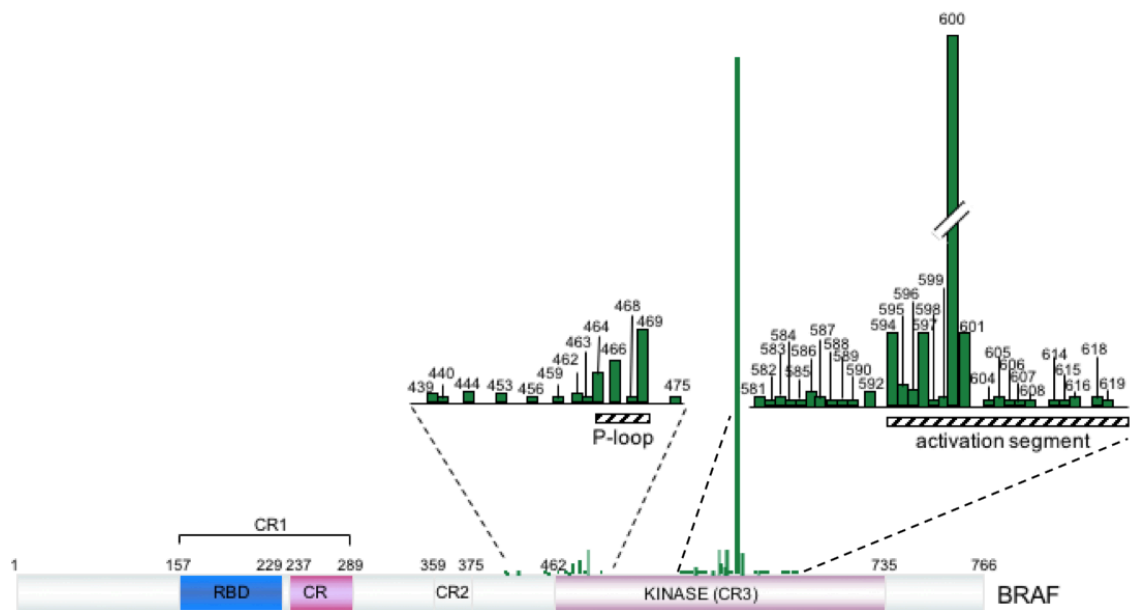


Figure 1.20 BRAF mutations in human cancers. Most of the mutations detected in the BRAF gene are in the P-loop as well as the activation segment of the kinase domain. More than 62 mutations have been detected in the human BRAF protein with V600E being the most frequent one, accounting for ~90% of human BRAF mutations. Substitution of valine to glutamic acid at position 600 of the protein corresponds to a single missense mutation of A-T at position 1799 of the gene which is located in exon 15. The V600E mutant version of the BRAF protein is detected in ~70% of malignant melanomas, 46% of papillary thyroid cancer, 41% of serous ovarian cancer and ~13% of colon cancer cases.

1.3.3. Senescence

Senescence is a cellular response to different types of stress signals, such as: telomere uncapping, DNA damage, oncogenic activation in particular RAS and its downstream effectors, and oxidative stress (Ben-Porath and Weinberg, 2005). Generally, senescent cells are irreversibly halted in the G0/G1 phase of the cell cycle and display particular characteristics such as sustained metabolic activity as well as unresponsiveness to growth factors, overexpression of senescence-associated β -galactosidase (SA- β -gal), dramatic changes to chromatin structure, and the inability to synthesise DNA. They also display some morphological changes such as an enlarged and flat appearance (Kong et al., 2011, Ben-Porath and Weinberg, 2005). Senescence happens either after a period of sustained cellular proliferation, known as replicative senescence/Hayflick limit, or in a premature way in response to stress signals. The latter is regarded as stress-induced premature senescence (Ben-Porath and Weinberg, 2005, Qian and Chen, 2010).

Replicative senescence occurs as result of telomere shortening. Telomeres are hexameric tandem repeats, located at the end of chromosomes, and shorten after each cell division due to a phenomenon known as the “end-replication problem”; this is the result of the inefficiency of DNA polymerase enzyme to replicate DNA at its very ends (Campisi, 2013). Two tumour suppressor pathways, p53/p21 and p16^{INK4a}/Rb, are known to play a critical role in generation of a cellular senescence response. Following telomerase shortening, once the length reaches a critical level, a DNA damage response (DDR) is triggered (Kong et al., 2011). Ataxia telangiectasia mutated (ATM), a serine threonine protein kinase phosphorylates Check point kinase2 (Chk2) on serine 20, which leads to p53 dissociation from MDM2 (an E3 ubiquitin ligase) and its subsequent stabilization. In the absence of ATM, ATM and Rad3-related (ATR) can activate p53 through Chk1 by phosphorylation of its serine 15 (Qian and Chen, 2013). Stabilized p53 trans-activates p21^(CIP1/WAF1), a cyclin dependent kinase inhibitor which can in turn inhibit the phosphorylation induced inactivation of pRb by Cdk2 cell cycle kinase (Muñoz-Espín and Serrano, 2014). Hypo-phosphorylated activated forms of Rb bind to E2F protein family members and

inhibit the transcriptional activity of target genes (Figure 1.21) (Ben-Porath and Weinberg, 2005).

p16^{INK4a}, a CDK inhibitor, is encoded by the *INK4A* gene that can bind to CDK4/6 and inhibit its activity, which is particularly important for tumour suppression (Takahashi et al., 2007, Ohtani et al., 2004, Rayess et al., 2012). This event also results in repositioning of the Cip/Kip family of CDK inhibitors, p21^{Cip1/Waf1/Sdi1} and p27^{Kip1} from cyclinD-CDK4/6 to cyclinE-CDK2 and suppression of the CDK2 activity (Figure 1.21) (Takahashi et al., 2007). p16^{INK4a}-induced senescence pauses the cell cycle at the G1-phase which is an irreversible growth arrest (Ohtani et al., 2004, Takahashi et al., 2007).

Oncogene-induced senescence (OIS) was first described following discovery of RAS oncogenic mutation. OIS is a preventive mechanism which occurs in benign tumours and prevents progression of the benign lesion to malignant tumours (Courtois-Cox et al., 2008). Activation of the oncogenic signal leads to high levels of DNA damage (DDR) which activates tumour suppressor pathways such as p19^{ARF}/p53/p21 and p16^{INK4a}/pRb therefore triggering OIS in the affected cells (Ben-Porath and Weinberg, 2005, Qian and Chen, 2013, Seoane et al., 2017). It is reported that cells undergoing OIS have senescence associated DNA damage foci (SDF) and senescence associated heterochromatin foci (Di Micco et al., 2006). There is evidence suggesting in human cells that the p53/p21 and p16^{INK4a}/pRb senescent pathways act in parallel and in a redundant fashion, which serve as a safety measure against tumorigenesis compared to mouse cells which have the two pathways acting in a linear manner (Ben-Porath and Weinberg, 2005). Evidence suggests that, while the p53/p21 pathway acts to initiate senescence and decreases after several days, the p16^{INK4a}/pRb pathway seems to moderately increase and maintains the level of senescence response in cells at latter stages (Ben-Porath and Weinberg, 2005).

In human colon adenomas there is evidence of a correlation between p16^{INK4a} expression level and cell cycle arrest (Kuilman et al., 2010). In 2004, Ohtani et al. suggested that the p16^{INK4a} expression is controlled by Ets1/2 transcription

factors which are downstream of the MAPK pathway and can get phosphorylated by MAPK at specific points of the cell cycle (Ohtani et al., 2004, Rayess et al., 2012). In 2010 Carragher et al., using mouse model, showed that after initial hyperplastic period in serrated adenoma, $V600E$ BRaf induced OIS occurs which is characterised by an increase in senescence associated β -galactosidase (SA- β -gal) as well as p16^{INK4a} but not p53, p19^{Arf} or p21^{Cip1} (Carragher et al., 2010). Using human colon tissue, Kriegl et al., shown that inactivation of the p16^{INK4a} through methylation of the *CDKN2A* gene promoter is the starting point for malignant transformation of the serrated lesions (Kriegl et al., 2011). Similar observations were reported by Bennecke et al., using Villin-Cre mice, in 2010 regarding $G12D$ Kras serrated tumours, in which elevated level of SA- β -gal as well as increased p16^{INK4a} mRNA and protein were detected; however, no change was detected in p19^{Arf} or p53 mRNA or protein levels (Bennecke et al., 2010). It is worth mentioning that in the $G12D$ Kras serrated pathway, OIS was only detected in the colon tissue but not in the small intestine for a reason unknown (Bennecke et al., 2010).

The senescence-associated secretory phenotype (SASP) is an important characteristic of senescent cells and is responsible for aging associated pathologies of organisms. SASP induces a number of factors, such as chemokines, cytokines, proteases and growth factors, which trigger immune surveillance of the senescent cells (Campisi, 2013, Yosef et al., 2017). Among the SASP proteins are pro-inflammatory cytokines interleukin 6/8 (IL6/8) which are important in cellular senescence responses to oncogenic BRAF (Kuilman et al., 2010).

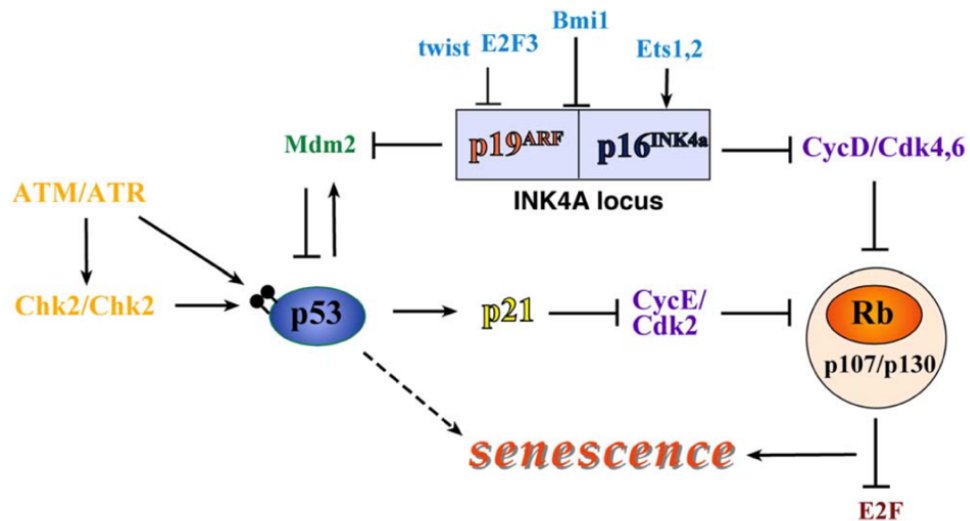


Figure 1.21 Schematic diagram of molecular pathways involved in cellular senescence (Ben-Porath and Weinberg, 2005). Two major tumour suppressor pathways p53/p21 and p16^{INK4a}/pRb play a crucial role in the senescence cellular response under various stress conditions. Under normal circumstances cells undergo senescence after a finite number of cell divisions, a phenomenon known as the Hayflick limit or replicative senescence. Replicative senescence is triggered once the telomere (hexameric tandem repeats at the end of chromosome) reaches a critical length which then is treated as DNA double strand break (DSB) and triggers p53 activation. Under stress conditions ATM/ATR kinases phosphorylate their downstream target proteins Chk1/Chk2 that leads to phosphorylation and stabilization of p53. Activated p53 can activate p21^(CIP1/WAF1), a cyclin dependent kinase inhibitor (CDKI) that can prevent Cdk2 from phosphorylating pRb. A second pathway that leads to irreversible cellular senescence is triggered by p16^{INK4a}, another CDKI that can bind to Cdk4/6 and inhibit their ability to phosphorylate the pRb protein. Hypo-phosphorylated Rb can then bind to E2F and prevent transcription of its target genes which are important in the G1/S transition of the cell cycle.

1.3.4. Other signalling pathways involved in intestinal homeostasis

Besides the pathways discussed above, other pathways such as Notch, Hedgehog, BMP, and Hippo are involved in intestinal homeostasis. Details of molecular mechanisms of these pathways, their involvement in intestinal homeostasis and role in disease development is beyond the scope of this project.

1.4. Inhibition of the RAF-MEK pathway

Because of the significant role that MAPK signalling pathway plays in human cancer development and progression, it has been an important target for drug development. Inhibitors have been predominantly developed against RAF and MEK.

Sorafenib was the first RAF inhibitor to be tested in clinical trials for melanoma patients. Sorafenib (Nexavar, Bayer) was well tolerated but showed no antitumor activity. It was shown, that sorafenib is a non-specific inhibitor of kinases such as RAF, both wild type and mutated, as well as receptor tyrosine kinases such as platelet derived growth factor (PDGF) and vascular-endothelial growth factor (VEGF) receptor 2, which may affect its efficacy in melanoma (Dhillon et al., 2007, McCain, 2013). Vemurafenib (PLX4032) is a new generation of RAF inhibitors which is highly selective towards the ^{V600E}BRAF mutant and was first synthesized in 2005 (Cseh et al., 2014). This compound is a small molecule, ATP-competitive, inhibitor that has high affinity to bind to the activation loop in the “DFG-in conformation” which is stabilized by the V600E mutation as a result of the bridge formation between Glu600 and Lys507 (Bollag et al., 2012).

Vemurafenib is a BRAF inhibitor which was approved in 2011 by the Food and Drug Administration (FDA) and later in 2012 by European Medicine Evaluation Agency (EMA) for treatment of metastatic melanoma, with proven effectiveness in V600E mutated melanoma, but generated a very poor response in colorectal cancer patient bearing the ^{V600E}BRAF mutation (Clarke and Kopetz, 2015). In 2012, Prahalled et al. reported that the poor patient response to PLX4032 in ^{V600E}BRAF CRC patients was the direct result of ERK-mediated feedback activation which in turn activates the EGFR receptor (Prahallad et al., 2012). In 2014 Sun et al. treated a fraction of patients with vemurafenib and showed they acquired resistance, which can be reversed by a period of drug holiday, which suggests an adaptive and reversible of drug resistance (Sun et al., 2014). In 2013, Mao et al. suggested an inhibitor combination of PLX4720 with a PI3K inhibitor could be used to overcome the primary and secondary resistance (Mao et al., 2013).

In a phase 3 trial, Dabrafenib (GSK2118436, Tafinlar), an ATP competitive inhibitor of BRAF, was also proven to be effective for treatment of metastatic melanoma (McCain, 2013). Dabrafenib was approved in 2014, for treatment of metastatic melanoma with $V600E$ BRAF mutation in combination with trametinib and in 2017 in combination with trametinib for metastatic non-small cell lung cancer (NSCLC) with $V600E$ BRAF mutation by FDA.

For inhibition of MEK1/2 kinases, a large number of potential inhibitors have been developed. PD98059 and U0126 are amongst the first generation of MEK1/2 inhibitors which were developed. PD98059 by D.T. Dudley et al. (Dudley et al., 1995) and U0126 by M. Favata et al. (Favata et al., 1998) are synthetic small molecule inhibitors that are ERK1/2 and ATP non-competitive. These inhibitors are valuable tools for research. They show low potency and off target effects, they therefore have never been used in clinical trials (Wu and Park, 2015). CI-1040 (PD184352) is a second generation MEK1/2 inhibitor which was developed in 1999. This molecule is a Mg-ATP and ERK1/2 non-competitive allosteric inhibitor, the first of this category to be tested in a clinical trial (Pearson et al., 2001, Wu and Park, 2015). Currently, trametinib also known as GSK1120212 is the only FDA approved MEK1/2 inhibitor. In 2014 trametinib, was approved by the FDA for use in a combination therapy with dabrafenib for the treatment of BRAF mutant melanoma (McCain, 2013, Wu and Park, 2015). Trametinib along with CH5126766 and GDC-0623 are among a newer generation of MEK1/2 inhibitors that can effectively inhibit the negative feedback loop, which results in reduced phosphorylation of MEKs by RAF (Caunt et al., 2015). AZD6244 (ARRY-142886) is also a potent orally bioavailable MEK1/2 inhibitor. AZD6244 shows anti-tumour activity in several human xenograft models such as NSCLC, colon, and melanoma; it is currently being evaluated in several phase II trials (Roberts and Der, 2007). Cobimetinib (GDC-0973/XL518/RG7421) is another, ATP-non-competitive, allosteric inhibitor of MEK1/2 with low potency toward RAS mutant tumour cells (Wu and Park, 2015). In November 2015, the FDA approved another MEK1/2 inhibitor known as cobimetinib (cotelllic), to be used in combination with vemurafenib (zelboraf), in the treatment of $V600E$ BRAF metastatic melanoma (Boespflug and

Thomas, 2016).

Several monoclonal antibodies (mAbs) have been developed against the extracellular domain of the EGFR receptor which vary in the recognition sequence and their binding affinity. The first that was approved by the FDA was Cetuximab (Erbix, Bristol-Myers Squibb and ImClone Systems), a chimeric IgG1 monoclonal antibody, which targets the EGFR extracellular domain (Gerber and Choy, 2010). Cetuximab was approved for monotherapy as well as in combination with traditional chemotherapy agents such as irinotecan, oxaliplatin and 5-fluorouracil for treatment of EGFR-detectable CRC patients (Roberts and Der, 2007, Jonker et al., 2007, Wen and Li, 2016). Cetuximab in combination with chemotherapy, was shown to improve anti-tumour activity and downstaging of unresectable tumours for the first line treatment of CRC patient with ^{WT}*KRAS* - as patients with mutated *KRAS* seem to resist EGFR inhibition (Gomez et al., 2013, Gerber and Choy, 2010).

1.5. Mouse models of colorectal cancer

Colorectal cancer is a very complicated type of cancer in which more than one mutation is responsible for disease initiation, progression and invasion. Moreover, CRC is affected by several different factors including environment, diet and other mutations in each individual. All of these characteristics make it a challenge for scientists to study the underlying mechanism of this vast and complicated type of cancer. Another challenging area is that, once the symptoms of CRC are obvious enough for the patient to go to the doctor, the disease is usually at its more advanced stages and it is difficult to study the initiation stages of the disease from tissue which is removed from patients. Although the use of human colorectal cell lines is important, the common use of cells has its own flaws; they often behave quite differently *in vitro* for multiple reasons such as gain of additional mutations due to prolonged laboratory use, which causes changes in the characteristics of cells. Therefore, there is always a need amongst scientists for a more accurate model of CRC.

There are three main categories of mouse models, to date, to study human cancer. These include the carcinogen induced model, such as the mouse model of colon carcinogenesis induced by azoxymethane (AOM) (MacFarlane et al., 2014), genetically engineered model (GEM) such as the ^{V600E}*Braf* model of CRC, and Xenograft models. Use of mouse tumour xenografts provides an alternative tool to study colorectal cancer, but it has its own limitations as the mice which receive the xenograft are immune compromised, which does not mimic human conditions. Genetically modified mouse models (GEMMs) that can mimic details of human cancer have been developed in order to study the role of various oncogenes and tumour suppressor genes in tumour initiation and progression. Further progress in the production of GEMMs has made it possible to produce more human-like mouse models in which oncogene expression and tumour mutation can be switched on and off at the right time; this can be used to study the mechanisms of tumour initiation and progression. The following provides details of various GEMMs and chemical models produced to mimic human colorectal cancer.

1.5.1. *Apc* mouse models

These mice carry a mutation in the adenomatous polyposis coli (*Apc*) gene and, even though they all show similarities such as embryonic fatality, tumour predisposition, the severity of the disease seems to be quite variable (Heyer et al., 1999).

In humans, *APC* mutation occurs in epithelial cells of the colon. APC is part of the WNT signalling pathway which acts through *TCF4* and *cyclinD1*, to target genes of the pathway affecting cell cycle at the S transition stage, causing growth dysregulation in the intestinal epithelium (Karim and Huso, 2013). APC is a large multi-domain protein consisting of 2843 amino acids with the function to down regulate the WNT signalling pathway (McCart et al., 2008) (Figure 1.22).

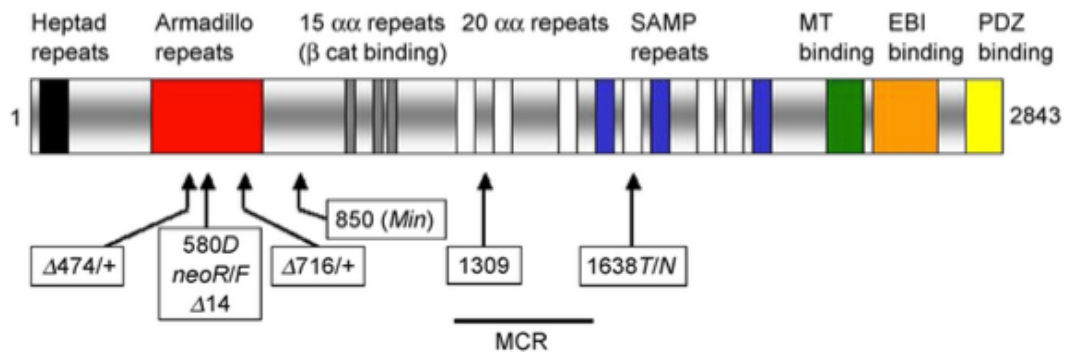


Figure 1.22 Schematic diagram of the 2843 amino acids structure of APC protein (McCart et al., 2008). Different mouse mutants are shown in black arrows.

The Multiple intestinal neoplasia (Min) mouse was generated by random mutagenesis with *N*-ethyl-*N*-nitrosourea (ENU) in 1990 by Moser et al. (McCart et al., 2008). The *Apc* Min mouse is an excellent model for human FAP which develops numerous adenomas in the small intestine and a few in the colon and rectum (McCart et al., 2008). It was established later that the *Apc* Min mouse model carries a point mutation at the position 850 of the gene codon which resembles FAP (Figure 1.22) (McCart et al., 2008, Young et al., 2013). Because of the Min mouse phenotypic resemblance to human FAP it has been used extensively in studies (Young et al., 2013). Homozygous mutation in these mice gives rise to embryonic fatality. Therefore, a heterozygous form affecting one allele of the gene is routinely bred (*Apc*^{Min/+}). Although all Min mice have the same mutation in their genome, they have showed diverse phenotypic characteristics of the disease such as polyp burden. The diversity is thought to be due to differences in diet, environmental factors and genetic modifiers (McCart et al., 2008). Genetic modifiers are defined as genes that affect the severity of the disease by direct or indirect interaction with the primary mutation which is responsible for disease formation. Modifiers of Min (Mom) strongly influence the tumour burden of the *Apc*^{Min/+} (McCart et al., 2008). Using different gene techniques, 13 modifiers of the Min mice have been identified (Johnson and Fleet, 2013).

Besides the *Apc* (Min) model, multiple other *Apc* mouse models have been generated to more accurately study sporadic CRC (Table 1.2). Shibata et al. showed that deletion of both copies of *Apc* (loxP site flanking exon 14; *Apc*^{fl/fl}; *Apc*^{580S/580S}) promotes adenoma formation (Shibata et al., 1997). Later, using *AhCre* under the *Cyp1a1* promoter which is inducible by β -naphthoflavone or with *Villin-CreER*^T, *Apc* deletion was detected at higher frequency within the small intestine and lower frequency in the colon tissue. Sansome et al. in 2004 and Andreu et al. in 2005, showed that deletion of *Apc* has a dramatic effect on proliferation rate as well as migration and differentiation (Sansom et al., 2004, Andreu et al., 2005). Recently, *Cre* strains that are more specific to the colon such as *Cdx2P-CreERT2*, *FABPCre*, *A33Cre* and *CDX2Cre*, have been used to

delete a single copy of *Apc* and also overcome the tumour burden in the small intestine (Jackstadt and Sansom, 2016).

Use of *Lgr5-CreER* to delete *Apc* in intestinal stem cells (ISC) was reported in order to determine the origin of intestinal cancer (Barker et al., 2008).

Since the *Apc* mutation on its own cannot cause tumorigenesis, in order to make the *Apc* models of CRC more patient relevant, additional mutations that come at later stages were introduced along with *Apc*. The *Apc* and *Kras*^{G12D/+} model, for sporadic colon cancer using adeno-Cre, successfully resulted in formation of metastatic cancer in the distal colon which resembles human disease (Hung et al., 2010).

GEM	Mutation	Polyp burden ^a	Histology/pathology	Comments
<i>Apc^{Mm/+}</i>	Truncating mutation at codon 850 (ENU induced).	~30 -> 100	Polypoid, papillary and sessile adenomas. Cystic crypts, no colonic ACF.	Canonical FAP model
<i>Apc^{A716/+}</i>	Neomycin inserted into exon 15; protein truncated at codon 716.	~300	Polypoid, papillary and sessile adenomas. No colonic ACF	Normal villous epithelium covering each polyp
<i>Apc^{T638N/+}</i>	Neomycin inserted in antisense orientation into exon 15; protein truncated at codon 1638.	< 10	Polypoid and hyperplastic polyps. Moderate to highly differentiated adenocarcinoma with infiltration into mucosa and submucosa. Gastric lesions and a single liver metastasis. Desmoids, cutaneous cysts and spontaneous colonic ACFs.	Truncated protein predicted, no expression detected
<i>Apc^{T638T/+}</i>	Hygromycin inserted in sense orientation into exon 15; protein truncated at codon 1638.	–	No increases in predisposition towards intestinal tumorigenesis. Smaller size, absence of preputial glands, nipple-associated cysts	Expression of 182 kDa protein detected.
<i>Apc^{T309/+}</i>	Frameshift at codon 1309.	~35	Polyps throughout duodenum to colon.	More colonic polyps than <i>Apc^{Mm/+}</i>
<i>Apc^{A14}</i>	Frameshift at codon 580.	~65	Increase in colonic polyps, ACF and rectal prolapse. Tubular adenomas and invasive carcinomas in animals > 12 months.	More severe than <i>Apc^{Mm/+}</i>
<i>Apc^{S80D}</i>	Frameshift at codon 580 following adenoviral derived cre exposure.	~6	Adenomas developed predominantly near anus.	Approach using adenovirus derived cre may account for localization of tumors
<i>Apc^{A580}</i>	Keratin 14 promoted excision of exon 14, resulting in a frameshift at codon 580 and truncation at codon 605	~120	Intestinal phenotype similar to <i>Apc^{A14}</i> with additional phenotypic manifestations in the skin, thymus and tooth.	Similar extra-colonic features to FAP patients (tooth defects)
<i>Apc^{A474/+}</i>	Neomycin inserted into exon 9, with duplication of exons 7, 8, 9 and 10. Frameshift at codon 474.	~30-00	Sessile polyps with a central depression. Mammary adenocarcinoma (18% between 3-5 months). Hyperproliferation of intestinal glands.	Influence of duplicated exons on expression?
<i>Apc^{neoR}</i> <i>Apc^{neoF}</i>	Neomycin inserted into intron 13, in reverse or forward orientation.	< 1 at 15 months		Hypomorphic alleles that reduce Apc by 80% and 90%, respectively.

Table 1.2 List of different *Apc* mutant mice (McCart et al., 2008). To generate better models of human colorectal cancer with the *Apc* mutation, different types of mutants were produced. These models are not only different in their codon but also show different phenotypic characteristics of the disease.

1.5.2. *Kras* mutant mouse model

KRAS is a membrane associated protein with GTPase activity which functions downstream of a range of tyrosine kinase growth factor receptors (Johnson and Fleet, 2013). Constant activation of KRAS leads to the activation of the ERK1/2 pathway (Janssen et al., 2002). Oncogenic missense mutations have been reported in codons 12, 13, and on rare occasions, 61 in the *KRAS* gene in human cancer (Johnson and Fleet, 2013, Luo et al., 2007). Substitution of aspartate with glycine in codon 12 ($G^{12}KRAS$) was reported to be present in 40% of human sporadic colorectal cancer cases, as well as 30% of non-small cell lung cancer (NSCLC) and 95% of pancreatic ductal Adeno-carcinomas (PDAC) (Johnson and Fleet, 2013). This mutation causes continuous activation of the protein which is the result of GTPase conformation lock (Luo et al., 2007).

To investigate the underlying role of $G^{12D}KRAS$ in cancer mutant, mouse models were reported some of which are listed below. Use of homologous recombination was reported in 2001 by Jackson et al., to replace one of *Kras* endogenous allele with an allele that had a translational floxed STOP sequence (Lox-Stop-Lox). The LSL sequence was located before the gene encoding a *Kras* oncogenic G12D allele (Jackson et al., 2001). In the presence of Cre activity, recombination removes the LSL cassette and as a result the oncogenic *Kras* G12 allele is expressed in the lung, and pancreas (Johnson and Fleet, 2013). This was initially done by use of a *CMV* promoter-Cre transgene, where the embryonic expression of $G^{12D}Kras$ proved to be lethal (Johnson and Fleet, 2013). Subsequently other *Kras* mouse models were reported in which Cre was induced using different promoters (Johnson and Fleet, 2013). Janssen et al. reported $G^{12V}KRAS$ as the most expressive, common oncogenic mutation in colorectal cancer (Janssen et al., 2002). Successful generation of a $G^{12V}Kras$ transgenic mouse, using 9kb murine *Villin* promoter in order to control selective expression of $V^{12D}Kras$ in the epithelial cells of the colon, was undertaken (Janssen et al., 2002)

In 2007 Luo et al. generated a $G^{12V}Kras$ mutation additional knockin model (Luo et al., 2007). The conditional *Kras* transgene was produced by insertion of a

human $G^{12}KRAS$ “minigene” sequence, into a vector with a Floxed STOP cassette. The minigene locates between $G^{12}Kras$ and the upstream *CMV* promoter (Luo et al., 2007).

In 2003 Guerra et al. reported a conditional $V^{12}Kras$ mouse model which was created by two separate recombination events. At first an IRES- β -geo cassette was introduced within the 3' untranslated region of the *Kras* allele by homologous recombination in mouse embryonic stem (ES) cells. Subsequently, resistant clones were subjected to the second recombination at the 5' end of the *Kras* allele. In the second recombination event, the endogenous exon one of *Kras* allele was replaced with the mutated sequence with a point mutation at the codon 12 which encodes valine. ES cell carrying both recombination on the same *Kras* allele expressed β -geo only after transfection with Cre recombinase (Guerra et al., 2003). In 2013 Davis et al. used the same method of recombination in order to create GEMs with $G^{12V}Kras$ and PTEN mutation to study the formation of intestinal serrated adenomas and metastatic carcinoma (Davies et al., 2014). *Pten*^{fl/fl}; *Kras*^{LSL/+} mice show an increase in crypt cell number with extended proliferative zone along the crypt-villus axis which result in villus branching. Villus branching is not the result of ectopic crypt formation but reduction of cell sloughing at the tip of the villus. Mice with *Pten*^{fl/fl}; *Kras*^{LSL/+} have a shortened life span with 30% having hyperplastic polyps, 78% with benign dysplastic serrated adenomas, 44% invasive adenocarcinomas and 41% metastatic intestinal carcinomas. The most prominent feature of the metastatic group of lesions is the serrated architecture of the neoplastic group resembling human serrated colonic neoplasm. Dysplastic sessile serrated adenoma, most commonly identified colonic neoplasm, is a non-polypoid tumour with a dysplastic epithelium, disorganized proliferation zone, lack of mature cells, and nuclear crowding (Davies et al., 2014).

1.5.3. ^{V600E}*Braf* mouse model

Conditional knockin GEMMs have been developed for the most common *BRAF* mutation in human cancer (V600E) in which the Cre-Lox system controls the endogenous *Braf* locus (Figure 1.23). Cre is a 38KDa recombinase enzyme extracted from bacteriophage P1 which mediates site recombination between LoxP sequences (locus of crossing over not P1 phage) sites (Schwenk et al., 1995). In this model ^{WT}BRAF protein is produced in the absence of Cre-recombinase with exons 15-18 being expressed from a minigene cDNA. Expression of Cre-recombinase causes deletion of the LSL cassette and, as a result, ^{V600E}*Braf* is expressed (Pritchard et al., 2007, Mercer and Pritchard, 2003). This model was developed in the Pritchard laboratory and was first reported in Mercer et al. published in 2005 (Mercer et al., 2005).

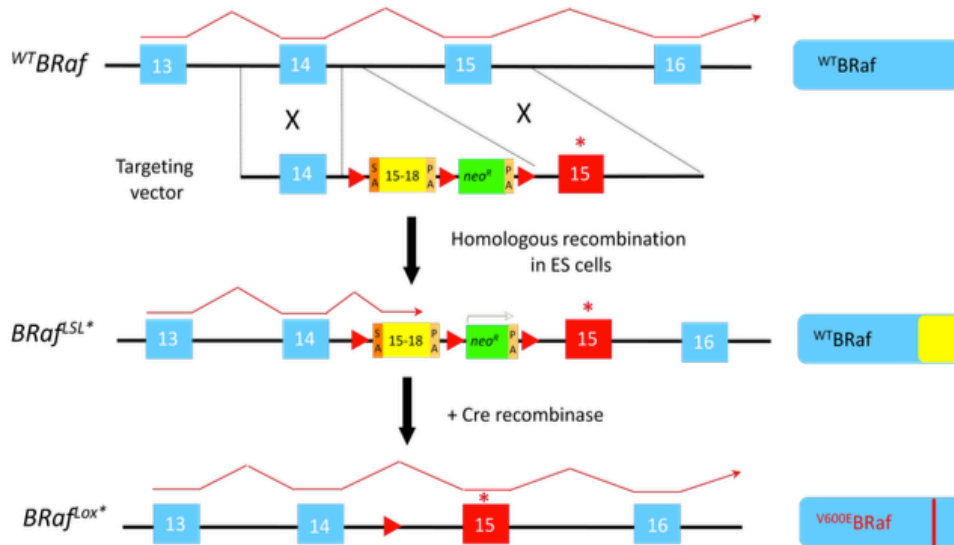


Figure 1.23 Conditional knockin allele for $v600E$ *Braf* in GEMMs (Pritchard et al., 2007). In this model modification of the *Braf* locus has been undertaken by insertion of a LSL (Lox-STOP-Lox), shown in red triangles, cassette in exon 14. LSL consists of a mini-cDNA encoding exons 15-18 of the *Braf* gene which has a β -globin splice acceptor sequence at the 5-end and a poly-A sequence at the 3' end. In exon 15 the gene sequence contains the T1799A mutation. Three LoxP sites are present in the LSL cassette: between exon 14 and the mini-cDNA, mini-cDNA and the *neo^R* cassette and the last one in between the *neo^R* cassette and genetically modified exon 15. Induction of $v600E$ *Braf* expression can be undertaken by expressing Cre. *Braf^{LSL-V600E}* allele converts to *Braf^{Lox-V600E}* after expression of Cre recombinase. "*" indicates the *Braf* exon 15 containing the point mutation.

In order to induce ^{V600E}BRaf in the intestine, the *AhCreER^T* mouse strain was used in which the *Cyp1A1* promoter induces expression of the tamoxifen (TM)-regulated Cre recombinase in transit amplifying cells in the gastrointestinal (GI) tract of the mouse (Kemp et al., 1993, Carragher et al., 2010). The strategy for generating the mouse model involved inter-crossing between heterozygous mice for *AhCreER^T* with heterozygous mice for a knockin *Braf^{LSL-V600E}*. The *CYP1A1* promoter which controls the *CreER^T* gene expression, is induced by β -Naphthoflavone (β -NF) and results in production of CreER^T fusion protein. Fusion of Cre with the ER leads to suppression of CreER^T by Hsp90 in the cytoplasm. To regulate the Cre fusion protein expression, the ER carries a mutation in its ligand binding domain which facilitates binding of the protein to Tamoxifen. The Hsp90 bound to ER is disrupted with TM which leads to the translocation of the CreER^T fusion protein into the nucleus, allowing LoxP recombination (Kemp et al., 1993, Carragher et al., 2010). By using *AhCreER^T*, the dual regulation of Cre recombinase is achieved (Figure 1.24).

Induction of crypt hyperplasia was detected following mice injection at 3 days post injection (p.i.). This was followed by evidence of senescence induction until 6 weeks p.i. Senescence was accompanied by a reduction in proliferative markers as well as an increase in senescence-associated β -galactosidase and p16^{INK4a} expression (Carragher et al., 2010). In mice aged >6 weeks an increase in proliferation of some of the cells in senescent tissue was observed, leading to formation of low grade dysplasia and at later time points occasional serrated adenomas were observed (Figure 1.25) (Carragher et al., 2010).

Following 3 days induction of ^{V600E}BRaf, nuclear β -catenin levels increased, particularly in the cells higher up in the crypt, which also corresponded to increased p-ERK staining (Figure 1.26). This was reversed following MEK inhibitor (PD184352) treatment and was also absent in senescent crypts (Figure 1.26) (Carragher et al., 2010). Phosphorylation of GSK3 β at serine 9 was induced at 3 days p.i., which was significantly downregulated following PD184352 treatment as well as at later time points (Figure 1.26). GSK3 β phosphorylation at serine 9 was shown to be AKT independent but MEK-

dependent (Figure 1.26)(Carragher et al., 2010). This finding opened opportunities for further investigation of canonical WNT pathway activation by ERK in more details that could have potential therapeutic values.

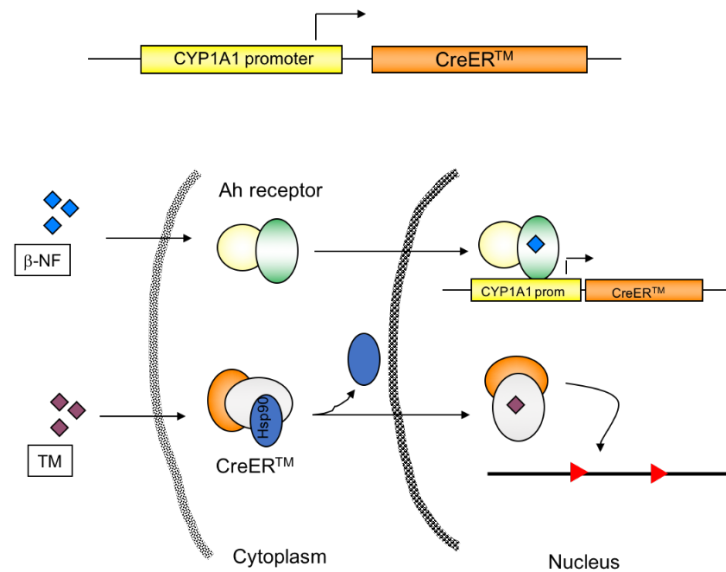
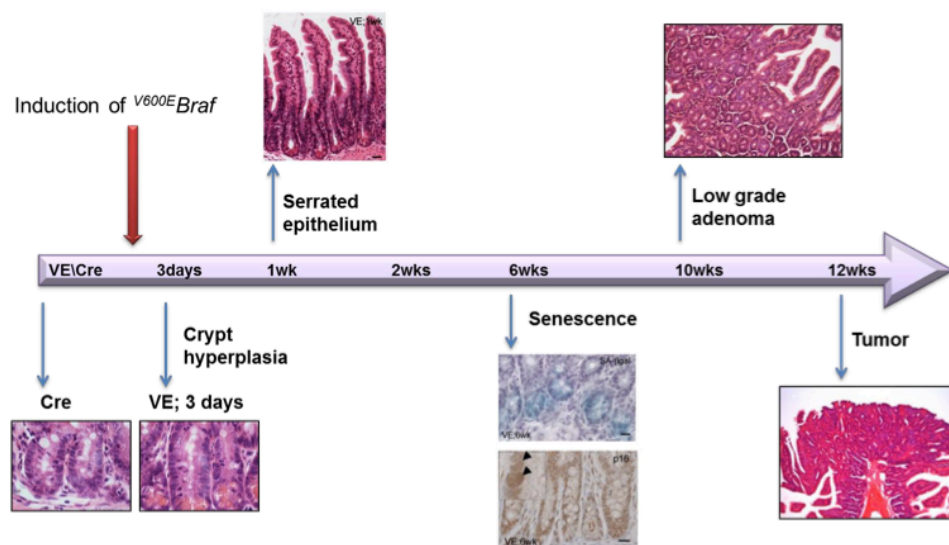


Figure 1.24 Control of Cre activity using the AhCreER^T system. The CYP1A1 promoter which controls CreER^T gene expression, is induced in the presence of β -NF. The resulting CreER^T fusion protein is suppressed by Hsp90 in the cytoplasm. In the presence of Tamoxifen (TM) HSP90 dissociates from the CreER^T fusion protein, which in turn leads to the fusion protein translocation into the nucleus and LoxP recombination occurs.



Carragher et al., 2010. EMBO Molecular Medicine. 2, 458-471

Figure 1.25 Timeline of $V600E$ BRaf induced small intestine hyperplasia followed by senescence and ultimately tumour development. Injection of mice with β -NF and TM took place at time zero. Three days after injection, crypt hyperplasia was detected, formation of serrated epithelium appears after one week and senescence occurs between 1-10 weeks. At 10 weeks p.i. some cells overcome senescence and start to proliferate which causes the formation of low grade adenomas. Formation of tumours was detected at around 12 weeks.

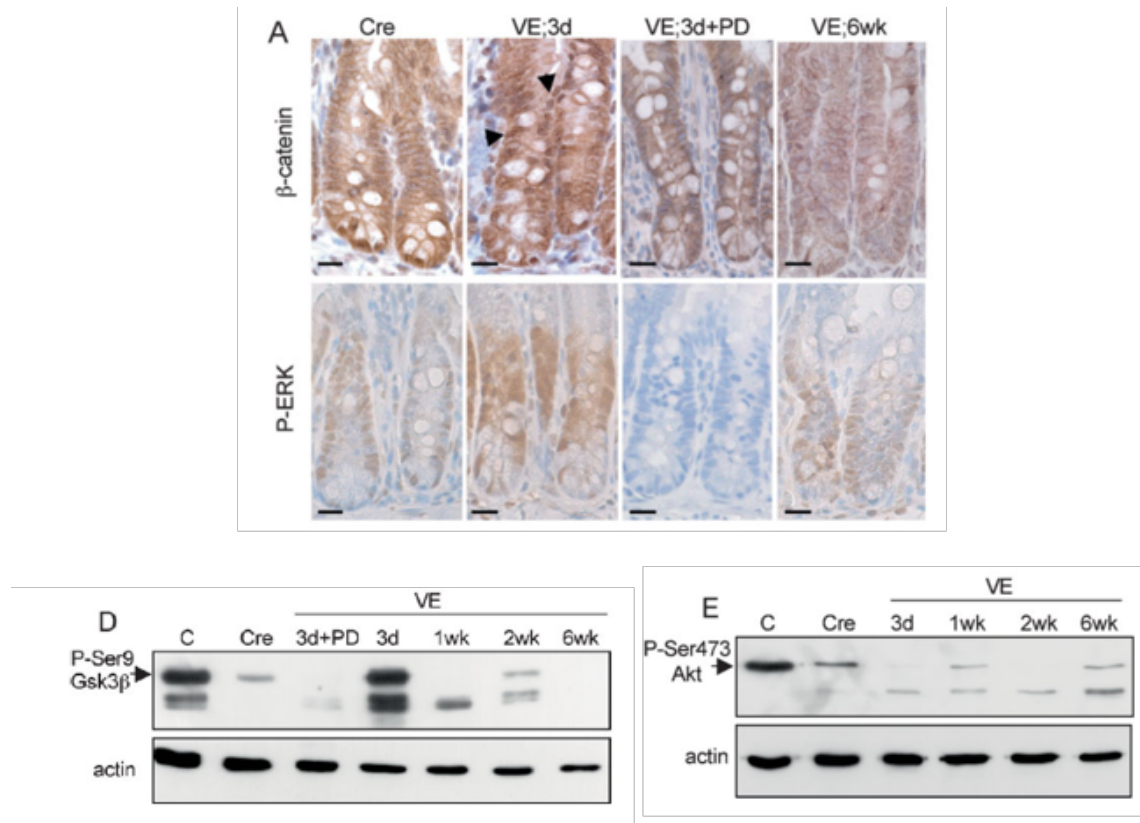


Figure 1.26 Evidence of crosstalk between MAPK/ERK and the WNT pathway in a V^{600E} Braf mouse model at various time points (Carragher et al., 2010).

A) Immunohistochemical analysis of V^{600E} Braf expressing gut tissue at 3 days p.i. as well as at 6 weeks p.i. and 3 days p.i. treated with PD184352. ERK phosphorylation increases 3 days p.i. in comparison to Cre control samples which was reversed following treatment with PD184352. At 6 weeks p.i. samples, ERK phosphorylation was lower in comparison to 3 days p.i. possibly because there was senescence pathway activation in the tissue at the later time points. Nuclear β -catenin expression was detected in 3 days p.i. at a higher level than Cre control samples and this was reversed following inhibitor treatment. Nuclear β -catenin was absent in the 6 weeks p.i. tissue.

D) Western blot analysis of the V^{600E} Braf expressing mouse tissue at various time points. 3 days p.i. tissue has high level of GSK3 β phosphorylation at serine 9 in comparison to control animals. This was reversed in 3 days p.i. tissue treated with PD184352. GSK3 phosphorylation was not detected at later time points, possibly due to senescence induction. "C" is a control sample of Mouse Embryonic Fibroblast (MEF). "Cre" refers to control AhCreER^T mice with WT Braf.

E) Western blot analysis of the tissue at different time points p.i., indicates that GSK3 β phosphorylation is AKT independent.

One problem with this model was that induction of *AhCreER^T* and Cre activity was also observed in other tissues besides the intestine and specifically in the stomach and lung tissue (Figure 1.27) (Carragher et al., 2010). This created problems with the long-term assessment of the mice and further tumour development. Therefore, the need for a better and more specific mouse model which is more patient relevant was needed so the disease could be monitored from a very early to later stage (formation of the tumours).

To make the ^{V600E}*Braf* expression more direct to intestinal epithelium *Villin-Cre* (*VilCre*) mice replaced *AhCreER^T*. The regulatory 9kb region of the mouse *Villin* gene was used, an actin-binding protein which is expressed from E9.5, embryonic age 9.5 days, in differentiated as well as undifferentiated cells in intestinal and renal epithelium as well as in stem cells of the crypts (Janssen et al., 2002). In 2013, Rad et al. reported the construction of a ^{V600E}*Braf* knockin allele which was activated in the intestine by *Villin-Cre*. They reported that ^{V637E}*Braf* mutation in exon 18 of mouse is equivalent to ^{V600E}*BRAF* mutation in exon 15 of the human gene (Rad et al., 2013). In this model, ^{V600E}*Braf* is expressed in cells determined by *Villin-Cre* expression. Adult animals showed crypt hyperplasia which leads to crypt thickening and formation of mucosal protrusions which looks like a villus structure in the large intestine. In the small intestinal tissue villus elongation and thickening with an abnormal branched like structure was detected (Figure 1.28) (Rad et al., 2013). In this model, hyperproliferation seemed to be the underlying molecular mechanism of the serration in the tissue as the apoptosis rate did not seem to change in compare to the control animal (Rad et al., 2013). In the Rad et al. study, mice developed dysplastic lesions at the age of 2-3 months, with some animals developing small (~2mm) lesions and at the age of 10 months almost all mice developed large dysplastic lesions with human TSAs like characteristics. Presence of carcinoma was confirmed in 13.8% of *Braf^{SL-V600E/+}; Villin-Cre* mice aged older than 10 months with both low-grade and high-grade tumours whereas in *p53^{LSL-172H/+}; Braf^{SL-V600E/+}; Villin-Cre* carcinoma was seen in 56% of the animals aged between 10-20 months (Rad et al., 2013).

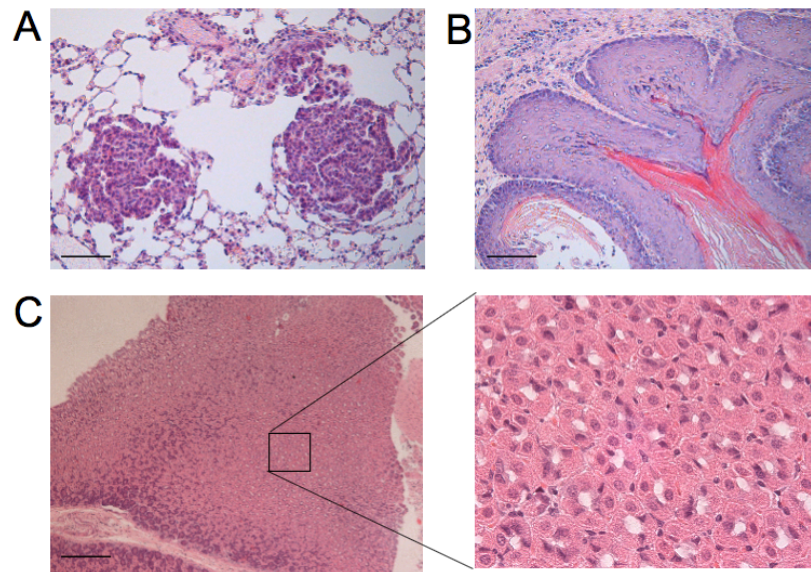


Figure 1.27 Formation of lung and stomach hyperplasia in $Braf^{+/LSL-V600E}; AhCreER^{T+/o}$ (Carragher et al., 2010).

A) Formation of lung adenomas in the tissue of the lung, 8-10 weeks post induction. This structure is similar to adenomas formed in conditional $V600E$ $Braf$ mice induced by nasal inhalation of the adenoviral-Cre.

B and C) In $Braf^{+/LSL-V600E}; AhCreER^{T+/o}$ mice, stomach hyperplasia following β -NF and TM was detected. Tissue was collected 8-10 weeks post induction. Hyperplastic stratified squamous epithelium of stomach was observed along with a large increase in hydrochloric acid secreting cells. These two phenotypes seem to be the main reason behind the limited life span of the mice (3 months) post induction.

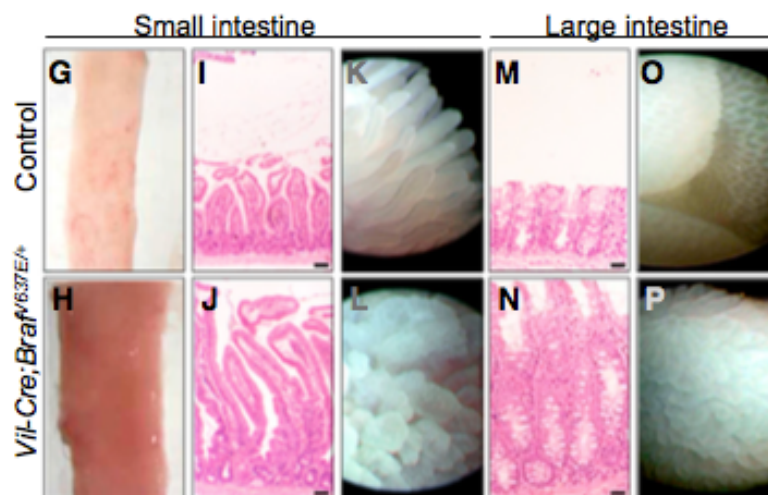


Figure 1.28 Pathological characteristics of the $Braf^{+/LSL-V600E}; Villin-Cre$ Mouse model (Rad et al., 2013). Macroscopic and microscopic characteristics of the small and large intestinal tissues in the control animal (top panel) and $Braf^{+/LSL-V600E}; Villin-Cre$ (lower panel). As shown, following the expression of the $V600E$ $BRAF$ oncogene, crypt elongation and thickening in both small and large intestinal tissues is observed.

1.5.4. *Gsk3* knockin mice

To investigate the details of GSK3 kinase regulation and the mechanism of action, considerable effort has been put into creation of different *Gsk3* mouse models. Several different genetic methods were employed in order to generate *Gsk3* mutant mice: conventional knockins and knockouts in which the *Gsk3* kinase mutation is expressed throughout the body, conditional knockouts which are tissue specific and transgenic mice (Table 1.3) (Kaidanovich-Beilin and Woodgett, 2011). *Gsk3* mouse models that are created belong to two major categories: mouse models with increased GSK3 activity such as *Gsk3 α* ^{S21A/S21A} and *Gsk3 β* ^{S9A/S9A} knockin (KI) models and the second category is mouse models with reduced GSK3 activity such as the *Gsk3 β* knockout (Gómez-Sintes et al., 2011).

Type of approach	Mouse design	Mouse name	Characterized by (reference)
CONVENTIONAL			
Knockout	Deletion of exon 2 (ATP-binding loop) of GSK-3 α	GSK-3 α KO	MacAulay et al. (2007), Kaidanovich-Beilin et al. (2009), Lee et al. (2011), Lipina et al. (2011)
Knockout	Deletion of exon 2 (ATP-binding loop) of GSK-3 β	GSK-3 β KO	Hoeflich et al. (2000)
Knockout	Deletion of exon 2 (ATP-binding loop) of GSK-3 β	GSK-3 β HET	Hoeflich et al. (2000), Beaulieu et al. (2004), O'Brien et al. (2004), Beaulieu et al. (2008), Bersudsky et al. (2008), Kimura et al. (2008)
TRANSGENIC			
Knock-in	Mutations GSK-3 α^{S21A} , β^{S9A}	GSK-3 α , β [S21A,S9A] KI	McManus et al. (2005), Eom and Jope (2009), Ackermann et al. (2010), Mines et al. (2010), Polter et al. (2010)
CONDITIONAL			
Double shRNA knockdown	GSK-3 α/β shRNA (shGSK-3-dh ^{+floxed}) \times Nestin-Cre	Nestin-Cre/shGSK-3-dh ^{+Δ}	Steuber-Buchberger et al. (2008)
Conditional knockout	GSK-3 α /GSK-3 β ^{flox/flox} \times Nestin-Cre	Nestin-GSK-3 α + β KO	Kim et al. (2009)
Double shRNA knockdown	GSK-3 β shRNA	DG-GSK-3 β knockdown (shRNA)	Omata et al. (2011)
TRANSGENIC			
Dominant-negative (DN) GSK-3 β	K85RGSK-3 β \times CamkII-tTA-Cre	DN-GSK-3 β	Gomez-Sintes et al. (2007)
Overexpression of GSK-3 β	TetO GSK-3 β \times CamkII-tTA-Cre	Tet/GSK-3 β	Lucas et al. (2001), Hernandez et al. (2002), Engel et al. (2006), Hooper et al. (2007)
Overexpression of constitutively active GSK-3 β [S9A]	S9AGSK-3 β in Thy-1 gene vector	GSK-3 β [S9A]	Spittaels et al. (2000), Spittaels et al. (2002), Prickaerts et al. (2006)
Overexpression of GSK-3 β	<i>Xenopus</i> GSK-3 β \times mouse prion promoter MoPrPXho	PrpGSK-3 β^{L56} and PrpGSK-3 β^{L64}	O'Brien et al. (2011)

Table 1.3 List of different models of *Gsk3* mouse (Kaidanovich-Beilin and Woodgett, 2011).

The *Gsk3* knockout (KO) animals first created were *Gsk3 β* knockouts which did not pass the late developmental stage as a result of hepatic apoptosis or cardiac patterning defects (Hoeflich et al., 2000, Kerkela et al., 2008). Heterozygous animals for *Gsk3 β* are morphologically normal and they show anti-depressant like behaviour like lithium treated animals. Animals exploratory activity is reduced, but they maintain normal general locomotion. Mice with a *Gsk3 β ^{+/-}* genotype demonstrate increased anxiety with reduced aggressive behaviour (Bersudsky et al., 2008, Beaulieu et al., 2008, Beaulieu et al., 2004, O'Brien et al., 2004). These animals seem to have an impaired ability to form long-term memory (Kaidanovich-Beilin and Woodgett, 2011). *Gsk3 α* null mice seem to have improved insulin sensitivity and hepatic glycogen accumulation on the ICR background (Kaidanovich-Beilin and Woodgett, 2011). *Gsk3 α* KO mice show unique phenotypic features decreased locomotion, social motivation, coordination and associative memory but increased sensitivity to environmental cues (Kaidanovich-Beilin et al., 2009).

Knockin mice were created by changing the codons, encoding serine 9 of GSK3 β and serine 21 of GSK3 α , to unphosphorylatable alanine. As a result, the protein kinase is insensitive to inhibition by the normal mode of regulation. This does not affect the kinase sensitivity to all regulatory pathways, for example the WNT (Kaidanovich-Beilin and Woodgett, 2011, McManus et al., 2005). *Gsk3* KI mice display normal development and growth and do not show any sign of diabetes (McManus et al., 2005). These mice have similar survival time of a normal mouse and are fertile with negligible alteration of small intestine molecular and morphological characteristics (Hey et al., 2016). Animals show 40% decrease in neurogenesis, which can be explained with reduction of vascular endothelial growth factor (VEGF) (Eom and Jope, 2009).

1.6. Aims and objectives:

Current research does not address the underlying mechanism of crosstalk between the MAPK and WNT pathways. Based on the 2010 publication by Carragher et al., crosstalk occurs at the ERK and GSK3 levels, and the crosstalk occurs with the help of intermediary kinase/s. Our hypothesis is that GSK3 phosphorylation plays a crucial role in this crosstalk and can be a potential therapeutic target, but this requires intensive research. To achieve this goal, we generated a novel mouse model by intercrossing the *Braf*^{SL-V600E/WT}, *Villin-CreER*^{T0/WT} with homozygous knockin for *Gsk3α/β*. Investigating the mechanism of the crosstalk required the following approaches:

- Investigation of crosstalk using ^{V600E}*BRAF* mutated cell lines.
- *In vivo* study using *AhCreER*^{T0/WT} and *Villin-CreER*^{T0/WT} strains.
- Use of *Gsk3* knockin (Serine-9-Alanine) mutant mice to confirm the role of GSK3 phosphorylation in ^{V600E}*BRAF*-driven CRC development.

Chapter 2. Materials and methods

The water which was used in all the experiments was always MilliQ water, unless stated otherwise.

I conducted all the work in this thesis, except for preparation of MEFs by Dr. C. Andreadi and Dr. L. Cheung. I genotype the mice collaboratively with Mr. D. Brown. All the injections and animal husbandry were performed by trained technicians at the CRF facility, University of Leicester. Processing the PFA fixed tissue, apart from paraffin embedding, was done by Mrs. J. Edwards. I subbed the glass slides along with Mr. D. Brown and Mrs. S. Giblett. Sectioning was performed by Mrs. S. Giblett. For the long-term survival study, tissue from BVE/Cre and WT/Cre mice were collected by Dr. H. Jin. Pathological analysis of the sections was carried out by Professor K. West. Dr. M. Viskaduraki and I performed statistical analysis. RNA extraction and microarray processing was carried out by Dr. S. Gibson and Dr. N. Sylvius. Analysis of Microarray data was carried out by Dr. J. Luo

2.1. Molecular biology

2.1.1. Cell line culture

All procedures were carried out in a class I tissue culture hood. All tissue culture plastic-ware was provided by Invitrogen, unless otherwise stated. Table 2.1 contains all reagents used in cell culture procedures.

2.1.1.1. A375P cells

Human melanoma (A375P) cells are primary malignant epithelial cells originally taken from a 54 years old Caucasian female patient (ATCC, 2019). A375P (Provided by Dr. S. Prigent) cells are bearing the homozygous ^{V600E}*BRAF* mutation. A375P cells were maintained in Dulbecco's Modified Eagle Medium (DMEM) supplemented with 10% [v/v] Foetal Bovine Serum (FBS) and 1% [v/v] Penicillin Streptomycin (10000µg of streptomycin and 10000 units of penicillin/ml). Cells were cultured in 10cm plates and maintained at 37°C in 10% CO₂.

2.1.1.2. HCC364 cells

Human lung non-small cell adenocarcinoma (HCC364) are primary cells originating from a 76 years old male patient (ExpASy, 2019a). HCC364 cells (purchased from ATCC) carry a heterozygous ^{V600E}*BRAF* mutation and were maintained in DMEM supplemented with 10% [v/v] FBS and 1% [v/v] Penicillin Streptomycin. Cells were cultured in 10cm plates and maintained at 37°C in 10% CO₂.

2.1.1.3. RKO cells

Three human colorectal cell lines (RKO143, RKO144 and Cook's RKO (Parental line) were directly provided by Professor B. Vogelstein. Human RKO

parental cells are primary colon carcinoma initially taken from a patient with unspecified sex and age (ExpASy, 2019b). Yun et al. reported presence of three BRAF alleles in RKO parental cells. These were used to produce RKO143 and RKO144 mutant cells through homologous recombination by inactivation of WT or mutant alleles (Yun et al., 2009). RKO cells were independently verified using qPCR by Dr. C. Rakhit from our laboratory. The parental RKO cell line carries 3 alleles of the *BRAF* gene, out of which two carry the V600E mutation and one is WT; whereas, RKO143 carries one WT and two knocked out *BRAF* alleles, and RKO144 contains one ^{V600E}*BRAF* and two knocked out *BRAF* alleles. These cells were maintained in McCoy's 5A Modified Medium supplemented with 10% [v/v] FBS and 1% [v/v] Penicillin Streptomycin. Cells were cultured in 10cm plates and maintained at 37°C with 10% CO₂. Cells were sub-cultured as needed, in a ratio of 1:3 when they reached 80% confluency, but the media was changed regularly.

2.1.1.4. Mouse Embryonic Fibroblasts (MEFs)

Mouse Embryonic Fibroblasts (MEFs) were prepared from embryos of *BRAF*^{L^{SL}-V600E/WT} mice. The embryos were isolated according to Home Office regulations (Andreadi et al., 2012). The head and liver were removed. A fresh scalpel blade was used to finely chop each embryo, and the tail was removed for genotyping. The tissue was incubated in 0.25% [v/v] trypsin-EDTA for 16 hours at 4°C. Then the trypsin-EDTA was removed and the cells were re-suspended in 10ml DMEM supplemented with 10% [v/v] FBS and 1% [v/v] Penicillin Streptomycin. The cell suspension was allowed to adhere to a 10cm plate at 37°C with 10% CO₂ overnight. The media was removed and replaced, 24 hours following plating, to remove dead cells. MEFs were maintained in 10ml of DMEM supplemented with 10% [v/v] FBS and 1% [v/v] Penicillin Streptomycin in a 10cm plate at 37°C in 10% CO₂. MEFs were split at 1:2 ratio when confluent.

2.1.2. Infection with Adenoviral Cre

All of the following procedures were carried out in a Class II hood.

To induce the expression of ^{V600E}BRaf, MEFs containing the *Braf*^{LSL-V600E/WT} alleles were infected with Adenovirus carrying Cre recombinase (AdCre) (AD5CMVCre, Gene Transfer Vector Core, University of Iowa Carver College of Medicine, USA). As a control for viral infection, MEFs were infected with Adenovirus carrying β -Galactosidase (Ad5CMVntLacZ, Gene Transfer Vector Core, University of Iowa Carver College of Medicine, USA). One day before infection, 2×10^5 MEFs were seeded into 6cm plates. Before infection, FBS and Penicillin Streptomycin were removed, and cells were rinsed twice with DMEM media without FBS and Penicillin Streptomycin. 2ml of DMEM media without FBS and Penicillin Streptomycin was left on the plate, and 2 μ l (8×10^7 pfu) of virus was added to the media. 2 hours after the addition of the virus, 3ml of DMEM supplemented with 10% [v/v] FBS and 1% [v/v] Penicillin Streptomycin was added, and the cells were cultured at 37°C in 10% CO₂ for relevant periods. A similar procedure was followed for WT control MEFs.

2.1.3. Freezing stock of the cells

Once a 10cm plate was confluent, media was removed and the cells were rinsed with 1X PBS. Cells were detached by the addition of 0.05% [v/v] trypsin-EDTA for 2 minutes at 37°C (checked regularly for the sign of detachment) and subsequently collected by gentle pipetting; and equal volumes of growth medium was added to neutralize the trypsin-EDTA. The cell suspension was transferred into a 15ml falcon tube and centrifuged at 1,100rpm for 5 minutes. The supernatant was removed and cells were re-suspended in 3ml of FBS containing 10% [v/v] DMSO. The suspension was then transferred into 3 cryovials. The vials containing cells were labelled and stored in liquid nitrogen permanently.

2.1.4. Thawing stock of the cells

A cryovial containing cells was kept in a 37°C water bath. The cell suspension was transferred into a 15ml falcon tube containing 7ml of culture medium with 10% [v/v] FBS, and 1% [v/v] Penicillin-Streptomycin, which subsequently was centrifuged at 1100rpm for 5 minutes. The supernatant was removed and the pellet was re-suspended in 10ml of medium containing 10% [v/v] FBS and 1% [v/v] Penicillin-Streptomycin and transferred in to 10cm plate and stored in an incubator at 37°C with 10% CO₂.

Chemical	Supplier/ Catalogue number
Dulbecco's Modified Eagle Medium (DMEM)	Invitrogen / 11995065
Foetal Bovine Serum (FBS)	Gibco Ltd / 10270
Penicillin-Streptomycin	Invitrogen / 15140
McCoy's 5A Modified Medium	Invitrogen / 26600023
Trypsin-EDTA	Gibco / 15400-054
Phosphate Buffered Saline (Dulbecco A) (PBS)	Oxoid / BR0014G
Dimethyl Sulfoxide (DMSO)	Sigma / D2650

Table 2.1 List of the reagents used in cell culture procedures.

2.1.5. Inhibition of MAPK pathway and S6K

All drugs were dissolved in DMSO. U0126 and rapamycin were stored at -20°C whereas PD184352 was stored, in the dark, at room temperature. On the day of treatment, cells were aimed to be ~90% confluent. Cells were treated with drugs listed in the Table 2.2, for both 5 and 24 hours, at the given concentrations. Control cells were treated with the same volume of DMSO for both 5 and 24 hours. Cell lysate were prepared as per Section 2.2.2.1.

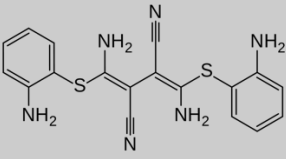
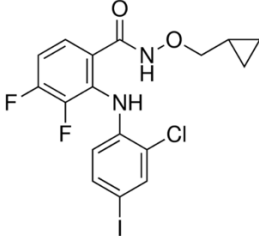
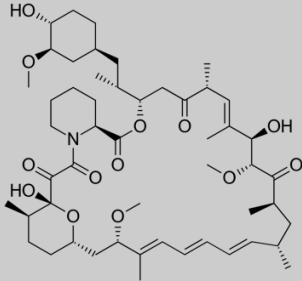
Chemical	Final concentration	Supplier/ Catalogue number	Structure
U0126	10 μ M	Cell signalling / 9903	
PD184352	1 μ M	Dr. Simon Cook, Babraham institute, UK	
Rapamycin	100nM	Cell Signaling / 9904	

Table 2.2 List of inhibitors used to treat cells.

2.2. Biochemistry

2.2.1. Immunofluorescence staining of cells

A list of chemicals and reagents used are in Table 2.3.

2.2.1.1. Cells preparation for immunofluorescence staining

Cells were seeded in 12 well plates, containing cover slips. Cover slips were coated with fibronectin (25 $\mu\text{g}/\text{ml}$), diluted from a stock solution (1 mg/ml) using filtered MilliQ water. Fibronectin solution was added to each well containing cover slips and incubated in the CO_2 incubator at 37°C overnight.

2.2.1.2. Immunofluorescence labelling

Cells on coverslips were fixed in 4% [w/v] PFA (8g of Paraformaldehyde powder in 80 ml of 0.2M Na_2HPO_4 , and heated until dissolved. This was kept at RT until cooled down; this was followed by addition of 20 ml 0.2 M NaH_2PO_4 and 100 ml of distilled water). They were permeabilised in 0.2% [v/v] Triton X-100 (made up in PBS), followed by blocking in 5% [w/v] BSA/PBS. Cells were incubated with a β -catenin antibody (1:100), followed by three washes in 0.2% [w/v] BSA/PBS. Fixed cells were then incubated with a rabbit secondary antibody diluted in 1% [w/v] BSA/PBS (1:400). DAPI with a 1:1000 dilution in PBS was added to cells for nuclear staining. Coverslips containing cells were mounted onto the slide. TE300 semi-automatic Nikon fluorescence microscope with a Hamamatsu ORCA-R² digital camera and an X-cite 120 fluorescence illumination system was used for the observation of slides.

Chemical	Supplier/ Catalogue number
Paraformaldehyde (PFA)	Sigma Aldrich / P6148
Na ₂ HPO ₄	Fisher Chemicals / S/4520/60
NaH ₂ PO ₄	Fisher Scientific / S/3720/60
Triton X-100	Sigma / 9002-93-1
Rabbit Secondary Antibody	Alexa Fluor / A21441
Phosphate Buffered Saline (Dulbecco A) (PBS)	Oxoid / BR0014G
BSA	Sigma / A3059
β-catenin Antibody	Sigma Aldrich / C2206
Rabbit Secondary Antibody	Alexa Fluor / A21441
DAPI	Invitrogen / D1306
Fibronectin	Sigma Aldrich / F1141

Table 2.3 List of the chemicals and reagents used in the immunofluorescence staining of cells.

2.2.2. Preparation of soluble protein lysates

All the chemicals and reagents are listed in Table 2.4.

2.2.2.1. Cell lysate preparation

Once cells were at 80-85% confluency, cell containing plates were taken from the incubator and immediately placed on ice. The media was drained and immediately replaced with 10ml of ice-cold 1X PBS (137mM NaCl, 8mM Na₂HPO₄, 2mM KH₂ PO₄, 2.7 mM KCl – pH 7.4), 3 times to wash out the last traces of media. Then PBS was drained and 200µl of ice-cold Gold Lysis Buffer (1% [v/v] Triton X-100, 50mM Tris – pH 7.0, 150mM NaCl, 10mM NaF, 5mM EGTA, 5mM EDTA, 0.5% [v/v] NP40) or RIPA buffer (50mM Tris – pH 8.0, 0.5% [w/v] sodium deoxycholate, 1% [v/v] NP40, 0.1% [w/v] SDS, 150mM NaCl) was added. Prior to use, 1% of phosphatase inhibitor cocktail 3 and protease inhibitor cocktail were added to the lysis buffer. Cells were harvested by use of a disposable cell scraper and collected into an ice-cold eppendorf tube, and incubated on ice for 10 minutes with vigorous vortexing every minute. Then tubes were transferred into a centrifuge which was pre-cooled at 4°C and centrifuged for 10 minutes at 12000rpm. The supernatant was transferred into an ice-cold fresh tube and was aliquoted, labelled and stored at -80°C.

2.2.2.2. Preparation of protein lysate from frozen tissue

Between 3-4 small pieces of each section of small and large intestine was cut and stored into a pre-labelled eppendorf tube; these were subjected to snap freezing using liquid nitrogen. These tubes were stored in a -80°C freezer. Frozen samples were placed into long, ice-cold disposable test tubes, 400µl of ice cold 1X RIPA lysis buffer, containing protease inhibitor cocktail, and phosphatase inhibitor cocktail was added to the tube. A mechanical homogeniser was used to break down the tissue; this was done on ice at all times to prevent protein degradation. The homogenised solution was transferred into a pre-labelled ice-cold eppendorf tube and was kept on ice for 10 minutes with vigorous vortexing every minute. Then tubes were then

transferred into a pre-cooled centrifuge, and were subjected to centrifugation for 10 minutes at 12000rpm, at 4°C. Supernatants were transferred into several ice-cold eppendorf tubes, labelled and stored at -80°C.

2.2.2.3. Calculation of protein concentration in lysate

Estimation of protein concentration in cell/tissue lysates was carried out using either Bradford or Lowry assays. Choice of the protein estimation assay depended on the concentration of SDS in the lysis buffer. The Bradford assay is not compatible with RIPA buffer due to the high concentration of SDS, so therefore for the samples which were lysed using RIPA buffer the Lowry method was used for these samples.

For the Bradford assay, 1µl of protein solution was mixed with 1 ml of Bradford Reagent. After mixing several times by inverting the cuvette containing the mixture, optical density (O.D.) readings were measured using a spectrophotometer (Biophotometer, Eppendorf) at 595nm. The concentration of protein was calculated by comparing the O.D. of a standard curve, using a series of volumes (0,1,2,3,4,5µl) of BSA protein. The standard graph was plotted with the help of Microsoft Office Excel which subsequently was used to calculate the final concentration of the tissue/cell protein lysate.

For the Lowry method, 1µl of protein was added into a cuvette containing 1ml of modified Lowry reagent mixed properly by inverting the cuvette. This was kept at room temperature for 10 minutes. 0.1ml of 0.1N Phenol Reagent was mixed, into the solution, by inverting the tube which was incubated at room temperature in the dark for 30 minutes. The O.D. was taken using a spectrophotometer (Biophotometer, Eppendorf) at 750nm. A similar standard curve to the Bradford assay was used.

Chemical	Supplier/ Catalogue number
Protease Inhibitor Cocktail	Calbiochem / 539134
Phosphatase Inhibitor	Sigma Aldrich / P0044
Bradford Reagent	Thermo Fisher Scientific / 23200
BSA protein	Thermo Fisher Scientific / 23209
Lowry Reagent	Thermo Fisher Scientific / 23240
NaCl	Fisher Chemicals / 7647-14-5
NaF	Sigma Aldrich / S7920
EGTA	Melford / E1102
EDTA	Melford / E57020
NP40	Sigma Aldrich / CA-630
Tris-Base	Fisher Scientific / BP152-1
KCl	FSA / P/4280153
Na ₂ HPO ₄	Fisher Chemicals / S/4520/60
KH ₂ PO ₄	Sigma Aldrich / P5655

Table 2.4 List of the chemicals and reagents used in preparation of protein lysate and estimation of protein concentration.

2.2.3. SDS-polyacrylamide gel electrophoresis

Table 2.8 contains detailed list of the chemicals and reagents used.

Appropriate percentages of SDS-gels, with 5% stacking gels, were prepared fresh (Table 2.5). The composition of the 5% stacking gel is as follows: 2.1ml of H₂O, 0.5ml of 30% [v/v] acrylamide, 380 μ l of 1M Tris-HCL at – pH 6.8, 30 μ l of 10% [w/v] SDS, 30 μ l of 10% [w/v] APS and 3 μ l of TEMED. Gels were prepared in a Miniprotean III cell (BioRad). After preparation, the gel was fitted into a cassette, and inserted into a running tank which was subsequently filled with electrophoresis buffer (pH 8.3) (192mM glycine, 25mM Tris-base, 0.1% [w/v] SDS). Protein lysates were thawed and were diluted to 1mg/ml concentration with 1X SDS loading buffer (1.0ml of 0.5M Tris-HCl – pH6.8, 3.0ml H₂O, 1.6ml of 10% [w/v] SDS, 0.4ml of 0.5% [w/v] Bromophenol blue, 1.6ml of glycerol, 0.4ml β -mercaptoethanol (100% stock)). Prior to loading, all diluted protein lysates were incubated at 95°C for 10 minutes. 15 μ l of each protein sample was loaded into each well, all samples were adjacent to a well containing 5 μ l of pre-stained molecular weight SDS-PAGE protein markers. Samples were electrophoresed at 100V until all the samples were aligned at the bottom of the stacking gel. Then voltage was then changed to 120V, and samples were run until the blue dye reached the bottom of the gel.

gel%	6	8	10	12
H ₂ O (ml)	5.3	4.6	4	3.3
30% Acrylamide (ml)	4.6	2.7	3.3	4.0
1.5M Tris-HCL, PH 8.8 (ml)	2.5	2.5	2.5	2.5
10% SDS (ml)	0.1	0.1	0.1	0.1
10% APS (ml)	0.1	0.1	0.1	0.1
TEMED (μ l)	8	8	8	8
Size of the protein (kDa)	55-200	36-97	22-66	14-50

Table 2.5 Detailed formulation of the SDS-PAGE gels used in the experiments.

2.2.4. Western-blot Semi-dry transfer

Nitrocellulose membrane of 0.2 μ m thickness was soaked in transfer buffer (192mM glycine, 25mM Tris, 0.01% [w/v] SDS, 20% [v/v] Methanol) before transfer. Semi-dry transfer blot (BioRad) was used to transfer the proteins from the SDS-PAGE gel onto the membrane as per manufacturer's instructions. 3mm blotting paper was pre-soaked in the transfer buffer, and placed on the blotting machine. Air bubbles were removed by rolling a stripette on the wet paper. The wet membrane was placed on top of the paper and air bubbles were removed. The gel was taken out of the tank and, using a gel opener, the glass panes were opened. Using a scalpel, the stacking part of the gel was cut off. The gel was lifted carefully, briefly dipped into the transfer buffer, and placed on top of the nitrocellulose membrane. Air bubbles were pushed out carefully from the space between the gel and membrane. One layer of pre-soaked 3mm blotting paper was placed on top of the gel. Once again, air bubbles were removed using a stripette. The blotting machine was assembled and proteins were transferred into nitrocellulose membrane at 12V for 1 hr and 10 minutes.

2.2.5. Immunostaining of western blots

Membranes were blocked in 5% [w/v] BSA (Sigma Aldrich, A3059) or in 5% milk [w/v] made in TBST (pH 7.4) (20mM Tris-HCl, 150mM NaCl, 0.1% [v/v] Tween-20) for 90 minutes (choice of blocking agent depended on the nature of the protein intended for detection), followed by incubation with a suitable antibody diluted in 5% BSA or 5% milk over night at 4°C on the shaker. Information regarding the concentration and suitable diluent for each antibody was found in the data sheets sent by each company (Table 2.6). The following day, the membrane was taken out of the antibody solution; it was then washed in TBST, 3 times with gentle shaking for 10 min each, and then incubated with a suitable secondary antibody (1:5000) at room temperature for 1 hour (Table 2.7), followed by TBST washes 3 times with gentle shaking. The products of this procedure were visualised using SuperSignal West Pico Chemiluminescent substrate kit. Two reagents in the kit were mixed at an equal ratio and placed on

the membrane for 4 minutes. Membranes were placed in between clear plastic sheets in a cassette and were exposed to Autoradiography film in the dark room.

Antibody	Size (kDa)	Species	Dilution	Diluent	Supplier /Catalogue number
BRAF	90	Mouse	1:1000	5% milk	Santa Cruz / sc-5284
p-ERK1/2	42-44	Rabbit	1:500	5% BSA	Cell Signaling / 9101S
p-MEK1/2	45	Rabbit	1:500	5% BSA	Cell Signaling / 9154S
ERK2	42	Mouse	1:1000	5% milk	Santa Cruz / sc-1647
DUSP6	37	Rabbit	1:500	5% milk	Abcam / Ab76310
p-GSK3 α	51	Rabbit	1:1000	5% BSA	Cell Signaling / 9316
p-GSK3 β	46	Rabbit	1:1000	5% BSA	Cell Signaling / 9323
p-GSK3 α/β	46,51	Rabbit	1:1000	5% BSA	Cell Signaling / 9331
pp-70S6K	70-85	Mouse	1:1000	5% BSA	Cell Signaling / 9206
pp-90RSK	90	Rabbit	1:1000	5% BSA	Cell Signaling / 9346
RSK1/2/3	90	Rabbit	1:1000	5% milk	Cell Signaling / 9355
β -catenin	88-94	Rabbit	1:10000	5% milk	Sigma Aldrich / C2206
p-AMPK α	62	Rabbit	1:500	5% BSA	Cell Signaling / 2535
AMPK α	62	Rabbit	1:1000	5% milk	Cell Signaling / 2603
ACC	280	Rabbit	1:1000	5% milk	Cell Signaling / 3676
p-ACC	280	Rabbit	1:1000	5% BSA	Cell Signaling / 3661
α -Actin	47	Mouse	1:5000	5% milk	Sigma Aldrich / A5228
p-AKT	60	Rabbit	1:1000	5% BSA	Cell Signaling / 4060

Table 2.6 List of primary antibodies used for immunoblotting.

Species	Supplier / Catalogue number
Rabbit HRP	Sigma / A6154
Mouse HRP	Sigma / A4416

Table 2.7 List of secondary antibodies used for immunoblotting.

Chemical	Supplier/ Catalogue number
30% Acrylamide-Bis	National Diagnostics / EC-890
Tris-base	Fisher Scientific / BP152-1
SDS	Melford / L22040
APS	Melford / A1512
TEMED	Fisher Bioreagents TM / BP150-20
Glycin	VWR / 10119CV
Bromophenol Blue	Raymond A LAMB / Batch 2600
Mercaptoethanol	Sigma Aldrich / M7522
Prestained Protein Ladder	Thermo Scientific / 26619
Nitrocellulose Membrane	Amersham / 10600043
Whatman paper	GE Healthcare Life Science / 4G426994
Methanol	Provided by Department of Chemistry
BSA	Sigma Aldrich / A3059
Milk Powder	MARVEL Original
Tween-20	Fisher Scientific / BP337-500
Chemiluminescent Substrate Kit	Thermo Fisher Scientific / 34580
Autoradiography Film	UltraCruz TM / SC-201696

Table 2.8 List of the chemicals and reagents used for SDS-polyacrylamide gel electrophoresis.

2.2.6. Genotyping

A list of chemicals and reagents is provided in Table 2.10.

2.2.6.1. DNA extraction from tissue

Tissue samples (ear snips) were collected and each sample was incubated with 100 μ l of GNTK buffer (50mM KCl, 10mM Tris-HCl – pH 8.3, 2.5mM MgCl₂, and 0.1mg/ml gelatin) supplemented with 40ng of Protease K and heated at 65°C for 2 hours; this was followed by heat inactivation step at 95°C for 10 minutes. The DNA samples were stored at 4°C.

2.2.6.2. Polymerase Chain Reaction (PCR)

To check the genotype of mice, PCR was performed in a final volume of 20 μ l composed of 16 μ l of 1X MyTaq™ Red Mix PCR master mix, 40nM of each primer listed in Table 2.9, and 2 μ l of DNA. The reactions were carried out in a G-Storm™ PCR machine. PCR conditions were as follows:

Name of gene	GSK3α V600E BRAF	AhCreER¹ and Villin-CreER¹ GSK3β
Heated Lid	112°C	112°C
Hot start	95°C - 2 minutes	95°C - 4 minutes
Strat cycle	94°C - 15 seconds	94°C - 20 seconds
	60°C - 15 seconds	60°C - 20 seconds
	72°C - 15 seconds	72°C - 25 seconds
End cycle	72°C - 5 minutes	72°C - 5 minutes
No of cycles	30	25

2.2.6.3. Recombination check for BRAF^{LSL-V600E/WT}

All mice carcasses were subjected to a check for ^{V600E}*BRAF* recombination, generating the Lox allele. The 20 μ l reaction volume was composed of 16 μ l of 1x MyTaqTM Red Mix PCR master Mix, 40nM of each primer listed in Table 2.9 and 2 μ l of DNA samples with the following condition:

Heated Lid	112°C
Hot start	95°C - 2 minutes
Start cycle	94°C - 15 seconds
	60°C - 15 seconds
	72°C - 15 seconds
End cycle	72°C - 5 minutes
No of cycles	30

Gene name	Primers	Sequence
^{S9A} <i>Gsk3β</i>	OCP 976 OCP 977	5' TCA-CTG-GTC-TAG-GGG-TGG-TGG-AGG-3' 5' GGA-GTC-AGT-GAC-AAC-ACT-TAA-CTT-3'
<i>AhCreER^l / Villin-CreER^T</i>	OCP 361 OCP 362	5' GCC-TGG-TCT-GGA-CAC-ATG-CC-3' 5' GTG-TCA-GCA-TCC-AAC-AAG-GC-3'
<i>BRAF^{LSL-V600E/W1}</i>	OCP 125 OCP 137 OCP 143	5' GCC-CAG-GCT-CTT-TAT-GAG-AA-3' 5' GCT-TGG-CTG-GAC-GTA-AAC-TC-3' 5' AGT-CAA-TCA-TCC-ACA-GAG-ACC-T-3'
^{S21A} <i>Gsk3α</i>	OCP 974 OCP 975	5' TTG-AAG-TGG-CTG-GTA-CTG-GCT-CTG-3' 5' GTG-TGC-TCC-AGA-GTA-GTA-CCT-AGC-3'
<i>BRAF LSL Recombination</i>	OCP 125 OCP143	5' GCC-CAG-GCT-CTT-TAT-GAG-AA-3' 5' AGT-CAA-TCA-TCC-ACA-GAG-ACC-T-3'

Table 2.9 List of primers used for genotyping.

Chemical	Supplier/ Catalogue number
KCl	FSA / P/4280153
Tris-Base	Fisher Scientific / BP152-1
MgCl ₂	Fisher Scientific / M10550153
Gelatin	Sigma Aldrich / 1001551566
Protease K	Sigma Aldrich / P2308
MyTaq™ Red Mix PCR Master Mix	BIOLINE / BIO-25044
1Kb Plus DAN Ladder	Invitrogen / 10787-026

Table 2.10 List of the chemicals and reagents used in genotyping.

2.3. Mouse breeding and Cre recombinase induction

Mice containing the heterozygous mutation for *AhCreER*^{T0/WT}/*Villin-CreER*^{T0/WT} alleles, *BRAF*^{LSL-V600E/WT} (Mercer et al., 2005), or alleles with the serine mutations in *Gsk3α*^{WT/S21A} and *Gsk3β*^{WT/S9A} (McManus et al., 2005) were intercrossed to gain litters expressing two or more alleles. Mice are fed with Labdiet (<https://www.labdiet.com/Products/StandardDiets/Rodents/index.html>) purchased from IPS. Mice were bred using 5LF5 (EU Rodent Diet 22%) and then maintained on 5LF2 (EU Rodent Diet 14%). Mice were maintained on a 7-7 light cycle (7 a.m. to 7 p.m.), the room temperature is maintained at 21°C +/- 2° with 55% +/- 10% humidity. Animals are housed in IVCs, so each cage is supplied with its own HEPA filtered sterile air.

Mice were genotyped using DNA from ear snips. Details of the strains and breeding strategy will be elaborated in the results chapter. Table 2.12 contains the list of reagents used.

Overall, tissue from 147 mice were used for this thesis.

2.3.1. Cre recombinase induction

Recombination of the ^{V600E}*Braf* LSL cassette was achieved by Cre recombinase, whose activity was dually regulated by β-Naphthoflavone and tamoxifen for the *AhCreER*^T model, and with just tamoxifen for the *Villin-CreER*^T model. β-Naphthoflavone was dissolved in pre-heated corn oil at 80 mg/ml at 100°C with continuous vortexing. Tamoxifen was prepared sterile in pre-heated sunflower oil at 100mg/ml and incubated at 65°C with occasional vortexing for an hour (until fully dissolved). Both drugs were aliquoted and stored at -20°C. Both drugs were injected into the abdominal cavity of mice between 8-12 weeks old. Injections were carried out by trained technicians in the Pre-Clinical Research Facility (PRF), University of Leicester. In the case of *AhCreER*^T, 200μl of β-naphthoflavone (8mg/ml) was given 24 hours prior to the 200μl i.p injection of tamoxifen (10mg/ml), whereas for the *Villin-CreER*^T model, mice received 200μl of tamoxifen i.p for 3 consecutive days. Mice were harvested 3

days after the last injection for short-term study and, for the long-term study, they were kept until they showed symptoms requiring them to be humanly terminated. According to our Home Office Project License, animals should be culled if they show signs of ill health such as piloerection and hunched posture, inactivity or inappetence for a period of 48 hours, also if animals show more serious clinical signs such as diarrhoea or dyspnoea should be terminated. All mice received 200 μ l of 20mM 5-Bromo-2'-deoxyuridine (BrdU) 3 hours prior to termination.

2.3.2. Inhibitor treatment of mice

Animals subjected to inhibitor treatment received two injections of 200 μ l tamoxifen (10mg/ml) on two consecutive days (at the same time) followed by 3 injections of freshly prepared inhibitor/carrier (Table 2.11) on three consecutive days exactly at the same time (24hrs intervals). On the last day of injection, each animal received 200 μ l of BrdU (20mM) 3 hours prior to humane culling. Carriers were prepared in the same way as their respective drug, the only difference was that the carrier does not contain the drug itself. PD184352 was prepared in 10% [v/v] DMSO, 10% [v/v] Cremophor EL, and 80% [v/v] distilled H₂O. All freshly prepared drugs were stored on ice and transferred into the PRF unit for injection on daily basis. From the total of 129 mice, 40 were used for the drug study.

Inhibitor	Concentration	Supplier/ Catalogue number	Carrier
PD184352	200mg/kg/day	Sigma Aldrich/ PZ0181	10% DMSO + 10% Cremophor +80% Distilled H ₂ O

Table 2.11 Inhibitor name and concentration used in animal study.

Chemical	Supplier/ Catalogue number
β -Naphthoflavone	Sigma Aldrich / N3633
Tamoxifen	Sigma Aldrich / 10540-29-1
BrdU	Sigma Aldrich / B5002
Cremophor EL	Callbiochem / 238470
DMSO	Sigma / D2650

Table 2.12 List of the reagents used in *in vivo* studies.

2.4. Histology

Table 2.15 contains details of the chemicals and reagents used.

2.4.1. Mouse tissue harvesting

Mice were humanly sacrificed following Home Office guidelines by trained technicians in the PRF unit. The entire GI tract (small and large intestines) was removed, rinsed in and flushed with 1X PBS. The length of the small intestine was measured and subsequently cut into 6 equal sections; they were numbered 1 to 6 with number 1 being the closest to caecum, 6 closest to stomach and the large intestine being number 7. A few small pieces of each section were cut and stored appropriately for RNA and protein extraction. The remainder was then cut open, swiss-rolled, and fixed in 10X volume of 4% [w/v] paraformaldehyde (PFA), 80mM Na₂HPO₄, 20mM NaH₂PO₄, and kept on the shaker at low speed for 24 hours at room temperature. After 24 hours of fixation, the PFA was removed and fixed tissues were submerged in 10X volume of 70% [v/v] ethanol and kept on the shaker for 2-3 hours at room temperature, and were then placed at 4°C.

2.4.2. Tissue processing

Tissues were infused with wax using a Shandon Citadel 2000 according to the manufacturer's protocol, by Mrs. J. Edwards (MRC Toxicology Unit, Leicester), followed by tissue embedding in wax. Pieces of tissue were placed in a metal case, in the correct orientation, covered with hot wax, and placed on a cold surface resulting in formation of solid blocks.

2.4.3. Pre-treatment of glass slides (Subbing)

Glass slides (VWR, 631-0907) were placed into polyacetyl racks and were soaked overnight in 5% [v/v] Decon. Slides were washed under hot running tap water for 30 minutes, rinsed in MilliQ H₂O five times for 5 minutes each time. Slides were dried in a 60°C oven, then submerged and agitated in subbing solution (2% [v/v] 3-aminopropyltriethoxysilane in acetone) for 2 minutes, and then placed in acetone twice for 2 minutes each time. Slides were rinsed twice in H₂O for 2 minutes. For the final step, slides were dried in a 60°C oven overnight.

2.4.4. Sectioning of wax embedded tissue samples

Paraffin blocks were kept at 4°C until they were completely cold, and then kept on a piece of tissue on top of ice; they were subsequently sectioned by Mrs. S. Giblett using a Leica RM2135 microtome. The sections were transferred into a 40°C water bath and then transferred onto pre-treated slides. The slides containing tissue sections were placed in a polyacetyl rack and then in a 37°C oven to dry.

2.4.5. Hematoxylin and Eosine (H&E) staining

The slides were placed into a polyacetyl rack and dewaxed (rehydration) by submerging into two consecutive tanks of xylene, followed by two tanks of 100% [v/v] ethanol, one tank of 90% [v/v] ethanol, and finally one tank of 70% [v/v] ethanol (slides were treated for 10 minutes at each stage). Racks containing slides were submerged into water, washed under a narrow stream of tap water for 3 minutes, and then submerged into Hematoxylin for 5 minutes. Then samples were placed in water and kept under a narrow stream of running tap water for 3 minutes (until the water was clean), and then submerged into a tank of 1% [v/v] acid alcohol (70% [v/v] ethanol, 1% [v/v] HCl) for 10 seconds to remove excess staining. The slides were washed under running tap water for 3 minutes (until the sections appeared blue). 1% [v/v] Eosin was used to stain the

cytoplasm for 1 minute. Slides were then submerged in a tank containing tap water and immediately subjected to dehydration by placing it into 70% [v/v] ethanol for 30 seconds, followed by two tanks of 100% [v/v] ethanol and two tanks of xylene for 5 minutes each. The slides were mounted with DPX. After drying, slides were observed under a Leica microscope (DM5000B), and photographed using a Leica DFC 420C camera. Pathological analysis of the sections was carried out by Professor Kevin West (University Hospital Leicester, NHS Trust).

2.4.6. Immunohistochemistry

Slides were placed into a polyacetyl rack and dewaxed by placing into two consecutive tanks of xylene, followed by two tanks of 100% [v/v] ethanol. Slides remained in each tank for 10 minutes. They were then submerged in 2% [v/v] hydrogen peroxide in methanol for 15 minutes to block endogenous peroxidases. Antigen retrieval was done by boiling the slides in pre-heated 10mM tri-sodium citrate buffer (10mM sodium citrate in dH₂O – pH 6.0 with acetic acid) for 20 minutes in a pressure cooker. Slides were left to cool down for at least 15 minutes in the same liquid, washed in 1X PBS (137mM NaCl, 8mM Na₂HPO₄, 2mM KH₂ PO₄, 2.7 mM KCl – pH 7.4), 3 times for 10 minutes each on a shaker at room temperature. Sections were marked by a hydrophobic PAP pen (ABcam) prior to incubation in 10% [v/v] swine serum that was diluted in 1X PBS for 1 hour at room temperature. Samples were then incubated with specific primary antibodies diluted in serum/PBS which was used for blocking overnight at 4°C (Table 2.13). The following day, samples were washed in 1X PBS 3 times, for 10 minutes each, and were then incubated with the secondary antibody (Table 2.14) 1:500 in serum/PBS solution, at room temperature for an hour. This was followed by 3 times 1X PBS washes for 10 minutes each. Sections were incubated in tertiary antibody Streptavidin-HRP, for 30 minutes and then once again washed 3 times in 1X PBS for 10 minutes each. Samples were incubated with DAB Peroxidase substrate kit in MilliQ H₂O, as instructed by the manufacturer, for up to 5 minutes depending on how fast the brown colour appeared and the intensity of the colour. Subsequently, slides were

washed in tap water on the shaker. Samples were processed through a round of dehydration in 70% [v/v] ethanol for 5 minutes, 90% [v/v] ethanol for 5 minutes, 2X 100% [v/v] ethanol and 2X of xylene for 10 minutes each. Finally, slides were mounted with DPX mounting solution.

2.4.7. Nuclear β -catenin IHC

Slides were placed into a polyacetyl rack and dewaxed by placing them successively into two consecutive tanks of xylene, followed by two tanks of 100% [v/v] ethanol and two tanks of 90% [v/v] ethanol. They were then submerged in 30% [v/v] hydrogen peroxide in 400ml of methanol for 30 minutes to block endogenous peroxidases. Slides then were washed in 90% [v/v] ethanol and were subsequently transferred and kept into 70% [v/v] ethanol for 10 minutes. Slides were washed in H₂O 3 times for 10 minutes each. Slides were then kept in preheated (10 minutes at 900W in microwave) TEG buffer (pH 9) (1.2gm Tris, 0.2gm EGTA in 1 liter of water) for 10 minutes and were subsequently left to cool down on a shaker at RT. Samples were then kept for 30 minutes in 50mM NH₄Cl (2.67gm NH₄Cl in 1 liter of PBS) on a shaker at RT. Tissue sections were marked by a hydrophobic PAP pen (ABcam) prior to three successive incubations with “wash 1” (1gm BSA, 0.05gm Saponin, 70ml PBS, 20ml of 1% [v/v] gelatine and was made up to final volume of 100ml with PBS), each wash was 10 minutes. Tissue was incubated overnight with β -catenin (1:1000) primary antibody (Table 2.13) diluted in the diluent (0.1% [w/v] BSA, 0.3% [v/v] Triton X-100 in PBS) at 4°C. On the subsequent day slides were washed 3 times with “wash 2” (0.1gm BSA, 0.05 gm Saponin, 70ml PBS, 1% [v/v] gelatine 20ml, and made up to final volume of 100 ml with PBS) for 10 minutes each time. Slides then, were incubated in Biotinylated host directed secondary antibody (1:200) (Table 2.14) for 1 hour at RT. “Wash 2” was used to wash samples 3 times, for 10 minutes each. Tissue was incubated with streptavidin-peroxidase for 30 minutes and were subsequently washed by “wash 2” twice, for 5 minutes each. Samples were incubated with the DAB Peroxidase substrate kit in MilliQ H₂O, as instructed by the manufacturer, for up to 5 minutes depending on how fast the brown colour appeared and the

intensity of this colour. Subsequently, slides were washed in tap water on the shaker. Samples were processed through a round of dehydration in 70% [v/v] ethanol for 5 minutes, 90% [v/v] ethanol for 5 minutes, 2X 100% [v/v] ethanol and 2X of xylene for 10 minutes each. Finally, slides were mounted using DPX mounting solution.

Primary Antibody	Catalogue Number	Species	Dilution	Serum	Supplier / Catalogue Number
BrdU	Cell Signaling / 5292	Mouse	1:100	Goat Serum	Dako / X0907
p-histoneH3	Cell Signaling / 9101	Rabbit	1:100	Swine Serum	Dako / X0901
p-ERK	Cell Signaling / 9101S	Rabbit	1:100	Swine Serum	Dako / X0901
β -Catenin	Sigma Aldrich / C2206	Rabbit	1:1000	Swine Serum	Dako / X0901

Table 2.13 Details of primary antibodies used for immunohistochemistry.

Species	Supplier / Catalogue number
Polyclonal Swine Anti-Rabbit	DAKO / E0353
Polyclonal Goat Anti-Mouse	DAKO / P0447

Table 2.14 List of secondary antibodies used for immunohistochemistry.

Chemical	Supplier / Catalogue number
PFA	Sigma Aldrich / P6148
Ethanol	Provided by Department of Chemistry
Glass Slide	VWR / 631-0907
Decon	Medline / R36138
Acetone	Fisher Chemicals / UN1090
Hematoxyline	Sigma Aldrich / GH S-132
Eosine 1% Aqueous	RA LAMB / 9619
HCl	Fisher Chemicals / H/1200/PB15
Xylene	Fisher Chemicals / UN1307
DPX	Sigma Aldrich / 44581
Hydrogen Peroxide	Sigma Aldrich / H1009
Tri-Sodium Citrate	Fisher Chemicals / S/3320/60
Acetic Acid Glacial	Fisher Chemicals / A/0400/P1317
NaCl	Fisher Chemicals / 7647-14-5
KCl	FSA / P/4280153
Saponin	Sigma / S-4521
NH ₄ Cl	Sigma / A4514
Streptavidin-HRP	Vector Laboratories / SA5704
DAB Peroxidase Substrate Kit	Vector Laboratories / SK4100

Table 2.15 List of the chemicals and reagents used in histology.

2.5. Statistical Analysis

Statistical analysis was collectively done by Dr. M. Viskuduraki and I. I performed unpaired and multiple T-tests to analyse the effect of genotype on crypt cell number, cell proliferation and animal survival.

Dr. Viskuduraki performed linear regression analysis to explore the effect of genotype on tumour (macroscopic + microscopic) formation, tumour size/stage and location while taking age into consideration.

2.6. Microarray assay

2.6.1. Tissue preparation for RNA extraction

2-3 small pieces of each section of intestinal tissue were freshly cut from animals, and kept in a 5ml labelled eppendorf tube containing RNAlater solution (Invitrogen, AM7021). Samples were kept at room temperature for 2 hours and then were transferred to -20°C for permanent storage.

2.6.2. RNA extraction from tissue sections and Microarray

Tissue from section 4 of the small intestine of 4 groups of mice, each group containing 6 mice, was subjected to experimentation: a) $Gsk3\alpha^{S21A/S21A}$; $Gsk3\beta^{S9A/S9A}$; $Villin-CreER^{T0/WT}$ (WT/Cre/Ki/Ki), b) $Braf^{L-SL-V600E/WT}$; $Villin-CreER^{T0/WT}$ (BVE/Cre), c) $Gsk3\alpha^{S21A/S21A}$; $Gsk3\beta^{S9A/S9A}$; $Braf^{L-SL-V600E/WT}$; $Villin-CreER^{T0/WT}$ (BVE/Cre/Ki/Ki), and the control group d) $Villin-CreER^{T0/WT}$ (WT/Cre). Each experimental group was composed of 3 males and 3 females. Tissues were handed to the Genomic Core Facility, Core Biotechnology service, University of Leicester. RNA extraction and microarrays assay were carried out by Dr. Spencer Gibson and Dr. Nicolas Sylvius. High quality RNA was subjected to microarray, using RNA Labelling and hybridization to SurePrint G3 Mouse Gene Expression v2 8x60K Microarray Kit (Agilent, G4852B). RNA extraction, microarray slide preparation and processing for all the samples were carried out simultaneously over 5 days. Samples consisted of 4 groups from different genetic background. Each group consisted of 6 biological replicates (equal number of male and female) to ensure high quality data. Figure 2.1 shows a simplified diagram of the microarray sample preparation and processing.

<http://www.genomics.agilent.com/literature.jsp?crumbAction=push&tabId=AG-PR-1118&contentType=User+Manual>

Results were subjected to bioinformatics analysis by Dr. Jin-Li Luo, Leicester Cancer Research Centre (LCRC), University of Leicester.

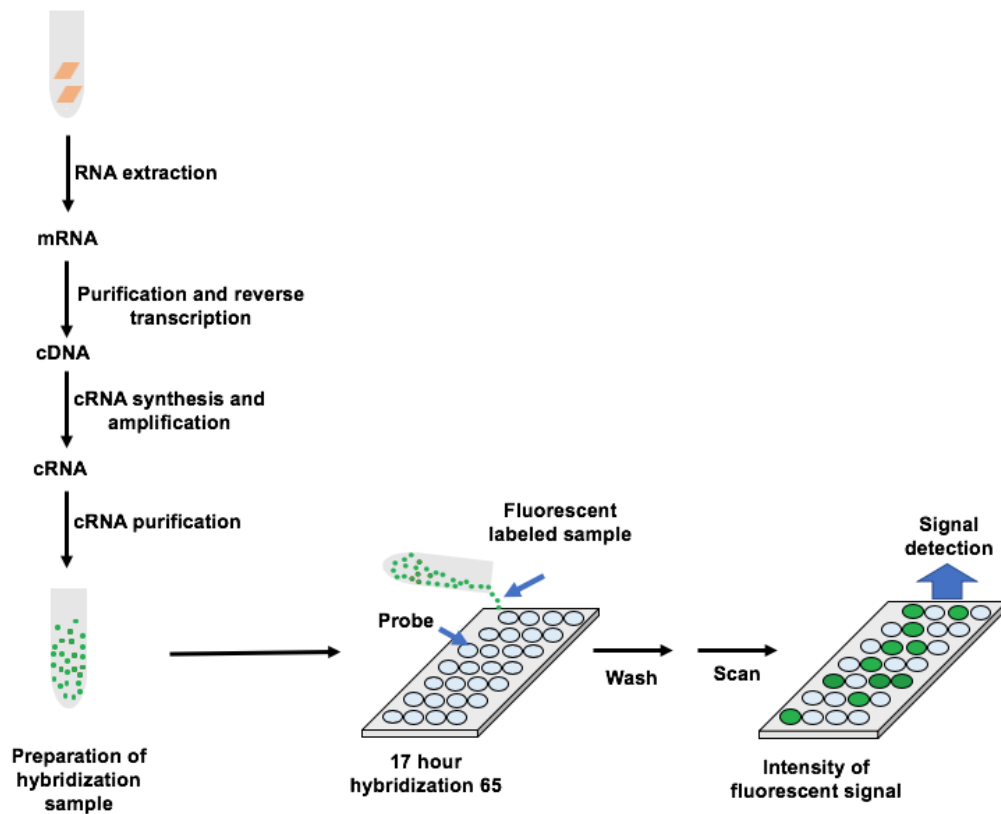


Figure 2.1 Schematic diagram showing the microarray gene expression analysis. Tissue sections were subjected to RNA extraction on a Promega Maxwell 16 Robot using the Promega simplyRNA cell purification Kit. RNA quality was checked using Agilent Bioanalyzer 2100 (with RNA Integration Number (RIN) of >7). 100ng of total RNA was subjected to reverse transcription and converted into complimentary RNA (cRNA). cRNA was then labelled with Cy3 using Agilent QuickAmp Labeling Kit One-Color, followed by labelled cRNA hybridisation overnight at 65°C onto a SurePrint G3 Mouse Gene Exp v2 Array which allows the quantification of ~60,000 transcripts. Microarrays were scanned using Agilent Microarray C-scanner. Raw data extraction and quality check was performed using Agilent feature extraction software 10.5.11.

Chapter 3. Investigation of the crosstalk between the MAPK and GSK3 pathways in ^{V600E}*BRAF* mutant cell lines

3.1. Introduction

^{V600E}*BRAF* mutation is the driver of sessile serrated colorectal cancer; it is detected in ~ 10% of patients and is associated with shorter overall survival and progression free survival compared to other CRCs. BRAF inhibitors are proven to be effective in melanoma patients carrying the ^{V600E}*BRAF* mutations but are not effective in CRC patients, due to resistant mechanisms that are a result of the activation of EGFR receptors on CRC cancer cells (Prahallad et al., 2012). On the other hand, intestinal tissue homeostasis and renewal depends on WNT pathway activation (Mah et al., 2016). We have previously detected crosstalk between the WNT and MAPK pathways at the level of GSK3 in our ^{V600E}*Braf* mouse models (Carragher et al., 2010). This raises the possibility of targeting GSK3 to manipulate ^{V600E}*BRAF*-driven CRCs therapeutically.

3.1.1. Evidence of crosstalk in ^{V600E}Braf mouse model (*in vivo*)

Published data from mice expressing ^{V600E}BRaf in the GI tract from our lab, showed the presence of crosstalk between the WNT and MAPK pathways in the 3 day p.i. gut tissue (Carragher et al., 2010). Tissue was taken from mice at different times post induction (p.i.) and also some induced animals received the MEK inhibitor PD184352 simultaneously. GSK3 β phosphorylation levels at Ser9 were found to go up significantly at 3 day p.i. which was the stage at which crypt hyperplasia was evident and was reversed in the animals which received PD184352 (Carragher et al., 2010). No changes in AKT phosphorylation were seen but an increase in β -catenin levels in crypts was observed that was reversed by PD184352. Based on this, Carragher et al. concluded that Ser9 phosphorylation of GSK3 is PKB/AKT independent, but induced by the MAPK pathway following ^{V600E}BRaf expression (Carragher et al., 2010).

3.2. Aims

Current research does not address the exact mechanism of crosstalk between the MAPK and WNT pathways which was initially shown by Carragher et al. By having a better understanding of the participant and facilitator proteins, using an *in vitro* system, we would have a better understanding of the early disease which could then inform more complicated model systems. This would also potentially help to unveil potential therapeutic targets. To this end, we used $V^{600E}BRAF$ mutated cell lines and primary cells. Our objectives were:

- To establish a good cell culture system to examine, in more detail, the link between $V^{600E}BRAF$, ERK, GSK3 and β -catenin.
- To identify intermediary kinases involved in phosphorylating GSK3 β at Ser9 in $V^{600E}BRAF$ mutant cells. Candidate kinases, examined here, are p70^{S6K} and p90^{RSK}.

3.3. Results

3.3.1. No correlation between activation of the MAPK pathway and phosphorylation of GSK3 in ^{V600E}*BRAF* mutant human CRC cell lines.

In order to investigate the crosstalk and identify possible intermediary kinases, a good cell culture system was needed. The human CRC cell line (RKO) was chosen for the study and was kindly provided by B. Vogelstein, Johns Hopkins University. RKO is a poorly differentiated colon carcinoma cell line. RKO143 (WT) and RKO144 (VE) are derivatives of the parental RKO cell line generated by homologous recombination (Sur et al., 2009). The parental cell line carries three alleles of the *BRAF* gene out of which two are V600E and one WT whereas RKO143 carries one WT allele and two knocked out alleles. RKO144 contains one V600E and two knocked out *BRAF* alleles.

As a first step, levels of various components of the two pathways were assessed by western blotting. There was an increase in the level of phospho-MEK and phospho-ERK in parental cells as well as RKO144 cells as a result of the ^{V600E}*BRAF* mutation in comparison to WT cells, as expected (Figure 3.1). However, there was no meaningful difference in the level of phosphorylation of GSK3 α/β with the ^{V600E}*BRAF* mutation. β -catenin expression levels also did not change in the presence or absence of ^{V600E}*BRAF* mutation. There was no correlation between changes in phosphorylation level of phospho-p70^{S6K} or phospho-p90^{RSK} and the ^{V600E}*BRAF* mutation. Overall, these data show no evidence of crosstalk between the MAPK pathway and GSK3 in this human CRC cell line.

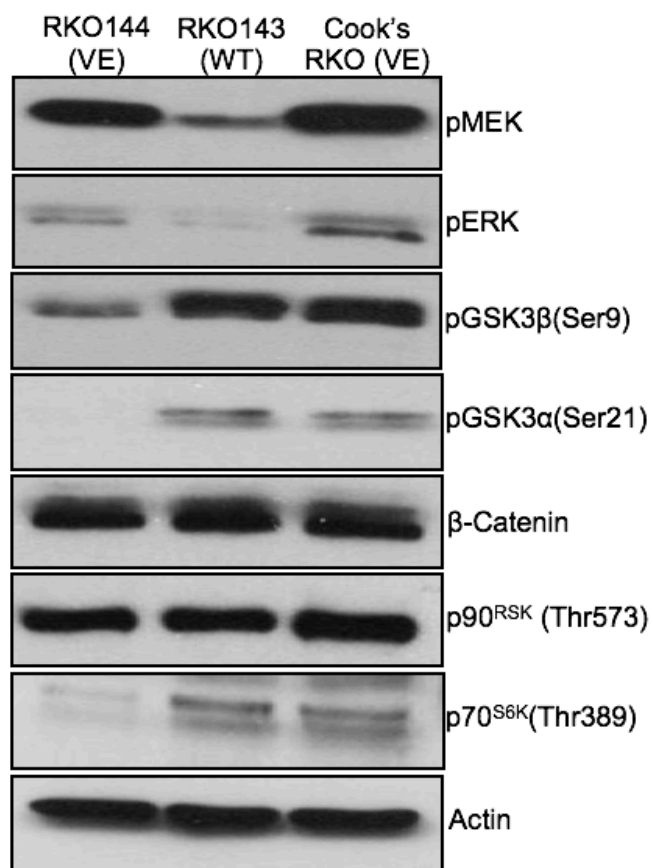


Figure 3.1 Western blot analysis of human CRC cell lines RKO. Activation of the MAPK pathway was observed by an increase in phosphorylation of MEK and ERK with the ^{V600E}BRAF mutation in Cook's RKO, as well as RKO144 cell lines, in comparison to RKO143 which carries the ^{WT}BRAF allele. The above figure is representative of three sets of biological replicates.

3.3.2. ^{V600E}BRAF induced activation of the MAPK pathway increases nuclear β -catenin levels in RKO human CRC cells.

Although the western blot data indicate that overall levels of β -catenin are not changed, the data do not address β -catenin localisation. To study the effect of the ^{V600E}BRAF on β -catenin level, immuno-fluorescent staining of RKO WT and both V600E cell lines was carried out. As shown in Figure 3.2, in WT cells the protein is quite evenly distributed in nuclear and cytoplasmic regions. However, in the presence of the ^{V600E}BRAF mutation there was an accumulation of β -catenin in the nuclear region of the cells and the level of cytoplasmic β -catenin protein seemed to be lower than in WT cells. This was potentially an interesting finding.

In order to further investigate the effect of the MAPK pathway on the sub-cellular localization of β -catenin, the RKO parental cell line was treated with the MEK inhibitor U0126 for a period of 16 or 24 hours (Figure 3.3). Control cells were treated with DMSO, the carrier used in inhibitor preparation. Following 16 hours of treatment with the MEK inhibitor, the distribution of β -catenin was more even throughout the cell; it was present in the nucleus as well as cytoplasm in comparison to the control (DMSO treated) cells which had more nuclear β -catenin than cytoplasmic. Similar results were observed following 24 hours treatment of cells with U0126. These results potentially indicate that the inhibition of the MAPK pathway alters translocation of β -catenin into the nucleus.

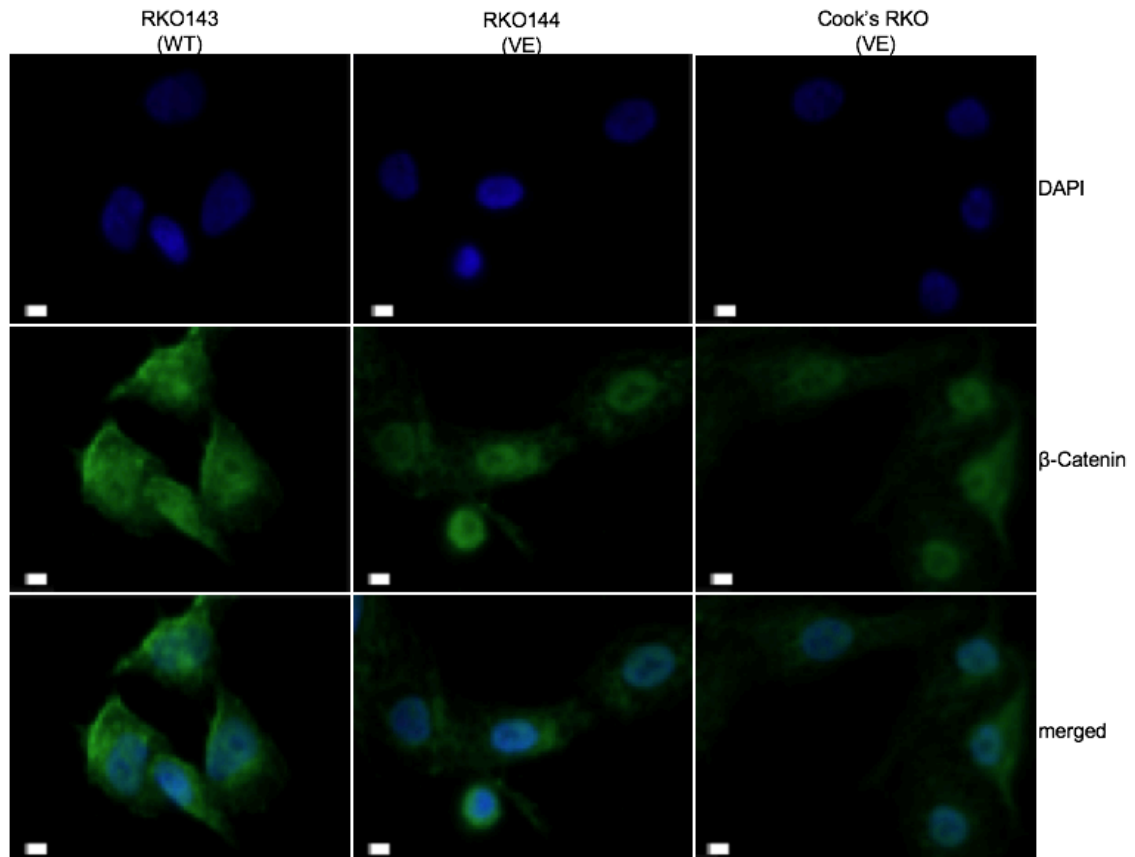


Figure 3.2 Immunostaining of RKO cell lines for subcellular localisation of β -catenin. In the WT cell line, β -catenin is distributed more evenly in the cytoplasm and the nucleus whereas β -catenin protein is more concentrated in the nuclear region in both cell lines with the V600E BRAF mutation. β -catenin immune fluorescence and DAPI were used in this experiment, and the images merged. Scale bars= $150\mu\text{m}$

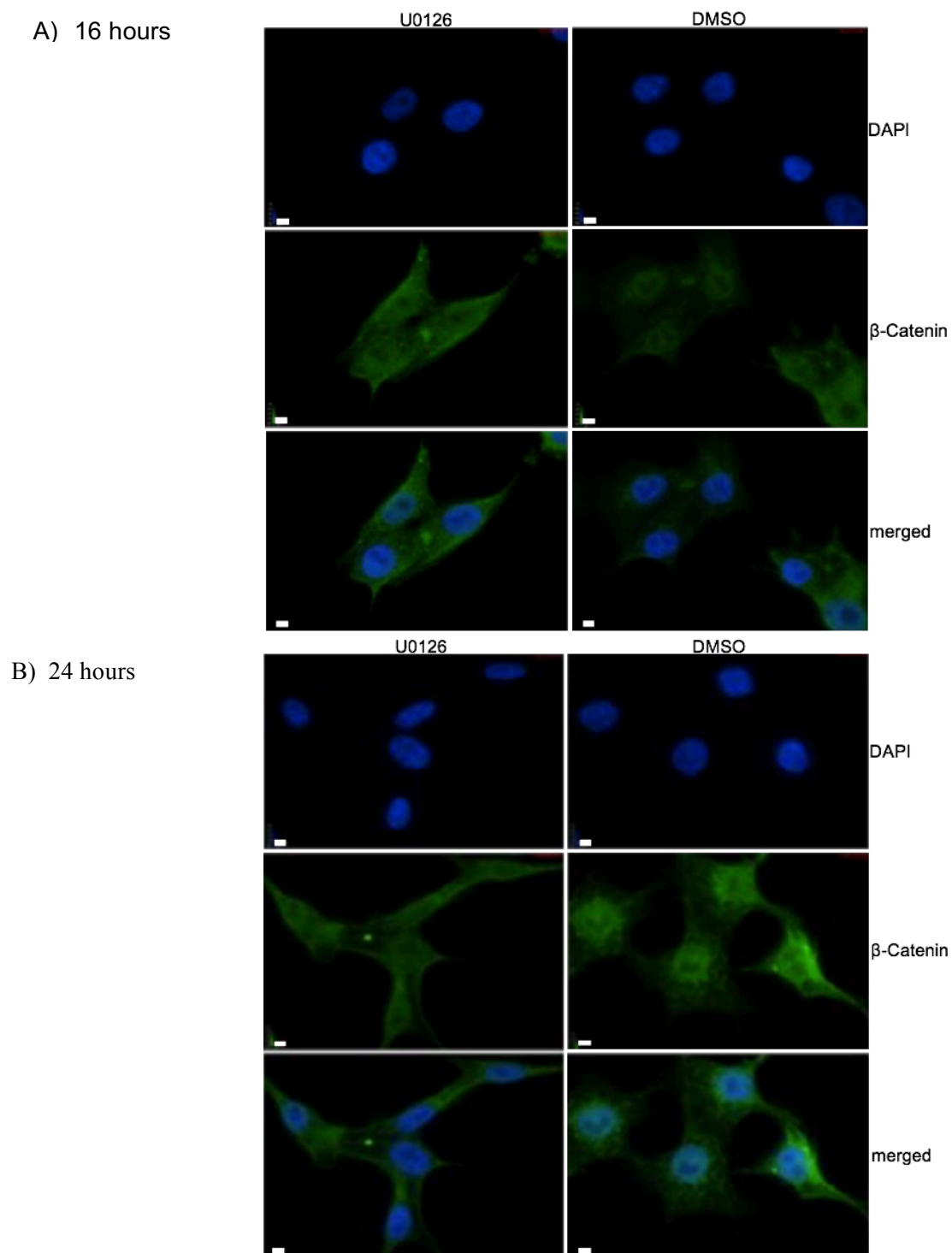


Figure 3.3 Immunostaining of the parental RKO cell line treated with U0126 (MEK inhibitor) for 16 or 24 hours. A) Two sets of cells treated for 16 hours with either U0126 or DMSO, were stained with DAPI or β -catenin antibody. B) Two sets of cells were treated for 24 hours with either DMSO or U0126 and stained with DAPI or β -catenin immunofluorescence and the images were merged. Even distribution of β -catenin throughout the cells after MEK inhibition. Scale bars= 150 μ m.

3.3.3. Investigation of crosstalk in ^{V600E}*Braf* mouse embryonic fibroblasts (MEFs).

In the next attempt to find a suitable *in vitro* model to study the crosstalk, MEFs were used. MEFs with a conditional Cre-regulated ^{V600E}*Braf* mutation were infected with adenoviral Cre, Ad β -gal, or no treatment for 96 hours, and cell lysates were subjected to western blot analysis. Following 96 hours of infection with Ad-Cre, levels of phospho-MEK increased in compare to Ad β -gal infection in ^{V600E}*Braf* cells. However, there was not a consistent change in phospho-ERK levels. This could be attributable to the high levels of DUSP6 expression in Ad-Cre infected MEFs in comparison to Ad β -gal infected MEFs (Figure 3.4). This fits with the result published by Andreadi et al. which showed an increase in expression of phospho-MEK, phospho-ERK and DUSP6 following 96 hours of Ad-Cre infection of ^{V600E}*Braf* MEFs (Andreadi et al., 2012). DUSP6 is a negative feedback regulator of ERK phosphorylation which, when expressed at high levels, de-phosphorylates phospho-ERK (Messina et al., 2011).

No consistent changes were observed in RSK or S6K phosphorylation levels across samples and there was also no change in β -catenin levels. With regard to GSK3 phosphorylation, there was no consistent change in phospho-GSK3 β or phospho-GSK3 α levels. Based on the above data, MEFs do not seem to be a good *in vitro* model to study the crosstalk as there was no meaningful correlation between MAPK activity and GSK3 phosphorylation (Figure 3.4).

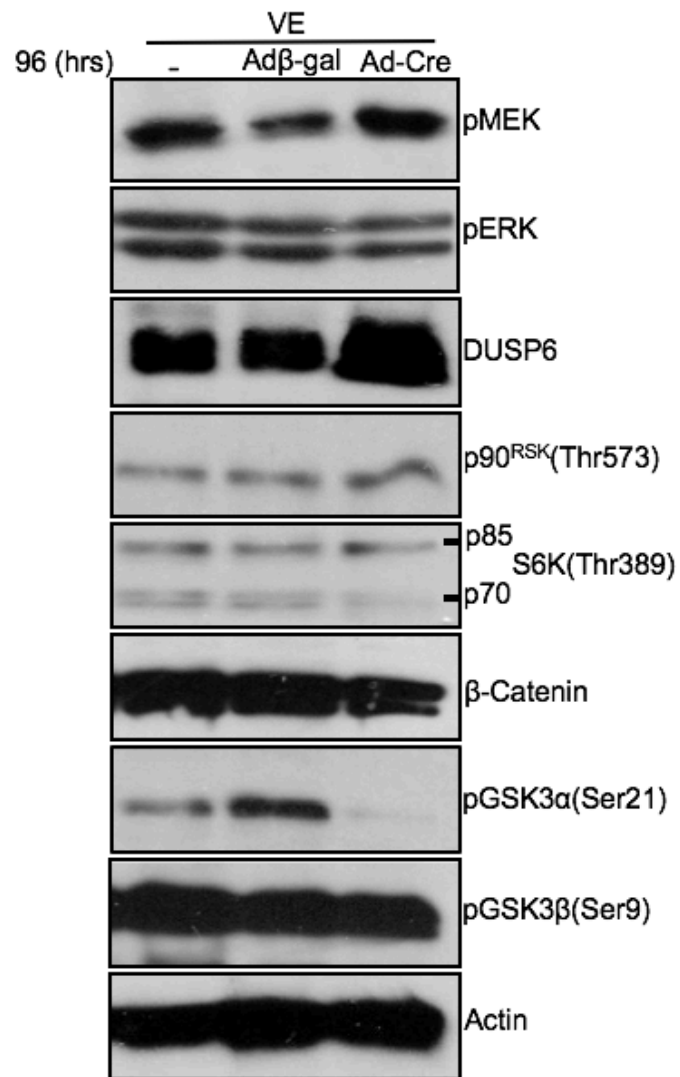


Figure 3.4 Western blot analysis of MEFs with conditional Cre regulated $V600E$ Braf. $V600E$ Braf MEFs were infected with Adenoviral Cre or β -gal for 96 hours. The above figure is representative of three sets of biological replicates.

3.3.4. Crosstalk between MAPK and WNT pathways in lung and melanoma cell lines.

One of the project aims was to establish a cell culture system in order to study the crosstalk in more detail. As the human CRC cell lines did not show any sign of pathway crosstalk, I decided to examine two non-colorectal cancer cell lines with the $V600E$ BRAF mutation: HCC364 (human lung adenocarcinoma cells) and A375P (human malignant melanoma cells). As shown in Figure 3.5, western blot analysis was carried out on the cell lysates prepared from the 3 RKO cell lines, as well as the lung and melanoma cell lines.

In HCC364 cells, MEK, the downstream target of RAF proteins was phosphorylated which in turn activates ERK through phosphorylation. Phosphorylation of MEK and ERK are indicators of MAPK activation which is the result of $V600E$ BRAF expression. High levels of DUSP6 expression, which is a negative feedback regulator of ERK phosphorylation, was also detected. Also, in HCC364 cells, GSK3 β was phosphorylated on Ser9 and β -catenin protein was expressed at high levels. This result indicates that there is potentially a link between activation of the MAPK pathway as a result of $V600E$ BRAF mutation and WNT pathway activation (Figure 3.5). GSK3 α phosphorylation was not detectable. Phosphorylation of p70 $S6K$ was at a low level but phosphorylation of p85 $S6K$ was at a high level, indicating that there was a possibility of S6Kinase participation in the crosstalk through the p85 isoform of S6K.

As shown in Figure 3.5, A375P melanoma cells have a high level of MEK phosphorylation as well as high ERK phosphorylation which is a strong indicator of MAPK pathway activation. DUSP6 was also expressed at high levels in melanoma cells. High levels of GSK3 β phosphorylation at Ser9 were detected as well as GSK3 α phosphorylation at Ser21. β -catenin was expressed at high levels and also there was a high phosphorylation level of p85 $S6K$, while lower levels of p70 $S6K$ phosphorylation. This result indicates that there is a potentially strong crosstalk between the MAPK pathway and the WNT pathway, with possibly the larger p85 isoform of S6K as a mediator.

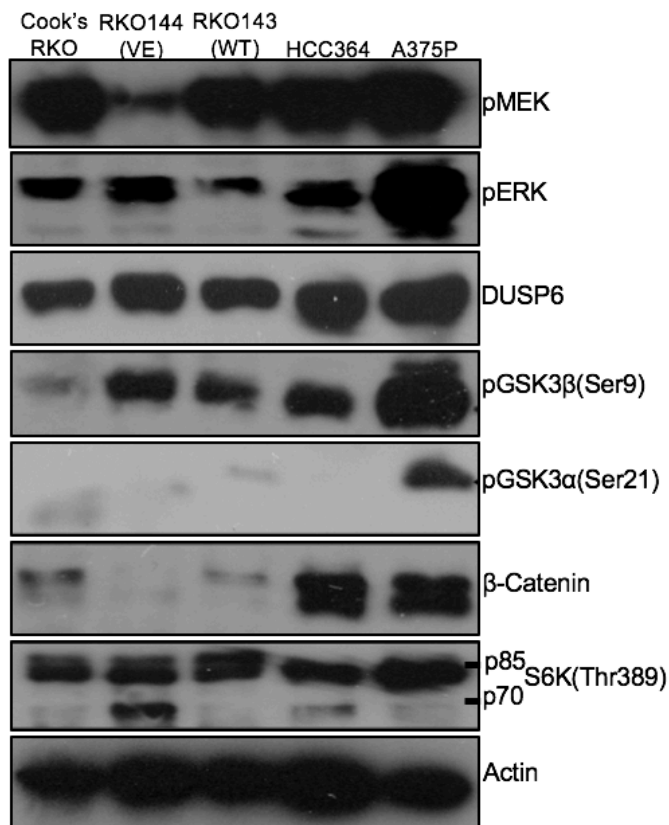


Figure 3.5 Western blot analysis of human cancer cell lines with the $V600E$ BRAF mutation. HCC364 (lung) and A375P (melanoma) cell lines were compared with RKO (colorectal) cancer cell lines. The above figure is representative of three sets of biological replicates.

3.3.5. MEK inhibition in human lung and melanoma cells with ^{V600E}BRAF mutation.

To further investigate the mechanism of the potential MAPK and WNT pathways crosstalk, the human lung and melanoma cell lines were treated with U0126 for both 5 or 24 hours. Cells were lysed and the cell lysates were used for western blot analysis. In the lung HCC364 cells, inhibition of MEK after 5 hours led to the downregulation of the activity of its immediate downstream target ERK, in comparison to control treatment. There was an increase in expression of the DUSP6 protein which can explain the low levels of ERK phosphorylation but suggests that DUSP6 is not a direct target of the ERK pathway in this cell type.

Although there was a significant decrease in activity of the MAPK pathway following 5 hours of inhibitor treatment, there was no correlation with phosphorylation of GSK3 α/β in comparison to control treatment. β -catenin expression levels also did not seem to change significantly after inhibitor treatment. No change was observed in the levels of phosphorylation of S6K or RSK proteins or AKT.

24 hours after treating the cells with U0126, there was a decrease of ERK phosphorylation, in comparison to the control treatment, although there was no difference in DUSP6 expression. Phosphorylation levels of GSK3 α/β and β -catenin levels were not obviously changed. Phospho-AKT or phospho-p90^{RSK} did not seem to change, whereas phospho-p85^{S6K} appeared to decrease in comparison to control treatment (Figure 3.6). Thus, there is no direct effect of ERK pathway on GSK3 phosphorylation or β -catenin levels in these cells. There was a delayed effect on phospho-p85^{S6K} suggesting there may be an autocrine/paracrine component.

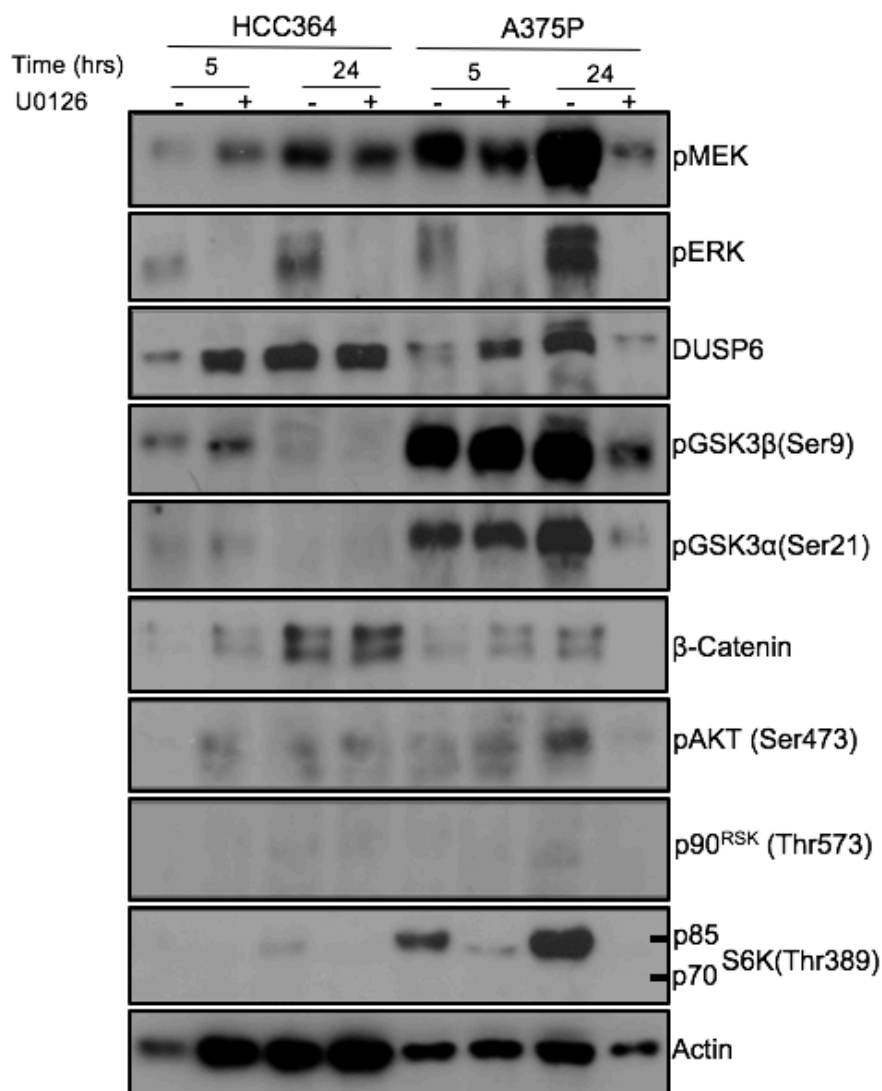


Figure 3.6 Analysis of protein and phospho-protein expression levels associated with the two pathways by western blot in human HCC364 lung and melanoma A375P cell lines treated with U0126 (MEK) inhibitor or DMSO for control cells. U0126 final concentration=10 μ M. The above figure is representative of three sets of biological replicates. "-" = cells treated with DMSO only.

Treatment of melanoma (A375P) cells with the MEK inhibitor for 5 hours reduced levels of phospho-ERK in comparison to the control sample; this was linked with an increase in expression of DUSP6 following 5 hours treatment with U0126 in comparison to control samples. There were no significant changes in the levels of GSK3 α/β phosphorylation, or β -catenin levels, or AKT phosphorylation or p90^{RSK} phosphorylation. Following 24 hours treatment of A375P with the MEK inhibitor, a significant decrease in the levels of phospho-ERK and DUSP6 were observed. GSK3 α/β phosphorylation levels of Ser21/9 decreased and β -catenin expression levels also went down. Phosphorylation of AKT, S6K, and RSK also decreased also after 24 hours. Thus, there is a delayed effect of MEK inhibition on other signalling pathways, possibly indicating an autocrine/paracrine component.

3.3.6. MEK inhibition in melanoma cells with ^{V600E}*BRAF* mutation.

To further confirm the crosstalk in A375P (melanoma) cells, they were treated with PD184352 inhibitor for either of 5 or 24 hours (Figure 3.7). Following 5 hours of MEK inhibition, the complete inhibition of ERK phosphorylation was observed. There was a slight decrease in GSK3 phosphorylation and β -catenin levels compared to the 5 hour DMSO treatment. Phosphorylation of S6K also decreased following 5 hours of treatment with PD184352. After 24 hours, inhibition of ERK phosphorylation was detected and there was also a slight downregulation in GSK3 phosphorylation in comparison to controls. There was no change in the levels of β -catenin. Once again there was a large decrease in p70^{S6K} phosphorylation. Although the separation between the two bands corresponding to both the p70 and p85 isoforms of S6K was not very clear, significant changes in expression seemed to be related to the band corresponding to the larger isoform - p85^{S6K}. Therefore, crosstalk occurs in A375P cells with S6K, particularly the p85 isoform, possibly playing a role as the intermediary kinase.

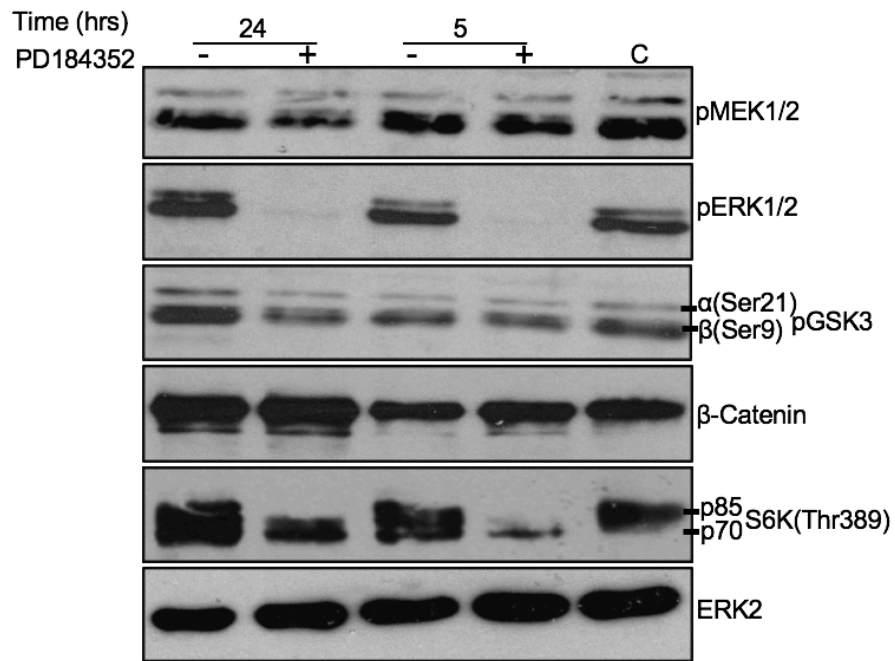


Figure 3.7 Western blot analysis of MEK inhibitor (PD184352) treated human melanoma (A375P) cells. A375P cells were treated with PD184352 for 5 or 24 hours. Control cells were treated with DMSO for 5 or 24 hours. PD184352 final concentration = 1 μ M. C = untreated A375P cell lysate, "-" = cells treated with DMSO only. The figure is representative of three sets of biological replicates.

3.3.7. S6K inhibition in melanoma cells with ^{V600E}BRAF mutation.

To investigate a role of S6K, A375P cells were treated with rapamycin, an inhibitor of S6K. Cells were treated for 5 or 24 hours. As shown in Figure 3.8, treatment of cells with rapamycin, decreased phosphorylation of GSK3 β to a small extent, but this did not affect β -catenin expression. Following 24 hours treatment of melanoma cells with rapamycin, a small reduction in GSK3 phosphorylation was again observed and no change was detected in β -catenin levels (Figure 3.8). The fact that no significant change in the expression level of phospho-GSK3 β was detected could be due to a sub-optimal concentration of rapamycin (100nM). It could also be because we inhibited the cells for 5 and 24 hours, in which time the rapamycin inhibitory effect on the pathway might have worn off, causing us to miss the inhibitor's effects on the downstream pathway.

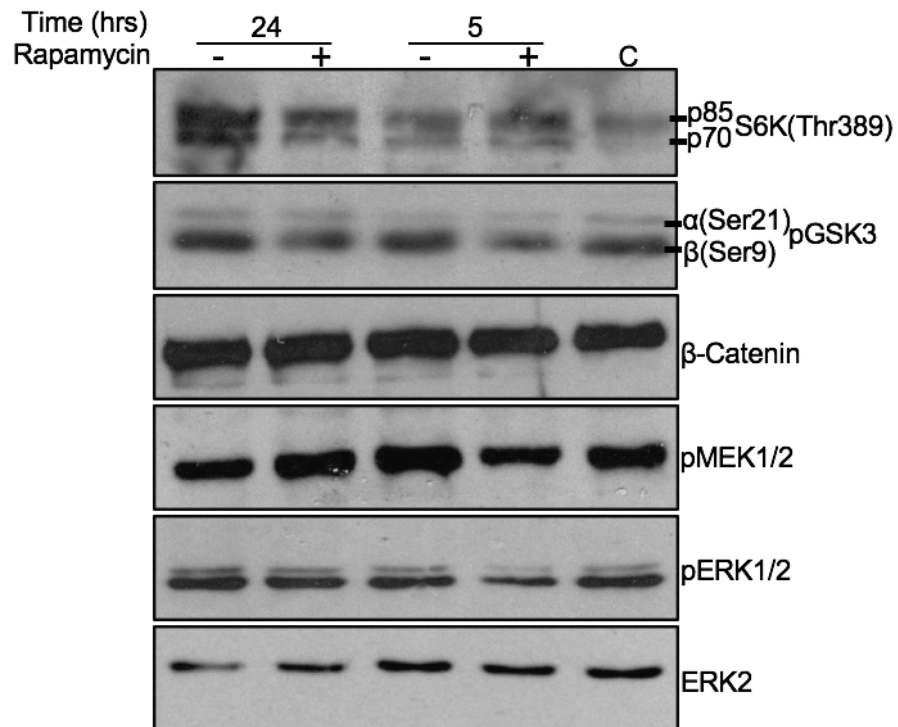


Figure 3.8 Western blot analysis of A375P melanoma cells treated with rapamycin for 5 or 24 hours. Control cells were treated with DMSO for 5 or 24 hours and analysed. Rapamycin final concentration=100nM. The figure is representative of two sets of biological replicates. C = untreated A375P cell lysate, "-" = cells treated with DMSO only.

3.4. Conclusion

In the mouse gut, changes in GSK3 phosphorylation were observed at around 3 days p.i. of ^{V600E}BRaf induction, a time at which formation of hyperplastic crypts occurs and this was reversed by MEK inhibition (Carragher et al., 2010). At later time points, senescence seems to be the reason behind suppression of both pathways in the tissue. At around 10 weeks post induction (p.i.) upregulation in expression of some proteins in both pathways was an indicator of some cells overcoming senescence and starting to proliferate again (Carragher et al., 2010). Based on these findings a model was hypothesized for crosstalk in hyperplastic crypts in which ^{V600E}BRAF activates the MAPK pathway through the phosphorylation of MEK; this is followed by ERK phosphorylation which leads to inactivation of GSK3 through phosphorylation of the kinase. We hypothesised that this increase in GSK3 phosphorylation may be a driver of intestinal cell proliferation. In this hypothesis, since the GSK3 α/β Ser21/9 phosphorylation site is not a MAPK consensus sequence, it cannot be a direct target of ERK, suggesting an intermediary kinase is involved. RSK, S6K and AKT have all previously been identified as potential intermediary kinases. Here we aimed to investigate this in more detail using cell lines (Figure 3.9).

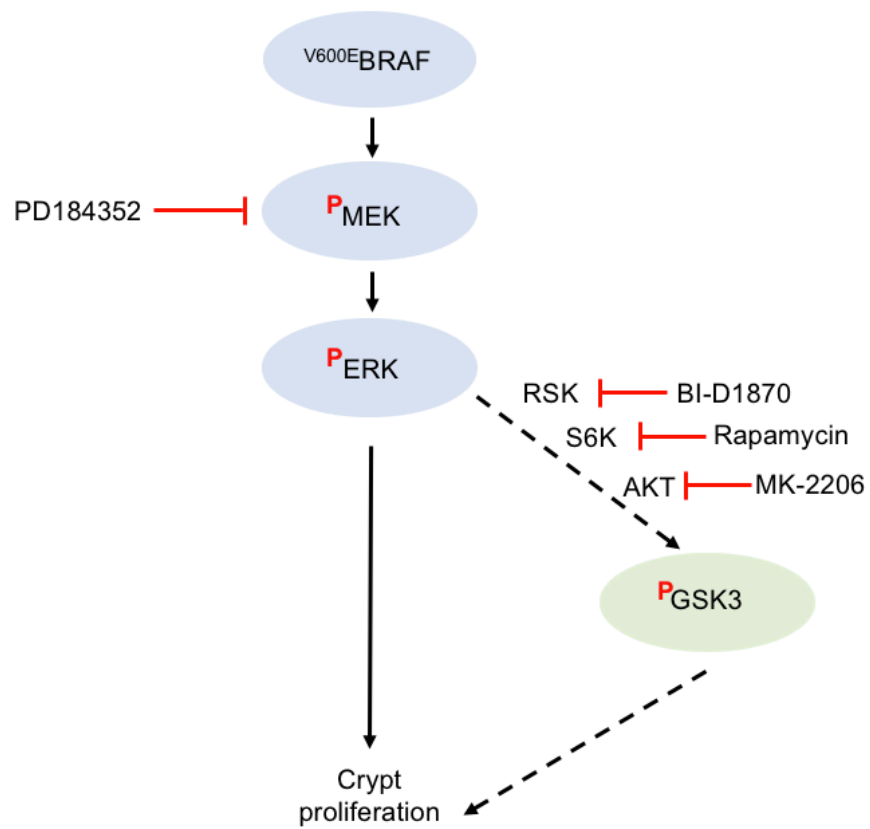


Figure 3.9 Schematic diagram of the RAF/MEK/ERK pathway and GSK3 crosstalk.

In order to establish a reliable *in vitro* model for the study of pathway crosstalk, the human colorectal cancer cell line RKO was chosen. Cook's RKO is the parental cell line with three alleles for *BRAF* one of which is *WT**BRAF* and two *V600E**BRAF*, other RKO lines were obtained from the parental line: RKO143 has one *WT**BRAF* allele and the two *V600E**BRAF* alleles are knocked out. RKO144 carries one *V600E**BRAF* allele and two other *BRAF* alleles are knocked-out. Western blot analysis of the RKO cell lines shows activation of the MAPK pathway as a result of the presence of the *V600E**BRAF* in comparison to WT cells but there was no link with GSK3 phosphorylation. This lack of evidence for the crosstalk in the human cells could be due to lack of micro-environmental factor/s of the gut. Another factor that could come into consideration is the fact that human RKO cell lines have several other mutations, including *H1047R**PI3K*, which might affect the crosstalk outcome and interfere with the phosphorylation level of GSK3. It has been proposed by Janku et al., that *PIK3CA* mutation can increase the production of some factors which leads to activation of oncogenic pathways independent of the PI3K pathway (Janku et al., 2013). Factors such as heregulin which can bind to ErbB3 and ErbB4 receptor tyrosine kinases and increase proliferation and invasion in the malignant tissue (Breuleux, 2007). ErbB ligands are expressed on intestinal epithelial cells and the activation of these ligands through dimerization can activate MAPK/ERK as well as PI3K/AKT signalling (Frey and Brent Polk, 2013). The above findings make the use of these cells for the study of the crosstalk more challenging.

Immunofluorescent staining analysis of RKO cells shows that the *V600E**BRAF*-driven MAPK activation affects sub-cellular localisation of β -catenin and cells with the mutation show more nuclear β -catenin in comparison to WT cells which has more even distribution of the protein in the cell, potentially suggesting a role for ERK pathway in this process. This effect on β -catenin localisation of the MAPK pathway in RKO cells appears to be independent of GSK3 phosphorylation.

Western blot analysis of MEFs with a conditional Cre-regulated *V600E**BRAF* mutation does not show any meaningful correlation between the MAPK pathway

and GSK3 phosphorylation or any change in activation of the intermediary kinases such as RSK and S6K. Thus, MEFs were not a good *in vitro* model system to study the crosstalk.

Some evidence of crosstalk between the MAPK pathway and GSK3 was evident in both human lung (HCC364) and melanoma (A375P) cells which harbour ^{V600E}BRAF mutation (Figure 3.6). Crosstalk was clearer in human melanoma cell lines as there was downregulation of GSK3 phosphorylation after 24 hours of inhibition of MEK, as well as downregulation in S6K phosphorylation levels. This finding fits with phospho-proteomic data by Old et al. of A375P cells published in 2009 that showed RSKs, S6K and GSK3 α/β sites are amongst 90 target genes whose phosphorylation is reversed following MEK inhibition. Phosphorylation of ERK1/2, S6K and GSK3 β at Ser9 was repressed in response to U0126 treatment in A375P melanoma cells. It was proposed that BRAF/MEK/ERK signalling inhibits GSK3 α/β through the inhibition of tyrosine residue phosphorylation essential for activation and also upregulation of inhibitory phosphorylation of Ser21/9 sites (Old et al., 2009).

The effect on the larger p85 isoform of S6K is potentially interesting. S6K has 2 isoforms p70 and p85, that are the products of alternative splicing of one gene. p85^{S6K} has a stretch of 23 extra amino acids at its N terminus end which is known to be the nuclear localisation signal (C Kozma and Thomas, 1994). It will be interesting to study the effect of the MAPK pathway on this isoform further, but this analysis is beyond the scope of the present study.

The delayed effect of MEK inhibition on other signalling pathways raises the possibility of an autocrine/paracrine mechanism in pathway crosstalk. In this possible mechanism, activation of the MAPK pathway following ^{V600E}BRAF mutation in some cells could lead to the secretion of protein/s. Secreted factor/s could then affect neighbouring cells through an interaction with cells surface receptor/s which could lead to changes in GSK3 phosphorylation and eventually increase proliferation (Figure 3.10). Melanoma cells could be used as an *in vitro* model for further investigation of this possible mechanism.

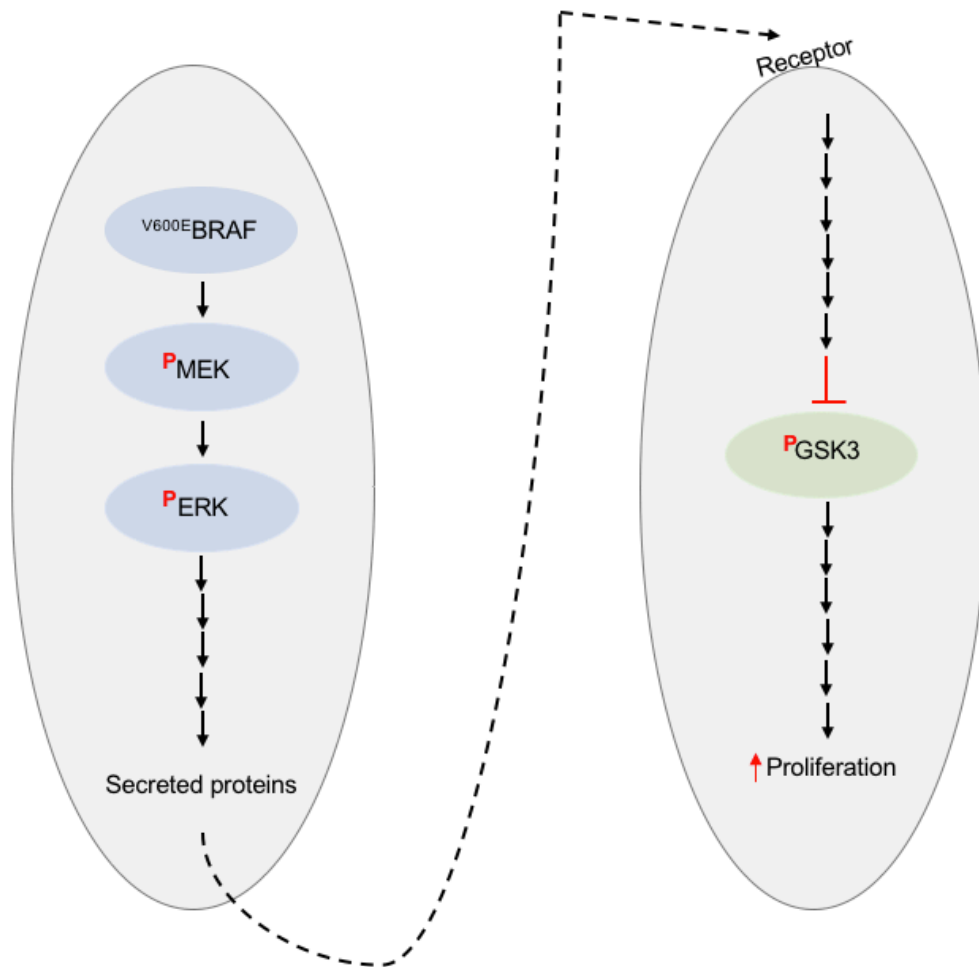


Figure 3.10 Schematic diagram of proposed autocrine/paracrine mechanism of crosstalk. In this model, activation of the MAPK pathway following $V600E$ BRAF mutation leads to secretion of proteins which then can affect the neighbouring cells and increase proliferation through changes in GSK3 phosphorylation.

The fact that A375P cells show some evidence of MAPK-WNT pathway crosstalk, but MEFs, CRC cells and lung cells do not, indicates how heterogeneous signalling pathways are in different contexts. Although human melanoma cells are a potential *in vitro* model, the focus of this project is on ^{V600E}BRAF-driven CRC. It is known that there are some fundamental differences between CRC and melanoma such as expression of EGFR receptors on the CRC cells at high levels (Prahallad et al., 2012). Therefore, it was decided not to pursue *in vitro* studies any further but to focus on *in vivo* mouse models.

Chapter 4. Setting up the *Braf*^{LSL-V600E/WT}/*Villin-CreER*^{T0/WT} model of serrated CRC: short-term study

4.1. Introduction

As work in chapter 3 did not identify a suitable CRC cell line for examining the link between ^{V600E}BRAF-ERK and GSK3, the focus of this work turned to the use of mouse models. As mentioned, work previously undertaken in the laboratory with the *Braf*^{LSL-V600E/WT}; *AhCreER*^{T0/WT} model, and published in 2010 by Carragher et al., showed evidence for the induction of crypt hyperplasia at 3 days p.i. of ^{V600E}BRaf, that was reversed by MEK inhibition. This publication also showed an increase in GSK3 phosphorylation and β -catenin levels that were reversed by MEK inhibition. Despite being a good model to study early changes, these animals did not survive beyond ~10-12 weeks p.i. as they developed tumours in the stomach and lung. Therefore, the *Braf*^{LSL-V600E/WT}; *AhCreER*^{T0/WT} model was not suitable for the long-term study.

During the course of this project a second ^{V600E}BRaf-expressing mouse gut model was generated using *Villin-Cre* (Rad et al., 2013). In this system, Cre recombinase expression is controlled by the 9kb *Villin* promoter which is specifically expressed in the GI tract. Rad et al. showed that MAPK activity did not increase significantly at the hyperplastic stage in comparison to wild type tissue, whereas it increased significantly at the adenoma and carcinoma stages. Also, an increase in the expression of MAPK target genes was slight at the hyperplastic stage but was higher at later stages of the disease. Activation of the WNT pathway was similar in the WT tissue and hyperplastic stage, but increased significantly at later stages of the disease and this was confirmed by immunohistochemical analysis of the tissue for nuclear β -catenin. Inhibition of GSK3 by CHIR-99021 had minimal growth inhibitory effect on the mutant CRC mouse cell lines, whereas it had a variable effect on human CRC cell lines (Rad et al., 2013).

For this project, we obtained the *Villin-CreER^{T0/WT}* mouse strain and combined it with *Braf^{LSL-V600E}* by interbreeding. This gave intestine-specific expression of ^{V600E}BRaf that also could be controlled temporally, using tamoxifen induction.

The results of the analysis of the *Braf^{LSL-V600E/WT}; Villin-CreER^{T0/WT}* mouse is shown in this chapter, focussing on the short-term expression of ^{V600E}BRaf.

4.2. Aims

As the *in vitro* model of ^{V600E}BRAF-driven CRC did not clarify the underlying mechanism involved in disease development, we switched to an *in vivo* system to gain a better understanding of the underlying mechanism of the crosstalk and to potentially pave the way to the discovery of possible preventive/therapeutic targets. To achieve this, we added the following objectives:

- To set up the *Braf*^{L^{SL}-V600E/WT}; *Villin-CreER*^{T0/WT} model.
- To use the *Braf*^{L^{SL}-V600E/WT}; *AhCreER*^{T0/WT} model.
- To compare the mechanism of crosstalk in two different models and to find the closest system that mimics the human disease.
- To study role of the MAPK pathway in the disease's short-term effects.
- To study the crosstalk between ^{V600E}BRaf-ERK and GSK3 following short-term ^{V600E}BRaf expression.
- To identify possible intermediary kinases. Candidate kinases AKT, S6K and RSK were examined here.

4.3. Results

4.3.1. ^{V600E}BRAF mouse gut models

In order to generate intestine-specific ^{V600E}*Braf* mouse models, two strains of Cre mice were used: *AhCreER*^{T0/WT} and *Villin-CreER*^{T0/WT}. Either *AhCreER*^{T0/WT} or *Villin-CreER*^{T0/WT} mice were intercrossed with *Braf*^{LSL-V600E/WT} mice. Resulting offspring were obtained as detailed in Figure 4.1. All offspring were subjected to PCR in order to check for the presence of the Cre allele as well as the ^{V600E}*Braf* allele (see section 4.3.2 below).

AhCreER^T mouse model**Genotype of the mouse**

AhCreER^{T0/WT} X Brat^{ΔSL-V600E/WT}
 Genotypes of offspring

Brat^{ΔSL-V600E/WT}; AhCreER^{T0/WT}

Brat^{ΔSL-V600E/WT}; AhCreER^{TWT/WT}

Brat^{WT/WT}; AhCreER^{T0/WT}

Brat^{WT/WT}; AhCreER^{TWT/WT}

Villin-CreER^T mouse model**Genotype of the mouse**

Villin-CreER^{T0/WT} X Brat^{ΔSL-V600E/WT}
 Genotypes of offspring

Brat^{ΔSL-V600E/WT}; Villin-CreER^{T0/WT}

Brat^{ΔSL-V600E/WT}; Villin-CreER^{TWT/WT}

Brat^{WT/WT}; Villin-CreER^{T0/WT}

Brat^{WT/WT}; Villin-CreER^{TWT/WT}

Figure 4.1 Schematic diagram of the mating strategy of AhCreER^{T0/WT} and Villin-CreER^{T0/WT} CRC mouse models. Genotypes of obtained offspring used in this study are shown in detail.

4.3.2. PCR analysis to determine mouse genotypes

As explained earlier, breeding was performed by using heterozygous $Braf^{LSL-V600E/WT}$ and heterozygous Cre mice which was either $AhCreER^{T0/WT}$ or $Villin-CreER^{T0/WT}$. All offspring were subjected to genotyping, using PCR primers for the Cre gene in either $AhCreER^{T0/WT}$ or $Villin-CreER^{T0/WT}$, which produced a single 300bp band (Figure 4.2A). Litters were also checked for the $Braf^{LSL-V600E}$ allele using PCR primers which produced two bands: a smaller band of 140bp representing the LSL-V600E allele and a larger band of 466bp representing the WT allele (Figure 4.2B). Mice which carried both heterozygous alleles were chosen for further study. At the age of 8-10 weeks, $Braf^{LSL-V600E/WT}; AhCreER^{T0/WT}$ mice were injected with β -NF on the first day and on the second day of injection with β -NF and TM; they were terminated at different time points p.i. $Braf^{LSL-V600E/WT}; Villin-CreER^{T0/WT}$ mice were subjected to two TM injections on two consecutive days at the same time each day (Figure 4.3). All mice also received BrdU injections 3 hours prior to humane termination. Tissue from the GI tract was subjected to DNA extraction followed by PCR in order to check for LSL-cassette recombination. In both Cre models, positive recombination was evident from the presence of two bands: a 466bp band for the $^{WT}Braf$ allele and a 518bp band for the $Braf^{LSL-V600E/WT}$ allele (Figure 4.2C).

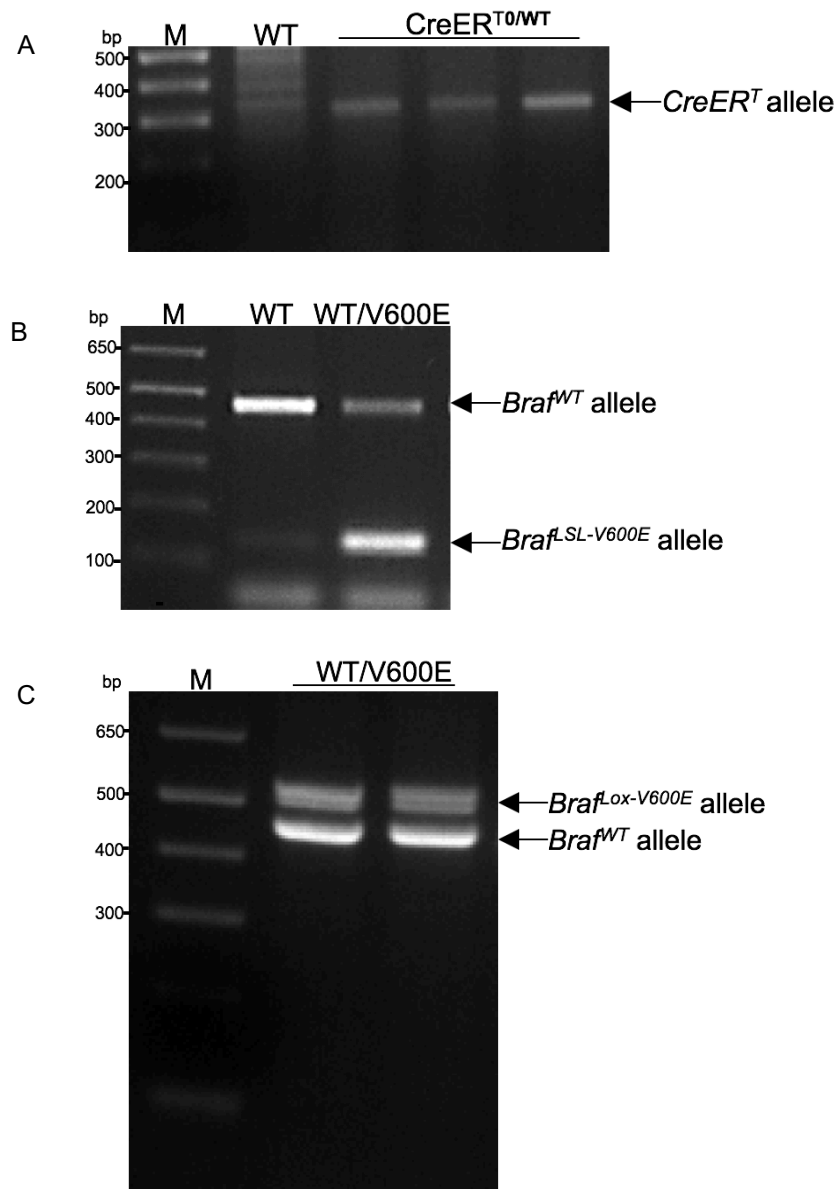


Figure 4.2 PCR genotyping to determine the genotype of the offspring as well as Cre-mediated recombination.

A) PCR genotyping to identify the presence of the Cre gene allele in heterozygous mice. A 300bp band corresponds to the allele.

B) PCR genotyping in order to identify the Braff^{LSL-V600E} allele. A 140bp band corresponds to the LSL-V600E allele and a 466bp band corresponds to the WT allele.

C) PCR using DNA from double heterozygous mice that have been induced to activate the Cre recombinase, showing the presence of the recombined Braff^{lox-V600E} at 518bp to check for Cre recombination. M=1kb ladder.

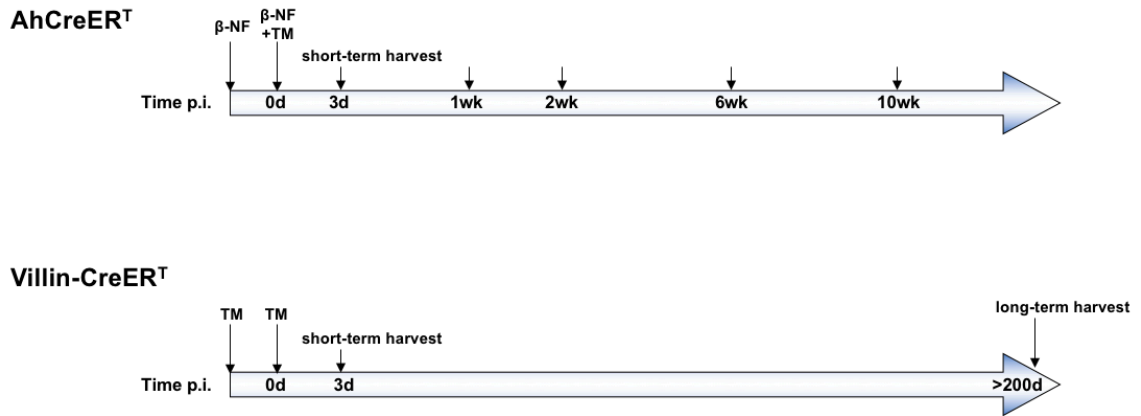


Figure 4.3 Schematic diagram showing treatment regime for AhCreER^{T0/WT} and Villin-CreER^{T0/WT} mouse models. In the AhCreER^{T0/WT} model, mice were injected with β-NF and β-NF+TM after 24 hours and were harvested at the time points indicated on the diagram. Time p.i. indicates the length of time after β-NF+TM injection. In the Villin-CreER^{T0/WT} model, mice were treated with two TM injections on two consecutive days and were terminated at 3 days p.i. for the short-term study and once signs of ill health appeared (according to the Home Office regulations) for the long-term study. Time p.i. indicates the length of time after the second TM injection.

4.3.3. Crosstalk between MAPK and GSK3 in the *Braf*^{LSL-V600E/WT}; *AhCreER*^{T0/WT} mouse model

In the first attempt and in order to study the crosstalk *in vivo*, tissue from the *Braf*^{LSL-V600E/WT}; *AhCreER*^{T0/WT} mouse model was analysed by western blot. As shown in Figure 4.4, at 3 days p.i., there was an increase in MEK phosphorylation levels as a result of the ^{V600E}*Braf* mutation. A small increase in ERK phosphorylation levels at 3 days p.i. was seen and can be explained by an increase in DUSP6 levels, a negative regulator of ERK phosphorylation. Also, there was upregulation in GSK3 α/β Ser21/9 phosphorylation as well as β -catenin levels following the expression of ^{V600E}BRaf. This is consistent with data from Carragher et al. (2010). Between ~1 week to ~6 weeks p.i. there was downregulation in MEK, ERK, GSK3 α/β phosphorylation and DUSP6 expression levels which could be related to the induction of senescence at these time points. At 10 weeks p.i. there was upregulation in MAPK pathway components as well as a slight increase in GSK3 β phosphorylation and β -catenin levels. This result potentially indicates that cells were overcoming the senescent phase (Figure 4.4).

An increase in phosphorylation of p85^{S6K} was detected at 3 days p.i. suggesting that this isoform could be the intermediary kinase facilitating the crosstalk. No changes in phosphorylation of AKT or RSK were detected (Figure 4.4). However, there was also an increase in phosphorylation of AKT as well as p85^{S6K} and p90^{RSK} at ~10 weeks p.i. potentially suggesting the activation of alternative pathways (Figure 4.4).

Overall, these data suggest that there is activation of the MAPK pathway shortly after ^{V600E}BRaf induction which is followed by senescence. At later time points, some cells overcome senescence and as a result there is reactivation of the MAPK and GSK3 pathways, potentially involving p85^{S6K}. Interestingly, AKT and RSK did not seem to play a role at earlier stages, but the data suggests that at later stages AKT as well as RSK might act as facilitators of pathway communication.

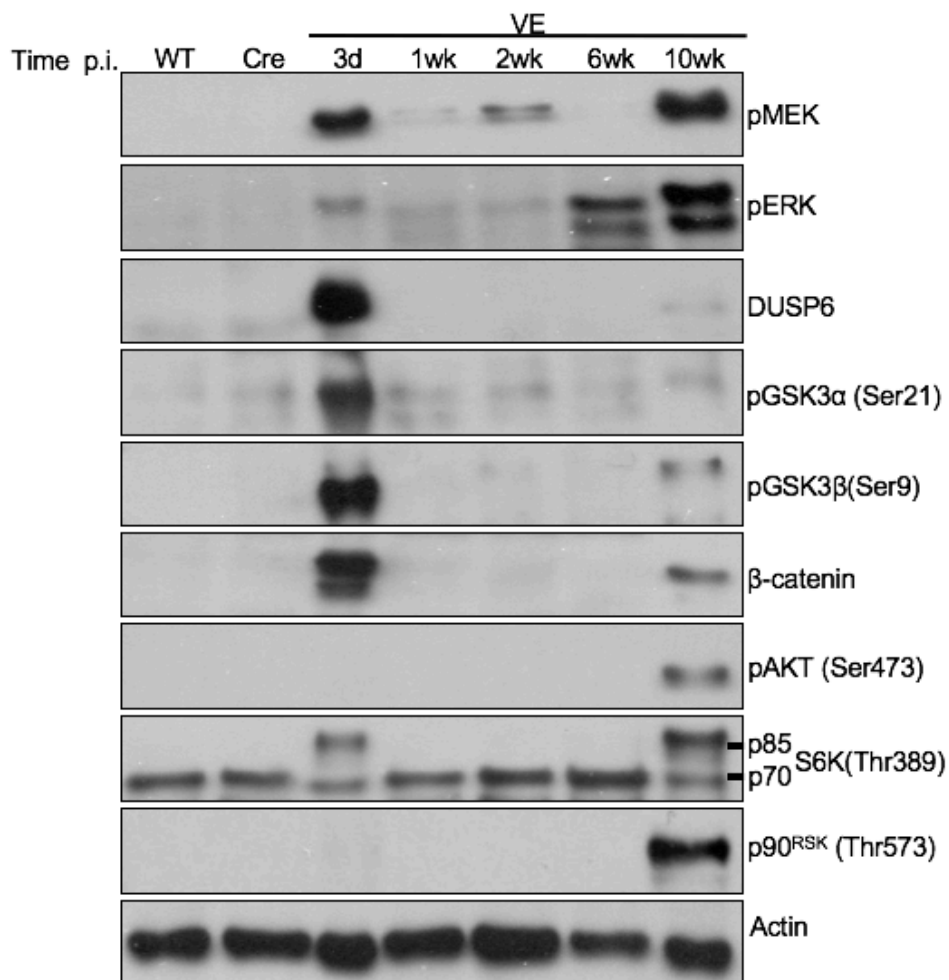


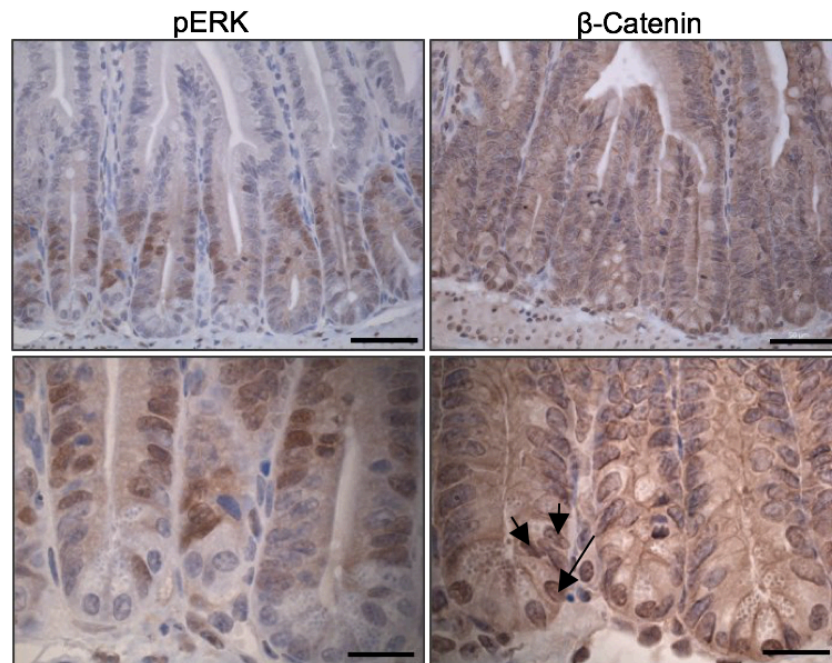
Figure 4.4 Western blot analysis of the *Braf*^{SL-V600E/WT}; *AhcreER*^{T0/WT} gut tissue at different times p.i. after animals were injected with β -NF and TM. Tissues from double heterozygous mice were harvested at different times; the lysate from the tissue was used for western blot analysis along with tissue lysate from single heterozygous *AhcreER*^{T0/WT}, induced for 3 days, as well as WT mice as controls. The above figure is representative of two sets of biological replicates. Tissue from section 4 of the small intestine, from 14 mice, were used.

4.3.4. Expression of MAPK and WNT pathway components using immunohistochemistry

In the next attempt to identify whether the crosstalk occurs in a cell intrinsic manner or not, tissue from *Braf*^{LSL-V600E/WT}; *AhCreER*^{T0/WT} mice at 3 days p.i. was subjected to immunohistochemistry. Staining for phospho-GSK3 was first attempted but this was not successful due to a lack of specificity of the antibody. Two adjacent sections from the same piece of tissue were then stained with phospho-ERK or β -catenin antibodies. Phospho-ERK was detected only in transit amplifying (TA) cells but not stem cells whereas β -catenin was detected in the nucleus of the crypt cells; most strongly in crypt base cells and more weakly in TA cells and cells further up the crypt as well as villi cells (Figure 4.5).

Therefore, there is some overlap in phospho-ERK and nuclear β -catenin, but not in all cells, suggesting some form of autocrine/paracrine component.

A



B

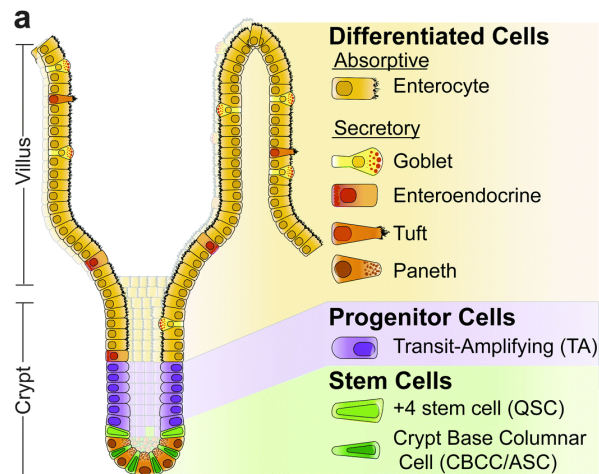


Figure 4.5 A) Immunohistochemical analysis of 3 days p.i. tissue samples taken from $Braf^{LSL-V600E/WT}; AhCreER^{T0/WT}$ mice. Adjacent sections from the same piece of tissue were stained for phospho-ERK and β -catenin. Photographs are taken at two different magnifications (top and bottom) but at the same spot on the tissue. Positive cells for nuclear β -catenin are indicated with black arrows. Scale bars= $50\mu m$ (top panels) and $20\mu m$ (lower panels). Tissue from section 4 of the small intestine of 4 mice were used.

B) A schematic diagram of intestinal epithelium structure. Intestinal epithelium consists of a crypt and villus structure composed of different cell types (Carulli et al., 2014). As illustrated, crypt structure contains stem, progenitor (TA) and crypt base columnar cells. TA cells differentiate into absorptive enterocytes or secretory goblet, tuft, enteroendocrine, or Paneth cells. Differentiated cells migrate upward towards villus, except for the Paneth cells which moves down and sits between the CBCCs.

4.3.5. Investigation of crosstalk in the *Villin-CreER^{T0/WT}* mouse model

As was stated before *Braf^{LSL-V600E/WT}*; *AhCreER^{T0/WT}* mice did not survive beyond 10-12 weeks of age due to the formation of tumours, in the stomach or lung, as a result of expression of ^{V600E}BRaf. Therefore, a more tissue specific mouse model of CRC was used, namely the *Villin-CreER^{T0/WT}* model. Tissue from 3 days p.i. mice from *Braf^{LSL-V600E/WT}*; *Villin-CreER^{T0/WT}* (BVE/Cre) was compared with controls.

In order to check the efficiency of recombination, a group of mice were injected with 1, 2, or 3 doses of TM on consecutive days and tissue was subjected to DNA extraction and PCR. High levels of recombination were seen in mice receiving either 2 or 3 TM injections but not those receiving 1 TM injection (Figure 4.6A).

In the BVE mouse, following ^{V600E}BRaf expression, MEK phosphorylation was not elevated compared to controls. ERK phosphorylation levels were only weakly elevated over controls, this is consistent with the Rad et al. (2013) published data. Following ^{V600E}BRaf expression, an increase in GSK3 α/β phosphorylation was detected, although the separation of the two α and β isoform bands was not clear. There was also an increase in phosphorylation of p70/85^{S6K} in comparison to controls, with possibly more changes in the p85 isoform. Although several attempts to detect phospho-p90^{RSK} were carried out, no positive band could be seen in several experiments (Figure 4.6B).

Overall, these data suggest that there is little, if any, activation of the MEK-ERK pathway following expression of ^{V600E}BRaf in the *Villin-CreER^{T0/WT}* model; this is a different result to what was seen in the *AhCreER^{T0/WT}* model. Although there is evidence for an increase in GSK3 phosphorylation, this may be partly ERK independent.

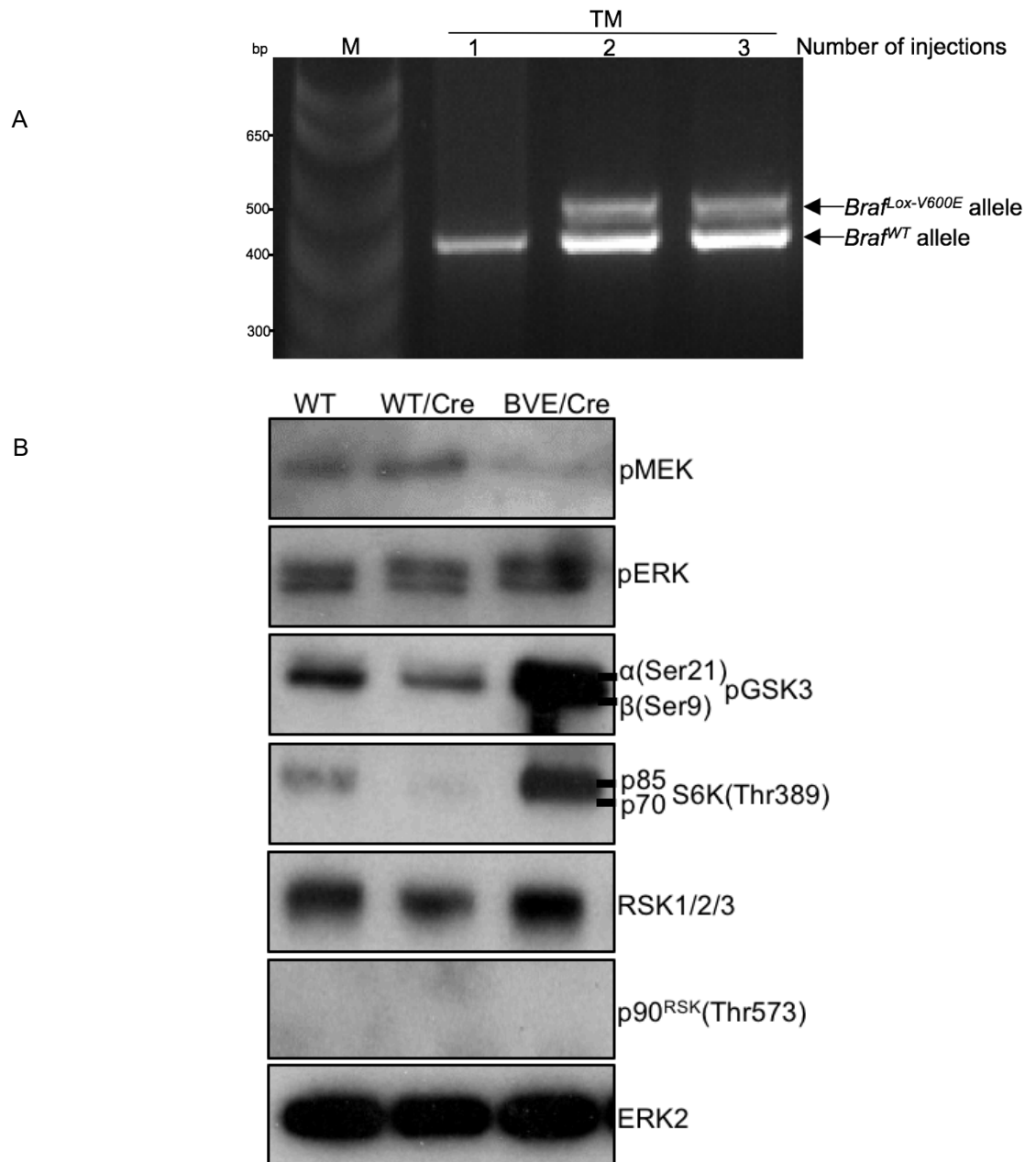


Figure 4.6 Analysis of BVE/Cre tissue following 3 days of induction of ^{V600E}BRaf.

A) PCR using DNA from double heterozygous mice induced for 1, 2 or 3 days with TM to check the efficiency of Cre recombination of the *Braf*^{Lox-V600E} allele. M=1kb ladder.

B) Western blot analysis of *Braf*^{LSL-V600E/WT}; *Villin-CreER*^{T0/WT} (BVE/Cre) mice. Animals were terminated 3 days after the last TM injection. Tissue was processed accordingly and the lysate was subjected to western blot analysis. The above figure is the representative of three sets of different biological replicates. Tissue from section 4 of the small intestine, from 9 mice, were used.

4.3.6. Crypt elongation in the small intestine as a result of the ^{V600E}Braf mutation

As a next step, in order to investigate the effect of the ^{V600E}Braf mutation on crypt hyperplasia in the *Villin-CreER*^{T0/WT} mouse model, mouse gut tissue at 3 days p.i. was subjected to H&E staining; tissue from *Villin-CreER*^{T0/WT} mouse induced for 3 days was used as a control. As stated before, after harvesting, small intestine tissue was cleaned and cut into 6 similar sized pieces from start of the caecum to end of duodenum as shown in Figure 4.7.

As shown in figure 4.8, the length of crypts in section 4 of the small intestine increased significantly following induction of ^{V600E}BRaf in comparison to controls (Figure 4.8).

Thus, although there was little if any MAPK pathway activation, crypt hyperplasia was seen.

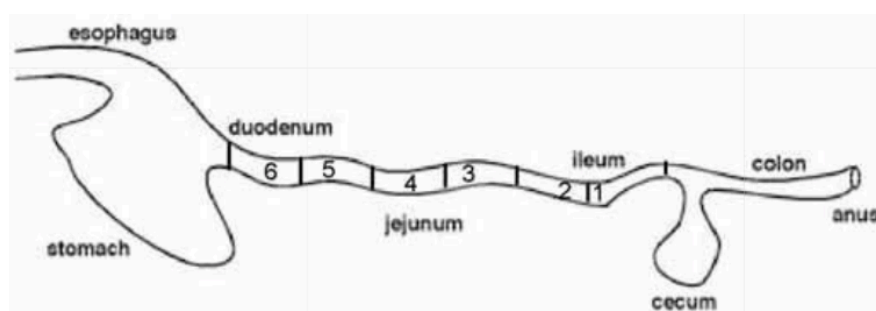


Figure 4.7 Schematic diagram of mouse small intestine (Carragher et al., 2010). The small intestinal tissue was cut into 6 sections of similar length, with section 1 being the ileum and section 6 being the duodenum. Individual sections were subjected to analysis.

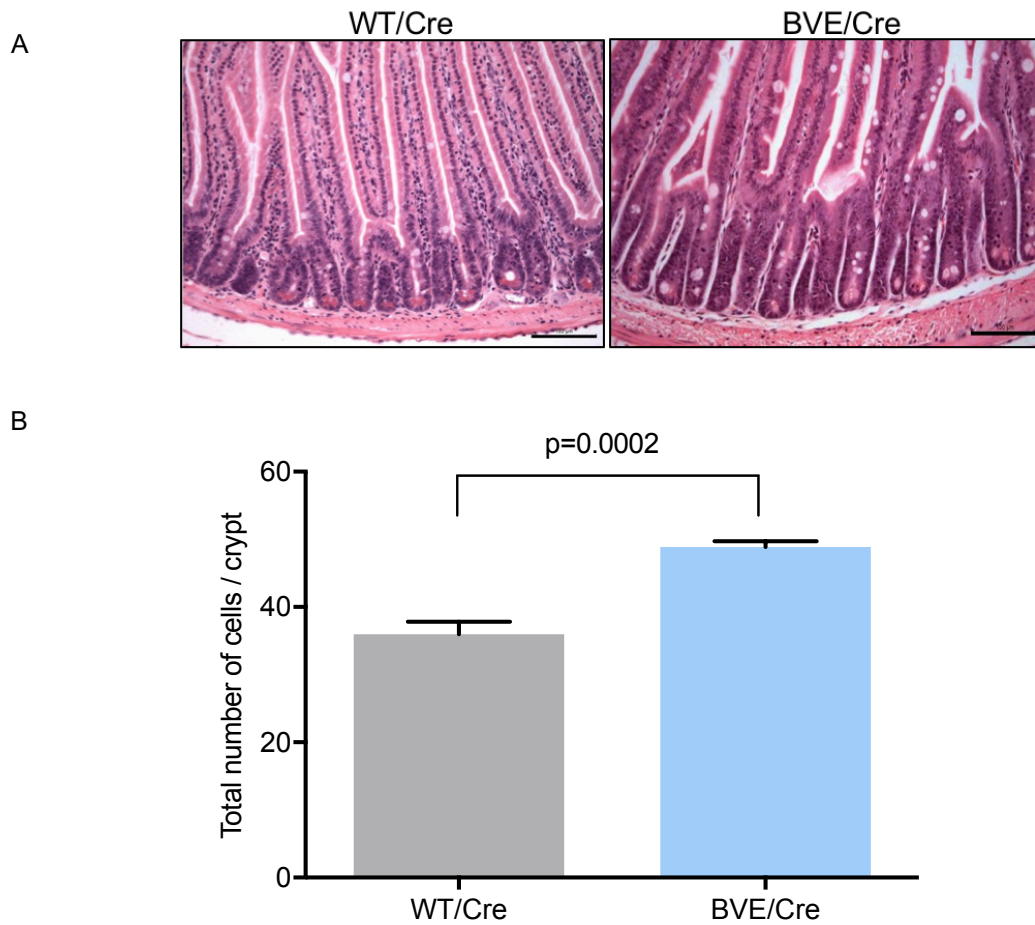


Figure 4.8 Crypt hyperplasia in $Braf^{LSL-V600E/WT}; Villin-CreER^{T0/WT}$ mice following TM induction at 3 days p.i.

A) H&E staining of 3 days p.i. gut tissue. Section 4 shows formation of hyperplastic crypts following $V600E$ $Braf$ induction in comparison to controls. Scale bars= $100\mu m$.

B) Graph showing total crypt cell counts in $V600E$ $Braf$ mice as well as control. In each group crypts from section 4 of the gut, in 5 mice, were subjected to H&E staining and 50 full crypts from each mouse was subjected to cell counting. Data shown mean \pm SD. Statistical analysis was carried out using an unpaired T-test. Total No. of mice used= 10.

4.3.7. Increase in number of proliferative cells in the small intestinal crypts

In order to find out if ^{V600E}BRaf impacted on crypt cells proliferation, tissue from *BVE/Cre* as well as control mice were subjected to immunohistochemical analysis.

Cells were first checked for BrdU positive staining which marks cells at S phase of the cell cycle. As shown in Figure 4.9, there was a significant increase in the number of proliferative cells in S phase of the cell cycle observed in *BVE/Cre* mice in comparison to controls (Figure 4.9).

The same tissues were subjected to phospho-Histone3 (pH3) staining which marks cells at the G2/M phase of the cell cycle. As shown in Figure 4.10, although there seemed to be a trend towards an increase in the number of proliferative cells positive for pH3 in comparison to controls, the increase was not statistically significant (Figure 4.10).

Overall, these data suggest that short-term ^{V600E}BRaf induces an increase in crypt cell proliferation with evidence for an increase in cells in S phase.

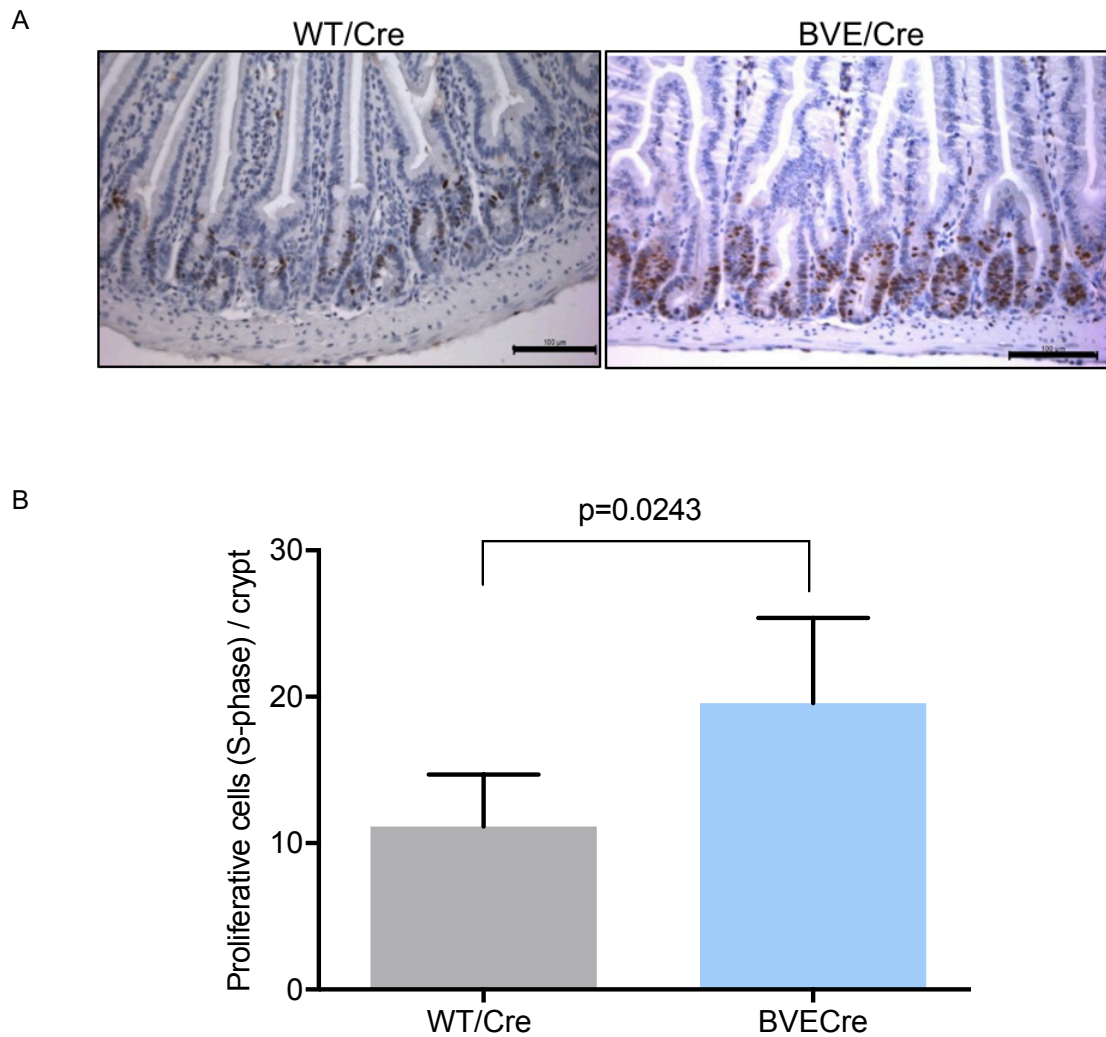


Figure 4.9 Immunohistochemical analysis of 3 days *p.i.* tissue for BrdU incorporation.

A) Immunohistochemical analysis of cells positive for BrdU, a proliferative marker. Mice were injected with BrdU 3 hours prior to termination. Tissue from section 4 of the gut of control and BVE/Cre tissue was subjected to analysis with a BrdU antibody. Scale bars= 100 μ m.

B) Graph showing a number of BrdU positive proliferative cells in intestinal crypts of BVE/Cre and control tissue. Section 4 of small intestine, from 5 mice in each category, was subjected to staining and cell counting. 50 full crypts from each animal analysed. Data shows mean \pm SD. Statistical analysis was carried out using an unpaired T-test. Total No. of mice used= 10.

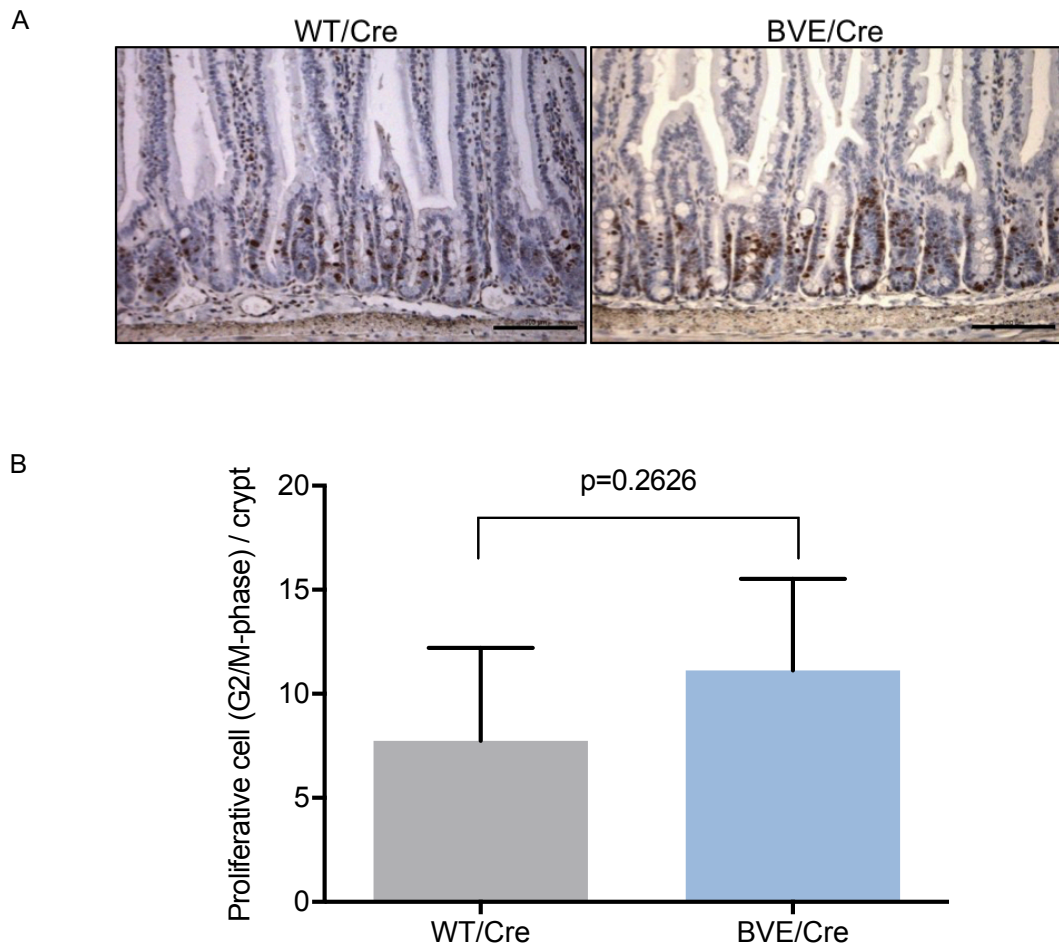


Figure 4.10 Immunohistochemical analysis of, 3 days p.i., tissue for phospho-H3.

A) Immunohistochemical analysis of the pH3 proliferative marker. Processed tissue from BVE/Cre and control gut tissue was subjected to analysis with a pH3 antibody. Scale bars= 100 μ m.

B) Graph showing a number of pH3 positive proliferative cells in the intestinal crypts of BVE/Cre and control mice. Tissues from section 4, of 5 mice, from each group were subjected to staining and cell counting. 50 full crypts from each animal were counted and data show mean \pm SD. Statistical analysis was carried out using an unpaired T-test. Total No. of mice used= 10.

4.3.8. Effect of MAPK pathway inhibition in the *Braf*^{SL-V600E/WT}; *Villin-CreER*^{T0/WT} mouse model

To conduct MAPK inhibition studies three groups of mice were subjected to investigation with 5 mice in each group. WT mice, as well as *Villin-CreER*^{T0/WT} and *Braf*^{SL-V600E/WT}; *Villin-CreER*^{T0/WT} mice were induced with TM for two consecutive days, 24 hours apart; then on days 1, 2 and 3 mice received intraperitoneal injections of PD184352 (MEK inhibitor) at 200mg/kg/day which was prepared freshly on each day. Animals were then terminated 6 hours after the final dose of PD184352 (Figure 4.11).

For controls, the same number of mice of each genotype, received TM injections on two consecutive days, but on days 1, 2, and 3 they have received intraperitoneal injection of carrier (10% DMSO+ 10% cremophor EL+ 80% H₂O) freshly prepared on the day of injection. Mice were then sacrificed 6 hours after the final carrier injection.

WT

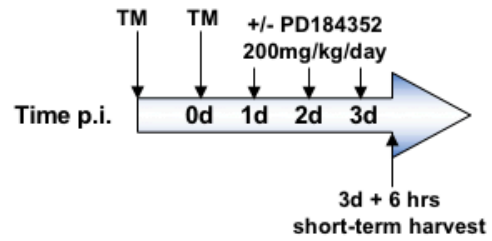
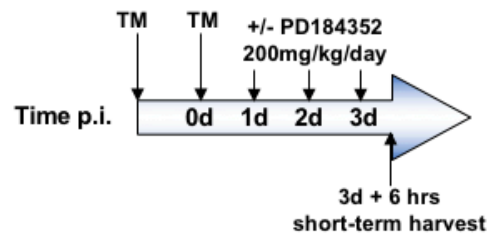
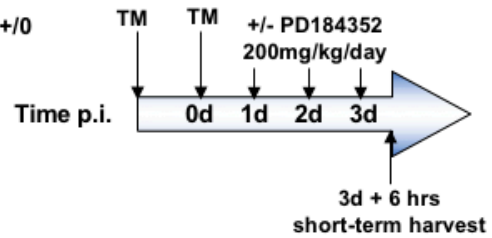
Villin-CreER^{T+/0}Braf^{LSL-V600E/+}; Villin-CreER^{T+/0}

Figure 4.11 PD184352 treatment regime. WT, Villin-CreER^{T0/WT}, Braf^{LSL-V600E/WT}; Villin-CreER^{T0/WT} mice were injected with TM for two consecutive days 24 hours apart. At 1, 2, and 3 days after the last TM injection, mice received PD184352 at 200mg/kg/day or carrier control by intraperitoneal injection. Mice were then terminated 6 hours after the last inhibitor injection.

In order to study the effect of MAPK pathway inhibition on the short-term expression of ^{V600E}BRaf, in the BVE/Cre model, mice were injected intraperitoneally with PD184352 or carrier for 3 consecutive days as shown in Figure 4.11. After harvesting, gut tissue lysate was subjected to western blot analysis. As shown in Figure 4.12, ERK phosphorylation was inhibited following PD184352 treatment in WT, WT/Cre and BVE/Cre mice, showing the drug treatment had been successful.

Interestingly, following the treatment of mice in this way there was an increase in GSK3 β phosphorylation at Ser9 in the carrier-treated WT/Cre control and BVE/Cre mice compared to WT mice. This is a different result to what was obtained previously which had indicated an increase in GSK3 β phosphorylation in BVE/Cre mice over the WT/Cre control and WT mice; this possibly indicates that Cre induction by TM and carrier injections are able to induce GSK3 β phosphorylation somewhat. However, in the WT/Cre control and BVE/Cre mice, there was a significant reduction in GSK3 β phosphorylation levels following MEK inhibition; this indicates that serine 9 phosphorylation is regulated by the MAPK pathway, regardless of whether MAPK activation is derived from signals from ^{V600E}BRaf or from other mechanisms. Unfortunately, for unknown reasons, GSK3 α western blots were not successful in this experiment. pS6K phosphorylation was also fully inhibited following MEK inhibition, whereas there was only a slight reduction in AKT phosphorylation (Figure 4.12), suggesting S6K is the intermediary kinase.

Altogether, this data suggests that in the *Braf*^{LSL-V600E/WT}; *Villin-CreER*^{T0/WT} mouse model of human CRC, communication between the MAPK pathway and GSK3 occurs, but this is not specific to ^{V600E}BRaf expression. S6K and AKT also seem to be downstream of MAPK in this model.

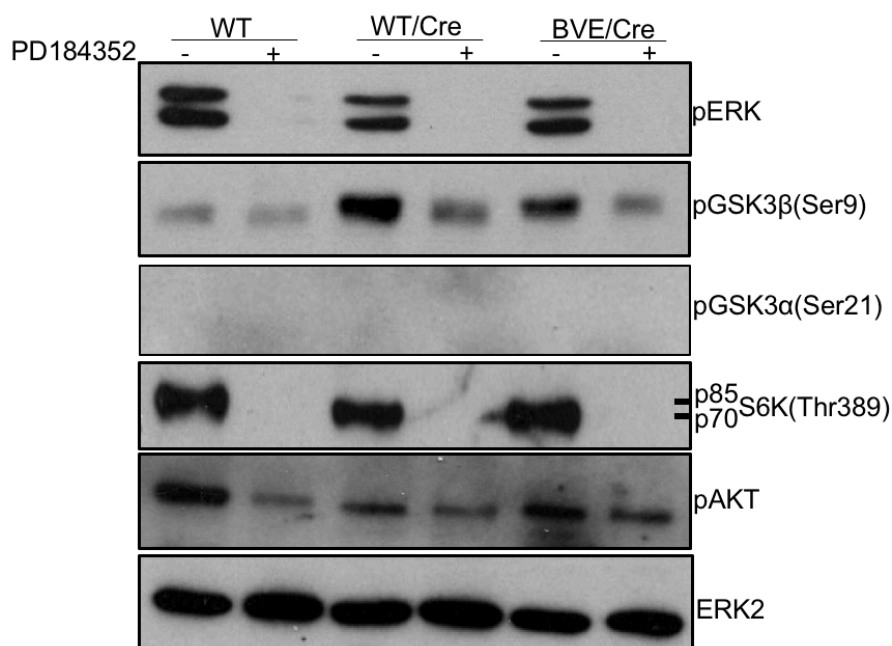


Figure 4.12 Western blot analysis of PD184352 treated, 3 days p.i., mouse tissue. Animals were injected with PD184352 or carrier control on 3 consecutive days at the same time every day after the last TM injection. Animals were terminated 6 hours after the last injection. Intestinal tissue was processed and the lysate was subjected to western blot analysis. The figure is representative of 2 sets of different biological replicates. Total No. of mice used= 12.

4.3.9. Effect of PD184352 treatment on crypt hyperplasia

In order to examine the effect of MAPK inhibition on crypt cell number, animals from the various treatments shown in Figure 4.11 were subjected to crypt cell counting.

As is shown in Figure 4.13, the total number of crypt cells does not change significantly following treatment with PD184352 in the WT, WT/Cre or BVE/Cre mice (Figure 4.13). These data confirm that the MAPK pathway is not involved in driving crypt hyperplasia downstream of ^{V600E}BRaf in the BVE/Cre model, suggesting this must be a MEK-ERK-independent effect.

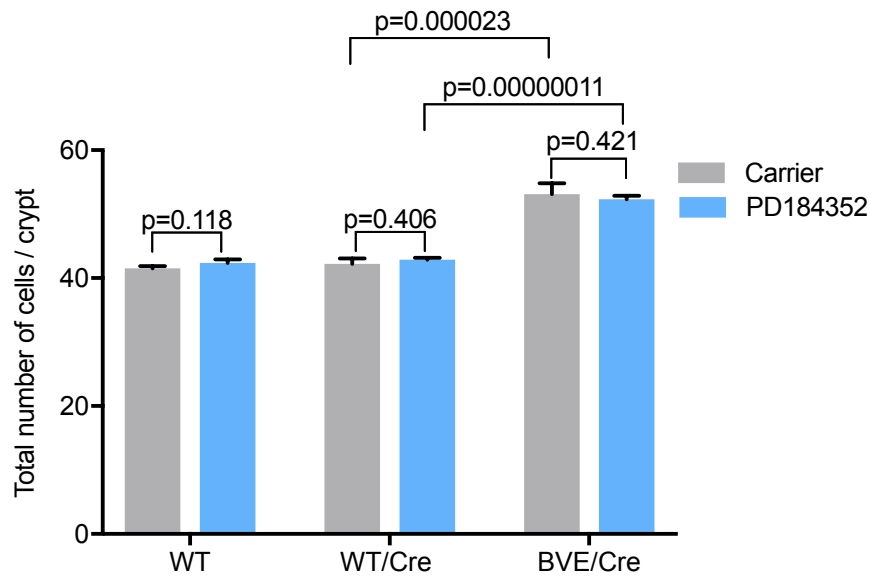


Figure 4.13 Number of cells per crypt following PD184352 or control treatment. Three groups of animals: WT, Villin-CreER^{T0/WT} (WT/Cre), *Braf*^{LSL-V600E/WT}; Villin-CreER^{T0/WT} (BVE/Cre) were used with 4 mice in each group. Mice were injected with TM on two consecutive days, followed by 3 days of PD184352 (200mg/kg/day) or equal volume of carrier (10% DMSO+ 10% cremophor EL+ 80% H₂O) and were sacrificed 6 hours after the last injection. Tissue was processed and subjected to H&E staining. 50 crypts, from section 4 of the gut, were subjected to cell count in each mouse and the result was subjected to statistical analysis. Data shows mean \pm SD. Statistical analysis was carried out using multiple T-test. Total No. of mice used= 24.

4.4. Conclusion

In the *AhCreER^{T0/WT}* mouse model of serrated CRC, expression of ^{V600E}BRaf in the short-term is associated with activation of the MAPK pathway, leading to an increase in phosphorylation of GSK3 (Figure 4.4); Crypt hyperplasia was also evident (Carragher et al., 2010). At ~1 week p.i., suppression of multiple signalling molecules was found to occur (Figure 4.4) and this seems to be the result of senescence induction which is then overcome at ~10 weeks p.i. These findings fit with the 2010 publication by Carragher et al. in which senescence was accompanied by an increase in senescence associated β -galactosidase and p16^{INK4A} expression (Carragher et al., 2010).

Data presented here show that crosstalk between MAPK and GSK may involve p85^{S6K}, but may also involve a paracrine component since phospho-ERK positive cells do not always correlate with nuclear β -catenin positivity (Figure 4.5). At later time points, apart from S6K, AKT may be activated. In the manuscript by Rad et al. (2013), tumour induction in the *Villin-Cre* model was accompanied by the acquisition of mutations in components of the WNT pathway and it is possible this is occurring in the *AhCreER^T* model to activate pathways involving AKT, although this remains to be proven.

As the *Braf^{LSL-V600E/WT}; AhCreER^{T0/WT}* mice do not survive beyond 10-12 weeks p.i., a more tissue specific *Villin-CreER^{T0/WT}* strain was used which allowed restricted expression in the intestinal tissue. In the *Braf^{LSL-V600E/WT}; Villin-CreER^{T0/WT}* mouse, following ^{V600E}BRaf short-term expression, crypt hyperplasia was observed in conjunction with weak phosphorylation of MEK and ERK. These data were consistent with the data from Rad et al. (Rad et al., 2013) who used the constitutive *Villin-Cre* strain. Some evidence for an increase in GSK3 phosphorylation was observed, which was AKT independent and our data show S6K may play a role.

Inhibition of the MAPK pathway by PD184352 in the *Braf^{LSL-V600E/WT}; Villin-CreER^{T0/WT}* animals, confirms that the MEK-ERK pathway does not play a role

in crypt hyperplasia induced by V^{600E} BRaf in this model. This is a startling result for two reasons.

Firstly, it is different to what was observed and reported in the *AhCreER^{T0/WT}* model by Carragher et al., (2010). This raises the possibility that the different *Cre* strains allow for expression of V^{600E} BRaf in different cell types in the gut; this generates a difference in the MAPK response. In the *AhCreER^{T0/WT}* mouse strain, β -NF and TM regulates expression of Cre recombinase in intestinal transit amplifying cells and stem cells (Carragher et al., 2010). Whereas in the *Villin-CreER^{T0/WT}* mouse strain, expression of the Cre recombinase is detected in the entire small and large intestinal epithelium including Paneth cells (Madison et al., 2002, Parry et al., 2013). Therefore, the MAPK-driven effects in the TA and stem cells of the *AhCreER^{T0/WT}* model may be overwhelmed by the non-MAPK-independent effects in the *Villin-CreER^{T0/WT}* model. In human, APC-driven CRCs, there is good evidence to suggest that the disease has a stem cell origin, with *Lgr5*- expressing stem cells being the cell of origin (Barker et al., 2007). It is not clear if this is the case for BRAF oncogene-driven CRCs, but it would be interesting to see if the serrated CRC phenotype can be driven, using a *Lgr5-Cre* strain and whether this involves the MAPK pathway at early stages or not. In the Rad et al. (2013) paper, crossing with the *Lgr5-EGFP-IRES-CreERT2* strain and TM induction, was reported in the supplementary section, and was shown to give rise to hyperplastic polyps but it was not shown whether this was associated with MAPK activation or not (Rad et al., 2013).

In 2013, Do et al. reported that in human hyperplastic polyps (HPs) there was a significant increase in phospho-ERK positive epithelial cells, in comparison to normal epithelial tissue ($p=0.0008$), with 65% of HPs expressing high levels of phospho-ERK. Moreover, activation of ERK was significantly higher in tissues expressing a high level of prostaglandin; these HP tissues represent less latent lesions with the higher potency to become malignant. In this study the *BRAF* mutation status was not looked at, therefore it remains unclear whether or not the increase in phospho-ERK was associated with *BRAF* mutation (Do et al., 2013).

Secondly, the data reveals that a MAPK-independent function for ^{V600E}BRaf. Although MEK-independent functions have been reported for CRAF, these are not so widely described or confirmed for BRAF (Hindley and Kolch, 2002). A MEK-independent function of ^{V600E}BRAF has been reported by Kang et al. (2015), in which an interaction between oncogenic ^{V600E}BRAF and 3-hydroxy-3-methylglutaryl-CoA (HMGCL), a ketogenic enzyme, was found to be the key event in communication between metabolic and cell signalling pathway in melanoma cells. HMGCL and ^{V600E}BRAF interaction was facilitated through Oct-1, leading to an increase in acetoacetate (AA), a HMGCL product. Increased AA could then in turn encourage a ^{V600E}BRAF and MEK1 interaction, leading to activation of the MEK-ERK signalling pathway (Kang et al., 2015). This may be one mechanism through which ^{V600E}BRaf operates in the BVE/Cre model and indeed links the oncogene with ketogenesis.

Other examples of MEK-independent functions of BRAF include inactivating mutations in the BRAF P-loop, which are independent of BRAF kinase activity and decrease formation of the BRAF-MEK1 complex but increase CRAF binding, resulting in MAPK activation through upregulation of CRAF activity (Haling et al., 2014).

Chapter 5. Investigation of the role of GSK3 phosphorylation in ^{V600E}Braf-driven early changes in the gut

5.1. Introduction

As shown in the previous chapter, induction of ^{V600E}BRaf leads to crypt hyperplasia in the *Villin-CreER^{T0/WT}* model which is MAPK-independent. An increase in GSK3 phosphorylation was observed, consistent with data from the *AhCreER^T* model. In order to explore the role of GSK3 α/β Ser21/9 phosphorylation in more detail, the double heterozygous, *Braf^{LSL-V600E/WT}*; *Villin-CreER^{T0/WT}* mice were intercrossed with double knockin mice for GSK3 α/β in which Ser21 of GSK3 α and Ser9 of GSK3 β had been changed to alanine. *Gsk3 α/β* knockin mice were kindly provided by Professor D. Alessi from the MRC protein phosphorylation unit, Dundee (McManus et al., 2005). This study reports successful breeding and use of a novel mouse model, *Gsk3 α ^{S21A/S21A}*, *Gsk3 β ^{S9A/S9A}*, *Braf^{LSL-V600E/WT}*; *Villin-CreER^{T0/WT}*, for the first time.

The results of the analysis of these various mouse strains is shown in this chapter, focussing on short-term expression of ^{V600E}BRaf.

5.2. Aims

Our finding in the previous chapter pointed at a role for GSK3 in pathways crosstalk following ^{V600E}BRaf induction, but the role of phosphorylation of Ser9/21 in this process was unclear and current research lacks the understanding of the mechanism by which GSK3 can induce crypt hyperplasia. We are hoping at the end of this chapter, our work can shed light on the role of GSK3 in ^{V600E}BRaf induced crypt hyperplasia. We sought the following objectives, in pursuing these goals:

- To inter-cross double knockin GSK3 α/β phosphorylation-deficient mice with *Braf*^{L^{SL}-V600E/WT}; *Villin-CreER*^{T0/WT} mice.
- To study the role of GSK3 phosphorylation on crypt hyperplasia induced by ^{V600E}BRaf.
- To study the molecular mechanisms by which GSK3 phosphorylation is involved in ^{V600E}*Braf*-driven crypt hyperplasia.

5.3. Results

5.3.1. *Gsk3* knockin mouse model

In order to study the role of GSK3 phosphorylation in pathway communication, *Gsk3 α / β* double knockin mice were used. At first, in order to obtain double heterozygous knockin (*Gsk3 α ^{S21A/WT}; Gsk3 β ^{S9A/WT}*) mice, a single heterozygous *Gsk3 α ^{S21A/WT}* mouse was intercrossed with a single heterozygous *Gsk3 β ^{S9A/WT}* mouse. Offspring obtained from this cross were obtained at the expected Mendelian ratio.

In the second round of breeding, double heterozygous knockin mice for *Gsk3 α ^{S21A/WT}; Gsk3 β ^{S9A/WT}* were intercrossed, which resulted in the production of offspring including *Gsk3 α ^{S21A/S21A}; Gsk3 β ^{S9A/S9A}* double homozygous mice. Additional crossings between double homozygous offspring were carried out to maintain the colony. The detailed mating strategies and analysis of these mice has been reported in 2016 by Hey et al., showing that *Gsk3 α / β* mutations have little effect on survival of mice or intestinal integrity (Hey et al., 2016).

All the offspring were subjected to PCR to check for the presence of the *Gsk3* knockin mutations. PCR primers produced two bands in the case of *Gsk3 α* ; a smaller 271bp band representing the *Gsk3 α ^{WT}* allele and a larger 371bp band representing the *Gsk3 α ^{S21A}* allele. PCR primers for *Gsk3 β* produced two bands: a smaller 233bp band corresponding to the *Gsk3 β ^{WT}* allele and a larger 352bp band corresponding to the *Gsk3 β ^{S21A}* allele (Figure 5.1).

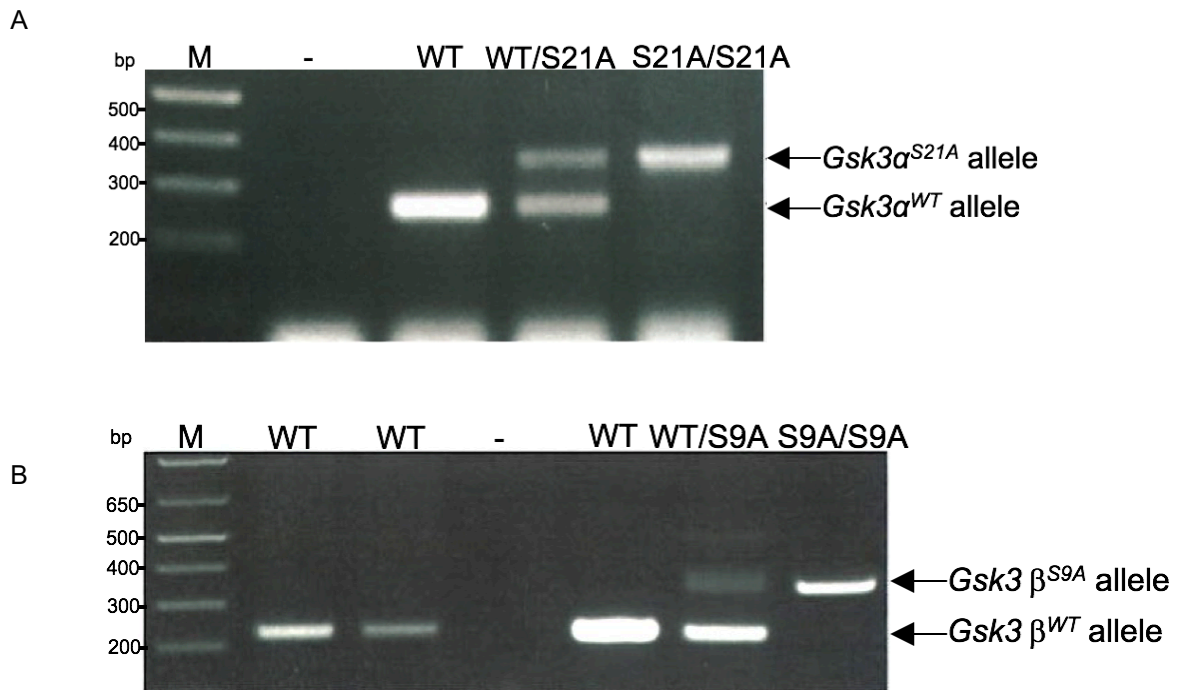


Figure 5.1 PCR genotyping to determine the genotype of Gsk3 offspring.

A) PCR genotyping in order to identify the presence of the Gsk3 α S21A knockin allele in mice; a 371bp band corresponds to the S21A knockin allele and a 271bp band corresponds to the WT allele. M=1kb ladder marker. “-” indicates an empty well.

B) PCR genotyping to identify the Gsk3 β S9A allele; a 352bp band corresponds to the Gsk3 β^{S9A} knockin allele and a 233bp band corresponds to the WT allele. M=1kb ladder marker. “-” indicates an empty well.

5.3.2. Inter-crossing of *Gsk3* knockin mice with ^{V600E}*Braf* mice

In the first round of breeding the *Gsk3α*^{S21A/S21A}; *Gsk3β*^{S9A/S9A} mice were intercrossed with *Villin-CreER*^{T0/WT} mice. The resulting offspring from this cross are shown in Table 5.1 (Mating1). In parallel, *Gsk3α*^{S21A/S21A}; *Gsk3β*^{S9A/S9A} mice were intercrossed with *Braf*^{LSL-V600E/WT} mice. The resulting expected offspring are shown in Table 5.1 (Mating 2).

At the next round of breeding, *Gsk3α*^{S21A/WT}; *Gsk3β*^{S9A/WT}; *Villin-CreER*^{T0/WT} mice, from Mating 1 were intercrossed with *Gsk3α*^{S21A/WT}; *Gsk3β*^{S9A/WT}; *Braf*^{LSL-V600E/WT} from Mating 2. The resulting offspring are shown in Table 5.2 (Mating 3). These included *Gsk3α*^{S21A/S21A}; *Gsk3β*^{S9A/S9A}; *Braf*^{LSL-V600E/WT}; *Villin-CreER*^{T0/WT} mice and relevant controls (Table 5.2).

Genotype of the mouse
Mating 1: $Villin-CreER^{T0/WT} \times Gsk3\alpha^{S21A/S21A}; Gsk3\beta^{S9A/S9A}$ Genotypes of offspring $Gsk3\alpha^{S21A/WT}; Gsk3\beta^{S9A/WT}; Villin-CreER^{TWT/WT}$ $Gsk3\alpha^{S21A/WT}; Gsk3\beta^{S9A/WT}; Villin-CreER^{T0/WT}$
Mating 2: $Braf^{LSL-V600E/WT} \times Gsk3\alpha^{S21A/S21A}; Gsk3\beta^{S9A/S9A}$ Genotypes of offspring $Gsk3\alpha^{S21A/WT}; Gsk3\beta^{S9A/WT}; Braf^{LSL-V600E/WT}$ $Gsk3\alpha^{S21A/WT}; Gsk3\beta^{S9A/WT}; Braf^{WT/WT}$

Table 5.1 Mating 1 and Mating 2 strategies conducted in parallel and genotypes of the offspring.

Genotype of the mouse
Mating 3: $Gsk3\alpha^{S21A/WT}; Gsk3\beta^{S9A/WT}; Braf^{\Delta SL-V600E/WT}$ X $Gsk3\alpha^{S21A/WT}; Gsk3\beta^{S9A/WT}; Villin-CreER^{T0/WT}$
Genotype of expected offspring
$Gsk3\alpha^{S21A/S21A}; Gsk3\beta^{S9A/S9A}; Braf^{\Delta SL-V600E/WT}; Villin-CreER^{T0/WT}$
$Gsk3\alpha^{S21A/S21A}; Gsk3\beta^{S9A/S9A}; Braf^{WT/WT}; Villin-CreER^{T0/WT}$
$Gsk3\alpha^{S21A/S21A}; Gsk3\beta^{S9A/S9A}; Braf^{\Delta SL-V600E/WT}; Villin-CreER^{TWT/WT}$
$Gsk3\alpha^{S21A/S21A}; Gsk3\beta^{S9A/S9A}; Braf^{WT/WT}; Villin-CreER^{TWT/WT}$
$Gsk3\alpha^{S21A/S21A}; Gsk3\beta^{S9A/WT}; Braf^{\Delta SL-V600E/WT}; Villin-CreER^{TWT/WT}$
$Gsk3\alpha^{S21A/S21A}; Gsk3\beta^{S9A/WT}; Braf^{\Delta SL-V600E/WT}; Villin-CreER^{T0/WT}$
$Gsk3\alpha^{S21A/S21A}; Gsk3\beta^{WT/WT}; Braf^{\Delta SL-V600E/WT}; Villin-CreER^{TWT/WT}$
$Gsk3\alpha^{S21A/S21A}; Gsk3\beta^{WT/WT}; Braf^{WT/WT}; Villin-CreER^{TWT/WT}$
$Gsk3\alpha^{S21A/S21A}; Gsk3\beta^{S9A/WT}; Braf^{WT/WT}; Villin-CreER^{T0/WT}$
$Gsk3\alpha^{S21A/S21A}; Gsk3\beta^{S9A/WT}; Braf^{WT/WT}; Villin-CreER^{T0/WT}$
$Gsk3\alpha^{S21A/WT}; Gsk3\beta^{S9A/S9A}; Braf^{\Delta SL-V600E/WT}; Villin-CreER^{TWT/WT}$
$Gsk3\alpha^{S21A/WT}; Gsk3\beta^{S9A/S9A}; Braf^{\Delta SL-V600E/WT}; Villin-CreER^{T0/WT}$
$Gsk3\alpha^{WT/WT}; Gsk3\beta^{S9A/S9A}; Braf^{\Delta SL-V600E/WT}; Villin-CreER^{TWT/WT}$
$Gsk3\alpha^{WT/WT}; Gsk3\beta^{S9A/S9A}; Braf^{\Delta SL-V600E/WT}; Villin-CreER^{T0/WT}$
$Gsk3\alpha^{S21A/WT}; Gsk3\beta^{S9A/S9A}; Braf^{WT/WT}; Villin-CreER^{TWT/WT}$
$Gsk3\alpha^{S21A/WT}; Gsk3\beta^{S9A/S9A}; Braf^{WT/WT}; Villin-CreER^{T0/WT}$
$Gsk3\alpha^{WT/WT}; Gsk3\beta^{S9A/S9A}; Braf^{WT/WT}; Villin-CreER^{TWT/WT}$
$Gsk3\alpha^{WT/WT}; Gsk3\beta^{S9A/S9A}; Braf^{WT/WT}; Villin-CreER^{T0/WT}$
$Gsk3\alpha^{S21A/WT}; Gsk3\beta^{S9A/WT}; Braf^{\Delta SL-V600E/WT}; Villin-CreER^{TWT/WT}$
$Gsk3\alpha^{S21A/WT}; Gsk3\beta^{S9A/WT}; Braf^{\Delta SL-V600E/WT}; Villin-CreER^{T0/WT}$
$Gsk3\alpha^{S21A/WT}; Gsk3\beta^{WT/WT}; Braf^{\Delta SL-V600E/WT}; Villin-CreER^{TWT/WT}$
$Gsk3\alpha^{S21A/WT}; Gsk3\beta^{WT/WT}; Braf^{\Delta SL-V600E/WT}; Villin-CreER^{T0/WT}$
$Gsk3\alpha^{WT/WT}; Gsk3\beta^{S9A/WT}; Braf^{\Delta SL-V600E/WT}; Villin-CreER^{TWT/WT}$
$Gsk3\alpha^{WT/WT}; Gsk3\beta^{S9A/WT}; Braf^{WT/WT}; Villin-CreER^{TWT/WT}$
$Gsk3\alpha^{WT/WT}; Gsk3\beta^{S9A/WT}; Braf^{\Delta SL-V600E/WT}; Villin-CreER^{T0/WT}$
$Gsk3\alpha^{WT/WT}; Gsk3\beta^{WT/WT}; Braf^{\Delta SL-V600E/WT}; Villin-CreER^{TWT/WT}$
$Gsk3\alpha^{WT/WT}; Gsk3\beta^{WT/WT}; Braf^{\Delta SL-V600E/WT}; Villin-CreER^{T0/WT}$
$Gsk3\alpha^{S21A/WT}; Gsk3\beta^{S9A/WT}; Braf^{WT/WT}; Villin-CreER^{TWT/WT}$
$Gsk3\alpha^{WT/WT}; Gsk3\beta^{WT/WT}; Braf^{WT/WT}; Villin-CreER^{T0/WT}$
$Gsk3\alpha^{S21A/WT}; Gsk3\beta^{WT/WT}; Braf^{WT/WT}; Villin-CreER^{TWT/WT}$
$Gsk3\alpha^{S21A/WT}; Gsk3\beta^{WT/WT}; Braf^{WT/WT}; Villin-CreER^{T0/WT}$
$Gsk3\alpha^{WT/WT}; Gsk3\beta^{S9A/WT}; Braf^{WT/WT}; Villin-CreER^{TWT/WT}$
$Gsk3\alpha^{WT/WT}; Gsk3\beta^{S9A/WT}; Braf^{\Delta SL-V600E/WT}; Villin-CreER^{TWT/WT}$
$Gsk3\alpha^{WT/WT}; Gsk3\beta^{WT/WT}; Braf^{WT/WT}; Villin-CreER^{T0/WT}$

Table 5.2 Mating 3 strategy and genotypes of offspring. Genotypes shown in red were used in Mating 4.

In order to maintain the colony population, $Gsk3\alpha^{S21A/S21A}$; $Gsk3\beta^{S9A/S9A}$; $Braf^{SL-V600E/WT}$; $Villin-CreER^{TWT/WT}$ mice were intercrossed with $Gsk3\alpha^{S21A/S21A}$; $Gsk3\beta^{S9A/S9A}$; $Braf^{WT/WT}$; $Villin-CreER^{T0/WT}$ mice obtained from Mating 4. The frequency of obtained genotypes is shown in Table 5.3 and shows that the mutations do not affect mouse survival (Table 5.3).

Genotype of the mouse	Observed number (%)	Expected number (%)
Mating 4: $Gsk3\alpha^{S21A/S21A}; Gsk3\beta^{S9A/S9A}; Braf^{LSL-V600E/WT}; Villin-CreER^{TWT/WT} \times Gsk3\alpha^{S21A/S21A}; Gsk3\beta^{S9A/S9A}; Braf^{WT/WT}; Villin-CreER^{T0/WT}$		
Genotype of offspring from 11 litters with 5.82 average litter size		
$Gsk3\alpha^{S21A/S21A}; Gsk3\beta^{S9A/S9A}; Braf^{LSL-V600E/WT}; Villin-CreER^{TWT/WT}$	18 (28.12%)	16 (25%)
$Gsk3\alpha^{S21A/S21A}; Gsk3\beta^{S9A/S9A}; Braf^{WT/WT}; Villin-CreER^{T0/WT}$	18 (28.12%)	16 (25%)
$Gsk3\alpha^{S21A/S21A}; Gsk3\beta^{S9A/S9A}; Braf^{LSL-V600E/WT}; Villin-CreER^{T0/WT}$	17 (26.56%)	16 (25%)
$Gsk3\alpha^{S21A/S21A}; Gsk3\beta^{S9A/S9A}; Braf^{WT/WT}; Villin-CreER^{TWT/WT}$	11 (17.19%)	16 (25%)
Total	64 (100%)	64 (100%)

Table 5.3 Mating strategy used to maintain the colony population used in this study.

5.3.3. Characterisation of intestinal tissue

In order to investigate the effects of the *Gsk3* knockin mutations on ^{V600E}Braf, mouse gut tissue from *Gsk3α*^{S21A/S21A}; *Gsk3β*^{S9A/S9A}; *Braf*^{LSL-V600E/WT}; *Villin-CreER*^{T0/WT} (BVE/Cre/Ki/Ki), induced for 3 days with TM was subjected to western blot analysis along with tissue from relevant controls such as WT, *Villin-CreER*^{T0/WT} (WT/Cre), and *Braf*^{LSL-V600E/WT}; *Villin-CreER*^{T0/WT} (BVE/Cre) which were also induced with TM. The results are shown in Figure 5.2.

In the BVE/Cre/Ki/Ki mouse gut tissue, following ^{V600E}BRaf expression, little induction of phospho-MEK was observed compared to controls, but seemed to be slightly higher than in BVE/Cre. Phospho-ERK seemed to be expressed at lower levels than BVE/Cre tissue. No phosphorylation of GSK3α/β proteins was detected as a result of mutation of Ser21/9 to Ala, as expected. An increase in phospho-p70/85^{S6K} was detected in the ^{V600E}BRaf-expressing tissue and this was not affected by the *Gsk3* mutations. Attempts to detect phospho-p90^{RSK} levels were not successful, unfortunately.

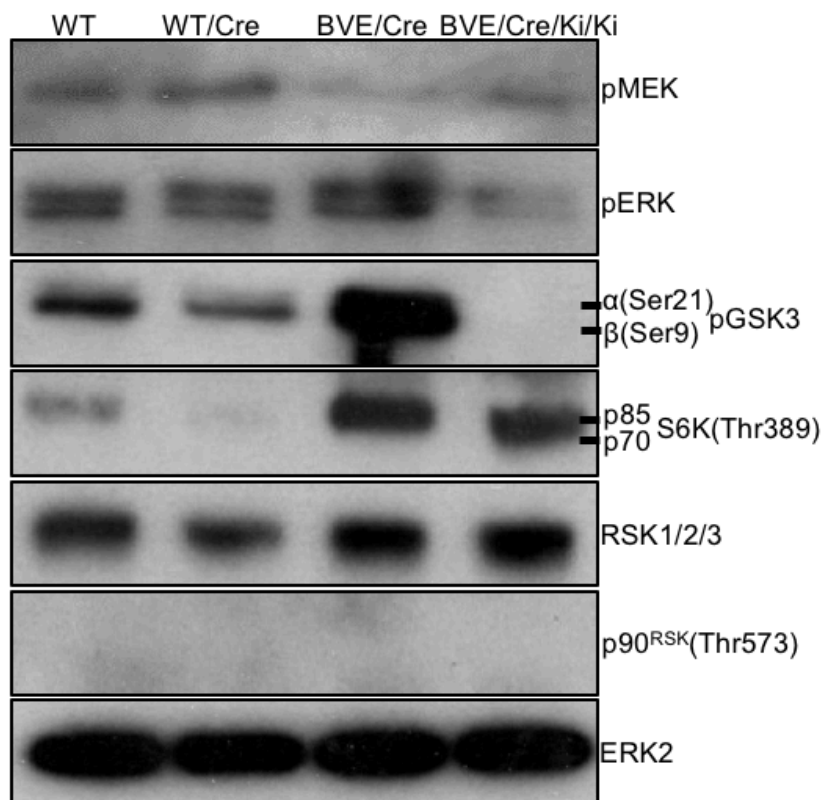


Figure 5.2 Western blot analysis of gut tissue from $Braf^{LS-V600E/WT}$; $Villin-CreER^{T0/WT}$ (BVE/Cre), $Gsk3\alpha^{S21A/S21A}$; $Gsk3\beta^{S9A/S9A}$; $Braf^{LS-V600E/WT}$; $Villin-CreER^{T0/WT}$ (BVE/Cre/Ki/Ki), $Villin-CreER^{T0/WT}$ (WT/Cre), and WT mice. Animals were injected with TM and terminated 3 days after the last TM injection. Tissue was processed accordingly and the lysate was subjected to western blotting. This blot is the same as shown in Figure 4.6 for the first three samples. The figure is representative of 3 sets of biological replicates. Tissue from section 4 of the small intestine from 12 mice were used.

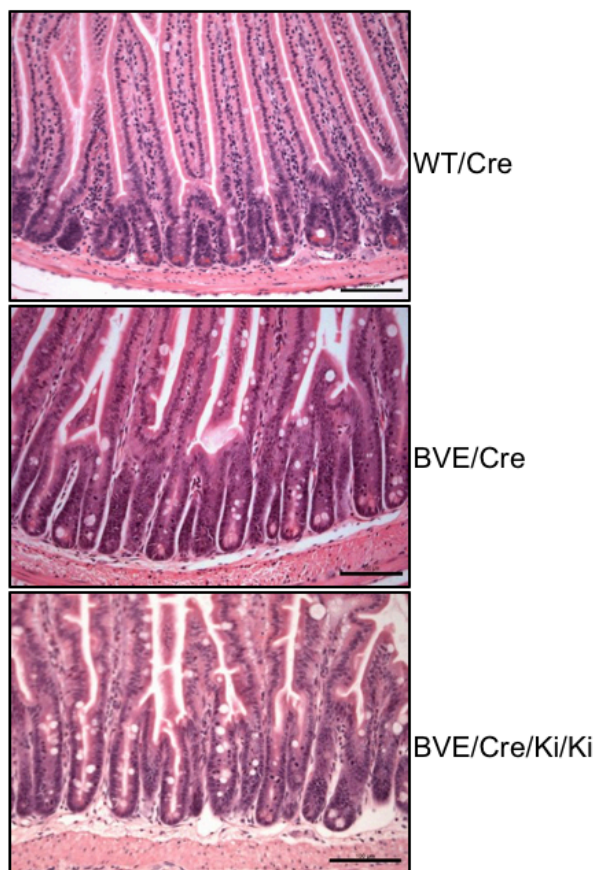
5.3.4. Effect of *Gsk3 α/β* knockin mutations on crypt hyperplasia following ^{V600E}BRaf induction

To investigate the effect of GSK3 on crypt hyperplasia, mouse gut tissue at 3 days p.i. from ^{V600E}BRaf expressing mice, with and without *Gsk3* double knockin mutations, was subjected to H&E staining. As stated before, after harvesting the small intestine, the tissue was cleaned and cut into 6 pieces of similar size, from the start of the caecum to the end of duodenum.

An increase in crypt length in section 4 of the gut was observed in BVE/Cre mice in comparison to controls (Figure 5.3A). Moreover, crypt cell number increased further in BVE/Cre/Ki/Ki animals. This increase was statistically significant (Figure 5.3).

These data suggest that ^{V600E}*Braf* mutation promotes crypt elongation. This is increased further following combined mutation of *Gsk3*. Therefore, GSK3 phosphorylation at Ser9/21 has a suppressive effect on ^{V600E}BRaf-driven crypt hyperplasia.

A



B

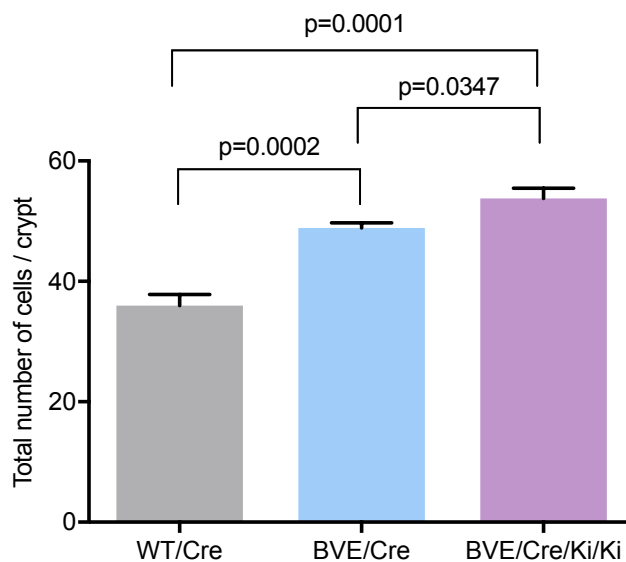


Figure 5.3 Examination of crypt length is observed following V^{600E} BRaf expression.

A) H&E staining of 3 days p.i. tissue from section 4 of the small intestine shows crypt elongation in BVE/Cre and BVE/Cre/Ki/Ki animals in comparison to control tissue. Scale bars = 100 μ m.

B) Graphs showing crypt cell number in different mice. Section 4 of the gut of 5 mice, for each of the 3 distinct genotypes, were subjected to H&E staining and 50 crypts of each section was subjected to crypt cell counting. Data show mean \pm SD. Statistical analysis was carried out using an unpaired T-test. Total No. of mice used= 15. Part of the data is the same as shown in Figure 4.8.

5.3.5. Effect of GSK3 phosphorylation on crypt cell proliferation

To study the impact of GSK3 phosphorylation on cell proliferation in the crypt, mouse gut tissue, at 3 days p.i., from BVE/Cre/Ki/Ki animals was subjected to immunohistochemical studies; the results were compared with data from BVE/Cre and control animals discussed in section 4.3.7 of chapter 4.

At first, cells were checked for BrdU positive staining which marks cells at the S phase of the cell cycle. As shown in Figure 5.4 there was a significant increase in the number of S phase proliferative cells, in BVE/Cre/Ki/Ki mice, compared to controls. Although there is a trend for an increase in BrdU+ cells compared to BVE/Cre tissue, this was not statistically significant (Figure 5.4).

The same tissue was subjected to a staining for the mitotic marker, phospho-Histone3 (pH3) staining. As shown in Figure 5.5, a significant increase in the number of pH3 positive cells, in BVE/Cre/Ki/Ki mice in comparison to both BVE/Cre as well as control samples, was observed (Figure 5.5). There was no significant increase of BVE/Cre compared to controls, but a trend towards an increase was observed.

Overall, these data suggest that GSK3, in the context of ^{V600E}BRaf, increases crypt cell proliferation with evidence for an increase in cells in the G2/M phase of the cell cycle.

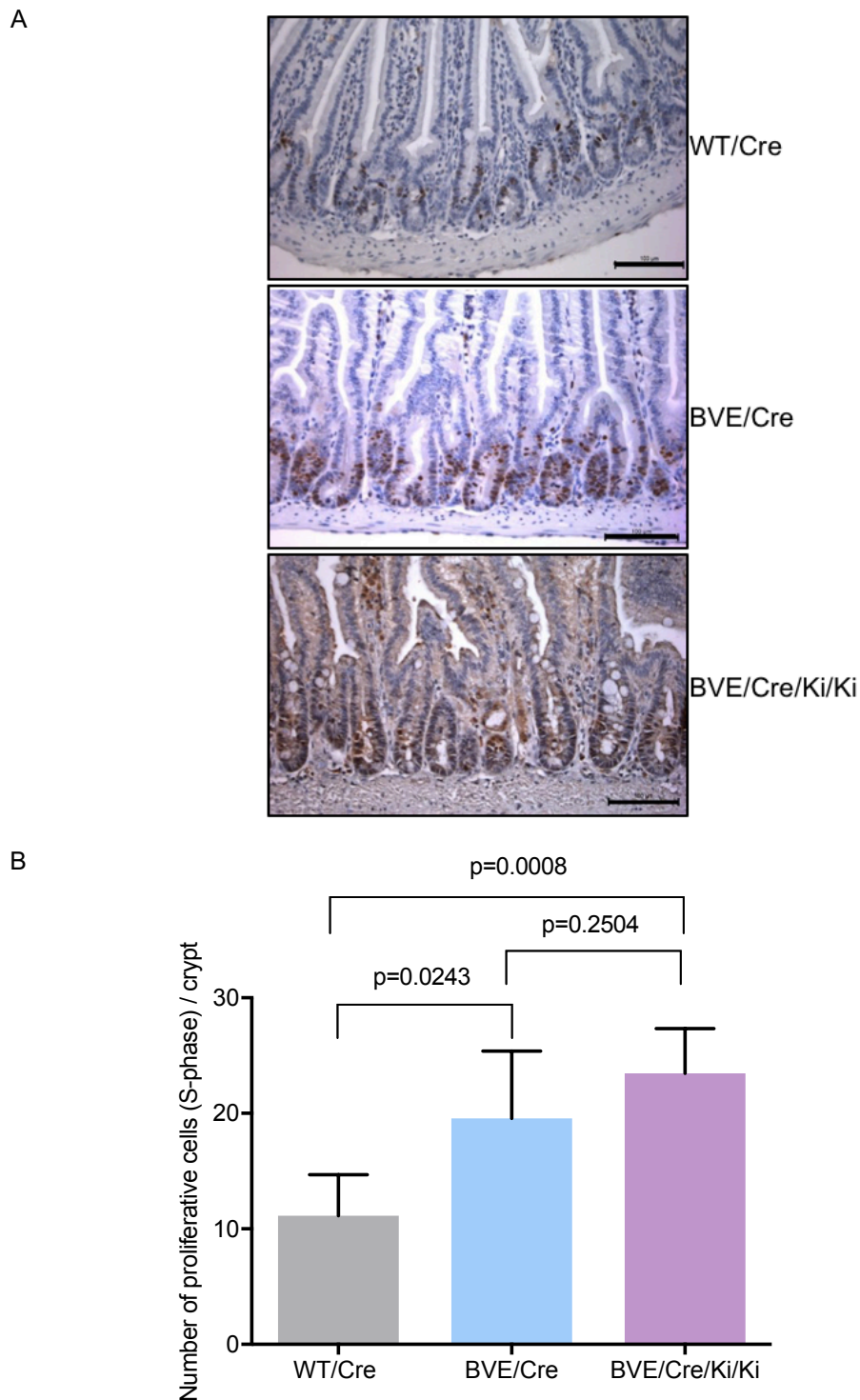


Figure 5.4 Immunohistochemical analysis for BrdU incorporation.

A) Immunohistochemical analysis of S phase proliferative cells positive for BrdU. Mice were injected with BrdU, 3 hours prior to termination. Processed tissue from section 4 of the gut was subjected to analysis with a BrdU antibody. Scale bar= 100 μ m.

B) Graph showing number of BrdU positive proliferative cells in intestinal crypts of each mice. Tissues from section 4 of the gut, from 5 mice, for each genotype, were subjected to staining and cell counting. 50 crypts from each animal were subjected to cell counting. Data show mean \pm SD. Statistical analysis was carried out using an unpaired T-test. Total No. of mice used= 15. Part of the data is the same as shown in Figure 4.9.

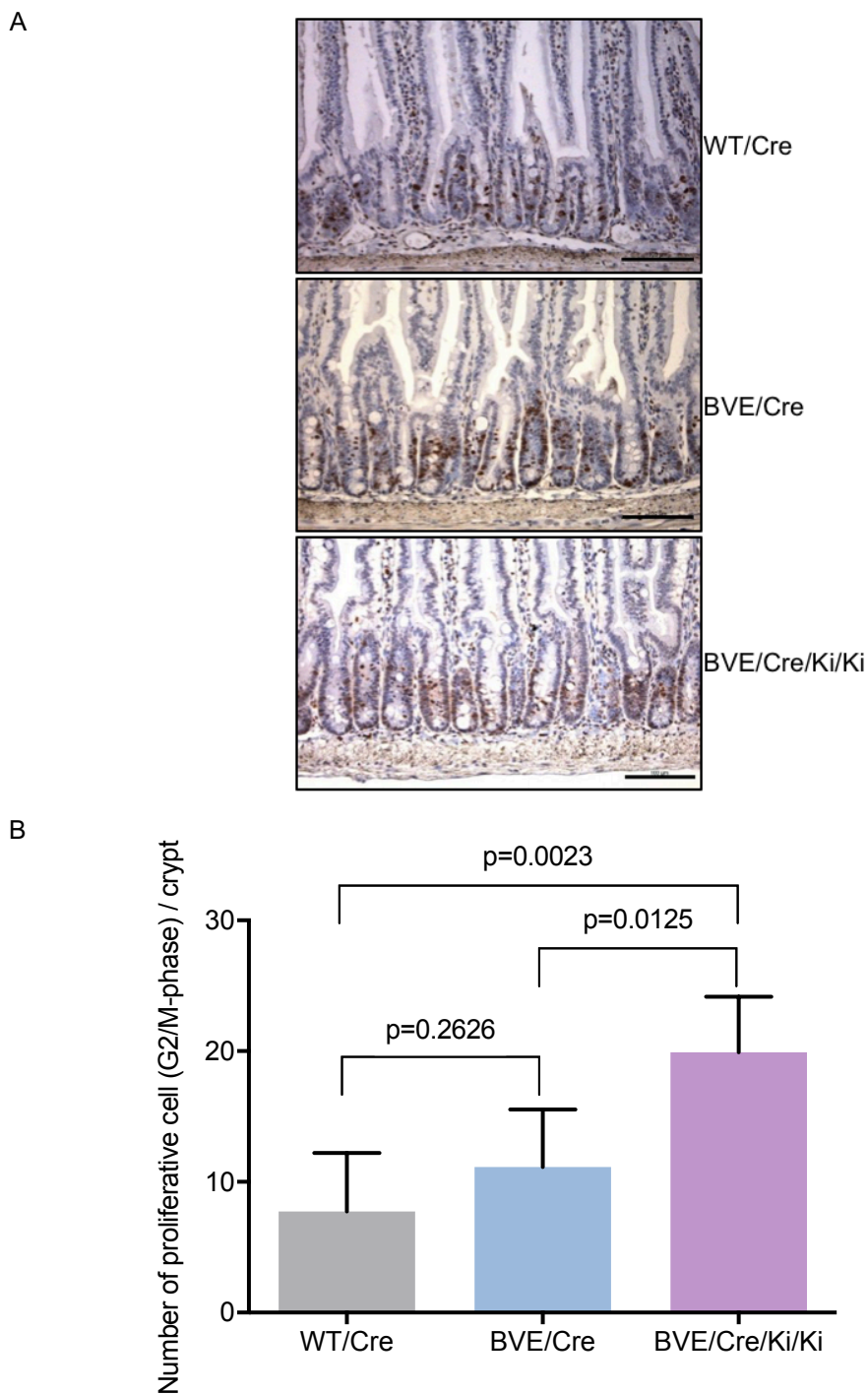


Figure 5.5 Immunohistochemical analysis for phospho-histone H3.

A) Immunohistochemical analysis of G2/M phase proliferative cells which are positive for the pH3 proliferative marker. Scale bar = 100 μ m.

B) Graph showing number of pH3 positive proliferative cells in the animals intestinal crypt. Tissues from section 4 of the gut, of 5 mice for each genotype, were subjected to staining and cell counting. 50 crypts from each animal were subjected to cell counting. Data show mean \pm SD. Statistical analysis was carried out using an unpaired T-test. Total No. of mice used= 15. Part of the data is the same as shown in Figure 4.10.

5.3.6. Gene expression analysis

In order to gain mechanistic insight, gene expression analysis was performed. Tissue from 4 groups of mice was subjected to experimentation: a) $Gsk3\alpha^{S21A/S21A}$; $Gsk3\beta^{S9A/S9A}$; $Villin-CreER^{T0/WT}$ (WT/Cre/Ki/Ki), b) $Braf^{L-SL-V600E/WT}$; $Villin-CreER^{T0/WT}$ (BVE/Cre), c) $Gsk3\alpha^{S21A/S21A}$; $Gsk3\beta^{S9A/S9A}$; $Braf^{L-SL-V600E/WT}$; $Villin-CreER^{T0/WT}$ (BVE/Cre/Ki/Ki), and d) $Villin-CreER^{T0/WT}$ (WT/Cre) which was used as the control group. Each experimental group contained a similar number of male and female individuals. All mice were injected with TM and tissues were harvested at 3 days post induction. Small pieces of fresh tissue from all sections of the gut (sections 1-6) and also the large intestine were stored in RNAlater solution at -20°C . Section 4, from 6 mice in each group (a total of 24 mice) was subjected to RNA extraction. RNA extraction and microarray analysis was performed by Dr. Spencer Gibson and Dr. Nicolas Sylvius from the Genomic Core Facility, Core Biotechnology service, University of Leicester. Bioinformatics analysis was performed by Dr. Jin-Li Luo, Leicester Cancer Research Centre (LCRC), University of Leicester.

In order to analyse the fold change in the expression of individual genes, gene values for six replicates were averaged. The average values for the control group were compared to the sample groups. Values that did not change two-fold, and those that did not maintain an adjusted p-value of 0.05 or less, were removed. These filters ensured that the remaining gene list were likely those that changed as a result of the genotype and were simultaneously statistically significant.

Pathway analysis was conducted using, the pathway enrichment analysis tools, WIKI pathway and KEGG pathway. The Kyoto Encyclopaedia of Genes and Genomes (KEGG) pathway and the WIKI pathway are two biological databases containing information on various biological systems such as cells, organism and ecosystem from molecular level information. Large scale molecular datasets were generated using genome sequencing and other experimental technologies. They contain information on diseases, drugs, metabolic pathways, signalling pathways, genes, proteins etc. KEGG pathway mainly uses scientific

publications to generate its data, whereas WIKI uses several established databases such as KEGG or Netpath (Soh et al., 2010).

5.3.7. Analysis of the impact of *Gsk3 α/β* knockin mutations on gene expression

At first, in order to study the effect of *Gsk3 α/β* knockin mutations alone on gene expression, a group of 6 mice with the WT/Cre/Ki/Ki genotype induced for 3 days with TM were subjected to microarray analysis; and the results were compared with the WT/Cre control group, also induced for 3 days with TM.

Microarray analysis showed 22 genes with >2-fold change in activity in expression compared to control. 3 of these genes were downregulated whereas 19 genes were upregulated (Appendix 1). Of these, only 4 genes (*Olfcr707*, *Olfcr1157*, *Srsf10*, and *Slbp*) were found to be involved in biological pathway enrichment using KEGG and WIKI pathway analysis databases. KEGG pathway analysis indicated an increase in the expression of 2 genes, *Olfcr707* (4.5-fold) and *Olfcr1157* (4.4-fold), which were involved in the Olfactory transduction pathway (adj P value= 0.0273), whereas WIKI pathway enrichment analysis showed an increase in expression of 2 genes; these were *Srsf10* (3.1-fold) and *Slbp* (3.6-fold), that were involved in RNA processing pathways (adj P value= 0.0068).

The data indicate that the *Gsk3 α/β* knockin mutations alone do not alter the expression of key genes in a noticeable way. Since WT/Cre/Ki/Ki survival time does not differ significantly, in comparison to WT/Cre control mice (data shown in chapter 6, Figure 6.1), these 22 genes are unlikely to be involved in mouse health or lifespan. This fits with the study published in 2016 by Hey et al., in which it was shown that *Gsk3 α/β* knockin mutations alone do not alter mouse survival or cause any changes in the anatomical or molecular characteristics of the small intestine. A small increase in apoptosis was reported at the tip of the villi in these mice (Hey et al., 2016). However, this microarray analysis has not indicated involvement of any key apoptotic genes.

As the 2-fold threshold for change of activity of the genes only revealed 22 genes which were not known to be involved in apoptosis, there was a possibility that our threshold might have filtered out some genes which would otherwise be shown to affect apoptosis. Therefore, in the re-analysis, all genes with adjusted P value of 0.05 or less were considered. Microarray data revealed only 34 genes of which 8 were downregulated while 26 were upregulated (Appendix 1A). Of 34 genes, 22 were discussed previously and shown not to be directly involved in apoptosis. Amongst the additional 12 genes found following new analysis, *Timmdc1* expression increased by 0.6-fold. *Timmdc1* can alter expression of genes which are involved in apoptosis, cell cycle arrest and regulation of cell migration. However, in this case, *Timmdc1* does not seem to alter any of the key genes involved in apoptosis confirming our previous conclusion on the effect of *Gsk3 α/β* knockin mutations alone on gene expression.

5.3.8. Molecular effect of ^{V600E}BRaf expression

To study the effect of ^{V600E}BRaf induction of gene expression, RNA from a group of 6 mice with the BVE/Cre genotype were subjected to microarray analysis and the results were compared with the, WT/Cre induced with TM for 3 days, control group.

815 genes with >2-fold altered expression were identified of which 381 genes were downregulated and 436 were upregulated (Appendix 2).

WIKI pathway enrichment analysis identified 81 genes involved in 10 different biological pathways. The pathways mostly affected by ^{V600E}BRaf induction were metabolic pathways (Figure 5.4).

Pathway Name	% Gene involvement	Adjusted P value
Cholesterol Biosynthesis	50%	1.65e-10
Amino Acid metabolism	~10%	1.65e-06
Glycolysis and Gluconeogenesis	~16%	1.95e-06
PPAR signalling pathway	~10%	1.58e-05
Adipogenesis	~7.5%	3.24e-05
Complement and Coagulation Cascade	~11.5%	5.65e-05
Alpha6-Beta4Integrin signalling pathway	~9%	7.01e-05
MicroRNA in cardiomyocyte hypertrophy	~8%	0.0002
Macrophage markers	30%	0.0008
Chemokine signalling pathway	~5%	0.0015

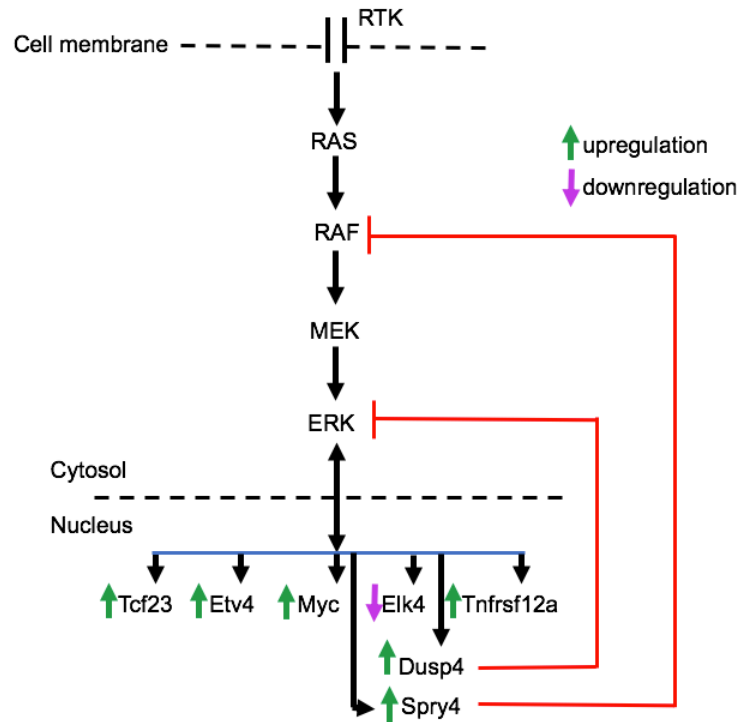
Table 5.4 WIKI pathway enrichment analysis indicating top pathways whose components change in expression following ^{V600E}BRaf induction.

To investigate the effect of ^{V600E}BRaf induction on the MAPK pathway, the microarray data was analysed for genes involved in the MAPK pathway. Enrichment analysis showed no significant changes in the MAPK pathway components, except for two negative feedback regulators, *Dusp4* and *Spry4*, which were shown to be slightly upregulated by 2.7, and 2.5-fold respectively. Some of the genes, which are known to be MAPK pathway targets, showed elevated expression; *Tcf23*, *Etv4*, *Tnfrsf12a*, and *Myc* showed increased expression by 22.5, 6.1, 3.2, and 2.0-fold, respectively, but many others such as *cyclin D1*, *c-fos*, *c-Jun*, etc did not change. However, the *Elk4* gene, a downstream target of MAPK pathway, was downregulated by 2.0-fold (Figure 5.6A). In 2009, Pratilas et al. showed an elevation in the activity of MAPK feedback inhibitors in human ^{V600E}BRAF tumour cells, and also transcription factors such as *MYC* and *ETV4* were shown to be the downstream targets of the ERK pathway (Pratilas et al., 2009). In 2013 Rad et al. showed slight changes in expression of some MAPK target genes at early stages, including *Etv4*, *Myc*, *Dusp4*, *Spry4*, and *Tnfrsf12a*, whereas a sharp increase in their expression was observed at later stages of the disease in the mouse intestine (Rad et al., 2013). Thus, there seems to be some evidence for partial induction of some MAPK target genes coupled with negative feedback regulation of the MAPK pathway, following short-term induction of ^{V600E}BRaf.

Although enrichment analysis of the microarray data did not indicate changes in the WNT signalling pathway, some WNT pathway target genes had >2-fold change in expression. These include *Wnt4*, *Tcf23*, *Dpp4*, members of the *Tnfrsf* family (*Tnfrsf12a*, *Tnfrsf19*, *Tnfrsf21*, *Tnfrsf23*, *Tnfrsf10*), members of the Keratin family (*Krt23*, *Krt31*, *Krt7*), *Vegfa*, *Stra6*, *Flrt3*, *Fgf2*, *Pparg*, *Ctgf*, *Sfrp5* and *Myc* (StanfordUniversity, 2017). For some, the expression was downregulated while it was upregulated for others. *Wnt4*, *Dpp4*, *Tnfrsf19*, *Tnfrsf10*, *Krt31*, *Vegfa*, *Stra6*, *Sfrp5* and *Fgf2* were downregulated by 2.3, 2.0, 2.1, 2.5, 2.3, 3.1, 2.3, 3.2 and 3.5-fold respectively. However, *Tcf23*, *Tnfrsf12a*, *Tnfrsf21*, *Tnfrsf23*, *Krt23*, *Krt7*, *Flrt3*, *Pparg*, *Ctgf*, and *Myc* genes were upregulated by 22.5, 3.2, 2.2, 2.1, 2.8, 3.7, 2.3, 2.4, 3.1, and 2.0-fold respectively (Figure 5.6B). Interestingly, amongst the WNT target genes, *Tcf23*

was upregulated by 22.5-fold. Rad et al. observed very small changes in WNT target gene expression, in their ^{V600E}BRaf mouse model, at early stages, but a more drastic elevation as the tumours progress (Rad et al., 2013). An increase in *MYC* expression is known to be a key component of the metabolic rewiring of colorectal carcinogenesis in human CRC tissue, irrespective of mutational background (Sato et al., 2017). An increase in *MYC* expression has also been reported in human CRC cells (Pratilas et al., 2009). In general, these data point towards some evidence for partial WNT activity at early stages in this ^{V600E}BRaf model.

A) MAPK



B) WNT

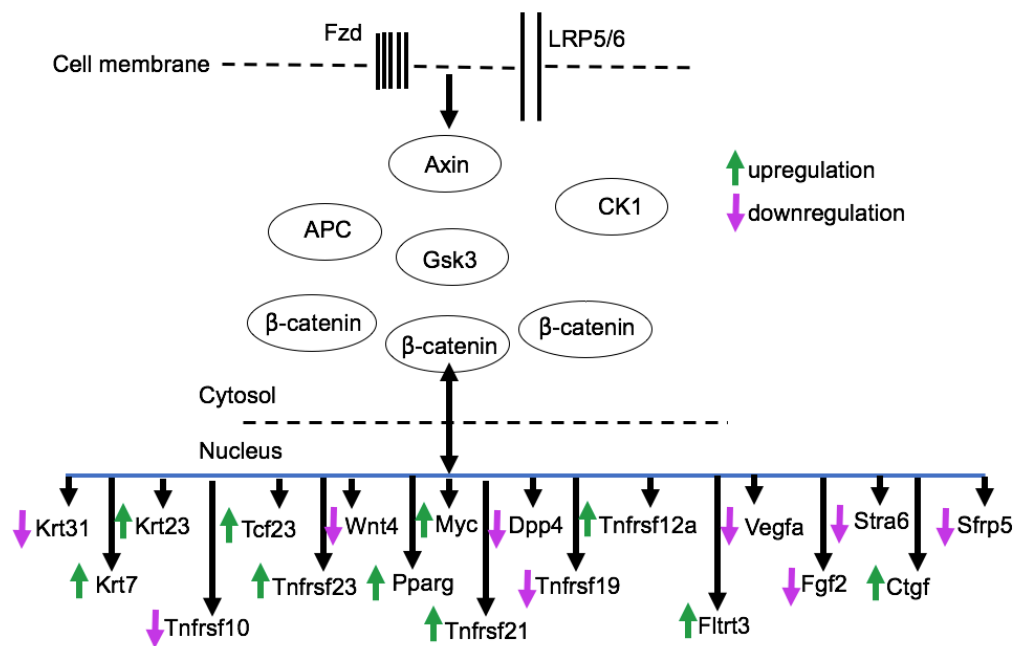


Figure 5.6 Simplified schematic diagram of V^{600E} Brat mutation's effect on the MAPK and WNT pathway.

A) Simplified diagram of V^{600E} Brat's effect on MAPK/ERK signature genes.

B) Simplified illustration on the effect of V^{600E} Brat's induction on WNT pathway signature genes.

Cholesterol biosynthesis has been reported to play an important role in the development of melanoma and colorectal cancer (Demierre et al., 2005). Our pathway enrichment analysis pointed to an enrichment in the cholesterol biosynthesis pathway, with 50% of genes involved in cholesterol biosynthesis changing following 3 days of ^{V600E}BRaf expression in the mouse gut. Multiple genes including *Mvd*, *Hmgcs1*, *Fdft1*, *Lss*, *Mvk*, *Cyp51*, *Nsdhl*, *Fdps* were upregulated by 2.8, 2.2, 3.1, 2.5, 2.3, 2.1, 2.5, and 3.0-fold respectively indicating a possible increase in pathway activity. *Abca1* gene expression was also shown to be downregulated by 4.5-fold. ABCA1 is not involved in cholesterol biosynthesis, but is known to be important in cellular cholesterol efflux. Loss of function in cancer increases intra-mitochondrial cholesterol levels, which is important for cancer cell survival (Smith and Land, 2012).

Other significant pathways altered in our enrichment analysis were in glycolysis and gluconeogenesis, with *Gapdh*, *Slc2a1*, *Gpi*, *Aldoa*, *Pfkl*, *Hk1*, and *Aldoc* genes increasing by 2.1, 3.5, 2.4, 2.0, 2.6, 2.4, and 3.2-fold, respectively, while *Fbp1* gene expression was reduced by 2.7-fold. An increase in the expression of two key regulatory genes; *Pfkl* (2.6-fold) and *Hk1* (2.4-fold), involved in glycolysis, was observed. *PFK* and *HK* are rate limiting enzymes in glycolysis whose upregulation increases glucose utilisation (Silva et al., 2012). Expression of human *FBP1* in the liver is known to be involved in an elevation of glycerol gluconeogenesis (Lamont et al., 2006). It appears that as a result of ^{V600E}BRaf induction, the rate of glycolysis is potentially increased while the gluconeogenesis pathway is reduced. Analysis of metabolite levels of human CRC tissue has shown activation of glycolysis by the Warburg effect, consistent with observations in the mouse model (Sato et al., 2017).

Enrichment analysis pointed at amino acid metabolism as an enriched pathway following 3 days of ^{V600E}BRaf expression in the mouse gut. Some of the genes involved in amino acid biosynthesis, including *Idh1*, *Gsta4*, *Farsb* and *Adh1*, respectively, showed increased expression by 2.1, 3.6, 2.1, and 2.3-fold. However, *Hmgcs2*, *Prodh*, *Aldh1a1*, *Glud1*, *Hadh*, *Oat*, and *Maoa* were downregulated by 2.1, 2.6, 7.3, 2.2, 2.0, 5.4, and 2.9-fold respectively. *ALDH1A1* in particular is known to be important in regulation of initiation and progression of colorectal and pancreatic cancers (Singh et al., 2015). Overall, although amino acid metabolism was altered, as observed by pathway analysis, there was no consistent trend towards upregulation or downregulation in any particular amino acid pathway.

Our analysis also indicated alterations in the expression of genes involved in chemokine signalling. Genes such as *Ccl9*, *Ccl6*, *Plcb4*, *Pik3r1*, *Ccl24*, and *Pik3ca* showed reduced expression by 3.2, 4.0, 2.3, 2.0, 2.2, and 2.0-fold respectively, whereas expression of *Cxcl16*, *Grk5*, and *Grk6* increased by 2.4, 2.1, and 2.0-fold respectively. Satoh et al. have reported abnormal expression of inflammatory cytokine genes in human CRC tissue (Satoh et al., 2017) consistent with what we observed. However, it should be noted that the expression average we observed may not be restricted to tumour cells but may also be due to changes in the stroma.

Altogether, the data shows that induction of ^{V600E}BRaf alters the expression of genes involved in different metabolic pathways, principally those in cholesterol biosynthesis and glycolysis. There also appears to be a partial effect on the activation of the MAPK and WNT pathways.

5.3.9. Effect of *Gsk3* mutation on gene expression changes induced by ^{V600E}BRaf

At the next stage, a comparison between gene expression changes in BVE/Cre and BVE/Cre/Ki/Ki was carried out. BVE/Cre/Ki/Ki mice were also injected with TM for 3 consecutive days and were subjected to RNA extraction and microarray analysis. The gene expression results were adjusted against the WT/Cre control group, which was also induced with TM for 3 days. Overall, BVE/Cre induced 815 gene changes (436 up and 381 down) and BVE/Cre/Ki/Ki induced 567 gene changes (293 up and 333 down). A Venn diagram indicating overlap in the gene expression changes in the two groups is shown in Figure 5.8.

The Venn diagram identified 3 groups of gene changes when comparing BVE/Cre and BVE/Cre/Ki/Ki: Group 1) 334 genes (~41% of the 815 genes from BVE/Cre and ~59% of the 567 genes from BVE/Cre/Ki/Ki) were expressed in both BVE/Cre and BVE/Cre/Ki/Ki genotypes, of which 178 were upregulated and 183 were downregulated (Appendix 3). This represents a group of genes that are induced following ^{V600E}BRaf expression, but are not affected by the *Gsk3* knockin mutations. Group 2) 481 genes unique to the BVE/Cre genotype (~59% of the 816 genes from BVE/Cre), of which 295 were upregulated and 222 were downregulated. These genes were induced by ^{V600E}BRaf, but since they do not change in the BVE/Cre/Ki/Ki group, then changes in their gene expression must be reversed by the *Gsk3 α/β* mutations (Appendix 4). Group 3) 233 genes (~41% of 567 genes from BVE/Cre/Ki/Ki) of which 114 were upregulated and 151 were downregulated (Appendix 5). These genes are new genes whose expression is changed when combining ^{V600E}BRaf expression with the *Gsk3 α/β* mutations, suggesting they occur as a result of an additive effect. A summary of these three groups and how they potentially operate in ^{V600E}*Braf/Gsk3 α/β* -induced changes is shown in Figure 5.9.

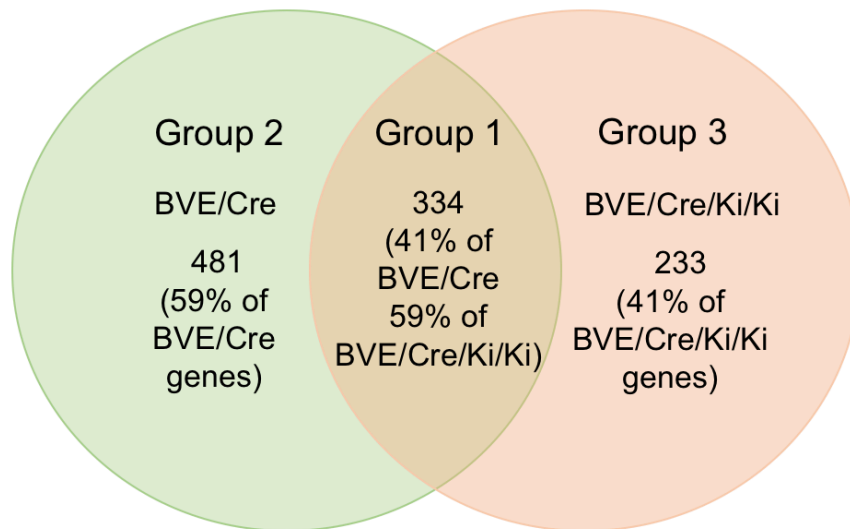


Figure 5.8 Venn diagram indicating number of genes with minimum of 2-fold change following V^{600E} BRaf induction or Gsk3 mutation. Comparison between BVE/Cre and BVE/Cre/Ki/Ki groups divides genes into 3 different groups.

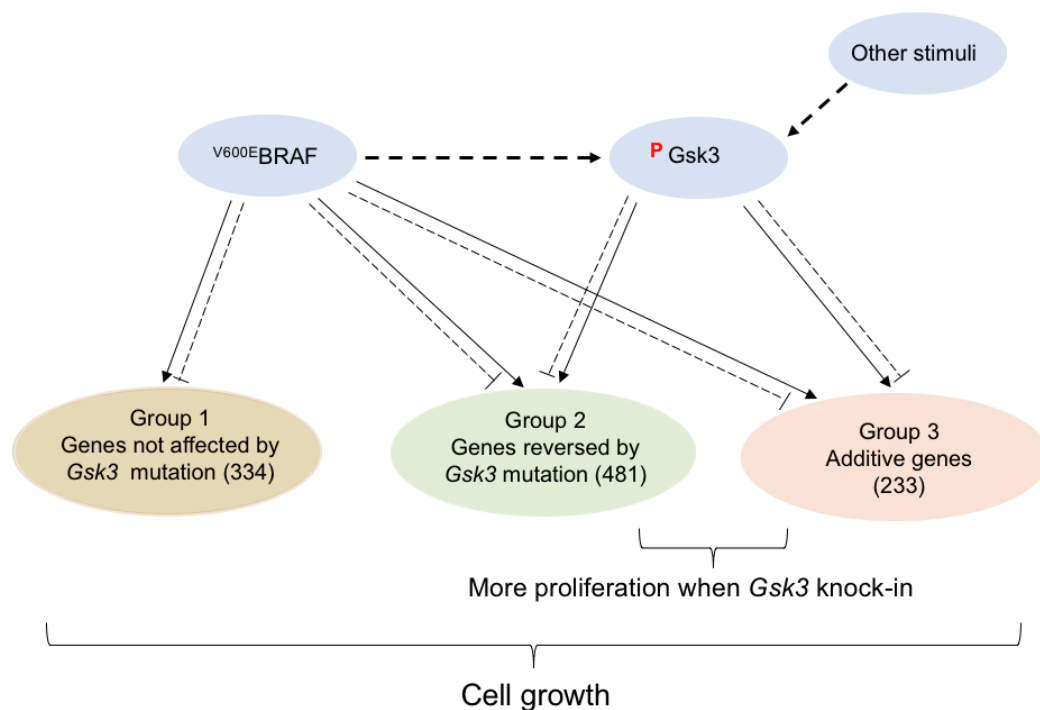


Figure 5.9 Schematic diagram of the proposed model on the effect of Gsk3 mutation on gene expression changes induced by V^{600E} BRaf. 3 groups of genes are indicated: Group 1) 334 genes whose expression are not affected by Gsk3 mutation; Group 2) 481 genes whose expression is reversed by Gsk3 mutations; and Group 3) 233 genes that are expressed as a result of V^{600E} BRaf induction and Gsk3 mutation giving an additive effect. The diagram indicates Gsk3 phosphorylation as being downstream of V^{600E} BRaf but it is potentially also induced by other stimuli.

5.3.10. Group 1 and Group 2 genes

Group 1: The expression of 334 genes were shown to have changed by more than 2-fold in both BVE/Cre and BVE/Cre/Ki/Ki samples (Figure 5.8) (Appendix 3). The difference in fold-change of these genes between BVE/Cre and BVE/Cre/Ki/Ki ranged from 0.5 to 2.94. The important gene changes in this group are discussed below.

Group 2: The expression of a total of 815 genes was shown to have changed by more than 2-fold in BVE/Cre, of which 481 genes (Group 2) were reversed by the *Gsk3 α/β* mutations in BVE/Cre/Ki/Ki (Figure 5.8) (Appendix 4). The important gene changes are also discussed below.

Of the 7 MAPK target genes shown to be differentially expressed in BVE/Cre (as discussed in Section 5.3.8), 6 were found to be differentially expressed in BVE/Cre/Ki/Ki to a similar extent, they therefore lie in Group 1. Two MAPK negative feedback regulators, *Dusp4* and *Spry4*, were similarly upregulated by 2.7 and 2.5-fold, respectively, in BVE/Cre and 2.3-fold and 2.2-fold in BVE/Cre/Ki/Ki. The MAPK target genes, *Etv4*, *Tnfrsf12a* and *Tcf23*, also increased in expression by 7.3, 3.2 and 22.5-fold, respectively, in BVE/Cre and 8.8, 2.7 and 21.3-fold in BVE/Cre/Ki/Ki. *Elk4* was shown to be downregulated by 2.01-fold in BVE/Cre and 2.25-fold in BVE/Cre/Ki/Ki. The only MAPK target gene whose expression was different in the BVE/Cre/Ki/Ki samples, and therefore lies in Group 2 was *Myc*, whose 2.0-fold induction in expression in the BVE/Cre sample was suppressed by *Gsk3* mutation. Thus, for the most part, *Gsk3* mutation does not impact on the ability of ^{V600E}Braf to partially induce MAPK target genes, although *Myc* clearly differs.

Of the 19 WNT target genes found to be differentially expressed in BVE/Cre (as discussed in Section 5.3.8), only 10 genes were found to be differentially expressed in BVE/Cre/Ki/Ki to a similar extent, they therefore lie in Group 1. These genes were: *Tnfrsf12a*, *Tnfrsf23*, *Tcf23*, *Krt7*, *Krt23*, *Krt31* and *Ctgf*. These were upregulated by 3.2, 2.1, 22.4, 3.7, 2.8, 2.3 and 3.1-fold

respectively, in BVE/Cre and 2.7, 2.6, 21.3, 2.9, 2.4, 2.0 and 2.7-fold in BVE/Cre/Ki/Ki. *Dpp4*, *Sfrp5* and *Tnfrsf19* were downregulated by 2.02, 3.21 and 2.1-fold, respectively, in BVE/Cre and 2.3, 3.12 and 2.0-fold in BVE/Cre/Ki/Ki. Expression of 9 WNT target genes previously shown to be differentially expressed in BVE/Cre was reversed by *Gsk3* mutation; they therefore lie in Group 2. *Wnt4*, *Tnfrsf10*, *Vegfa*, *Stra6* and *Fgf2* were downregulated by 2.3, 2.5, 3.1, 2.3 and 3.5-fold, respectively; whereas, *Tnfrsf21*, *Flrt3*, *Pparg* and *Myc* were upregulated by 2.2, 2.3, 2.4 and 2.0-fold, respectively, in BVE/Cre but did not change in BVE/Cre/Ki/Ki. Thus, although ^{V600E}BRaf can regulate the expression of a subset of WNT target genes, mutation of *Gsk3* can reverse the expression of ~1/2 of these genes, including *Myc*.

One of the pathways shown to be enriched in BVE/Cre samples was cholesterol biosynthesis, with ~44% of genes in the pathway showing elevated expression. Of the 8 genes shown to be involved in cholesterol biosynthesis in BVE/Cre (as discussed in Section 5.3.8), 7 of these were not affected by *Gsk3* mutation and therefore lie in Group 1. The expression of *Fdft1*, *Mvd*, *Hmgcs1*, *Lss*, *Mvk*, *Cyp51*, and *Fdps* were elevated by 3.1, 2.8, 2.2, 2.7, 2.7, 2.1 and 3.0-fold respectively, in BVE/Cre and were elevated in BVE/Cre/Ki/Ki to a similar extent. *Nsdhl* gene (2.5-fold) was the only gene in BVE/Cre whose expression was reversed by *Gsk3* mutation; it therefore lies in Group 2. Altogether, this result indicates the potential increase in the activity of cholesterol biosynthesis following ^{V600E}BRaf expression is not affected by *Gsk3* mutation.

Enrichment analysis pointed at the expression of 8 genes involved in glycolysis and gluconeogenesis in BVE/Cre (discussed in Section 5.3.8). Of these, 3 genes (*Pfk1*, *Aldoc* and *Slc2a1*) were detected to have elevated expression by 2.6, 3.6 and 3.5-fold in BVE/Cre and to similar extent (3.7, 2.5 and 3.1-fold) in BVE/Cre/Ki/Ki (Group 1). Expression of 5 genes was suppressed by *Gsk3 α/β* mutation, and therefore lie in Group 2: *Fbp1* was downregulated by 2.7-fold whereas, *Gapdh*, *Gpil*, *Aldoa*, and *Hk1* expression were increased by 2.7, 2.3, 2.1 and 2.4-fold respectively in BVE/Cre. As stated previously, *Pfk1* and *Hk1* are two key regulatory genes in glycolysis. *Pfk1* is shown not to be affected by

the *Gsk3* mutation whereas *Hk1* is. Therefore, the outcome on glycolysis and gluconeogenesis by *Gsk3* mutation is mixed.

11 genes involved in amino acid metabolism were found to change in BVE/Cre (as discussed in Section 5.3.8), of which 6 were changed in BVE/Cre/Ki/Ki to a similar extent and therefore lie in Group 1. *Gsta4* was upregulated by 3.6-fold in BVE/Cre and 2.9-fold in BVE/Cre/Ki/Ki, whereas *Aldh1a1*, *Glud1*, *Hadh*, *Maoa* and *Oat* were downregulated by 7.3, 2.2, 2.0, 2.9 and 5.4-fold, respectively, in BVE/Cre and 6.7, 2.0, 2.0, 2.6 and 5.9-fold in BVE/Cre/Ki/Ki. Expression of 5 genes was suppressed by *Gsk3* mutation in BVE/Cre/Ki/Ki and therefore these genes lie in Group 2. *Idh1*, *Farsb* and *Adh1* showed increased expression by 2.1, 2.1 and 2.3-fold respectively whereas, *Hmgcs2* and *Prodh* were downregulated by 2.1 and 2.6-fold respectively, in BVE/Cre. Thus, *Gsk3* mutation reverses the effect of ~1/2 of the genes involved in amino acid metabolism whose expression is changed by ^{V600E}BRaf.

Of the 9 genes involved in chemokine signalling in BVE/Cre (as discussed in Section 5.3.8), expression of 3 genes was also changed in BVE/Cre/Ki/Ki and therefore these genes are in Group 1. *Ccl9*, *Ccl6* and *Pik3r1* were shown to be downregulated by 3.2, 4.0 and 2.0-fold in BVE/Cre and 2.5, 4.1 and 2.2-fold in BVE/Cre/Ki/Ki. The remaining 6 genes that were shown to be differentially expressed in the BVE/Cre were reversed by *Gsk3* mutation and therefore lie in Group 2. *Plcb4*, *Ccl24* and *Pik3ca* were downregulated by 2.3, 2.2 and 2.0-fold respectively, whereas, *Cxcl16*, *Grk5* and *Grk6* were upregulated by 2.4, 2.1 and 2.0-fold in BVE/Cre. Therefore, *Gsk3* mutation suppresses ~2/3rds of the genes involved in chemokine signalling which are otherwise expressed as a result of ^{V600E}BRaf induction.

Group 3: Additive effect of *Gsk3* mutation and ^{V600E}BRaf induction

567 genes were differentially expressed in BVE/Cre/Ki/Ki, as a result of *Gsk3 α/β* mutation and ^{V600E}BRaf induction in the mouse gut, of which 334 genes were expressed in both BVE/Cre and BVE/Cre/Ki/Ki (discussed in Section 5.3.10). The remaining 233 genes were new genes shown to arise from an additive effect of the two mutations (Figure 5.8) (Appendix 5). These genes were uniquely expressed in BVE/Cre/Ki/Ki, of which 114 were upregulated, while 151 were downregulated. Pathway analysis of these genes is shown in Table 5.5.

Pathway Name	% Gene involvement	Adjusted P value
Insulin signalling	~2.5%	0.0048
Statin pathway	~10.5%	0.0048
PluriNetWork	~1.7%	0.0048
IL-5 signalling pathway	~3.7%	0.0048
B cell receptor signalling pathway	~2.5%	0.0048
MAPK signalling pathway	~2.4%	0.0048
Kit receptor signalling pathway	~4.3%	0.0048
Focal adhesion	~2.1%	0.0054
MicroRNAs in cardiomyocyte hypertrophy	~2.9%	0.0069
Androgen receptor signalling pathway	~2.4%	0.0112

Table 5.5 WIKI pathway enrichment analysis indicating top pathways whose components change in expression as a result of additive effect of *Gsk3 α/β* mutations and *V600E*BRaf induction. These genes were uniquely expressed in BVE/Cre/Ki/Ki group.

Differential expression of 7 new MAPK target genes (*Dusp6*, *Dusp8*, *Dusp26*, *Etv5*, *Elk1*, *Ptnp*, *Acvr1c*) as a result of combining *Gsk3* mutation and ^{V600E}BRaf induction were found. *Dusp6*, *Dusp8*, *Etv5* and *Elk1* were upregulated by 2.1, 2.0, 2.2 and 2.2-fold respectively while *Acvr1c*, *Dusp26* and *Ptpn5* were downregulated by 2.0, 2.2 and 5.8-fold respectively (Figure 5.10). *Ptpn5* is a downstream target of the MAPK pathway which acts as a negative feedback regulator of ERK1/2, limiting its nuclear translocation (Paul et al., 2002, Muñoz et al., 2003). The fact that there are changes in expression, of these additional MAPK targets, would suggest elevated activity through the MEK/ERK pathway in the BVE/Cre/Ki/Ki samples. However, the overall effect on the pathway is complex due to many of these genes being negative regulators.

The combination of ^{V600E}BRaf induction and *Gsk3* mutation did not alter the expression of any of the WNT target genes.

Insulin signalling was shown to be enriched in our analysis through changes in expression of a few of the genes involved. An increase in expression of *Elk1* by 2.2-fold was observed, whereas *Rhoq*, *Cblb*, and *Sh2b2* were downregulated by 2.3, 2.6, and 2.1-fold respectively. As only a small number of genes involved in insulin signalling were affected, and their expression changes were only 2-3-fold, the overall effect on the pathway is thought to be minor.

Our analysis indicated alterations in the expression of two genes involved in statin signalling. *Ldlr* was shown to be upregulated by 2.2-fold, whereas *ApoE* was downregulated by 2.8-fold compared to controls. Thus, there is no clear indication of a significant effect on the statin pathway.

PluriNetwork, the name given to an underlying network involved in Pluripotency in mouse, was amongst the signalling pathways shown to be enriched following combined ^{V600E}BRaf induction and *Gsk3* mutation. Reduction in expression of *Acvr1c*, *Hck*, *Smarca4*, and *Tfcp2l1* by 2.0, 2.0, 2.2, and 2.2-fold respectively was observed, while *Etv5* expression increased by 2.2-fold. *Tfcp2l1* (LBP-9, CRTR-1) is a transcription factor, important in pluripotency and self-renewal of

embryonic stem cells, and is known to be involved in different cancers (Kotarba et al., 2018). *Tfcp2l1* is a downstream target of the canonical WNT pathway and is important in the WNT promoted self-renewal of embryonic stem cells (Qiu et al., 2015).

IL-5 signalling was enriched with altered expression of 3 of the genes involved. *Elk1* was upregulated by 2.2-fold, whereas *Hck* and *Sh2b2* were downregulated by 2.0, and 2.0-fold respectively.

Overall, the result is indicative of the fact that the combined mutation does not give clear changes in the activity of any new pathways. The most noticeable change is an increase in the expression of MAPK pathway targets.

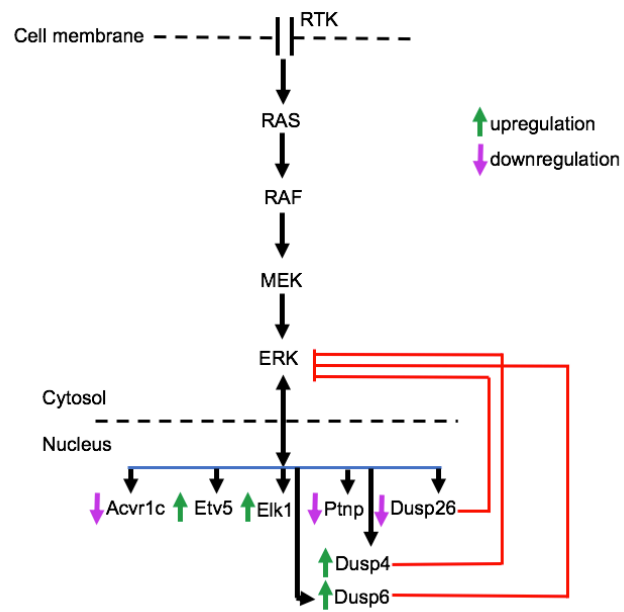


Figure 5.10 Simplified schematic diagram indicating the combined effect of Gsk3 mutation and $V600E$ BRAF induction on the MAPK signalling pathway.

5.3.11. Group 3a: *Gsk3* knockin mutation alters expression level of some common genes

While analysing the 334 genes which are commonly expressed in both BVE/Cre and BVE/Cre/Ki/Ki (Group 1), (discussed in Section 5.3.10), a subset of 13 genes were identified; that, although they were commonly expressed in both BVE/Cre and BVE/Cre/Ki/Ki samples, their expression level was significantly different between the two genotypes (Appendix 6). These genes are classified as Group 3a genes. The difference in fold change between BVE/Cre and BVE/Cre/Ki/Ki ranged from 2.01 to 2.94.

Amongst the Group 3a genes were 3 Angiopoietin genes. *Ang3*, *Ang4* and *Ang6* were downregulated by 4.0, 3.4 and 3.2-fold respectively in BVE/Cre but by 9.1, 9.9, and 7.6-fold respectively in BVE/Cre/Ki/Ki. Angiopoetins are protein ligands, that bind to Tier 1-2 receptors, which trigger angiogenesis during embryonic development and adult vessel homeostasis (Fagiani and Christofori, 2013). The higher level of downregulation in BVE/Cre/Ki/Ki suggests a suppressive role of the *Gsk3* mutations.

4 of the Defensin alpha genes were found to be significantly downregulated in BVE/Cre/Ki/Ki in comparison to BVE/Cre. *Defa-ps1*, *Defa-rs7*, *Defa25* and *Defa26* were downregulated by 5.1, 7.5, 9.6 and 5.0-fold respectively in BVE/Cre, but by 11.7, 15.2, 20.2 and 14.8-fold respectively in BVE/Cre/Ki/Ki. Alpha defensins are neutrophil peptides that are seen to be elevated in tumour tissues and are produced in response to gram-positive and gram-negative bacteria, fungi, and pro-inflammatory cytokines in humans (White et al., 1995, Zou et al., 2007). Zou et al. reported elevation in alpha-defensin 1-3 levels in stool samples of patient with CRC and argued that this can be used as a diagnostic marker (Zou et al., 2007). The higher level of downregulation in BVE/Cre/Ki/Ki suggests a suppressive role of the *Gsk3* mutation.

Expression of 2 of the Cytochrome P450 genes were further downregulated in BVE/Cre/Ki/Ki in comparison to BVE/Cre. *Cyp2b10* and *Cyp2b9* were

downregulated by 12.0 and 9.3-fold respectively in BVE/Cre and 31.9 and 21.9-fold in BVE/Cre/Ki/Ki.

5.3.12. Effect of ^{V600E}BRaf induction on the expression of AMP-activated protein kinase α

As was explained previously, gene expression analysis indicated an impact of ^{V600E}BRaf induction on glycolysis and other metabolic pathways. As a next step, we analysed AMPK, since AMPK is a serine threonine protein kinase which plays an important role as a cellular fuel sensor. Activated AMPK can phosphorylate and activate a number of metabolic enzymes involved in cellular ATP-consumption such as cholesterol, protein and fatty acid biosynthesis. AMPK is also known to be involved in the regulation of mTOR and cellular proliferation. AMPK is proposed to act as a suppressor of proliferation in normal as well as cancer cells (Motoshima et al., 2006). Tissue lysates from BVE/Cre, and BVE/Cre/Ki/Ki as well as control mice, induced with TM for 3 days, were subjected to western blot analysis for AMPK.

As previously discussed, ^{V600E}BRaf induction over a short time-frame results in only weak elevation of phospho-ERK, with no changes in MEK phosphorylation compared to controls (Figure 5.11A). Induction of ^{V600E}BRaf in BVE/Cre samples reduced AMPK α protein expression, in comparison to control samples, and this remained the same once *Gsk3 α / β* knockin mutations were introduced with ^{V600E}BRaf. Expression of phospho-AMPK α was similar in all samples, although it was slightly elevated in BVE/Cre.

To further analyse the effect of ^{V600E}BRaf on phospho-AMPK α expression, samples from animals treated with PD184352 were subjected to western blot analysis. As explained in chapter 4, following inhibition of MAPK with PD184352, the inhibition of phospho-ERK was detected. Western blot analysis detected both phospho-AMPK α 1/2 isoforms. Phospho-AMPK α 1 levels decreased in PD184352 treated samples, compared with untreated samples, while in PD184352 treated BVE/Cre phospho-AMPK α 2 was reduced, compared to the untreated sample (Figure 5.11B).

Thus, these data show that AMPK α is downstream of the MAPK pathway in the mouse intestine, but this occurs irrespective of ^{V600E}*Braf* mutation or *Gsk3* mutation status suggesting AMPK is not the mediator of metabolic changes observed in the microarray studies.

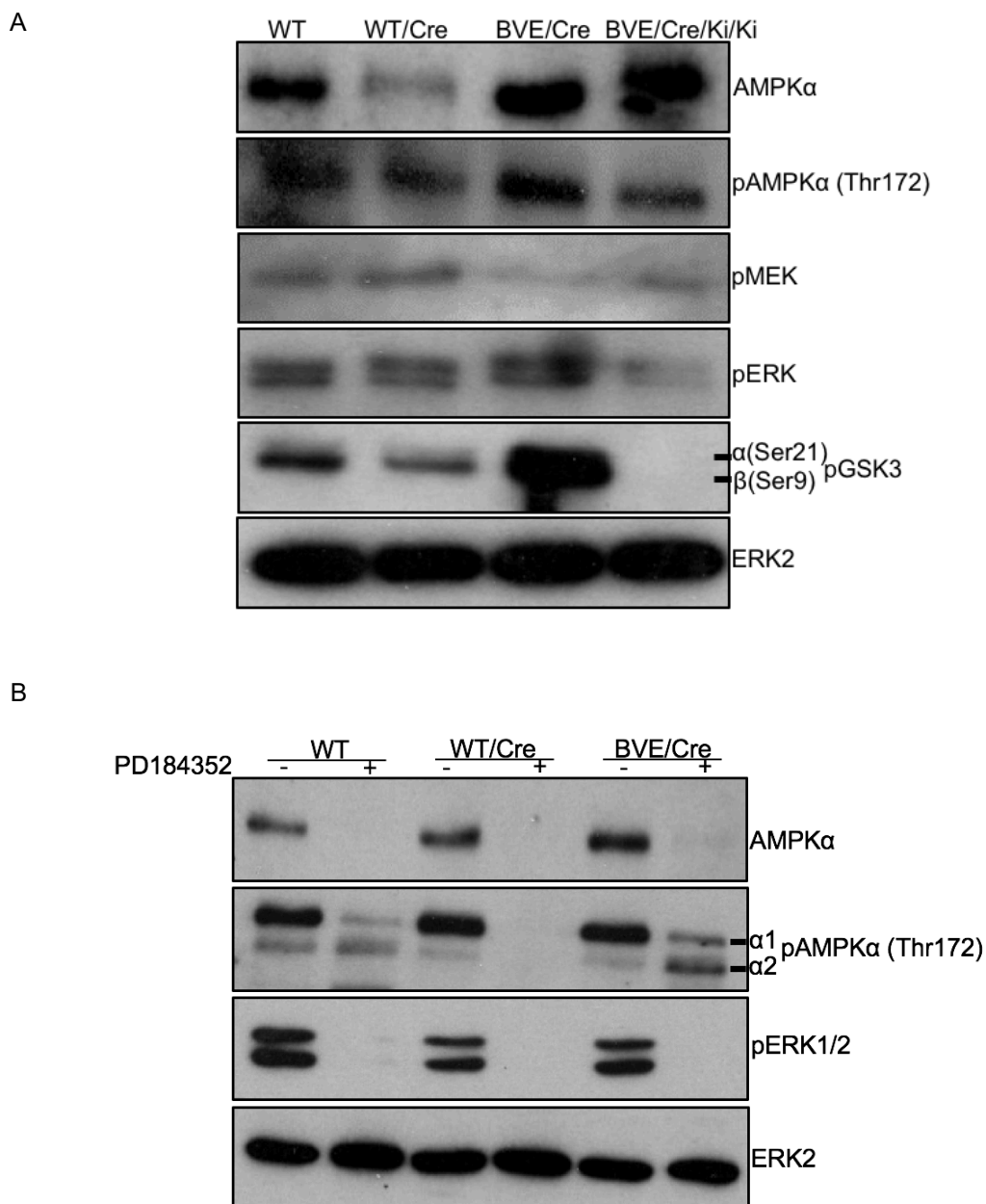


Figure 5.11 Expression and phosphorylation of AMPK- α protein kinase following $V600E$ BRaf induction with or without Gsk3 α/β mutations.

A) Western blot analysis of samples from WT, WT/Cre, BVE/Cre as well as BVE/Cre/Ki/Ki mice. Animals were terminated 3 days after the last TM injection. Tissue was processed and the lysates were subjected to western blotting. Some of these panels are the same as shown in Figure 5.2. The figure is representative of 3 sets of biological replicates. Total No. of mice used=12.

B) Western blot analysis of PD184352-treated mouse tissue. Animals were injected with PD184352 or carrier control on 3 consecutive days at the same time every day after the last TM injection. Animals were terminated 6 hours after the last injection. Intestinal tissue was processed and the resulting lysates were subjected to western blot analysis. Some of the blots are the same as shown in Figure 4.12. The figure is representative of 3 sets of biological replicates. Total No. of mice used=18.

5.4. Conclusion

In chapter 4 the *Villin-CreER^{T0/WT}* mouse model was introduced and subjected to experimentation in order to investigate the effect, of ^{V600E}BRaf induction, on crypt hyperplasia and protein expression. An increase in GSK3 α/β phosphorylation at Ser21/9 was observed, which is similar to observations reported in the *AhCreER^{T0/WT}* mouse model (Carragher et al., 2010). In order to study the role of GSK3 in the crosstalk in more detail, double knockin mutations of *Gsk3 α/β* at Ser21/9 were introduced.

As shown in chapter 4, in the ^{V600E}*Braf* mouse, lengthening of the crypt occurs which is the result of an increase in cell number in comparison to controls. It is shown that there was an even further increase in crypt cell number/length following introduction of the *Gsk3* mutation. An increase in crypt cell number was associated with further increases in the number of proliferative cells. Thus, GSK3 phosphorylation acts as a suppressor of ^{V600E}BRaf-induced crypt proliferation at early stages. In order to study the effect of these mutations at the molecular level, in this chapter, the tissue was subjected to RNA extraction and subsequent microarray analysis.

Molecular analysis shows that *Gsk3 α/β* knockin mutations on the wild type background changes the expression of very few genes - 22 in total. Thus, changes in these genes do not affect the phenotype of the mouse, or their normal life span, since it is known that survival of these mice is normal. This fits with the data of Hey et al. (2016), in which it was shown that *Gsk3 α/β* double knockin mice are fertile, and have a normal life span, with very few morphological and molecular alterations in the small intestine. Although, they were shown to have a very small increase in apoptosis at the tip of villi (Hey et al., 2016), the microarray analysis shown here does not indicate an involvement of apoptotic genes/pathways. Therefore, the slight increase in apoptosis reported in Hey et al. might be due to a combined effect of the 22 genes.

In BVE/Cre mice, a group of 815 genes with altered expression, as a result of ^{V600E}BRaf induction, was observed of which 81 were found to be involved in enrichment of 10 different biological pathways. Although, the MAPK pathway was not one of the enriched pathways, of 30 MAPK downstream target genes that were assessed, 8 were found to have alterations in their expression in comparison to controls. Two negative feedback regulators of the MAPK pathway showed an increase in expression; this may explain why BVE/Cre tissue does not show an increase in ERK phosphorylation following ^{V600E}BRaf induction. In 2013, using the *Villin-Cre* mouse model, Rad et al. examined expression of MAPK pathway target genes at different stages of progression using qRT-PCR. A significant increase in expression of MAPK target genes was shown at later stages of the disease for example LGD, HGD, and carcinoma, but this was weak at the earlier hyperplastic stage (Rad et al., 2013). Overall, these data show evidence for weak induction of a subset of ~30% of MAPK target genes. This is consistent with our previous observation that MEK inhibition does not reverse crypt hyperplasia.

The WNT pathway was not shown to be enriched in expression in BVE/Cre animals but, of 135 WNT target genes assessed, 19 (~14%) were shown to be expressed differentially. Changes in expression of some WNT pathway target genes was also previously reported by Rad et al. However, a significant increase in their expression was only seen at the dysplastic and carcinoma stages of the disease, whereas at the earlier hyperplastic stage, changes were very small in comparison to WT tissue (Rad et al., 2013). Our analysis shows induction of some WNT pathway targets and in particular a ~23-fold expression in *Tcf23*. Members of TCF transcription factors are known to be important in maintaining cell cycle progression and proliferation. Ding et al. reported an increase in nuclear localisation of the TCF- β -catenin complex during S and G2 phases of the cell cycle (Ding et al., 2014). Therefore, the sharp increase in *Tcf23* expression potentially corresponds to our observation of an increase in S phase proliferation in BVE/Cre samples. *Myc*, a key gene in the gut was also upregulated by ~2.0-fold. In 2007, Sansom et al. reported *Myc* as an important intermediary protein, at the early stages of neoplasia, which is induced by *Apc*

loss. It was shown that loss of *Myc* can rescue the phenotype which was created by the *Apc* loss, even in the presence of high nuclear β -catenin, using the *AhCre* mouse model. It was proposed that *Myc* is the most important downstream target of the WNT pathway, which itself is crucial for the activation of the majority of WNT downstream target such as *Tcf4* in colorectal cancer (Sansom et al., 2007). Activation of a subset of WNT pathway targets is consistent with previous observations in the *AhCreER^{T0/WT}* model in which an increase in nuclear β -catenin was observed following ^{V600E}BRaf induction (Carragher et al., 2010).

Genes involved in cholesterol biosynthesis showed increased expression following ^{V600E}BRaf induction. Of 16 genes involved in the pathway, 8 were shown to be upregulated by at least two-fold. Moreover, the gene coding for *Abcab1*, an important factor in cholesterol efflux (Smith and Land, 2012), showed reduced expression by 4.5-fold. Therefore, it is plausible that an increase in cholesterol biosynthesis and reduction of cholesterol efflux occurs as a coordinated event at the hyperplastic stage, which results in increased cholesterol levels in BVE/Cre cells. In 2012, Smith et al., using young adult mouse colon, showed *Abca1* gene mRNA was downregulated by a minimum of 3-fold in tumour cells and *Abca1*-restored cells were shown to be excluded quickly from the tumour. In addition to reduction in *Abca1* activity, cholesterol biosynthesis was shown to increase in cancer cells (Smith and Land, 2012). *ABCAB1* promoter methylation has been reported in high grade prostate cancers, but is not evident in benign prostate. It is suggested that an increase in intracellular cholesterol, as a result of loss of ABCA1 protein function, sets the stage for prostate tumour progression in humans (Lee et al., 2013).

Our microarray analysis showed a potential increase in glycolysis. Of 51 genes involved in the pathway, 8 were differentially expressed by >two-fold, 2 of which, *Hk1* and *Pfkl*, are key regulators of glycolysis. An increase in glycolysis in cancers is known as the Warburg effect. Most cancer cells are known to have high level of glycolysis and production of lactic acid (Martins et al., 2016). Recently a new concept, known as “reverse Warburg effect”, has been introduced in which it has been proposed that mitochondria of tumour cells have

the ability to manipulate stromal cells towards catabolism. The tumour microenvironment then produces the required fuel for anabolic cancer cells to use via the TCA cycle and OXPHOS. This phenomenon was shown to occur in breast cancer cells, ovarian cancer, head and neck, and lymph node metastasis and osteosarcoma (Sotgia et al., 2011, Chekulayev et al., 2015). In 2015, Chekulayev et al. suggested that CRC should not be considered a hypoxic tumour, as it consumes higher than the normal level of oxygen, but refuted the idea that CRC stromal cells fuelled malignant cells through OXPHOS system (Chekulayev et al., 2015). Therefore, it is possible that an increase in glycolysis and the Warburg effect in our study could be occurring in the hyperplastic epithelial cells and not in stromal tissue.

Of 112 genes involved in amino acid metabolism, 11 were found to be differentially regulated as the result of V^{600E} BRaf induction. However, there was no consistent or a particular trend towards a particular pathway. Of 186 genes known to be involved in the chemokine signalling, 9 were shown to be differentially expressed following induction of V^{600E} BRaf. However, no pathway was reproducibly altered. Given the effect of V^{600E} BRaf on several metabolic pathways, we examined AMPK α . Although we found evidence for phosphorylated and non-phosphorylated forms of AMPK α being downstream of the MAPK pathway, this effect was not restricted to V^{600E} BRaf-expressing tissue.

At the next stage, in order to investigate the role of GSK3 phosphorylation on gene expression at early stages, gene expression patterns in BVE/Cre and BVE/Cre/Ki/Ki gut tissue were compared. 3 groups of genes were identified: Group 1) 334 genes whose expression is not affected by *Gsk3 α/β* mutations and which are commonly expressed in both BVE/Cre as well as BVE/Cre/Ki/Ki; Group 2) 481 genes uniquely expressed in the BVE/Cre, whose expression is reversed by *Gsk3 α/β* knockin mutations in the BVE/Cre/Ki/Ki; Group 3) 233 genes whose expression is the result of additive effect, of V^{600E} BRaf induction and *Gsk3 α/β* knockin mutations, and are only expressed in BVE/Cre/Ki/Ki (Figure 5.8). Another small group (Group 3a) of 13 genes had expression that

was common to BVE/Cre and BVE/Cre/Ki/Ki, but showed substantial differences in expression between the two.

Induction of ^{V600E}BRaf can affect the expression of a subset of ~15% of WNT target genes (*Tnfrsf12a*, *Tnfrsf23*, *Tcf23*, *Krt7*, *Krt23*, *Krt31*, *Ctgf*, *Dpp4*, *Sfrp5*, *Tnfrsf19*, *Wnt4*, *Tnfrsf10*, *Vegfa*, *Stra6*, *Tnfrsf21*, *Flrt3*, *Pparg*, *Myc* and *Fgf2*), ~50% of which were reversed by *Gsk3* mutation (*Wnt4*, *Tnfrsf10*, *Vegfa*, *Stra6*, *Fgf2*, *Tnfrsf21*, *Flrt3*, *Pparg* and *Myc*). This result suggests that phosphorylation of Ser21/9 of GSK3 plays a role in regulation of a subset of WNT target genes.

The main additive effect of the two mutations was on MAPK target genes. ^{V600E}BRaf alone was found to alter the expression of 7/30 MAPK pathway targets; *Gsk3* mutation additionally changed the expression of 8 of these. This observation of higher activity, through the MAPK pathway, may explain why expression of phospho-MEK is slightly higher in BVE/Cre/Ki/Ki in comparison to BVE/Cre (Figure 5.2A). A higher activity, through the MAPK pathway, may also explain the observation of a higher number and proliferation of crypt cells in BVE/Cre/Ki/Ki compared to BVE/Cre (Figure 5.3). It would be interesting to test this possibly by treating BVE/Cre/Ki/Ki samples with MEK inhibitors to examine if the higher crypt cell number and proliferation can be reversed.

In summary, these molecular studies suggest that induction of ^{V600E}BRaf alone mostly alters the expression of genes involved in cholesterol biosynthesis, with partial effects on glycolysis/gluconeogenesis pathways, chemokine signalling, and the MAPK and WNT pathway. *Gsk3* mutation reverses the expression of a subset of WNT pathway genes; it also alters the expression of a new group of MAPK target genes, which are mostly negative feedback regulators. Figure 5.12 shows a detailed hypothesised model of the ^{V600E}BRaf and GSK3 crosstalk to summarise these results (Figure 5.12).

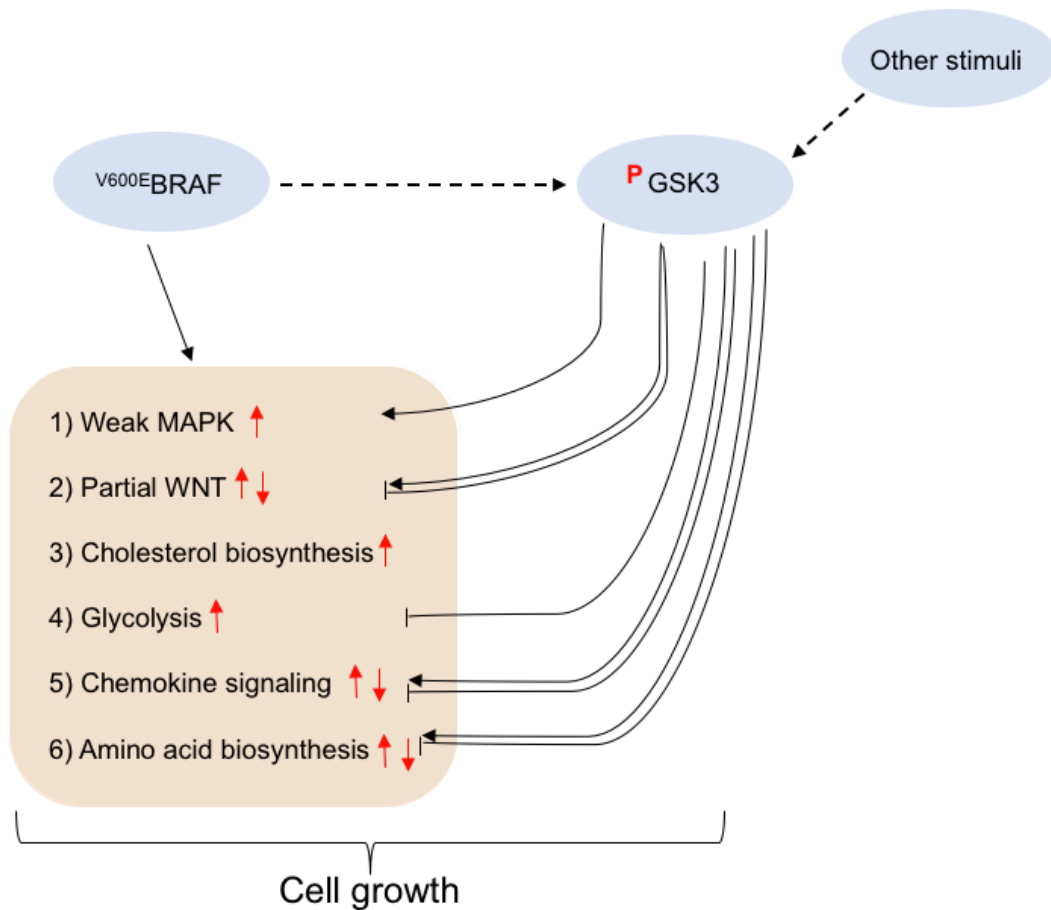


Figure 5.12 Schematic diagram of $V600E$ BRaf and GSK3 crosstalk based on the gene expression study. 3 groups of genes and affected pathways are indicated: Group 1) 334 genes whose expression not affected by Gsk3 mutation. Group 2) 481 genes whose expression is reversed by Gsk3 mutation. Group 3) 233 genes that are expressed as a result of combined, $V600E$ BRaf induction Gsk3 mutation, additive effect. Group 3a) 13 genes, whose expression differs by a minimum of 2-fold between BVE/Cre/Ki/Ki and BVE/Cre. Besides $V600E$ BRaf, GSK3 phosphorylation may also be induced by other stimuli in the cell.

Chapter 6. Investigation of the role of GSK3 phosphorylation in ^{V600E}BRaf-induced tumour development: long-term study

6.1. Introduction

The work in previous chapters indicated that *Gsk3 α/β* knockin mutation of Ser21/9 increases crypt cell number, once it is introduced on the back of the ^{V600E}*Braf* mutation, possibly through an increase in cell proliferation. We also wanted to study the long-term effect of the mutation on tumour burden and the survival of the animals. As was mentioned, work was previously done in the laboratory on *Gsk3 α* ^{S21A/S21A}; *Gsk3 β* ^{S9A/S9A} mice on the *Braf* wild type background, which indicated that the knockin mutations on their own did not have any significant effect on crypt phenotype and the animals survived a normal life span (Hey et al., 2016). Here, we examined tumour development and survival in the long-term following introduction of the *Gsk3 α/β* knockin mutations onto the ^{V600E}*Braf* background.

6.2. Aims

Current research indicates that induction of ^{V600E}BRaf, in the small intestine, results in reduction of animal life span. It leads to the formation of tumours in the small intestine, but it does not address how GSK3 affects tumour formation, grade and mouse lifespan. We hope to clarify if GSK3 Ser9/21 phosphorylation has an additive effect to the ^{V600E}*Braf* mutation on the animals' quality of life. To address this, we sought the following objectives:

- To study the effect of *Gsk3 α/β* knockin mutations on animal survival in the context of ^{V600E}BRaf.
- To study the effect of *Gsk3 α/β* knockin mutations, on tumour burden and stage, in the context of ^{V600E}*Braf*.
- To compare BVE/Cre and BVE/Cre/Ki/Ki mice on survival, tumour burden and stage.

6.3. Results

6.3.1. Effect of *Gsk3* mutation on long-term survival following ^{V600E}BRaf induction

In order to study the effect of genotype on survival, 4 groups of animals were part of this study: a) *Villin-CreER*^{T0/WT} (WT/Cre), b) *Braf*^{LSL-V600E/WT}; *Villin-CreER*^{T0/WT} (BVE/Cre), c) *Gsk3α*^{S21A/S21A}; *Gsk3β*^{S9A/S9A}; *Villin-CreER*^{T0/WT} (WT/Cre/Ki/Ki), d) *Gsk3α*^{S21A/S21A}; *Gsk3β*^{S9A/S9A}; *Braf*^{LSL-V600E/WT}; *Villin-CreER*^{T0/WT} (BVE/Cre/Ki/Ki). All mice received TM injections, and were kept under standard conditions in the animal facility, and monitored routinely for their health. Based on the severity of the symptoms, sick mice were humanely terminated according to Home Office protocols. 3 hours prior to termination, mice received BrdU injections. Tissue was harvested according to standard protocols. In all cases, survival time was represented as the duration between the last TM injection and the termination day. Tissue from BVE/Cre and WT/Cre mice were kindly collected by Dr. Hong Jin from our laboratory.

As shown in Figure 6.1, a significant reduction in mouse survival time was observed in BVE/Cre (13 Females, 14 males and 4 of unknown sex) mice, in comparison to the WT/Cre (sex is unknown) control. A significant reduction in survival time was also observed in BVE/Cre/Ki/Ki (5 females, and 6 males) mice, compared with WT/Cre/Ki/Ki (3 females and 8 males) mice. No significant difference in survival of the WT/Cre/Ki/Ki mice was observed, compared to WT/Cre mice, which is consistent with data of Hey et al. (Hey et al., 2016). A marginal reduction was observed in animal survival of BVE/Cre/Ki/Ki mice, compared to BVE/Cre mice, but this difference was not statistically significant. Thus, ^{V600E}BRaf expression has a large effect on survival, whereas the *Gsk3* knockin mutations have little effect (Figure 6.1).

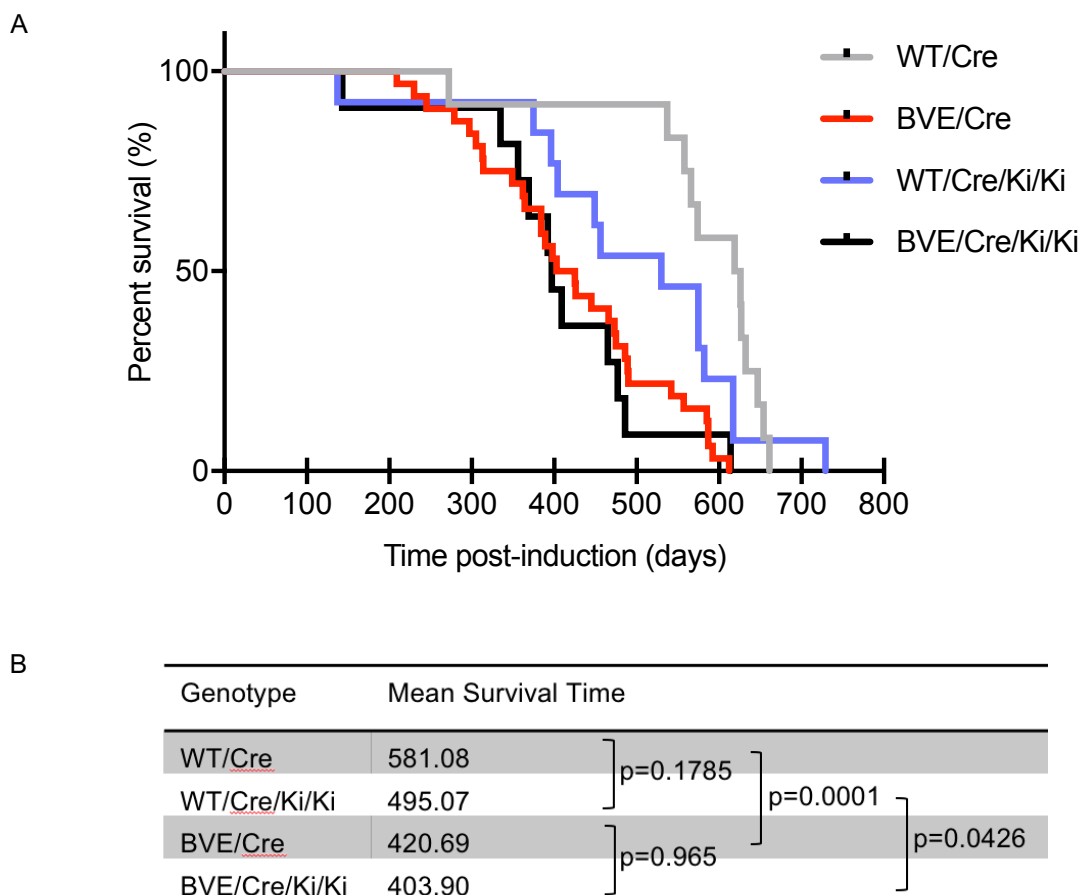


Figure 6.1 Effect of the genotype on mouse survival.

A) Kaplan-Meier survival graph indicating the effect of genotype on overall survival. Mice were injected with TM, and were kept under standard conditions, and were monitored routinely for the signs of poor health. Sick animals were terminated humanely, once their health deteriorated to the point that they could not be kept alive any longer, according to Home Office criteria BVE/Cre/Ki/Ki ($n=11$ comprising of 5 females and 6 males), WT/Cre/Ki/Ki ($n=11$ comprising of 3 females and 8 males), WT/Cre ($n=11$ with unknown sex), and BVE/Cre ($n=31$ comprising of 13 females, 14 males and 4 of unknown sex).

B) Table showing Mean Survival Time of mice with different mutations. Statistical analysis was carried out in order to calculate the significance of the data following comparison between each group. Statistical analysis was carried out using paired T-test. Total No. of mice used= 64.

6.3.2. Effect of *Gsk3* mutation on tumour burden following ^{V600E}*BRAF* induction

In order to study the impact of *Gsk3* mutation on tumour burden, small intestinal tissue was harvested, and subjected to analysis. As the number of BVE/Cre mice used in the survival analysis (Figure 6.1) was larger than the other groups (n=31), this number was reduced to n=11, by age matching, in order to analyse a similar number of mice in each group. Of the 11 mice in BVE/Cre group (4 females, 6 males and 1 of unknown sex). Mice in BVE/Cre/Ki/Ki included 5 females and 6 males. Once animals were sacrificed, the small intestine tissues were harvested, cleaned using PBS and cut into 6 pieces of similar size from the start of the caecum to the end of the duodenum (Figure 6.2A). The tissue then was cut, and flattened on a clean surface, and was monitored for the presence of tumours visible to the naked eye. These were referred to as macroscopic tumours. A photograph of typical serrated macroscopic tumours is shown in Figure 6.2B. Control mice with WT/Cre, and WT/Cre/Ki/Ki, did not develop any macroscopic tumours (data not shown).

Tissues were processed according to standard protocols and subjected to sectioning. Tissue sections were H&E stained and sent to gastrointestinal pathologist Professor Kevin West, (University Hospital Leicester, NHS Trust) for subsequent staging analysis. 'Microscopic tumours' is a term that was used for tumours which could be seen under the microscope. All macroscopic tumours were expected to be visible under the microscope. As serial sectioning of all tissues from all the animals was impractical - the middle sections of each tissue block, from 1-6 sections of the small intestine, of each of the 11 mice in each group were analysed. As shown in Figure 6.2C, *Gsk3 α/β* knockin mutation, in the context of ^{V600E}*Braf*, did not change the appearance of microscopic tumours in comparison with ^{V600E}*Braf* only mice (Figure 6.2C).

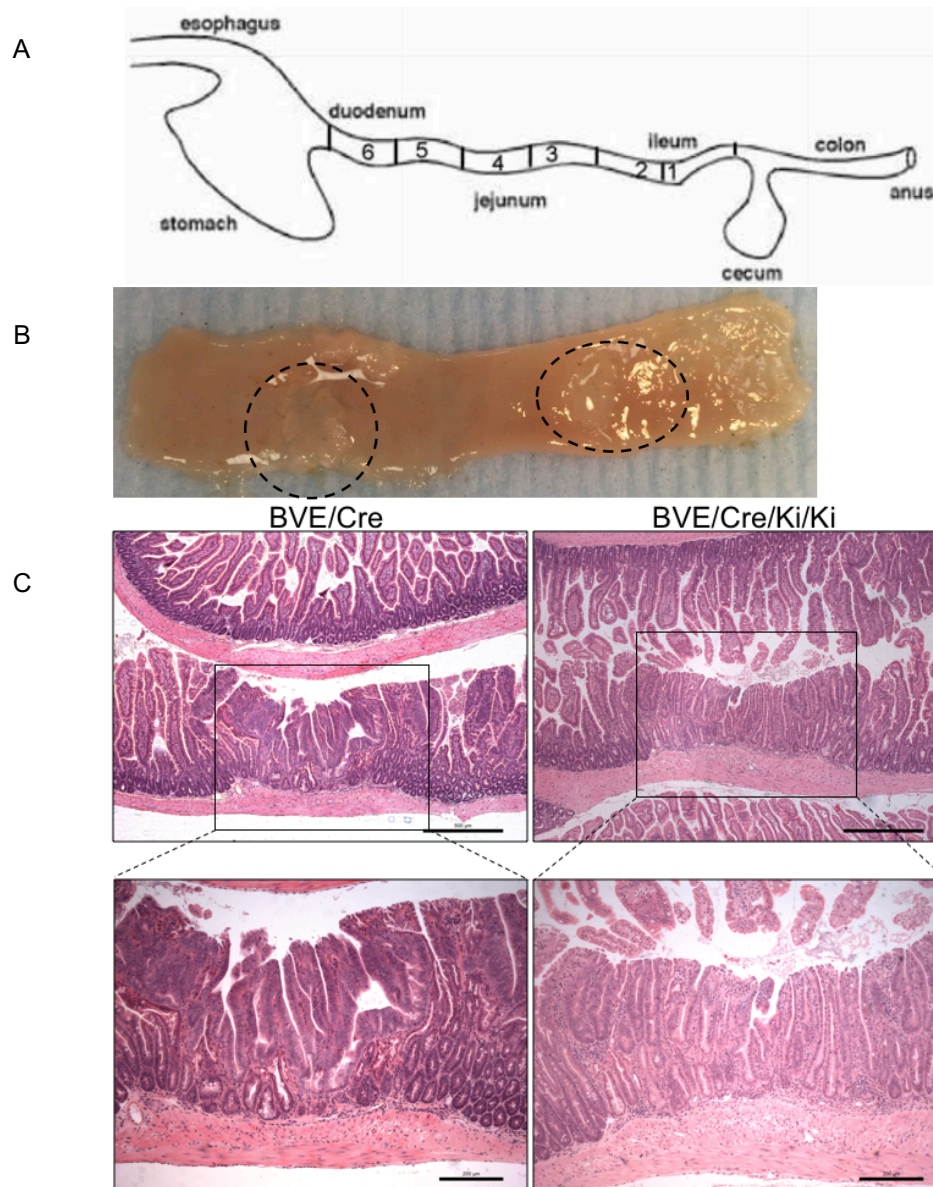


Figure 6.2 Appearance of macroscopic and microscopic tumours in mouse gut tissue.

A) Schematic diagram of mouse small intestine (Carragher et al., 2010). The small intestinal tissue was cut into 6 sections of similar length, with section 1 being the ileum and section 6 being the duodenum. Individual sections were subjected to analysis.

B) Typical appearance of macroscopic tumours, shown in black circles. Once the animal was terminated, the small intestine was harvested, washed with PBS and was subsequently cut into 6 pieces. Each section was cut open and flattened on a clean surface and was monitored for tumours visible to the naked eye (macroscopic tumours). A photograph of macroscopic tumours was taken using an iPhone6 camera. Macroscopic tumours with V^{600E} BRaf have a flattened appearance and are pale in colour as shown in the photograph. The tissue sample is from 1 mouse.

C) Microscopic tumour from V^{600E} BRaf mice without (left hand side) and with (right hand side) Gsk3 α/β double knockin mutations. Tissue sections were subjected to H&E staining and photographed. Scale bars= 500 μ m (top panels) and 200 μ m (lower panels). Total No. of mice used= 22.

As shown in Figure 6.3A, the genotype of the mouse did not affect the number of macroscopic tumours in BVE/Cre (4 females, 6 males and 1 of unknown sex) mice, compared to BVE/Cre/Ki/Ki (5 females and 6 males) mice. Regression analysis was performed by Dr. Maria Viskaduraki from the BBSAH facility, University of Leicester, to explore the association between number of macroscopic tumours and genotype or age. As expected, age was significantly associated with the number of macroscopic tumours (P value= 0.004). However, there was no significant difference in the number of tumours between the different genotypes, after accounting for age (P value= 0.40) (Figure 6.3B). To determine, by age matching from a cohort of 31, whether our selection of 11 BVE/Cre mice affected our observation regarding the association between number of tumours and the genotype, a comparison between all 31 mice from BVE/Cre group and 11 mice from BVE/Cre/Ki/Ki group was carried out. As shown in Figure 6.3C, no significant association between the number of macroscopic tumours and the genotype of mice was observed (P value= 0.3327).

The number of microscopic tumours showed more of a trend towards higher tumour burden in BVE/Cre/Ki/Ki, but this was not quite significant in comparison to ^{V600E}BRaf only mice (Figure 6.4A) (P value= 0.08). The number of microscopic tumours also did not increase with age, suggesting they develop early following ^{V600E}Braf expression and many of them stay around for the lifetime of the mouse without progressing further (P value= 0.63) (Figure 6.4B).

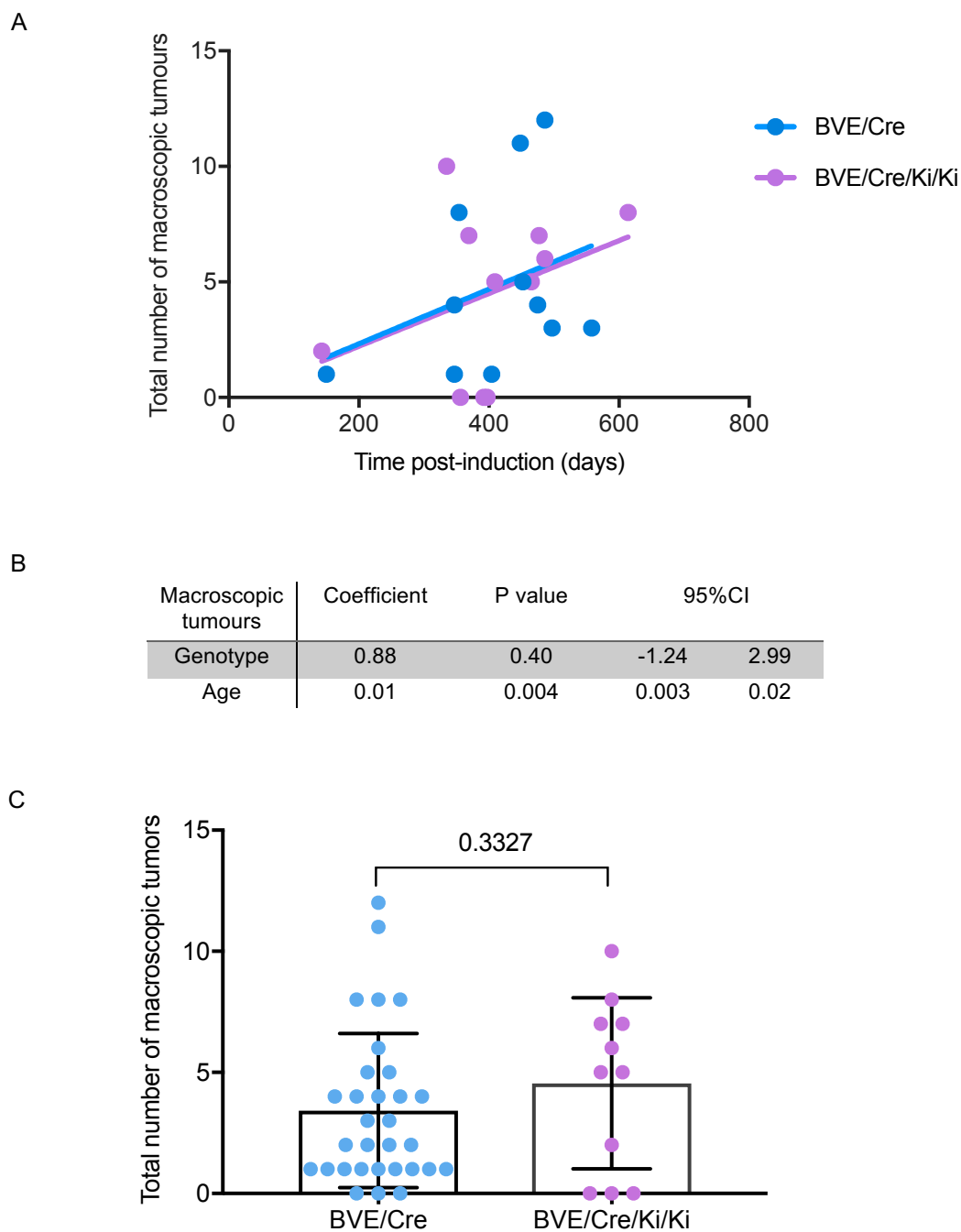


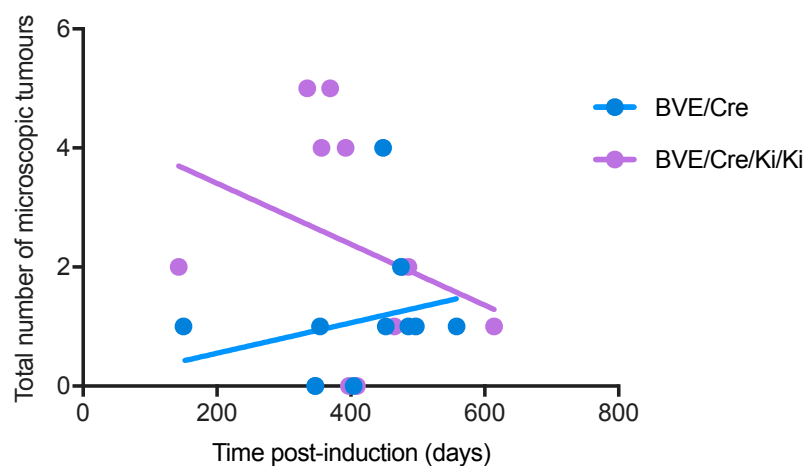
Figure 6.3 Analysis of number of macroscopic tumours in $V^{600E}BRaf$ mice small intestine, with or without $Gsk3\alpha/\beta$ knockin mutations, over time.

A) Scatter graph of number of macroscopic tumours in $V^{600E}BRaf$ mice, with and without $Gsk3\alpha/\beta$ knockin mutations, taking age into consideration ($n=11$). Total No. of mice used=22. BVE/Cre included 4 females, 6 males and 1 of unknown sex. BVE/Cre/Ki/Ki group composed of 5 females and 6 males.

B) Table showing statistical analysis on the effect of genotype and age on macroscopic tumour burden. Statistical analysis was carried out using linear regression.

C) Graph showing number of macroscopic tumours in $V^{600E}BRaf$ mice with and without $Gsk3\alpha/\beta$ knockin mutations. In this graph all 31 BVE/Cre mice (13 females, 14 males and 4 with unknown sex) were included and compared with 11 mice (5 females and 6 males) in the BVE/Cre/Ki/Ki group. Statistical analysis was carried out using unpaired T-test. Data shows mean \pm SD.

A



B

Microscopic tumours	Coefficient	P value	95%CI	
Genotype	1.26	0.08	-0.14	2.66
Age	0.00	0.63	-0.01	0.00

Figure 6.4 Analysis of the number of microscopic tumours in V^{600E} Braf mice small intestine with or without Gsk3 α/β knockin mutations, over time.

A) Scatter graph of number of microscopic tumours in V^{600E} Braf mice, with and without Gsk3 α/β knockin mutations, taking age into consideration (n=11). Total No. of mice used=22. BVE/Cre included 4 females, 6 males and 1 of unknown sex. BVE/Cre/Ki/Ki group composed of 5 females and 6 males.

B) Table showing statistical analysis of the effect of genotype and age on microscopic tumour burden. Statistical analysis was carried out using linear regression.

As shown in Figure 6.3, the average number of macroscopic tumours was also investigated and was found to not change significantly between the two genotypes (P value= 0.87) (Figure 6.5A and B).

The average number of microscopic tumours was significantly changed across the two genotypes, with higher numbers of tumours in the BVE/Cre/Ki/Ki in comparison to BVE/Cre mice (P value= 0.02) (Figure 6.5A and B).

It is worth mentioning that all the macroscopic tumours are expected to be seen under the microscope in addition to all the small tumours that are not visible to the naked eye. As a result, in theory, the total number of microscopic tumours should exceed the total number of macroscopic tumours. However, this was not the case in our observations. This could be due to the fact that serial sectioning was not carried out as it was impractical, to serial section all samples, within the time frame of this study. Therefore, some of the microscopic tumours could have been missed by looking at the middle section of each paraffin block.

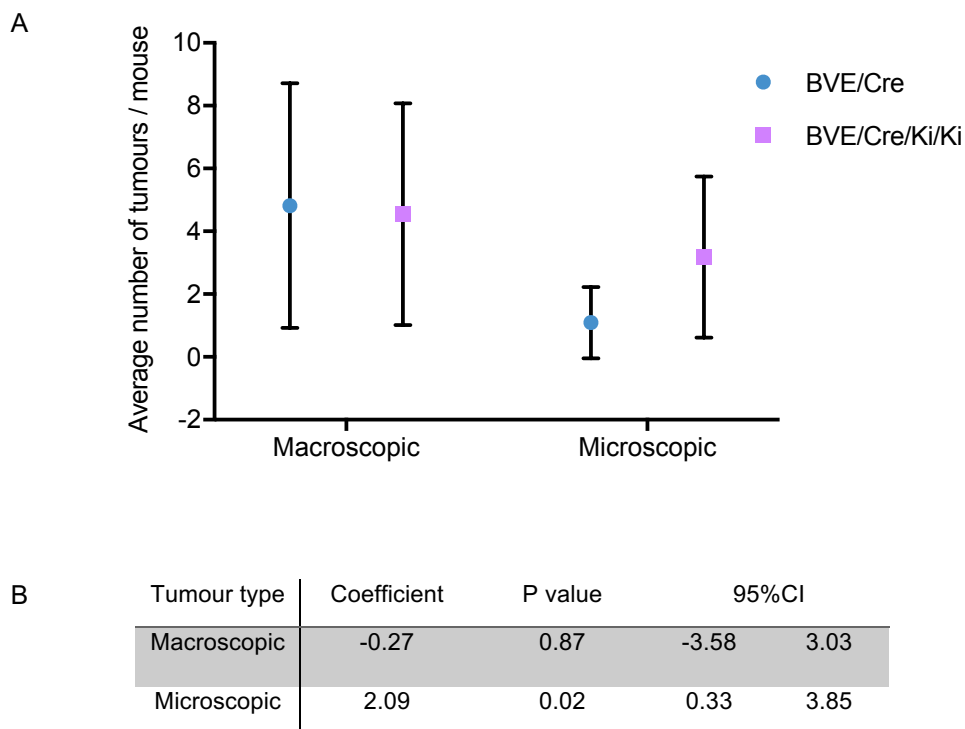


Figure 6.5 Impact of $Gsk3\alpha/\beta$ mutations on macroscopic and microscopic tumour burden in $V600E$ BRaf mice small intestine.

A) Graph showing average number of macroscopic, microscopic tumours per mouse for each genotype ($n=11$). Data shows mean \pm SD. Total No. of mice used=22. BVE/Cre included 4 females, 6 males and 1 of unknown sex. BVE/Cre/Ki/Ki group composed of 5 females and 6 males.

B) Statistical analysis indicating association between average number of tumours and the genotype of animals. Statistical analysis was carried out using linear regression.

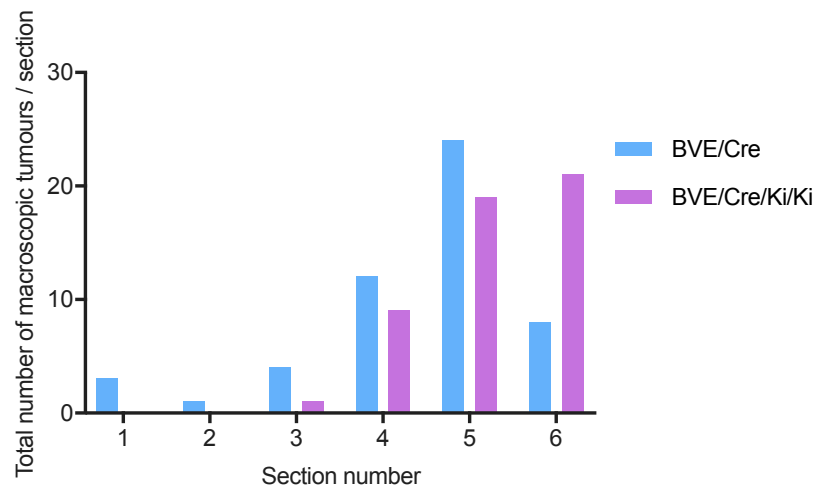
6.3.3. Tumour burden in different regions of the intestine

The total number of macroscopic tumours across different sections of the gut were analysed. In BVE/Cre mice (4 females, 6 males and 1 of unknown sex), the majority of macroscopic tumours were located in sections 4, 5 and 6 near the duodenum and jejunum, similar to what was observed for BVE/Cre/Ki/Ki (5 females and 6 males). Moreover, no tumours were observed in sections 1 and 2 in BVE/Cre/Ki/Ki mice in the ileum (Figure 6.6A). Multiple linear regression analysis showed no statistical correlation between the genotype of the mouse and the number of macroscopic tumours in different sections of the gut (P value = 0.84). However, the number of macroscopic tumours was significantly different when comparing different regions of the gut within one genotype (P value = <0.001) (Figure 6.6B).

The total number of microscopic tumours in both genotypes appeared to be quite similar in sections 1-4 of the small intestine. However, there was an increase in the number of microscopic tumours in sections 5 and 6 of the gut in BVE/Cre/Ki/Ki mice, in comparison to BVE/Cre mice (Figure 6.7A). Multiple linear regression analysis showed a significant statistical correlation between the number of microscopic tumours, developing in each section of the gut, and the genotype of the mice (P value = 0.02). Moreover, the number of microscopic tumours was significantly different when comparing different regions of the gut within one genotype (P value = <0.001) (Figure 6.7B).

Taken together, Expression of ^{V600E}BRaf in gut increases tumour burden in the duodenum as compared to the ileum and this is not affected by *Gsk3 α/β* knockin mutations.

A



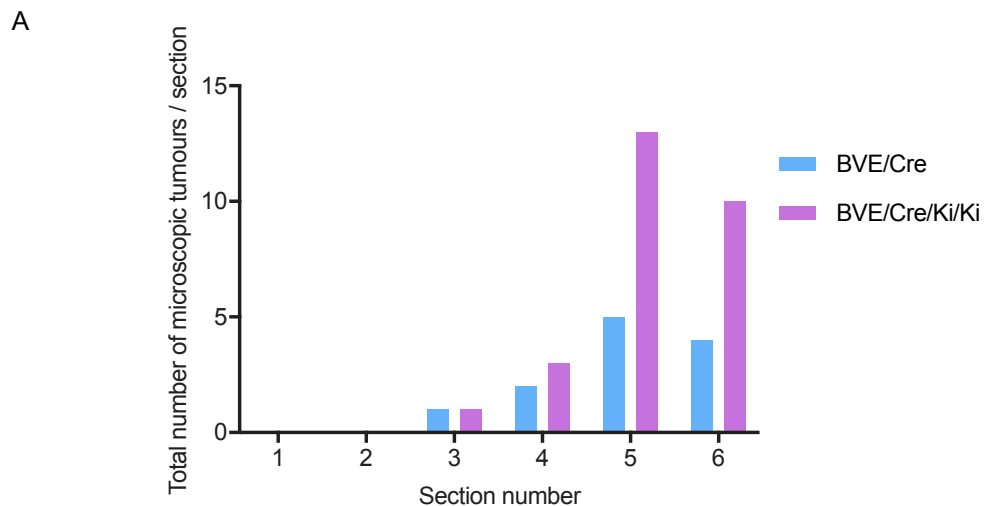
B

Macroscopic tumours	Coefficient	P value	95%CI	
Genotype	-0.05	0.84	-0.50	0.41
S.I. section	0.35	<0.001	0.22	0.49

Figure 6.6 Impact of the genotype on the number of macroscopic tumours in different sections of the small intestine.

A) Bar graph showing the effect of different mutations on the total number of macroscopic tumours developed in each section of the gut using BVE/Cre and BVE/Cre/Ki/Ki mice ($n=11$). Total No. of mice used=22. BVE/Cre included 4 females, 6 males and 1 of unknown sex. BVE/Cre/Ki/Ki group composed of 5 females and 6 males.

B) Statistical analysis indicating the association between the total number of macroscopic tumour burden, in different regions of the intestine, and the genotype. Statistical analysis was done using linear regression.



B

Microscopic tumours	Coefficient	P value	95%CI	
Genotype	0.24	0.02	0.04	0.44
S.I. section	0.17	<0.001	0.11	0.23

Figure 6.7 Impact of genotype on the number of microscopic tumours in each section of the small intestine.

A) Bar graph showing total number of microscopic tumours in each section of the gut using BVE/Cre and BVE/Cre/Ki/Ki mice (n=11). Total No. of mice used=22. BVE/Cre included 4 females, 6 males and 1 of unknown sex. BVE/Cre/Ki/Ki group composed of 5 females and 6 males.

B) Statistical analysis indicating the association between the total number of microscopic tumour burden in different regions of the intestine and the genotype. Statistical analysis was done by using linear regression.

6.3.4. Impact of *Gsk3* mutation on tumour grade

In order to investigate the impact on the tumour development stage, tissue from BVE/Cre (4 females, 6 males and 1 of unknown sex) and BVE/Cre/Ki/Ki (5 females and 6 males) mice were subjected to pathological grading. In low-grade dysplastic tissue, the muscle layer is intact and the structure of the villus is not affected, but there is nucleus to cytoplasmic ratio changes in the epithelial cells. A high-grade dysplastic tumour, also known as severe dysplasia, is characterised by the presence of large nuclei, abundance of mitotic figures and the structures of the crypt and villi are disrupted but still recognisable. An invasive carcinoma shows loss of cell polarity and infiltration of the tumour into the muscle layer. Figure 6.8 shows examples of H&E stained gut tissue with different grades of tumours (Figure 6.8).

As shown in Figure 6.9, there was an increase in the total number of low-grade dysplastic (LGD), and high-grade dysplastic (HGD) tumours in BVE/Cre/Ki/Ki mice in comparison to BVE/Cre mice (n=11) (Figure 6.9A). However, statistical analysis using a multiple linear regression test showed this was not significant (P value= 0.19), but the number of tumours increased significantly when comparing HGD with LGD grades within the same genotype (P value= <0.001). No significant difference in the number of tumours was observed when carcinoma and LGD were compared within the same genotype (P value= 0.35) (Figure 6.9B).

Altogether, these data suggest that introduction of *Gsk3 α/β* knockin mutations, in addition to ^{V600E}*Braf*, increases number of tumours but does not affect the grade.



Figure 6.8 H&E staining of mouse gut tissue containing tumours at different stages. On the left-hand panel, is an example of a low-grade dysplastic tissue. At this stage, the muscle layer is intact, the structure of the villus is not affected, but there is nucleus to cytoplasmic ratio changes in the epithelial cells. The middle panel is an example of a high-grade dysplastic tumour, also known as severe dysplasia. There is the presence of large nuclei, abundance of mitotic figures and the structures of the crypt, and villi are disrupted but still recognisable. On the right-hand side, the tissue shows an invasive carcinoma in which there is loss of polarity and infiltration of tumour into muscle layer. Scale bar= 200 μ m.

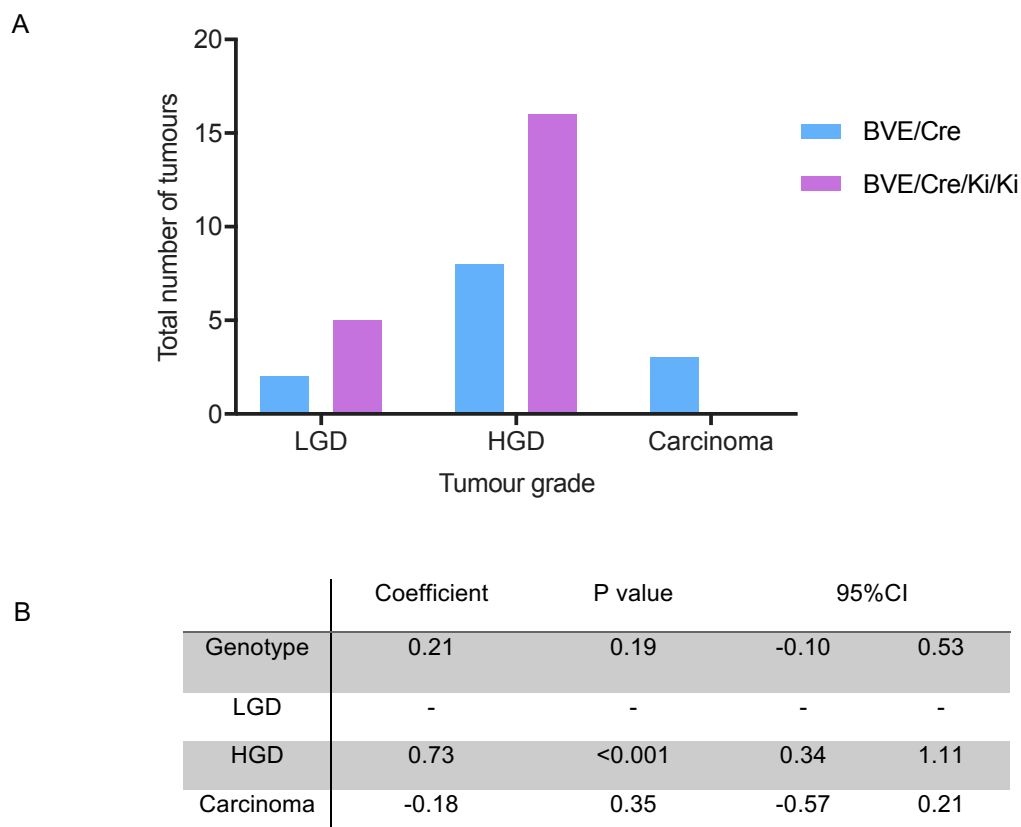


Figure 6.9 Impact of $Gsk3\alpha/\beta$ knockin mutations on tumour grade. A) Bar graph indicating the total number of microscopic tumours of different stages in $V600E$ BRAf, mouse small intestine, with and without $Gsk3\alpha/\beta$ knockin mutations. Tissue sections with microscopic tumours were subjected to pathological grading by Professor Kevin West ($n=11$). Total No. of mice used=22. BVE/Cre included 4 females, 6 males and 1 of unknown sex. BVE/Cre/Ki/Ki group composed of 5 females and 6 males.

B) Statistical analysis showing the association between the animal genotype and the tumour grade. Statistical analysis was done using linear regression.

6.3.5. Conclusion

As shown in chapter 5, the introduction of the *Gsk3 α/β* knockin mutations, in the context of *V600E*Braf, increases the total number of crypt cells in comparison to *V600E*Braf alone. This finding suggests that the inability of GSK3 α/β to become phosphorylated on Ser21/9, in the context of *V600E*BRaf, has an accelerating role in terms of crypt proliferation; whereas, this is not seen in the wild type intestine, when analysed in the short-term.

In order to investigate the long-term effect of *Gsk3 α/β* knockin mutations in the context of *V600E*BRaf, on animal survival and tumour development, mice received TM injections, and were left to live a normal life, with their health was monitored regularly. Although the survival of animals decreased significantly as a result of *V600E*BRaf induction, in comparison to controls, *Gsk3 α/β* knockin mutations, in the context of *V600E*Braf, did not reduce mouse survival further. Thus, any impact of GSK3 in crypt proliferation or tumour burden does not have an effect on overall survival. Therefore, if GSK3 α/β Ser21/9 has a tumour suppressive effect, it is only marginal. However, *V600E*Braf mice with *Gsk3 α/β* knockin mutations were found to have significantly higher numbers of microscopic tumours, in comparison to *V600E*Braf only, which may be linked to the effect on crypt proliferation at earlier stages. Overall, these findings show that *Gsk3 α/β* knockin mutations have an accelerating effect on crypt proliferation and tumour burden, but this does not translate into an effect on animal overall survival. Therefore, GSK3 phosphorylation is important as a tumour suppressive mechanism in early disease, but is not involved in progression. There was also no significant correlation between mouse genotype and tumour grade. This confirms our hypothesis that the GSK3 phosphorylation does not affect disease progression.

Tumour burden in different sections of the small intestine varied with higher tumour burden in the duodenum regardless of genotype, which is consistent with what was reported in the case of humans. In 2004 Dabaja et al. reported that in humans most cases of small bowel adenoma are detected in the

duodenum as well as the jejunum (SBA) (Dabaja et al., 2004). A similar observation was reported by Chang et al. (Chang et al., 2010). Aparicio et al. in 2013 reported that human dMMR tumours are seen mostly in the proximal site (duodenum and jejunum) in comparison to ileum (Aparicio et al., 2013). This could possibly be linked to morphological and functional differences as a result of homeobox genes (Hox) gradient between proximal and distal sections of small intestine. Pdx-1 transcription factor, is a Hox gene which is only found in the duodenum and pancreatic islets, but not in other parts of small intestine (Walters et al., 1997). Pdx-1 is shown to be low or absent in cancer cell lines as well as mouse gastric cancer tissue. Upregulation in Pdx-1 expression is involved in the inhibition of cancer cell growth or xenograft tumour formation (Ma et al., 2008). The difference in tumour burden could also be the result of differences in metabolic gene expression in duodenum, jejunum and ileum. GATA4, a zinc finger transcription factor is expressed in both duodenum and jejunum, but not in the ileum and it is known to be involved in the expression of Lactase (Lct), Sucrose isomaltase (Si) as well as Fatty acid binding protein 1 (Fabp1) in the gut and is crucial in lipid and cholesterol uptake (Battle et al., 2008). It will be interesting to investigate the link between ^{V600E}*Braf* and the *Hox/GATA4* genes.

Overall, the data show *GSK3 α/β Ser21/9* is a weak tumour suppressor; *Gsk3* knockin mutations have an impact only on early stages of tumour development, but not mouse survival.

Chapter 7. Summary and Discussion

7.1. Background to the project

Colorectal cancer (CRC) is the third most common cancer and the fourth most common cause of cancer death worldwide. In the UK, CRC was reported as being the third most common cancer and the second most common cause of cancer death in 2014. The traditional type of CRC which accounts for ~84% of reported cases is associated with chromosomal instability, of which ~80% show *APC* mutation, while ~5-10% carry mutations in other WNT signalling components (e.g. *CTNNB1*). It is estimated that, besides the well-known traditional CRC pathway, ~10-20% of carcinomas develop through a different series of biological and molecular changes known as the serrated pathway. A class of CRC developing through the serrated pathway, are characterised by having *BRAF* or *KRAS* mutations; this then leads to hyperactivation of the MAPK pathway. Serrated CRCs with ^{V600E}*BRAF* mutation accounts for ~8% of cases and are known as sessile serrated CRCs. Sessile serrated CRCs have a poor prognosis, as they develop in the proximal colon, and are difficult to detect because of their awkward location and pale flat appearance.

Unlike melanoma, sessile serrated CRCs do not respond to treatment with the *BRAF* inhibitor PLX4032 (Kopetz et al., 2010). This was shown to be because of paradoxical activation of EGFR receptors associated with relief of ERK inhibition of EGFR - leading to activation of the ERK pathway through CRAF (Prahallad et al., 2012). At present, there are no effective treatments for ^{V600E}*BRAF*-mutated CRCs. Therefore, there is a need to develop better treatment strategies. To do so, a clear understanding of the underlying mechanisms of disease initiation and progression is crucial.

Due to the impracticality of having access to human tissue samples at the early stages, mouse models of human CRC have proven to be a good tool to study the mechanisms of disease initiation and progression *in vivo*. In 2010, Carragher et al., using the *Braf*^{LSL-V600E/WT}; *AhCreER*^{T0/WT} mouse, reported the

presence of crosstalk between ERK and GSK3, following $V600E$ BRaf induction, which was detected using samples at 3 days post $V600E$ BRaf expression (hyperplastic stage). Activation of the ERK pathway as a result of $V600E$ BRaf induction increased phosphorylation, of GSK3 α/β at serines 21/9, in an AKT-independent manner. Inhibition of GSK3 phosphorylation was reported following PD184352 treatment, suggesting that GSK3 phosphorylation is directly downstream of $V600E$ BRaf-ERK. Induction of crypt senescence was shown from ~1 week to ~10 week p.i. and *AhCreER*^{T0/WT} mice did not survive beyond ~12 week p.i. due to the formation of tumours in the stomach and lung. Therefore, the need for a more tissue-specific Cre strain to mimic human serrated CRC condition was necessary.

In 2013, Rad et al., using a constitutive *Villin-Cre* strain (active from E9.5), reported the presence of hyperplastic crypts in adult mice which was suggested to be the direct result of hyperproliferation of crypt cells - as no significant change in apoptosis was observed. They observed thickened and branched villi in the small intestine, whereas in the large intestine, crypt hyperplasia with mucosal protrusions resembling villi structure was detected. There was a lack of evidence for senescence at early stages, although an increase in *p16*^{INK4A} expression was detected at later stages of neoplasia (Rad et al., 2013). The absence of *p16*^{INK4A} in hyperplastic samples with the *BRAF* mutation was also reported by Kriegl et al., but *p16*^{INK4A} was found to be upregulated in serrated adenomas (Kriegl et al., 2011).

For the current study, the tamoxifen inducible *Villin-CreER*^{T0/WT} strain was chosen which specifically expresses $V600E$ BRaf in the small and large intestinal epithelium of the adult mouse; this allows for Cre-regulated expression in the adult using tamoxifen (TM) administration.

7.2. Summary of results

7.2.1. CRC cell lines as model system

As a starting point, human RKO cell lines were used in this study in order to attempt to establish an *in vitro* model for examining crosstalk between ERK and GSK3 (Chapter 3). Despite observing increased activity of the MAPK pathway, as a result of ^{V600E}BRaf expression, no link with GSK3 phosphorylation was observed. There are several explanations for this. Firstly, it could be that lack of stromal factors present in the gut which affects the crosstalk in the cell lines. Alternatively, RKO cells have other mutations which can affect GSK3 phosphorylation. RKO cells carry the ^{H1047R}PI3K mutation, which is known to cause enhanced catalytic activity and activation of downstream signalling through AKT (Yueh et al., 2016). AKT activation induced by ^{H1047R}PI3K can inactivate GSK3 α/β , through phosphorylation of Ser21/9, as shown in Figure 7.1. This potentially could override any effect of ^{V600E}BRAF-MAPK on GSK3 phosphorylation. ^{V600E}BRAF-driven activation of the MAPK pathway in RKO cells did affect the subcellular localisation of β -catenin, but this was found to be GSK3 phosphorylation-independent.

Using other human cell lines harbouring the ^{V600E}BRAF mutation, some evidence of crosstalk between the MAPK and GSK3 was observed, an example being in human lung (HCC364) and melanoma (A375P) cells. The best evidence for crosstalk was observed in the A375P cells, with S6 Kinase (S6K) identified as being a candidate intermediary kinase. Inhibition of MEK in melanoma cells led to downregulation of both GSK3 and S6K phosphorylation after 24 hours. This is consistent with data from Old et al., who demonstrated suppression of ERK1/2, S6K and GSK3 β phosphorylation following the treatment of A375P cells with U0126. It was proposed that BRAF/MEK/ERK signalling inhibits GSK3 α/β through the inhibition of tyrosine residue phosphorylation which is essential for activation and also regulation of inhibitory Ser21/9 phosphorylation sites (Old et al., 2009). Thus, there is strong evidence

for crosstalk between the MAPK and GSK3 which can be reversed through MAPK inhibition in human melanoma cells, but this study has found that this was not the case in RKO CRC cells.

A more prominent effect of MEK inhibition in gut tissue and melanoma cells was seen on the p85 isoform of S6K; this has a stretch of extra 23 amino acids acting as the nuclear localisation signal in contrast to the p70 isoform, which is cytoplasmic. The reasons for the p85 isoform specific effect are not clear.

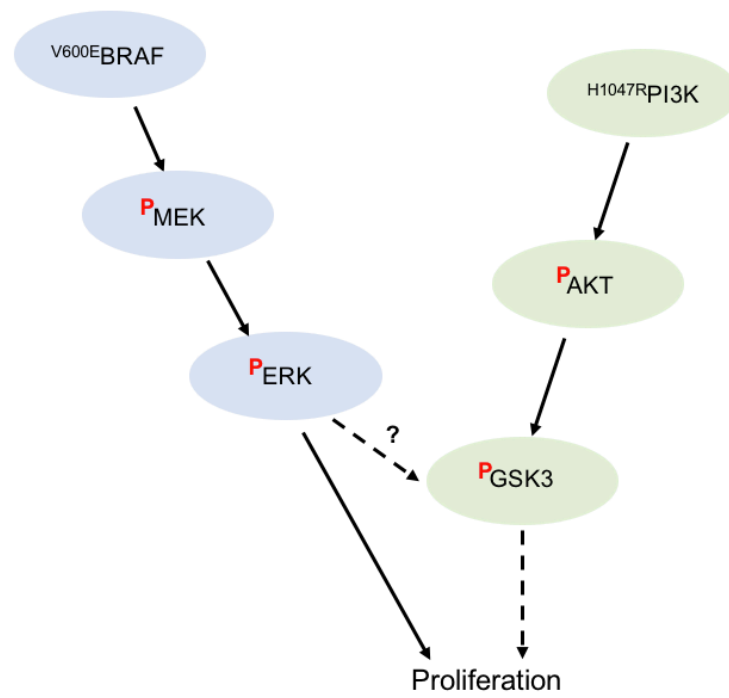


Figure 7.1 Schematic diagram of the potential effect of activated H^{1047R} PI3K on AKT and GSK3 phosphorylation in RKO cells.

7.2.2. *Villin-CreER^{T0/WT}; Bra^f^{SL-V600E/WT}* (BVE/Cre) as a model of serrated CRC

Use of the BVE/Cre mouse model of serrated CRC gave us the opportunity to study the disease at early stages but also over a long period of time. Following 3 days of ^{V600E}BRaf induction, we observed crypt hyperplasia resulting from the hyperproliferation of crypt cells, with a particular increase in the number of S phase cells. This observation is consistent with the 2010 report by Carragher et al. which used the *AhCreER^{T0/WT}* model and also with the *Villin-Cre* model published by Rad et al. in 2013. We did not investigate the induction of senescence in this model, but studied the long-term effects on tumour development.

The average survival time for BVE/Cre mice p.i. was ~400 days which was significantly shorter in comparison to control mice. Macroscopic tumours had a flat pale appearance with higher tumour burden detected in the duodenum. Most tumours detected were HGD, although some tumours were LGD and only a few carcinomas were detected in these mice. No macroscopic tumours were observed in the large intestine. In all, the data is very similar to disease progression observed in the Rad et al. publication, which was identified as being a good model of human serrated CRC.

7.2.3. MAPK-independent crypt hyperplasia in the BVE/Cre model

Using the BVE/Cre model of CRC, crypt hyperplasia at early stages appeared to be MAPK-independent. This is demonstrated by two lines of evidence: a) the fact that MEK and ERK phosphorylation were not observed to increase (Chapter 4 - Figure 4.6) and b) inhibition of the MAPK pathway by PD184352 treatment did not reverse crypt hyperplasia (Chapter 4 - Figure 4.13). MAPK-independent proliferation at early stages in the BVE/Cre model is interesting as this is different from what was observed previously in the *AhCreER^T* mouse model. However, Rad et al. using the *Villin-Cre* model suggested that ^{V600E}Braf-induced MAPK activation occurs only at the adenoma and carcinoma stages

and not at the hyperplastic crypt stage, although, details of MAPK-independent hyperplasia was not studied in depth in this report (Rad et al., 2013).

The difference in the two models raises the possibility that different Cre strains express ^{V600E}BRaf in different cell types in the small intestine and that these different cell types have different dependencies on the MAPK pathway. Carragher et al. reported the presence of Cre recombinase in intestinal transit amplifying cells and stem cells driven by *AhCreER^T* (Carragher et al., 2010) and in 2004, Ireland et al. reported that Cre recombination in intestinal stem cells can persist for up to 6 months (Ireland et al., 2004). Multiple manuscripts have reported that expression of Cre recombinase in the *Villin-CreER^T* mouse model occurs throughout the GI epithelium and persists for 60 days p.i. It will be interesting to further examine MAPK pathway activity in these different Cre strains and cell types.

Gene expression analysis of the BVE/Cre mice showed that ~30% of 30 MAPK target genes altered expression in response to short-term induction of ^{V600E}BRaf (Chapter 5). Two of these genes are negative feedback regulators i.e. *Dusp4* and *Spry4* which increased by 2.7 and 2.5-fold respectively. This may explain the lack of ERK phosphorylation in BVE/Cre samples but does not explain the ineffectiveness of PD184352 treatment on crypt proliferation.

In all, the above data suggest that ^{V600E}BRaf is uncoupled from MEK/ERK at this stage, consistent with data from some melanoma models. Kang et al. demonstrated that, in melanoma, ^{V600E}BRAF increases expression of HMGCL, a rate-limiting enzyme in ketogenesis, through the Oct-1 transcription factor in an ERK-independent manner. This results in an increase in production of acetoacetate, which in turn encourages binding of ^{V600E}BRAF to MEK1 resulting in delayed activation of the ERK pathway (Kang et al., 2015). Potentially, this mechanism could occur in hyperplastic crypts but then release MAPK activity in later adenomas. In 2017, Xia et al. reported on the effect of high fat diet on increases in serum acetoacetate level which then can accelerate proliferation in ^{V600E}BRAF-expressing melanoma cells through the mechanism proposed by Kang et al. Moreover, it was proposed that lowering serum acetoacetate level or

use of dehydroacetic acid to antagonise ^{V600E}BRaf-acetoacetate binding can reduce cell proliferation underlying the importance of diet on proliferation of ^{V600E}BRAF-expressing melanomas (Figure 7.2) (Xia et al., 2017).

An important future step would be to look at the effect of BRAF kinase inhibitors on the downstream pathway as well as crypt phenotype to investigate MAPK-independent effects in more detail.

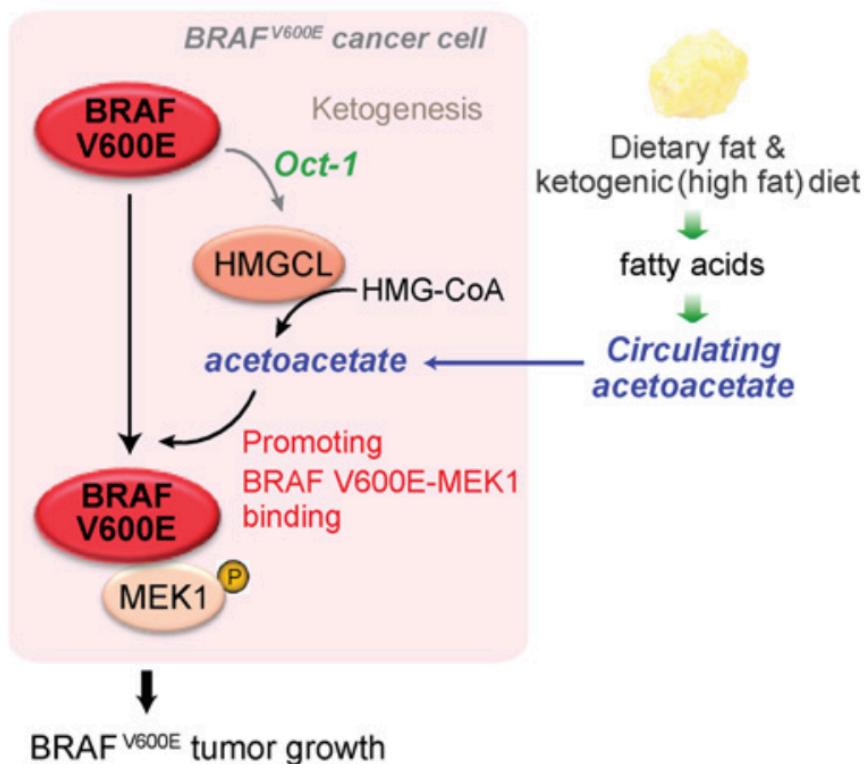


Figure 7.2 Schematic diagram of the proposed model on the effect of dietary fat on tumour growth in $BRAF^{V600E}$ BRAF-induced melanoma (Xia et al., 2017). $BRAF^{V600E}$ increases expression of HMGCL through the Oct-1 transcription factor in an ERK-independent manner resulting in an increase in production of acetoacetate, which in turn encourages binding of $BRAF^{V600E}$ to MEK1 resulting in delayed activation of the ERK pathway. Increase in serum acetoacetate level by use of high fat diet can also accelerate tumour growth in $BRAF^{V600E}$ BRAF-induced melanoma. This diagram is taken from Xia et al., 2017.

7.2.4. WNT pathway involvement in crypt hyperplasia

In the *AhCreER^T* model an increase in GSK3 β phosphorylation and nuclear β -catenin were observed suggesting WNT pathway activation but this was not supported in the study of Rad et al. Our gene expression analysis showed that induction of ^{V600E}BRaf in the short-term altered expression of ~15% of the total of 135 WNT target genes including *Tcf23* by 22.5-fold and *Myc* by 2-fold. This indicates induction of a subset of the WNT target genes at the hyperplastic stage by ^{V600E}BRaf.

Myc is known to be an important downstream target of WNT which itself can regulate the majority of WNT target genes including *Tcf4* (Sansom et al., 2007). Therefore, it is plausible that *Myc* is also responsible for the increase in *Tcf23* expression found in this study. The TCF family of proteins are important in maintenance of the cell cycle and nuclear localisation of TCF- β -catenin increases during G2-S of the cell cycle (Ding et al., 2014). It will be interesting to further examine the role of these ^{V600E}BRaf-induced WNT target genes, particularly *Tcf23* and *Myc*, in crypt hyperplasia in more detail.

7.2.5. Cholesterol biosynthesis is induced by ^{V600E}BRaf

Gene expression analysis also identified that ^{V600E}BRaf induces expression of genes involved in cholesterol biosynthesis. *Hmgcs1* is one of the genes whose expression was found to be elevated by 2.2-fold. HMGCS has two isoforms; HMGCS1 (cytoplasmic) and HMGCS2 (mitochondrial). Cytoplasmic HMGCS1 is known to be the upstream enzyme regulating the activity of HMGCL and HMGCRC. HMGCL a rate-limiting enzyme participating in ketogenesis whereas, HMGCRC a rate-limiting enzyme involved in cholesterol biosynthesis (Figure 7.3). Therefore, potentially, the ^{V600E}BRaf-driven increase in HMGCS could induce an increase in ketogenesis and cholesterol levels which could potentially drive the increase in cell proliferation and crypt hyperplasia observed at early stages in a MAPK-independent manner (Figure 7.4).

An increase in cholesterol biosynthesis components coincided with a 4.5-fold downregulation in expression of *Abca1* gene, which is known to be important for

maintenance of cholesterol efflux. An increase in cholesterol biosynthesis coupled with *Abca1* activity was reported in cancer cells (Smith and Land, 2012, Lee et al., 2013). This observation possibly suggests an important role for cholesterol biosynthesis in development and progression of CRC with HMGCS1 as a potent candidate for future drug development studies. This also points at an increase in cholesterol level as a possible diagnostic marker of early stages of serrated CRCs, but this remains to be examined.

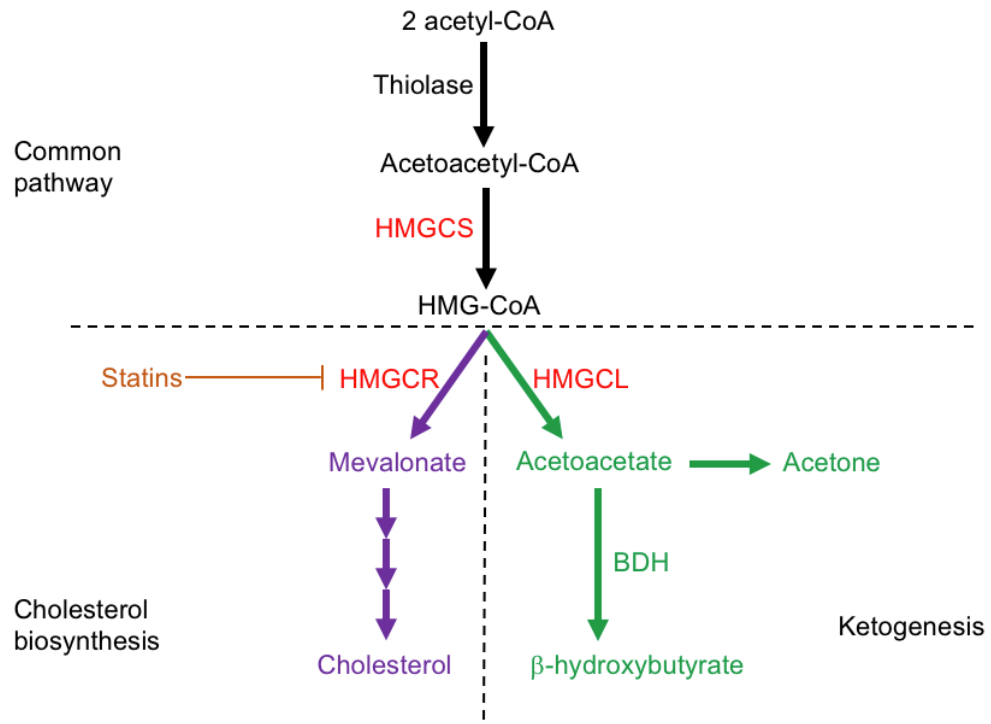


Figure 7.3 Simplified schematic diagram of cholesterol biosynthesis and ketogenesis pathways showing some of the important enzymes involved in the pathways deregulated by V^{600E} BRaf (in red).

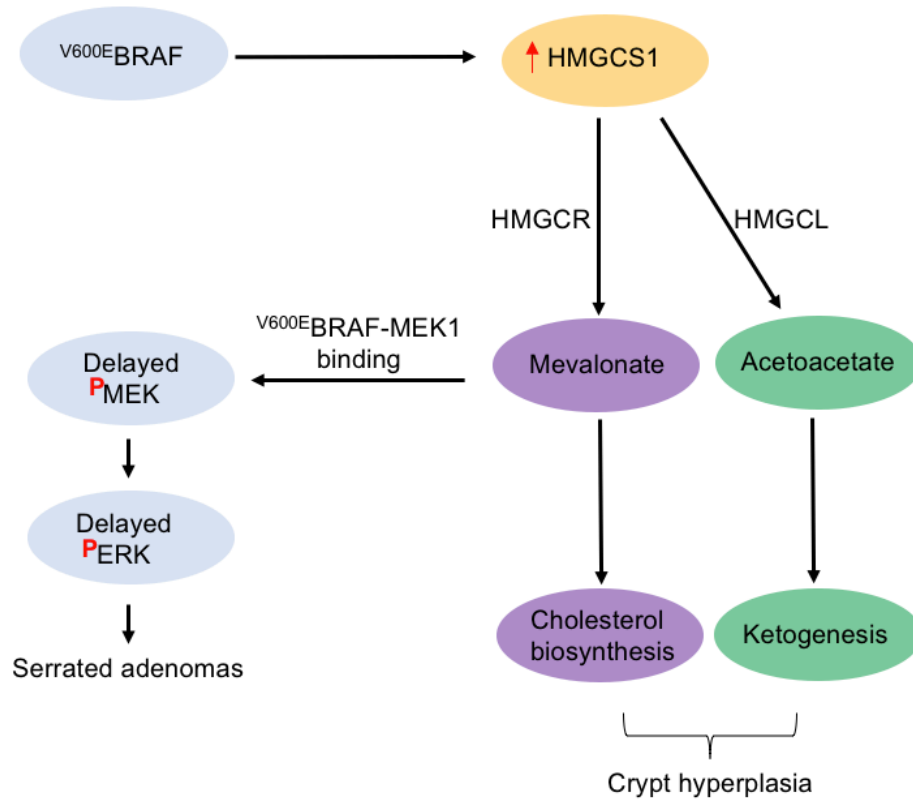


Figure 7.4 Schematic diagram of the proposed model of the mechanism involved in interaction between $V600E$ BRAF and HMGCS1 in early stages of serrated CRC. Expression of $V600E$ BRAF leads to increase in expression of HMGCS1 which in turn can increase the production of acetoacetate through HMGCL activity and mevalonate levels through HMGCR activity. Potentially, this could result in an increase in cell growth. This promotes the $V600E$ BRAF-MEK1 interaction leading to delayed activation of MAPK signalling resulting in serrated adenoma formation.

7.2.6. ^{V600E}BRaf induces components of glycolysis

Gene expression analysis indicated a potential increase in glycolysis following induction of ^{V600E}BRaf. A high rate of glycolysis to generate ATP is one of the characteristics of tumours irrespective of oxygen availability (Sato et al., 2017) and also tumour cells have high levels of lactic acid production (Martins et al., 2016). In 2017, a manuscript by Sato et al. using tumour and normal tissue samples from 275 patients with colorectal cancer reported a decrease in glucose level while lactate was increased in tumour tissues in comparison to control, indicating an increase in glycolysis. They showed a direct correlation between *MYC* expression and activation of glycolysis and downregulation of gluconeogenesis which could be reversed by *MYC* inhibition. Sato et al. proposed that expression of *MYC* can induce the Warburg effect in adenoma and early stages of the adenoma-carcinoma sequence (Sato et al., 2017). This is potentially consistent with our observation, although further validation is needed in our model.

In 2016, Ferretta et al. reported that in ^{V600E}BRAF-mutated melanoma high levels of phospho-ERK expression is coupled with decreased OXPHOS activity and increased glycolysis suggesting this as a compensatory survival mechanism. Inhibition of glycolysis was proposed as a suitable target for novel combinational therapy in ^{V600E}BRAF metastatic melanoma (Ferretta et al., 2016). Parmenter et al. stated that inhibition of oncogenic ^{V600E}BRAF leads to significant and consistent reduction in glycolysis through a network of BRAF-regulated transcription factors including *MYC* which are responsible in driving glycolysis downstream of ^{V600E}BRAF. It was proposed that combination therapy of BRAF inhibitors with glycolysis inhibitors is an important step to induce cell death in BRAF inhibitor resistant melanoma cells (Parmenter et al., 2014). It will be interesting to look into this in more detail in our model to get an insight into possible mechanisms of glycolysis and *MYC* cooperation in the initiation and progression of serrated CRC, which potentially could be used to develop therapies.

7.2.7. Effect of GSK3 phosphorylation on crypt hyperplasia and tumour burden

In the BVE/Cre model V^{600E} BRAF induced GSK3 phosphorylation was observed. This appeared to be MAPK-dependent as GSK3 phosphorylation levels were decreased in MEK inhibitor treated mice but occurred irrespective of whether the mice expressed V^{600E} BRAF or not. To investigate the role of this in more detail, mutation of Ser21/9 of *Gsk3 α/β* were obtained and intercrossed with BVE/Cre mice.

Mice carrying only the *Gsk3* mutations did not develop tumours and survived their normal life span. Gene expression analysis of the gut indicated few changes in gene expression with no apparent effect on mouse health. McManus et al. using the same single and double homozygous *Gsk3 α/β* knockin mice reported the animals are born at normal Mendelian ratio and had normal development and growth without being diabetic (McManus et al., 2005), consistent with our observation.

Upon combining the *Gsk3* mutations with V^{600E} *Braf* mutation an enhancement in crypt cell proliferation was observed (Chapter 5). These mice were also found to develop higher numbers of tumours at late stages but the combined mutations had no effect on tumour grade or life span. Thus, the data point to a role of GSK3 phosphorylation at the early stages (Chapter 6), which then manifests itself as an increase in tumour burden later on.

Gene expression analysis (Chapter 5) indicates that the main influence of the combined effect of *Gsk3* mutation and V^{600E} *Braf* mutation was on the expression of additional MAPK target genes, mostly negative feedback regulators of the pathway. An increase in expression of negative feedback regulators of the pathway such as *Dusp6* and *Dusp8*, both MAPK phosphatases, by 2.1 and 2.0-fold may be the reason behind slightly lower levels of phospho-ERK in BVE/Cre/Ki/Ki tissue in comparison to BVE/Cre tissue. However, in the BVE/Cre/Ki/Ki tissue a slight increase in phospho-MEK level was observed as well as an increase in crypt proliferation. Potentially this may arise as a result of

a decrease in phospho-ERK, resulting in less feedback inhibition of EGFR and more paradoxical activation of the MAPK pathway through CRAF as proposed in Figure 7.5. This model needs to be further studied by examining expression of the DUSPs and EGFR phosphorylation.

However, the protein tyrosine phosphatase, non-receptor type 5 (*Ptpn5*) was downregulated by 5.8-fold. *PTPN5* is known to code for a tyrosine phosphatase (STEP) with several known targets including ERK1/2 and p38^{MAPK} (Paul et al., 2002). *PTNP5* plays a role in synaptic function and is involved in different neurological disorders such as Alzheimer's and Parkinson's disease as well as schizophrenia. *PTPN5* is shown to interact with Mob1a, a conserved coactivator of NDR and the LATS family of kinases and functions as a tumour suppressor by reducing proliferation and activating apoptosis. Moreover, Mob1 is also important during mitotic exit in cytokinesis. *PTNP5* depleted cells were shown to normally proceed through mitosis. However, these cells shown to have defective cytokinesis and remained connected through cytoplasmic bridges involving unseparated persistent midbodies (Kumar et al., 2017). As *Ptpn5* was downregulation by ~6-fold, potentially this could lead to an increase in proliferation through Mob1a. It will be interesting to investigate its role in early and late stage of serrated CRC through its interaction with Mob1 in detail.

The expression of a subset of ~15% of WNT target genes (*Wnt4*, *Tnfrsf10*, *Vegfa*, *Stra6*, *Fgf2*, *Tnfrsf21*, *Flrt3*, *Pparg* and *Myc*) were reversed by *Gsk3* mutation suggesting a role for Ser21/9 phosphorylation site of GSK3 protein in determining the outcome of the WNT signalling pathway. This is unexpected as it contradicts current understanding of GSK3 Ser21/9 phosphorylation which has suggested it is not involved in the WNT pathway (Hey et al., 2016). Therefore, as part of future studies it will be important to examine the involvement of Ser21/9 phosphorylation of GSK3 α/β in the canonical WNT pathway in the early stages of serrated CRCs in more detail and the link with ^{V600E}BRAF.

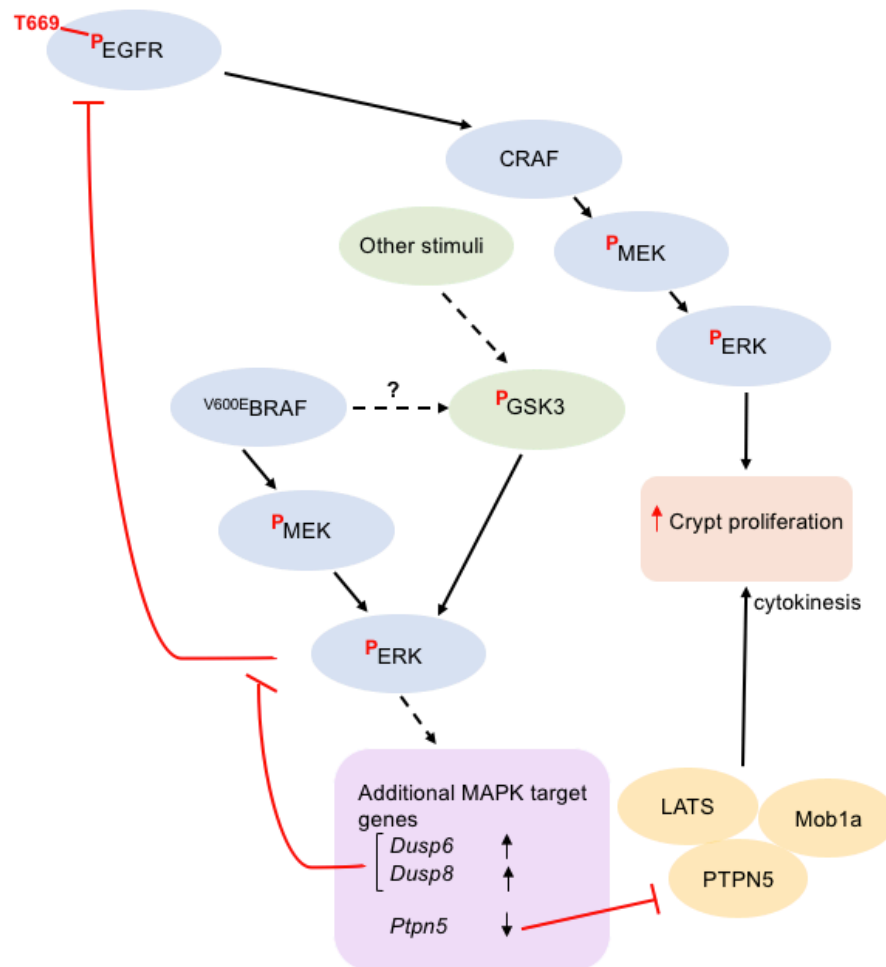


Figure 7.5 Schematic diagram of proposed model on the effect of MAPK target genes on crypt hyperplasia. The additive effect of $V600E$ BRaf and Gsk3 mutation upregulates the expression of additional MAPK phosphatases which can in turn suppress phospho-ERK. This may lead to reduction in its inhibitory effect on the EGF receptor which is otherwise inhibited by phospho-ERK. Increased EGFR activity may induce increased crypt proliferation through CRAF. The large decrease in Ptpn5 expression may also lead to increased crypt proliferation through Mob1a.

7.2.8. Conclusion

This study confirms that $V^{600E}Braf$ mutation is an initiator of serrated colorectal cancer, acting in a MAPK-independent manner to induce formation of hyperplastic crypts. The data would suggest a possible role of ketogenesis, cholesterol metabolism and glycolysis in hyperproliferation, which would need to be examined further. Induction of $V^{600E}BRaf$ expression also leads to the activation of a subset of WNT target genes, some of which are affected by GSK3 phosphorylation. GSK3 phosphorylation is a suppressor of $V^{600E}BRaf$ -driven hyperproliferation; it possibly acts by altering the expression of MAPK phosphatases, which influences the paradoxical activation of the EGFR receptor or the activity of Mob1a.

A deeper understanding of the $V^{600E}BRaf$ induction of serrated CRC can be determined by studying the metabolic rewiring of CRC cells, specifically, ketogenesis, cholesterol biosynthesis and glycolysis; moreover, WNT signalling appears to play an outsized role in this process. A better understanding of crosstalk between the signalling and metabolic pathways would, therefore, bring new insights into the mechanism that drives this incurable cancer. Furthermore, future work would help to identify and validate potential therapeutic targets for this devastating disease.

Chapter 8. Appendix

Appendix 1- List of genes expressed as a result of *Gsk3 α/β* knockin mutations. A total of 22 genes showed a positive or inverse correlation with expression of *Gsk3 α/β* mutations.

“+” indicates genes upregulated by *Gsk3 α/β* mutations, whereas “-“ indicates downregulated genes.

Agilent ID	Gene symbol	Fold change	Regulation
A_55_P2130039	5830477G23Rik	2.30572206	+
A_52_P400999	Arhgap31	2.33304601	-
A_55_P2717633	Btbd3	3.47231258	+
A_55_P2727793	Ckap5	3.45993074	+
A_51_P137184	Fam209	5.40636183	+
A_51_P248857	Fam212a	4.39517548	+
A_55_P1977938	Fcgbp	5.8653884	-
A_55_P2186230	Gm3317	2.18662648	+
A_51_P147422	Kctd19	48.7793775	+
A_51_P436051	Necap2	6.37877619	+
A_55_P2181134	Olf1157	4.36390244	+
A_55_P2837175	Olf1707	4.47684252	+
A_51_P157270	Plekhd1	3.15353078	+
A_55_P1987817	Skint8	2.60316504	+
A_55_P2620126	Slbp	3.63103045	+
A_55_P1978810	Srsf10	3.11828487	+
A_66_P137918	Upk1b	2.67783387	-
A_30_P01022449		2.90207359	+
A_30_P01026786		9.30356488	+
A_30_P01030866		15.3742557	+
A_55_P2776311		3.36435788	+
A_66_P137918		2.58617689	+

Appendix 1A- List of genes expressed as a result of *Gsk3 α/β* knockin mutations.

A total of 34 genes (Adj.P.Value 0.05 or less) showed a positive or inverse correlation with expression of *Gsk3 α/β* mutations.

“+” indicates genes upregulated by *Gsk3 α/β* mutations, whereas “-“ indicates downregulated genes.

Agilent ID	Gene symbol	Adj.P.Value	Fold change	Regulation
A_55_P2130039	5830477G23Rik	0.04022214	2.30572206	+
A_66_P137918	AK050218	0.04394539	2.58617689	+
A_55_P2776311	AK143382	0.01057861	3.36435788	+
A_55_P2798408	Alad	0.01584807	1.9461378	+
A_52_P400999	Arhgap31	0.01726504	2.33304601	-
A_55_P2181753	Bdh1	0.00117544	1.88894966	-
A_51_P163106	Bdh1	0.01726504	1.45533176	-
A_55_P1991585	Blvrb	0.01516221	1.5205462	+
A_55_P2717633	Btbd3	0.03847012	3.47231257	+
A_55_P1973501	Ceacam16	0.02776841	1.76850053	+
A_55_P2727793	Ckap5	0.01584807	3.45993074	+
A_52_P19016	Clasrp	0.04684837	1.31864262	-
A_51_P137184	Fam209	0.00141865	5.40636183	+
A_51_P248857	Fam212a	0.02711775	4.39517548	+
A_55_P1977938	Fcgbp	0.00117544	5.8653884	-
A_55_P2186230	Gm3317	0.02887158	2.18662648	+
A_51_P147422	Kctd19	0.000406	48.7793775	+
A_55_P2036894	Med29	0.01113607	1.68806062	+
A_51_P436051	Necap2	0.03847012	6.37877619	+
A_55_P2181134	Olf1157	0.00117544	4.36390244	+
A_55_P2837175	Olf1707	0.01071889	4.47684252	+
A_55_P2741784	Pif1	0.03847012	1.47385817	+
A_51_P381618	Pla1a	0.03847012	1.56856058	-
A_51_P157270	Plekhd1	0.03659238	3.15353078	+
A_51_P127464	Ppp1r37	0.01057861	1.49535107	+
A_55_P2167025	Pvrl2	0.04468665	1.67674431	-
A_55_P1987817	Skint8	0.03847012	2.60316504	+
A_55_P2620126	Slbp	0.01584807	3.63103045	+
A_55_P1978810	Srsf10	0.01584807	3.11828487	+
A_55_P1975095	Timmdc1	0.04779914	1.50570409	+
A_55_P2932738	Upk1b	0.00117544	2.67783387	-
A_30_P01030866		0.03659238	15.3742557	+
A_30_P01022449		0.03847012	2.90207359	+
A_30_P01026786		0.03847012	9.30356488	+

Appendix 2- List of genes expressed following V^{600E} BRaf induction. A total of 815 genes showed a positive or inverse correlation with V^{600E} BRaf induction.

“+” indicates genes upregulated following induction of V^{600E} BRaf, whereas “-“ indicates downregulated genes.

Agilent ID	Gene symbol	Fold change	Regulation
A_51_P116687	1700010I14Rik	3.81759886	-
A_55_P2514383	1700016C15Rik	2.12588862	-
A_55_P2227217	1700123M08Rik	2.42721974	-
A_66_P115236	1810010D01Rik	2.70476915	-
A_55_P1970436	2010107G12Rik	2.87515614	+
A_51_P179565	2010204K13Rik	2.19678691	+
A_51_P295365	2610021A01Rik	3.95584793	-
A_52_P614417	3000002C10Rik	2.12032583	+
A_51_P208152	3930402G23Rik	7.04068245	+
A_52_P119350	4732419C18Rik	2.39344862	+
A_66_P110966	4930402H24Rik	5.54253439	-
A_51_P428316	4930539N22Rik	4.91614265	-
A_55_P2327853	4931431B13Rik	4.77744114	-
A_55_P2286493	4933405E24Rik	2.5605532	-
A_52_P110070	5730416F02Rik	4.28177137	+
A_55_P2349148	5830408B19Rik	3.3740403	+
A_55_P1971264	6530403M18Rik	2.10229153	+
A_52_P499028	9130008F23Rik	2.11125988	+
A_55_P2508704	9430091E24Rik	4.88880053	-
A_55_P2470474	9530082P21Rik	2.06373547	+
A_55_P2238059	A730091E23Rik	2.1593641	-
A_55_P2137049	AA467197	2.80386495	+
A_51_P453043	Aacs	2.24283872	+
A_52_P665675	Abca1	4.54707964	-
A_52_P671534	Abhd8	2.32901985	-
A_51_P435068	Acadsb	2.97424089	+
A_66_P101407	Acat3	2.14459622	+
A_51_P451574	Acot1	3.14926882	+
A_55_P2165324	Acsl3	3.94838105	+
A_65_P09709	Acsl3	2.87442537	+
A_55_P2935081	Acss2	3.49177633	-

A_66_P118038	Ada	4.54825386	+
A_51_P430423	Ada	2.73677169	+
A_55_P2025760	Adam9	2.50403837	+
A_51_P311038	Adamts15	2.12718149	+
A_52_P313217	Adgrd1	2.2716298	-
A_55_P2502426	Adh1	2.30556267	+
A_55_P2101776	Adora1	2.10467035	-
A_55_P2021505	Adra2a	3.01598122	-
A_51_P510891	Afp	16.7478883	-
A_51_P238563	Agpat2	2.19476071	+
A_51_P346165	Agpat4	2.15586105	-
A_51_P323712	Agt	2.20298348	-
A_52_P162509	Ahcyl2	2.35412458	+
A_55_P2153620	Ahnak	2.99962922	-
A_55_P2510197	Airn	3.41068729	-
A_55_P2089223	Ak4	2.41779931	+
A_55_P2174743	Akap7	2.50262989	-
A_51_P331288	Akr1b7	2.26198525	-
A_51_P128987	Akr1b8	5.6970612	+
A_52_P346037	Akr1c12	2.32807327	+
A_51_P284177	Akr1c14	3.79748439	-
A_51_P334942	Aldh1a1	7.26974612	-
A_51_P383399	Aldh1a7	3.29677774	-
A_55_P2007196	Aldoa	2.05691617	+
A_51_P220681	Aldoc	3.65546839	+
A_66_P133314	Aldoc	3.25564212	+
A_55_P2070992	Aldoc	3.19219026	+
A_51_P423813	Alpi	3.56714859	+
A_51_P132685	Alpl2	3.83352224	+
A_51_P343350	Amn	2.40282661	-
A_51_P349888	Ang2	2.39989751	-
A_66_P134474	Ang3	4.00757746	-
A_52_P98778	Ang4	3.41449623	-
A_55_P2716491	Ang6	3.19815373	-
A_51_P481679	Angptl3	2.73086096	+
A_52_P520607	Ankrd22	5.88624243	+

A_52_P319438	Ankrd37	3.7638202	+
A_66_P134542	Anln	2.49856084	+
A_55_P2733277	Anxa11	2.01581152	+
A_52_P662711	Anxa13	3.22448685	+
A_51_P296737	Anxa13	2.52146107	+
A_51_P165342	Anxa2	2.53323534	+
A_51_P451032	Anxa3	3.74039071	+
A_55_P2056325	Anxa3	3.23601342	+
A_52_P534355	Anxa7	3.58950866	-
A_51_P451482	Anxa9	2.37947727	+
A_55_P2092869	Anxa9	2.24858713	+
A_51_P359315	Apobec2	3.05136065	+
A_55_P2117155	Apoc3	2.87838084	-
A_51_P310629	Apoc3	3.13260563	-
A_66_P120380	Apol10b	5.23275672	-
A_55_P2181752	Apol7a	2.06516646	-
A_51_P497724	Apol7a	2.14456414	-
A_51_P125205	Aqp1	2.7270354	-
A_55_P1990121	Aqp5	8.29388185	+
A_52_P527106	Arhgap12	2.16639295	+
A_55_P2327577	Arhgef38	2.0848469	+
A_55_P2505115	Armc2	2.21081339	-
A_55_P2504175	Arrdc4	2.51451181	+
A_66_P103456	Arsb	2.31592308	-
A_65_P16786	Ascc2	2.172527	+
A_55_P2033725	Ascl2	2.70957772	-
A_51_P259975	Aspa	2.45323269	-
A_55_P2719684	Aspa	3.4792232	-
A_55_P2089804	Atf7	4.59787417	-
A_66_P118819	Atg9b	2.27387034	+
A_55_P2715192	Atp13a4	3.15882285	-
A_55_P2002602	Atp5l	2.03157324	-
A_52_P565847	AU018091	4.66753433	-
A_55_P2130024	AY761184	5.5874184	-
A_55_P2509073	B430010I23Rik	2.06169414	+
A_55_P2084611	B4galt6	2.57233995	+

A_55_P2807306	Bambi	2.10090506	-
A_55_P2507986	Bambi-ps1	2.10466127	+
A_51_P215559	BC021614	2.23544119	+
A_66_P132970	BC049987	2.64508183	+
A_51_P121915	BC089597	2.24942627	-
A_51_P158018	Bend5	2.51672554	+
A_52_P340669	Bhlha15	2.06469885	-
A_51_P411926	Bmp8b	2.30181245	+
A_52_P674759	Btbd3	3.51562388	+
A_55_P2113633	Bzw1	2.0679539	+
A_51_P497985	C2	2.83081771	-
A_51_P110301	C3	3.64603898	-
A_52_P60194	C4bp	2.24955369	-
A_55_P2509454	C4bp-ps1	2.35971098	+
A_52_P458790	C530008M17Rik	2.2460618	-
A_55_P2021572	C87414	2.02905676	-
A_52_P188261	Camk2d	2.37885553	+
A_55_P1998631	Capg	2.61101468	+
A_55_P2747166	Capn2	3.52383999	+
A_52_P610923	Car9	3.99552472	+
A_55_P2092750	Car9	3.57246927	+
A_55_P2100585	Cass4	3.08900705	-
A_51_P484978	Cblc	2.37694833	+
A_51_P481159	Cbr3	2.99520553	+
A_51_P124719	Ccdc93	2.34612748	+
A_52_P18116	Ccl24	2.18085557	-
A_51_P460954	Ccl6	3.98402032	-
A_51_P185660	Ccl9	3.22589625	-
A_55_P2925449	Ccser1	2.59741939	-
A_55_P2125912	Cct6a	2.16672989	+
A_51_P385718	Cd177	2.07127557	+
A_55_P2004511	Cd300lf	3.04917898	-
A_55_P2185605	Cd48	3.06328217	-
A_55_P2101585	Cd55	2.40101244	+
A_51_P388412	Cd55	2.27973234	+
A_66_P109404	Cd55	2.19932487	+

A_55_P2715366	Cd86	2.6394723	+
A_52_P141384	Cdcp1	3.80559003	-
A_51_P450033	Cdk1	2.12792155	+
A_52_P284658	Cdkn2aipnl	2.01739013	+
A_51_P370008	Ceacam18	2.44063366	+
A_51_P444447	Cebpd	2.02674493	-
A_51_P219970	Cela1	2.14288053	+
A_55_P2713446	Cenpq	2.19737382	-
A_51_P380587	Cep72	2.01630118	+
A_55_P2850037	Ces1d	2.17554692	-
A_51_P369784	Ces1e	2.41834654	-
A_51_P358316	Chga	3.62874193	-
A_55_P2120354	Cib2	2.02659396	-
A_52_P385606	Ckb	2.687476	+
A_51_P394715	Cklf	6.1889485	-
A_55_P2738062	Clasp2	2.03683584	-
A_52_P251450	Cldn2	4.22584269	+
A_66_P109468	Cldn24	4.4598803	-
A_55_P2183453	Cldn4	2.59725223	+
A_55_P2500178	Clic1	2.2223426	+
A_65_P01958	Clpb	2.02889698	+
A_55_P2015878	Clps	6.90569662	-
A_55_P2747563	Cml2	2.18313175	-
A_55_P2610621	Col1a2	2.68259802	-
A_66_P129600	Commd1	3.36935748	-
A_51_P140731	Cops5	2.02794702	+
A_52_P320261	Cpa2	2.10900565	+
A_51_P427674	Cpt1a	2.8889856	+
A_51_P264695	Crym	3.53173625	-
A_51_P157042	Ctgf	3.07832403	+
A_55_P2935306	Cttnbp2nl	2.70478614	-
A_55_P2047639	Cubn	22.5226449	-
A_51_P374198	Cxcl16	2.45434499	+
A_55_P2046563	Cym	4.37829316	-
A_52_P472486	Cyp2b10	6.76358593	-
A_55_P2044653	Cyp2b10	12.0417853	-

A_51_P467076	Cyp2b9	9.27450468	-
A_55_P2487509	Cyp2c55	5.58072591	-
A_51_P447785	Cyp2c55	13.7060056	-
A_55_P2058433	Cyp2c68	2.07436477	-
A_51_P355301	Cyp3a11	3.40019677	-
A_51_P482051	Cyp3a16	4.71224116	-
A_51_P489367	Cyp3a25	3.11867867	-
A_51_P341203	Cyp3a41a	5.19663205	-
A_55_P2162880	Cyp3a57	3.0176612	-
A_55_P2028046	Cyp3a59	3.4515038	-
A_52_P302345	Cyp4v3	2.83373408	-
A_51_P485791	Cyp51	2.48428953	+
A_55_P2792294	Cyp51	2.13003057	+
A_55_P1988113	Cyth2	2.05015232	-
A_55_P1954820	D1Ert622e	2.14487912	+
A_66_P106385	Daf2	2.25538684	+
A_52_P452747	Dao	2.22240952	-
A_55_P2108933	Dao	4.26958278	-
A_52_P256569	Dbn1d2	2.50567876	+
A_51_P110471	Ddah1	5.72512997	+
A_51_P307168	Ddah1	4.94501756	+
A_51_P326229	Ddx25	4.00922631	-
A_51_P491470	Ddx47	2.21100333	+
A_55_P2054373	Defa-ps1	5.14844547	-
A_55_P2076994	Defa-rs10	11.3636594	-
A_55_P2045213	Defa-rs12	10.4204255	-
A_55_P2004208	Defa-rs2	2.82958532	-
A_55_P2018863	Defa-rs7	7.51735979	-
A_55_P2018862	Defa-rs7	14.1460448	-
A_55_P1961407	Defa2	20.8148712	-
A_55_P1971928	Defa21	12.8541543	-
A_55_P1969960	Defa25	9.62054647	-
A_55_P1954799	Defa26	5.03901767	-
A_51_P319093	Dgka	2.12431276	+
A_51_P312437	Dhrs7	2.06080912	+
A_55_P2046657	Dio1	2.49223813	-

A_55_P2592137	Dio1	2.74628496	-
A_51_P368394	Dnajb8	2.02901733	+
A_55_P2501636	Dnm3	2.97872858	+
A_51_P329818	Dpep3	2.86678676	+
A_52_P417368	Dpp4	2.01729563	-
A_55_P2806464	Dpysl5	2.15471053	-
A_52_P481279	Drc1	2.82724175	+
A_51_P347333	Dusp4	2.74539755	+
A_51_P161946	E130012A19Rik	6.65119368	+
A_51_P120448	Echdc1	2.46188487	+
A_55_P1956418	Efr3b	2.01258235	-
A_52_P387009	Egln3	4.82903433	+
A_51_P330428	Eif4ebp1	2.04044398	+
A_55_P1977096	Elk4	2.01638049	-
A_55_P2797109	Eln	2.43383247	+
A_55_P1989921	Eml2	2.00018791	+
A_55_P2087561	Eno1b	2.20616018	+
A_66_P103820	Enpep	2.83333033	-
A_51_P332917	Enpp3	2.58796747	+
A_52_P379277	Enpp3	2.29550213	+
A_52_P630563	Ept1	2.14680822	+
A_55_P2094292	Erp27	8.50332292	-
A_55_P2016105	Errfi1	3.27023125	+
A_55_P1959521	Etv4	7.26329444	+
A_55_P2078780	Etv4	5.07246287	+
A_51_P204486	Exoc3l4	2.19314455	-
A_51_P174961	F10	3.29295839	-
A_55_P1971889	F3	2.56779469	+
A_65_P20641	Fads2	2.47191533	+
A_55_P2913071	Fam101b	2.45681214	+
A_51_P329949	Fam13a	2.50348375	+
A_51_P115159	Fam162a	2.48571812	+
A_51_P431734	Fam185a	2.19294655	+
A_52_P416727	Fam210a	2.01978028	+
A_55_P2430221	Fam35a	2.01482135	-
A_51_P447976	Fam46c	2.01155007	-

A_65_P00912	Fam46c	2.33001467	-
A_55_P2061036	Fam83e	2.11956737	+
A_52_P410520	Farsa	5.4131116	-
A_55_P2626499	Farsb	2.13378677	+
A_52_P588483	Fbln1	2.60111783	-
A_55_P2740354	Fbln1	2.94947404	-
A_51_P474701	Fbp1	2.68994528	-
A_55_P1965194	Fbxl5	2.25255052	+
A_55_P2033250	Fdft1	3.12860168	+
A_66_P111208	Fdft1	2.14153771	+
A_55_P1966804	Fdps	3.00590605	+
A_66_P138027	Fgd6	2.04423278	+
A_51_P399845	Fgf2	3.46554563	-
A_55_P2021921	Fkbp1a	2.31741542	-
A_52_P222350	Flnb	2.12371346	+
A_55_P2144556	Flrt3	2.2813642	+
A_66_P122700	Fpgs	2.24649696	+
A_51_P383270	Fras1	2.22476473	-
A_52_P367294	Fsd1l	2.08976464	+
A_55_P2483347	Fut1	2.66308607	-
A_66_P129538	Gale	2.13644657	+
A_55_P1994258	Gapdh	3.0262952	+
A_55_P1965725	Gapdh	2.7096528	+
A_55_P1984284	Gapdh	2.13203662	+
A_51_P406253	Gcg	3.42111317	-
A_55_P2106175	Gch1	3.17869603	+
A_55_P1989813	Gcm1	2.50694408	-
A_52_P53144	Gcnt3	2.50986777	+
A_65_P11011	Gcnt3	2.22359819	+
A_55_P2727267	Ggps1	2.99931573	-
A_52_P313098	Gip	2.38566364	-
A_52_P463340	Gjd3	2.11572554	-
A_51_P267700	Gkn3	3.88899272	+
A_51_P169087	Gls2	3.50965315	+
A_51_P376258	Glud1	2.16333373	-
A_55_P2487095	Glyctk	2.07667128	-

A_65_P20683	Gm1070	2.32737692	-
A_66_P130315	Gm11210	2.63211677	-
A_55_P2200054	Gm11266	3.68360945	-
A_55_P2051039	Gm11937	2.03766164	-
A_55_P2737234	Gm11974	3.71225529	-
A_55_P2059323	Gm13315	2.18917075	+
A_55_P2098971	Gm14085	5.25782321	+
A_66_P118249	Gm14137	2.02272619	+
A_55_P2054372	Gm15299	2.66212221	-
A_55_P2736480	Gm15658	2.5413604	-
A_66_P103164	Gm15764	2.10404355	-
A_66_P114103	Gm19434	3.1681395	-
A_55_P2829137	Gm20684	2.01914451	+
A_55_P1972868	Gm21498	6.66169584	-
A_65_P07827	Gm2701	3.80229476	-
A_51_P187579	Gm31711	2.0033284	+
A_66_P121715	Gm32894	2.30909376	+
A_55_P2930354	Gm33586	2.83370397	-
A_55_P2549189	Gm35622	2.6419219	+
A_55_P2730996	Gm38413	2.42461281	-
A_66_P127146	Gm38419	2.17252858	+
A_55_P1992571	Gm41468	2.11306164	-
A_66_P121785	Gm41781	2.68662678	-
A_55_P2150248	Gm4787	7.96394821	-
A_55_P2749956	Gm4841	2.26995072	-
A_55_P1967533	Gm5069	2.72731888	+
A_66_P121502	Gm5485	2.39145303	-
A_55_P2722684	Gm5592	4.29038729	-
A_55_P2322120	Gm5617	4.10908613	+
A_55_P2004721	Gm766	5.78914152	+
A_55_P2482301	Gm7861	3.59999948	-
A_55_P2108690	Gm8709	2.24669339	+
A_52_P463271	Gm ds	3.66307645	+
A_55_P2157814	Gm ds	2.46238683	+
A_51_P171200	Golm1	2.07367877	+
A_55_P2744563	Gpi1	2.36196964	+

A_52_P597775	Gprc5a	5.19338334	+
A_52_P141488	Grk5	2.09204233	+
A_52_P46419	Grk6	2.0221292	+
A_55_P1961423	Gsta3	2.68943125	+
A_51_P112223	Gsta4	3.57607494	+
A_55_P2062190	Gstm1	2.22601523	-
A_51_P454949	Gstm3	2.54996102	-
A_55_P2094060	Gzma	2.17719405	-
A_55_P1962747	H2-Ab1	2.37292153	-
A_52_P683598	H2-Ab1	2.43102461	-
A_55_P2146560	H2-Ab1	2.65289187	-
A_51_P278868	H2-DMb1	2.39581411	-
A_55_P2037343	H2-Q10	2.53650091	+
A_55_P2074035	Hao	7.89153918	-
A_55_P2032272	Habp2	4.90617184	-
A_51_P196590	Hadh	2.02084681	-
A_55_P1984886	Hcst	2.00233395	-
A_55_P2106429	Herc2	2.69706692	-
A_55_P2748958	Hhat	2.07494652	-
A_66_P107191	Hif1a	3.41329591	+
A_55_P2027999	Hk1	2.39086272	+
A_55_P2032966	Hmgcs1	2.19608874	+
A_55_P2109033	Hmgcs2	2.09857644	-
A_55_P2912004	Hmgcs2	2.45454406	-
A_52_P535623	Hook1	2.06407046	+
A_55_P1997936	Hsd17b7	2.00765069	+
A_52_P515036	Htati2	2.87532824	+
A_51_P228883	Htati2	2.0561794	+
A_52_P562054	Ick	2.14315931	+
A_51_P467668	Ick	2.08610358	+
A_51_P132978	Idh1	2.13407961	+
A_52_P257502	Igfbp4	2.12054365	-
A_55_P2376423	Igkv4-72	2.67447127	-
A_51_P503757	Iglv1	2.15453162	-
A_55_P2825279	Il22ra1	2.3858523	-
A_51_P290207	Insig1	3.05639653	+

A_55_P1983708	Insrr	2.31817811	-
A_52_P99531	lppk	2.46044868	+
A_51_P152550	lqcg	2.32779159	-
A_52_P518922	ltga1	5.41659494	-
A_66_P119869	ltln1	4.17447703	-
A_55_P2035117	ltln1	6.34832614	-
A_55_P1975917	ltlnb	6.70710738	-
A_51_P269663	ltpr1	2.16423608	-
A_51_P191262	Jsrp1	4.07628047	+
A_52_P570240	Kbtbd11	2.38332601	-
A_55_P2106926	Kcna3	5.62329463	-
A_52_P642488	Kcnk1	2.2000032	+
A_51_P389636	Kcnn4	2.97966619	+
A_55_P2745114	Kcnq1	5.07968578	-
A_51_P218975	Kcns3	2.48150269	-
A_51_P331805	Kctd15	2.47522248	-
A_55_P2044389	Kif6	3.14719561	-
A_55_P2022074	Klf10	2.4913085	+
A_55_P2793729	Klf15	3.12169226	-
A_55_P2004551	Klra1	3.82871646	-
A_55_P2170350	Klra22	3.5964526	-
A_51_P287691	Kremen2	2.68194555	+
A_51_P287198	Krt23	2.85035821	+
A_55_P2140042	Krt31	2.26798258	-
A_52_P410685	Krt7	3.71226807	+
A_51_P167489	Lama3	2.10885257	+
A_51_P223656	Lamb3	2.63652536	+
A_55_P1967196	Lamb3	2.42486902	+
A_55_P1981366	Lamc2	3.14816996	+
A_55_P2018697	Ldhd	3.14034592	+
A_52_P413492	Ldlrap1	2.88206585	+
A_51_P117881	Leap2	3.08708099	-
A_51_P249909	Lect2	2.96944965	-
A_55_P2529154	Lhcgr	2.05377112	-
A_51_P286946	Lhpp	3.26052897	-
A_51_P403564	Lhx5	2.58348502	+

A_66_P134488	Lif	3.69615034	-
A_51_P334118	Lin7c	2.37073902	+
A_65_P12904	Lmna	2.54284427	+
A_52_P137765	Lmna	2.37310457	+
A_51_P313566	Lmna	2.36069307	+
A_52_P103628	LOC102637129	2.90712308	+
A_51_P150835	LOC102641619	2.11893751	-
A_55_P2723934	LOC102642530	6.08099851	-
A_55_P2552889	LOC102643017	2.07351672	-
A_55_P2057189	LOC105242475	11.5310401	-
A_55_P2727165	LOC105243184	3.55821487	+
A_51_P200484	Lrp12	2.58631306	-
A_55_P2930128	Lrrc16b	3.14340118	-
A_55_P2054967	Lrrc49	2.61868483	-
A_52_P365342	Lrrn2	3.2587244	-
A_55_P2924612	Lsamp	3.53619559	-
A_55_P2807240	Lss	2.6967456	+
A_51_P296487	Lss	2.49458959	+
A_55_P2015292	Ltc4s	2.78230041	-
A_51_P491635	Ly6g6e	4.64027034	+
A_66_P118567	Lypd6b	4.18836753	-
A_55_P2181738	Lyz1	3.50558225	-
A_51_P321150	Lyz2	2.62895668	-
A_52_P238027	Lyz2	3.28861681	-
A_51_P243514	Macc1	2.88377363	+
A_51_P213030	Macrod1	2.49505934	-
A_66_P119238	Maoa	2.87985176	-
A_55_P1988664	Map3k14	4.61061488	-
A_55_P2105843	Mbd1	2.14320845	-
A_51_P349495	Mboat1	18.1122972	+
A_55_P2016842	Me1	3.65702719	+
A_55_P2009952	Me1	3.27438021	+
A_51_P490817	Me2	2.07682049	-
A_51_P376313	Med8	2.04446857	+
A_51_P455997	Meg3	2.09722814	-
A_55_P2736010	Meg3	2.17346632	-

A_66_P102500	Meis2	3.17915614	+
A_55_P2067707	Mep1a	7.9292874	-
A_51_P279437	Mfsd2a	2.03715055	+
A_55_P2928183	Mgam	2.33186209	-
A_55_P2118916	Mgat4c	2.46181828	+
A_55_P2727629	Mgea5	2.01447847	-
A_55_P2041723	Mid1ip1	2.14722404	+
A_55_P2068265	Mif	2.38671712	+
A_55_P1994947	Mif	2.31006867	+
A_51_P426096	Mmp7	3.45440397	-
A_66_P118835	Mmp7	4.60343002	-
A_55_P2814955	Mpp3	2.91172234	+
A_51_P497039	Mpp3	2.2559183	+
A_55_P2044282	Mpp6	2.02605765	+
A_55_P2092633	Mptx1	9.52037061	-
A_66_P109060	Mptx2	12.7218068	-
A_51_P289249	Mpzl3	2.0450316	+
A_55_P2180854	Mrgprg	4.47546651	-
A_55_P2077158	Mro	2.18306012	-
A_55_P2739272	Ms4a8a	2.81608832	+
A_66_P104901	Msmo1	2.68640299	+
A_51_P282179	Mtor	2.06887826	+
A_55_P2025687	Muc4	2.59445054	+
A_51_P355943	Mvd	2.75745035	+
A_55_P2058861	Mvk	2.69557514	+
A_51_P169527	Mvk	2.33450871	+
A_52_P108346	Myc	2.03713298	+
A_51_P170536	Mycbpap	2.6323993	-
A_51_P288746	Myo18b	3.96536904	-
A_66_P121695	Naaladl1	3.85948137	-
A_55_P2130855	Nap111	2.10772491	+
A_51_P479230	Nat8	2.33310062	-
A_55_P2910874	Ncald	2.06634651	-
A_55_P2609901	Ncald	2.15472099	-
A_52_P443427	Ncoa4	2.37967774	+
A_51_P191649	Ndc80	2.23859355	-

A_66_P108184	Ndfip2	2.03475623	+
A_65_P09473	Neat1	2.00713663	+
A_55_P2628192	Nebi	4.51980296	-
A_52_P140005	Nipal1	2.11580074	+
A_52_P650180	Nipal2	4.2284531	+
A_51_P232708	Npff	9.61909993	-
A_55_P2074281	Nr2f1	2.56319699	-
A_55_P2115330	Nrg4	2.00621608	-
A_55_P2185900	Nrg4	2.12263871	-
A_52_P297803	Nsdhl	2.50591024	+
A_51_P425696	Nt5c2	2.52588617	+
A_52_P77837	Nt5c3	2.29713531	+
A_55_P2641968	Nt5c3	2.09633174	+
A_52_P574668	Nt5e	3.57244673	+
A_55_P2716786	Nudt5	2.98238172	-
A_55_P2802986	Oat	5.43414744	-
A_55_P2094916	Ocm	2.42790096	-
A_55_P2073825	Ocm	3.57307969	-
A_55_P2915840	Oit1	2.66127863	+
A_66_P110850	Olfr1385	4.36306737	+
A_66_P115118	Olfr1513	3.02539696	-
A_66_P116004	Olfr699	3.90353118	-
A_51_P316199	Olfr73	2.22476485	+
A_51_P368894	Onecut1	2.4108186	+
A_55_P2208579	Onecut2	2.08723703	+
A_52_P547795	Opa1	2.13975871	+
A_55_P2718563	Opcml	3.14870623	-
A_52_P215176	Opn3	3.68790814	+
A_66_P108770	Oxct1	2.28885489	+
A_51_P107326	Oxct1	2.17283619	+
A_55_P2039556	Pak6	3.25812942	-
A_66_P102877	Pald1	2.60873877	-
A_55_P2019751	Paox	2.57544225	+
A_51_P180613	Paox	2.17170595	+
A_52_P37123	Pard6b	2.45870426	+
A_55_P2745124	Park2	3.56191961	-

A_51_P298843	Pcbd2	2.49774125	-
A_55_P2722458	Pcdh15	4.91436255	-
A_51_P397673	Pcsk9	5.1809386	+
A_52_P452787	Pcd6ip	2.02532605	+
A_55_P2131964	Pdia2	4.3700222	-
A_51_P406429	Pdk1	2.34845519	+
A_66_P132039	Pdx1	4.71527225	+
A_55_P2118076	Pdzd7	2.81068402	+
A_66_P127455	Pdzk1	3.04776378	-
A_55_P2011410	Pdzk1	6.27420338	-
A_51_P303397	Pepd	2.09116283	-
A_51_P212491	Pfkfb3	2.48250716	-
A_51_P310896	Pfkl	2.62851759	+
A_55_P1963184	Pgap1	4.50288761	+
A_55_P2081488	Pglyrp1	2.50515641	+
A_51_P427530	Pgm1	3.87333542	+
A_51_P195958	Phlda1	3.74891883	+
A_52_P350786	Phlda2	4.02409905	+
A_65_P09318	Pik3ca	2.03139975	-
A_52_P307938	Pik3r1	2.05923125	-
A_51_P337195	Pipox	4.1913206	-
A_55_P2797212	Pir	3.13063999	+
A_52_P654624	Pisd-ps3	2.01284118	-
A_66_P139646	Pla2g4c	8.82842044	+
A_52_P17207	Pla2g4c	3.51755837	+
A_55_P2499113	Pla2g5	2.40047829	+
A_55_P1997696	Plbd1	2.16486399	-
A_55_P2121980	Plcb4	2.31049705	-
A_51_P278163	Plcd3	4.49531995	-
A_52_P488437	Plek2	3.53730614	+
A_51_P375201	Plk3	2.61317972	+
A_51_P328817	Plk5	3.26445168	-
A_52_P121502	Plip	2.67115391	+
A_52_P418644	Plp2	3.80179483	+
A_55_P2042606	Pls1	3.34099182	-
A_55_P2088995	Plscr1	2.84051851	+

A_52_P4598	Pmm1	2.17897156	+
A_55_P1999962	Podn	2.58652087	-
A_55_P2077098	Pof1b	3.28206739	+
A_55_P2727524	Pole2	5.00516671	-
A_55_P2824501	Pou4f1	2.34876829	-
A_55_P2741134	Pou5f1	7.61585645	-
A_51_P106799	Pparg	2.43600947	+
A_51_P224564	Ppm1f	2.54442487	-
A_51_P332652	Pqlc3	2.22968064	+
A_55_P2130555	Prdm11	2.06156498	+
A_55_P2744082	Prelid2	2.56262529	+
A_66_P109368	Prex2	4.80294808	-
A_51_P215438	Prodh	2.58149256	-
A_51_P225793	Prr5l	2.77717499	-
A_51_P477682	Prss12	2.69629282	-
A_51_P429335	Prss16	3.02166181	+
A_55_P2052290	Psat1	2.90098797	+
A_52_P570266	Psmb10	2.01486411	-
A_51_P345367	Psmb8	2.00542643	-
A_51_P207988	Ptger4	2.6933843	+
A_52_P571290	Ptms	2.55455478	-
A_66_P110662	Ptn	4.38178107	-
A_52_P605812	Ptrh1	2.61776494	+
A_66_P119926	Pus7	2.65772837	-
A_52_P366462	Pyy	3.27779478	+
A_51_P209280	Rab31	2.4339198	+
A_55_P1956687	Rab37	2.01768847	-
A_55_P2161923	Rabgap1	3.55678971	-
A_52_P430628	Rabggtb	2.6412537	+
A_51_P115817	Ralgps2	2.08324675	+
A_52_P551476	Raph1	3.21521185	+
A_51_P348433	Rasal1	2.89250324	+
A_55_P2035315	Rasgef1b	3.1973149	+
A_52_P574759	Rbpjl	2.33305986	-
A_55_P2898235	Rdh9	2.52664529	-
A_51_P329811	Reg1	14.720603	-

A_51_P267969	Reg3a	15.1566743	-
A_51_P169671	Reg3b	8.46381216	-
A_51_P354126	Reg3g	5.89322542	-
A_55_P2167486	Resp18	2.63549843	-
A_52_P343326	Rgp1	2.56411944	+
A_55_P2905246	Rgs12	2.02632758	-
A_66_P126313	Rhof	2.06140566	+
A_55_P2071329	Rhog	2.47496371	-
A_66_P107583	Rhox3a	4.35260825	-
A_55_P2000399	Rhox4a	5.05383142	-
A_55_P1975667	Rhox4g	4.63443604	-
A_51_P491987	Ripk3	3.13255327	+
A_52_P249798	Rnase1	2.45733292	-
A_55_P2935946	Rnf150	2.6370543	-
A_51_P517672	Rnf152	2.24384606	+
A_51_P148494	Rnft1	2.09541284	+
A_55_P2723769	Rnu1a1	2.43703418	-
A_55_P2723745	Rnu1b1	2.06332642	-
A_55_P1987290	Rnu1b6	2.03777953	-
A_55_P2065991	S100a11	3.30629814	+
A_51_P419226	S100a14	11.9693649	+
A_66_P114627	S100a16	2.78506095	+
A_55_P2148912	S100a16	2.65526969	+
A_51_P108812	S100a5	2.95247365	+
A_51_P281089	S100a6	6.10242214	+
A_51_P166886	Saa2	2.87489127	-
A_52_P198898	Samd5	2.56273467	+
A_51_P129464	Scd2	6.22784077	+
A_55_P2481829	Scmh1	2.08959377	+
A_55_P2030736	Scmh1	2.00002888	+
A_51_P212741	Scn2b	2.25208316	-
A_52_P409711	Sec24a	2.01993357	+
A_55_P2165414	Serpina1a	2.21773467	-
A_55_P2010301	Serpina1c	2.23401215	-
A_55_P2113857	Serpina1e	2.15475974	-
A_51_P187602	Serpinb5	4.00811191	+

A_66_P138465	Setd1a	3.91153129	+
A_52_P220190	Sf3b1	2.05175929	-
A_55_P2020203	Sfrp5	3.21605773	-
A_51_P454196	Sh2d4a	2.15311258	+
A_51_P313761	Shmt2	2.08987917	+
A_66_P132493	Siglece	5.69201659	-
A_55_P2022890	Slc12a8	2.19740297	+
A_55_P2505205	Slc13a1	2.81882393	+
A_55_P2143923	Slc13a2	3.73637876	-
A_55_P2822857	Slc16a12	2.41995303	+
A_51_P110759	Slc1a1	2.00021958	-
A_51_P408631	Slc20a1	2.23030934	+
A_55_P2107987	Slc22a13b-ps	3.03869283	-
A_55_P2185362	Slc25a18	2.19852806	-
A_51_P211616	Slc27a6	2.72329544	+
A_51_P464738	Slc2a1	3.46886007	+
A_52_P883557	Slc30a10	2.25338338	+
A_51_P338563	Slc36a1	3.33108857	-
A_51_P279997	Slc4a7	2.67749278	+
A_51_P253207	Slc51a	2.49121638	-
A_52_P229943	Slc51b	2.30660432	-
A_55_P2101088	Slc5a11	6.29586334	-
A_55_P1965030	Slc5a12	14.1408338	-
A_51_P228971	Slc5a4b	2.94715843	-
A_66_P139208	Slc6a8	2.33339888	+
A_55_P2883452	Slc7a8	2.43626428	-
A_51_P112734	Slc7a8	2.65557205	-
A_55_P2941602	Slco2a1	4.93549398	-
A_51_P423578	Slfn2	2.03709882	-
A_51_P496569	Slit2	6.55144779	+
A_51_P383140	Slk	2.71369224	+
A_52_P472324	Slpi	3.19275551	-
A_51_P164270	Snrpa1	2.21086073	+
A_55_P2647378	Spag9	4.74660787	-
A_51_P325552	Spert	2.36762958	-
A_51_P365516	Spink1	2.73501194	-

A_55_P2048853	Sprr2a2	3.26242147	+
A_51_P459894	Sprr2b	3.19046855	+
A_51_P491758	Sprr2j-ps	4.06382097	+
A_52_P204311	Spry4	2.4856726	+
A_51_P209261	Sqrdl	2.13863989	+
A_51_P489313	Sri	2.14270735	+
A_55_P2738763	Ssfa2	2.56012933	+
A_55_P2603685	St3gal6	2.57796109	+
A_55_P2740019	St3gal6	2.20531936	+
A_55_P2603690	St3gal6	2.19124934	+
A_55_P2118609	St6galnac1	2.8505826	-
A_51_P236267	St8sia4	2.05074404	-
A_51_P471177	Stra6	2.33036577	-
A_66_P118256	Strn3	2.09921686	+
A_51_P394814	Svep1	4.01888461	-
A_55_P2741163	Swi5	2.09427605	+
A_55_P2370250	Syn3	4.55857699	-
A_51_P216456	Tac1	2.42732495	+
A_55_P2017645	Tap2	2.03368428	-
A_55_P2183597	Tbc1d2	2.25270857	+
A_55_P2089565	Tbx22	2.99829809	-
A_52_P161297	Tcea3	2.36105235	-
A_52_P300451	Tcf23	22.4609843	+
A_51_P164030	Tcp1	2.49985601	+
A_55_P1968028	Tdgf1	3.50731538	-
A_55_P1994418	Teddm3	4.70199584	+
A_52_P949440	Tgfb1i1	2.06464998	-
A_52_P220879	Tgm2	2.44059749	-
A_51_P249989	Tifa	4.90379011	-
A_55_P2011385	Tifa	8.0572635	-
A_55_P2153990	Tldc2	2.05694506	+
A_52_P330694	Tle1	2.16470003	+
A_51_P371001	Tm4sf4	12.3091984	+
A_66_P126582	Tmem181a	2.00753209	+
A_51_P495485	Tmem55a	3.19749198	-
A_55_P1976953	Tmprss9	2.82692082	-

A_51_P131408	Tnfrsf12a	3.20458298	+
A_51_P399305	Tnfrsf19	2.09826522	-
A_52_P451073	Tnfrsf21	2.21470929	+
A_55_P2071132	Tnfrsf23	2.06822007	+
A_55_P2018017	Tnfsf10	2.52042163	-
A_55_P2010038	Tnfsf9	2.04279551	+
A_55_P2742131	Tom11l1	2.44585321	+
A_52_P657286	Trim39	2.95020296	-
A_55_P2732428	Trp53rkb	2.32954881	-
A_55_P2043782	Trpm1	2.08676304	-
A_52_P605387	Tsg101	2.08684164	+
A_55_P2724059	Tsga10	2.95202515	+
A_51_P333923	Tspan1	2.80678544	+
A_55_P2011061	Tspan12	2.06125139	+
A_55_P2724669	Tspan8	2.11371613	+
A_65_P19832	Ttr	3.26596512	+
A_51_P490023	Tubb2a	2.65914278	+
A_55_P2175245	Tusc3	2.35324285	+
A_55_P2163729	Tvp23a	2.13400149	-
A_52_P463365	Twf1	2.13604883	+
A_55_P2095019	Ubash3b	9.8700017	-
A_55_P2718015	Ube2f	2.24895062	-
A_55_P1980543	Ube2i	2.39935204	+
A_51_P297105	Ucp2	2.70646407	+
A_52_P90265	Ucp2	2.30751148	+
A_66_P108247	Ucp3	2.16975228	+
A_66_P106021	Usf2	2.37270159	-
A_55_P2491668	Usp2	2.58547387	-
A_65_P19862	Vdr	2.05206733	+
A_55_P2741794	Vegfa	3.13899228	-
A_52_P96552	Vkorc11l1	2.53696218	+
A_55_P2072150	Vpreb2	4.99130261	-
A_55_P1953861	Vstm2l	2.04463291	+
A_51_P220934	Vstm5	2.15870612	+
A_52_P561650	Vwa1	3.58094649	-
A_55_P2844759	Wdr92	2.15621816	-

A_55_P2298029	Whsc111	3.52166103	-
A_66_P139703	Wnt4	2.31115065	-
A_55_P1985950	Xpnpep2	4.5713438	-
A_51_P373609	Yars2	2.20259814	+
A_55_P2763719	Zbed4	4.84473046	-
A_55_P2496052	Zfp934	3.34278871	-
A_55_P2054703		5.36203145	+
A_66_P101652		3.92502845	+
A_55_P2021908		3.89063759	+
A_55_P2016623		3.34749774	+
A_55_P2185359		3.30459398	+
A_55_P2723989		3.29822582	+
A_55_P2081137		3.12158234	+
A_55_P2092046		3.10219287	+
A_55_P2017116		3.0874653	+
A_30_P01019037		3.07825672	+
A_66_P105956		3.03106954	+
A_30_P01017441		2.97791984	+
A_55_P2005719		2.97077132	+
A_52_P226489		2.9206491	+
A_52_P532370		2.86539983	+
A_55_P2182077		2.84933589	+
A_52_P221024		2.845959	+
A_66_P106968		2.82881184	+
A_55_P2185628		2.78403084	+
A_55_P2133680		2.78269581	+
A_66_P139927		2.72856338	+
A_55_P2112797		2.7179039	+
A_55_P2088690		2.68101282	+
A_30_P01024971		2.66470281	+
A_66_P140076		2.65226061	+
A_66_P117863		2.63232785	+
A_66_P128490		2.62117413	+
A_66_P137413		2.59430712	+
A_66_P100016		2.58711436	+
A_55_P2026761		2.57420603	+

A_55_P1971093	2.56996212	+
A_55_P2021455	2.56768995	+
A_52_P53507	2.55705998	+
A_55_P2168267	2.54520467	+
A_55_P2155593	2.53485976	+
A_52_P437084	2.5265546	+
A_52_P229210	2.51049788	+
A_65_P07032	2.49041664	+
A_52_P272054	2.4826356	+
A_66_P136793	2.47107626	+
A_52_P654437	2.46518851	+
A_66_P136364	2.45071807	+
A_55_P1968664	2.44918359	+
A_55_P2001072	2.41178395	+
A_55_P2156504	2.4107448	+
A_52_P644984	2.40816322	+
A_30_P01026945	2.39536248	+
A_55_P1961414	2.39447174	+
A_30_P01019015	2.38902441	+
A_66_P116430	2.3730527	+
A_66_P116378	2.36276512	+
A_66_P102046	2.34805578	+
A_55_P2167005	2.32047442	+
A_55_P2135023	2.32036468	+
A_52_P89683	2.31488259	+
A_55_P1984070	2.29899903	+
A_52_P395508	2.29356686	+
A_30_P01024970	2.29300797	+
A_55_P2112701	2.28964498	+
A_66_P127084	2.28870149	+
A_66_P107454	2.28308095	+
A_66_P134733	2.28089189	+
A_55_P2108689	2.26957988	+
A_55_P2060938	2.26249241	+
A_55_P2067947	2.26170583	+
A_52_P61549	2.26150979	+

A_55_P2060854	2.25856736	+
A_66_P126101	2.25668804	+
A_30_P01031905	2.25562598	+
A_30_P01029178	2.25459583	+
A_66_P105518	2.24364807	+
A_30_P01026822	2.24335813	+
A_52_P92404	2.24273262	+
A_65_P01046	2.22543232	+
A_55_P2139587	2.22197068	+
A_55_P1975087	2.21257548	+
A_55_P2133679	2.21089872	+
A_66_P118307	2.21068721	+
A_65_P08042	2.20396155	+
A_55_P2037424	2.20206525	+
A_30_P01020518	2.20023447	+
A_66_P104393	2.19375491	+
A_55_P2160204	2.19146912	+
A_55_P2186929	2.19143474	+
A_30_P01025368	2.17305862	+
A_55_P2091247	2.17087837	+
A_55_P2067153	2.16981599	+
A_55_P2144003	2.16975146	+
A_55_P2054128	2.16055742	+
A_55_P2037689	2.15660917	+
A_52_P430427	2.15474776	+
A_55_P1992470	2.15148672	+
A_55_P1972892	2.14623549	+
A_30_P01027445	2.14508465	+
A_55_P1979694	2.14249798	+
A_66_P122949	2.13887979	+
A_55_P2013273	2.12991058	+
A_55_P2069995	2.11810514	+
A_55_P2020080	2.09825535	+
A_30_P01032460	2.07024538	+
A_30_P01026145	2.06889957	+
A_55_P2136334	2.05507384	+

A_30_P01024929	2.05355504	+
A_55_P1975837	2.0532757	+
A_30_P01021243	2.03435779	+
A_30_P01029927	2.03081225	+
A_55_P2021094	2.02889324	+
A_66_P102988	2.02217531	+
A_30_P01018414	2.01860142	+
A_51_P152725	2.00937643	+
A_30_P01020196	2.00907569	+
A_30_P01029853	2.05286689	-
A_51_P124315	2.05744882	-
A_55_P2116650	2.06361644	-
A_30_P01026385	2.08807447	-
A_55_P1954092	2.09814269	-
A_55_P1974114	2.19019148	-
A_30_P01033068	2.24219635	-
A_55_P1987406	2.26631644	-
A_30_P01028589	2.29215523	-
A_55_P2040775	2.30230593	-
A_30_P01032372	2.36480553	-
A_30_P01018122	2.37244203	-
A_55_P2183369	2.44019531	-
A_55_P2088720	2.48763755	-
A_55_P2077522	2.65908412	-
A_66_P119679	2.70969318	-
A_30_P01032404	2.73052776	-
A_30_P01024756	2.78631924	-
A_55_P1965079	2.84611994	-
A_51_P502906	2.86186974	-
A_30_P01021863	2.90423802	-
A_55_P2151672	2.93398431	-
A_66_P112995	2.93856459	-
A_55_P2187235	2.96650206	-
A_30_P01020013	2.99296827	-
A_30_P01024857	3.48931187	-
A_30_P01018083	3.49104967	-

A_55_P2173672	3.51789569	-
A_30_P01023602	3.61498302	-
A_30_P01021853	3.89029929	-
A_30_P01030381	3.94379696	-
A_30_P01024471	3.96199925	-
A_55_P2713325	4.04520172	-
A_66_P108887	4.127366	-
A_30_P01028216	4.16550978	-
A_30_P01019373	4.16624269	-
A_30_P01025695	4.20178204	-
A_30_P01028595	4.25387371	-
A_55_P2726807	4.27531512	-
A_30_P01033661	4.35454438	-
A_30_P01018274	4.49438419	-
A_30_P01022466	4.89468214	-
A_30_P01020171	5.01619957	-
A_30_P01018255	5.2256452	-
A_30_P01031955	5.97825331	-
A_52_P379474	6.00734849	-

Appendix 3- List of genes expressed in both *Braf*^{LSL-V600E/+}; *Villin-CreER*^{T0/WT} and *Gsk3α*^{S21A/S21A}; *Gsk3β*^{S9A/S9A}; *Braf*^{LSL-V600E/+}; *Villin-CreER*^{T0/WT} genotypes (Group 1).

A total of 334 genes whose expression was not affected by *Gsk3α/β* mutations. "+" indicates genes that are upregulated, whereas "-" indicates downregulated genes.

Agilent ID	Gene symbol	Fold Change- List1	Fold Change-List2	Regulation
A_51_P116687	1700010I14Rik	3.817598859	4.747866447	-
A_55_P2514383	1700016C15Rik	2.125888617	2.03747604	-
A_66_P115236	1810010D01Rik	2.704769147	2.629264062	-
A_51_P179565	2010204K13Rik	2.196786905	2.625891503	+
A_51_P295365	2610021A01Rik	3.955847926	3.472392779	-
A_51_P208152	3930402G23Rik	7.040682453	7.092338189	+
A_52_P119350	4732419C18Rik	2.39344862	2.555000581	+
A_66_P110966	4930402H24Rik	5.542534387	5.052795463	-
A_52_P110070	5730416F02Rik	4.281771369	3.898610738	+
A_55_P2137049	AA467197	2.803864955	2.161516951	+
A_51_P453043	Aacs	2.242838718	2.45550484	+
A_52_P665675	Abca1	4.547079645	5.28084675	-
A_51_P451574	Acot1	3.149268817	2.962036637	+
A_55_P2165324	Acsl3	3.948381053	3.08514453	+
A_51_P311038	Adamts15	2.127181492	2.656232413	+
A_52_P313217	Adgrd1	2.271629797	2.16347686	-
A_55_P2101776	Adora1	2.104670353	2.086910752	-
A_55_P2021505	Adra2a	3.015981215	2.870103012	-
A_51_P510891	Afp	16.7478883	13.01655062	-
A_55_P2089223	Ak4	2.417799306	3.012057251	+
A_51_P128987	Akr1b8	5.697061203	6.595042987	+
A_52_P346037	Akr1c12	2.32807327	2.41824582	+
A_51_P284177	Akr1c14	3.797484394	6.212026241	-
A_51_P334942	Aldh1a1	7.269746125	6.705518979	-
A_51_P383399	Aldh1a7	3.296777741	2.773283588	-
A_51_P220681	Aldoc	3.655468394	2.532088067	+
A_66_P133314	Aldoc	3.255642123	2.528688527	+
A_55_P2070992	Aldoc	3.192190262	2.188106213	+
A_51_P349888	Ang2	2.399897506	4.718275307	-
A_66_P134474	Ang3	4.007577464	9.106061323	-

A_52_P98778	Ang4	3.414496232	9.937558961	-
A_55_P2716491	Ang6	3.198153729	7.584071566	-
A_52_P520607	Ankrd22	5.886242429	4.881114579	+
A_52_P319438	Ankrd37	3.763820204	3.217732303	+
A_52_P662711	Anxa13	3.22448685	2.776034612	+
A_51_P296737	Anxa13	2.521461066	2.673935112	+
A_51_P451032	Anxa3	3.740390711	2.531860267	+
A_51_P451482	Anxa9	2.379477266	2.597224753	+
A_55_P2092869	Anxa9	2.248587133	2.362621627	+
A_51_P359315	Apobec2	3.051360653	3.466624848	+
A_66_P120380	Apol10b	5.232756723	5.32389073	-
A_51_P125205	Aqp1	2.727035398	3.384006147	-
A_55_P1990121	Aqp5	8.293881853	8.761372446	+
A_55_P2327577	Arhgef38	2.084846903	2.076889541	+
A_55_P2505115	Armc2	2.210813386	2.263981683	-
A_55_P2504175	Arrdc4	2.514511815	2.383054378	+
A_55_P2033725	Ascl2	2.709577722	2.811099002	-
A_51_P259975	Aspa	2.453232687	2.358365772	-
A_55_P2719684	Aspa	3.479223195	2.510889607	-
A_55_P2089804	Atf7	4.597874172	6.145067092	-
A_66_P118819	Atg9b	2.273870341	2.741880766	+
A_55_P2130024	AY761184	5.5874184	12.86176097	-
A_51_P215559	BC021614	2.235441193	2.586486099	+
A_66_P132970	BC049987	2.645081828	2.519492899	+
A_51_P497985	C2	2.830817712	2.123214217	-
A_52_P60194	C4bp	2.24955369	2.704334136	-
A_55_P2509454	C4bp-ps1	2.359710982	2.75601853	+
A_55_P1998631	Capg	2.611014676	3.407781845	+
A_55_P2747166	Capn2	3.523839987	2.549093254	+
A_52_P610923	Car9	3.995524725	3.622641253	+
A_55_P2092750	Car9	3.572469271	3.2953796	+
A_51_P481159	Cbr3	2.995205527	2.729136455	+
A_51_P460954	Ccl6	3.984020318	4.127113868	-
A_51_P185660	Ccl9	3.22589625	2.473079489	-
A_51_P385718	Cd177	2.071275575	2.053221996	+
A_55_P2185605	Cd48	3.063282174	3.186206344	-

A_51_P370008	Ceacam18	2.440633659	2.280059868	+
A_55_P2713446	Cenpq	2.197373816	2.106389678	-
A_55_P2850037	Ces1d	2.175546917	2.408647634	-
A_51_P369784	Ces1e	2.418346543	2.181137789	-
A_51_P358316	Chga	3.628741926	3.257538139	-
A_52_P385606	Ckb	2.687475996	2.049701781	+
A_51_P394715	Cklf	6.1889485	8.539557745	-
A_55_P2015878	Clps	6.905696623	9.842716062	-
A_55_P2610621	Col1a2	2.682598018	3.361031729	-
A_52_P320261	Cpa2	2.109005651	2.745970788	+
A_51_P264695	Crym	3.531736246	3.706161778	-
A_51_P157042	Ctgf	3.078324027	2.772902326	+
A_55_P2047639	Cubn	22.52264493	36.25655313	-
A_55_P2046563	Cym	4.37829316	3.644386995	-
A_52_P472486	Cyp2b10	6.763585935	15.56736475	-
A_55_P2044653	Cyp2b10	12.0417853	31.97723654	-
A_51_P467076	Cyp2b9	9.274504684	21.89423648	-
A_55_P2487509	Cyp2c55	5.58072591	6.254027318	-
A_51_P447785	Cyp2c55	13.70600562	18.4572753	-
A_55_P2058433	Cyp2c68	2.074364768	2.631859438	-
A_51_P355301	Cyp3a11	3.40019677	4.902257115	-
A_51_P482051	Cyp3a16	4.712241162	5.701079782	-
A_51_P489367	Cyp3a25	3.118678668	3.503589928	-
A_51_P341203	Cyp3a41a	5.196632054	6.226552729	-
A_55_P2162880	Cyp3a57	3.017661198	3.329227465	-
A_55_P2028046	Cyp3a59	3.451503803	4.202718895	-
A_52_P302345	Cyp4v3	2.833734082	4.178934937	-
A_55_P2792294	Cyp51	2.130030571	3.15939868	+
A_52_P256569	Dbnnd2	2.505678762	2.020075107	+
A_51_P110471	Ddah1	5.725129973	5.038996845	+
A_51_P307168	Ddah1	4.945017556	4.082785631	+
A_55_P2054373	Defa-ps1	5.148445469	11.67485889	-
A_55_P2076994	Defa-rs10	11.36365938	18.03062248	-
A_55_P2045213	Defa-rs12	10.42042548	11.0634862	-
A_55_P2004208	Defa-rs2	2.829585317	3.047987882	-
A_55_P2018863	Defa-rs7	7.517359792	15.17535517	-

A_55_P2018862	Defa-rs7	14.14604485	25.39646142	-
A_55_P1961407	Defa2	20.81487115	19.9819434	-
A_55_P1971928	Defa21	12.85415435	15.21380118	-
A_55_P1969960	Defa25	9.620546471	20.21261398	-
A_55_P1954799	Defa26	5.039017672	14.82352575	-
A_51_P312437	Dhrs7	2.060809117	2.017775743	+
A_55_P2046657	Dio1	2.492238127	2.684635796	-
A_55_P2592137	Dio1	2.746284963	4.281960066	-
A_52_P417368	Dpp4	2.017295633	2.304573185	-
A_55_P2806464	Dpysl5	2.154710532	2.035358402	-
A_52_P481279	Drc1	2.827241755	3.985239594	+
A_51_P347333	Dusp4	2.745397546	2.300272525	+
A_51_P161946	E130012A19Rik	6.651193684	4.309772471	+
A_52_P387009	Egln3	4.829034327	2.910371953	+
A_51_P330428	Eif4ebp1	2.040443975	2.368080319	+
A_55_P1977096	Elk4	2.016380494	2.251253589	-
A_55_P2797109	Eln	2.43383247	2.420449781	+
A_66_P103820	Enpep	2.833330329	3.578467614	-
A_55_P2094292	Erp27	8.503322918	11.11782816	-
A_55_P2016105	Errfi1	3.270231251	2.561433624	+
A_55_P1959521	Etv4	7.263294443	8.780739887	+
A_55_P2078780	Etv4	5.072462871	8.233225959	+
A_55_P2913071	Fam101b	2.456812143	2.720851042	+
A_51_P329949	Fam13a	2.503483747	2.522757551	+
A_51_P115159	Fam162a	2.485718123	3.018494796	+
A_51_P447976	Fam46c	2.011550073	2.042791116	-
A_55_P2061036	Fam83e	2.119567373	2.289765695	+
A_52_P410520	Farsa	5.413111601	5.141416686	-
A_55_P2740354	Fbln1	2.949474035	2.588139221	-
A_55_P2033250	Fdft1	3.128601679	2.338069547	+
A_66_P111208	Fdft1	2.141537711	2.017846627	+
A_55_P1966804	Fdps	3.005906053	2.874970604	+
A_55_P2021921	Fkbp1a	2.317415415	2.40382624	-
A_51_P383270	Fras1	2.224764732	2.148473313	-
A_51_P406253	Gcg	3.421113172	2.137635303	-
A_55_P2106175	Gch1	3.178696025	2.722127534	+

A_52_P313098	Gip	2.385663644	2.12996186	-
A_52_P463340	Gjd3	2.115725545	2.038315883	-
A_51_P169087	Gls2	3.509653148	3.702712	+
A_51_P376258	Glud1	2.163333727	2.007054438	-
A_55_P2054372	Gm15299	2.662122205	4.438733284	-
A_55_P1972868	Gm21498	6.661695841	14.52163068	-
A_66_P121715	Gm32894	2.309093758	2.030616992	+
A_55_P2150248	Gm4787	7.963948209	9.121777828	-
A_66_P121502	Gm5485	2.391453028	3.645249251	-
A_55_P2482301	Gm7861	3.599999477	8.433339079	-
A_52_P463271	Gmgs	3.663076447	2.299186757	+
A_55_P2157814	Gmgs	2.462386829	2.08351164	+
A_52_P597775	Gprc5a	5.193383339	4.513927594	+
A_55_P1961423	Gsta3	2.689431252	2.188346966	+
A_51_P112223	Gsta4	3.576074935	2.883293696	+
A_51_P454949	Gstm3	2.549961024	2.434476911	-
A_55_P2037343	H2-Q10	2.536500913	4.407517904	+
A_55_P2074035	Haa0	7.891539183	7.974933473	-
A_55_P2032272	Habp2	4.906171841	6.290439113	-
A_51_P196590	Hadh	2.020846813	2.023192508	-
A_66_P107191	Hif1a	3.413295913	2.954428068	+
A_55_P2032966	Hmgcs1	2.196088743	2.263746725	+
A_51_P503757	Iglv1	2.154531621	5.630848749	-
A_51_P290207	Insig1	3.056396527	2.793779384	+
A_55_P1983708	Insrr	2.318178109	2.188423803	-
A_52_P99531	Ippk	2.46044868	2.136588382	+
A_66_P119869	Itln1	4.17447703	7.703977956	-
A_55_P2035117	Itln1	6.348326143	11.34971842	-
A_55_P1975917	Itlnb	6.707107382	9.715114802	-
A_52_P570240	Kbtbd11	2.38332601	2.0819845	-
A_55_P2106926	Kcna3	5.623294629	4.254750352	-
A_51_P389636	Kcnn4	2.979666187	2.528585466	+
A_51_P218975	Kcns3	2.481502692	2.600890722	-
A_55_P2793729	Klf15	3.121692258	3.584910362	-
A_51_P287691	Kremen2	2.681945546	2.390322195	+
A_51_P287198	Krt23	2.850358212	2.400011482	+

A_55_P2140042	Krt31	2.267982584	2.008643663	-
A_52_P410685	Krt7	3.712268073	2.988653005	+
A_55_P1981366	Lamc2	3.148169956	2.451106666	+
A_55_P2018697	Ldhd	3.140345916	2.917089377	+
A_52_P413492	Ldlrap1	2.882065854	2.782737229	+
A_51_P249909	Lect2	2.969449649	2.89088529	-
A_51_P286946	Lhpp	3.260528969	2.791021001	-
A_51_P403564	Lhx5	2.583485021	3.725589737	+
A_65_P12904	Lmna	2.542844269	2.837107975	+
A_52_P137765	Lmna	2.37310457	2.677945873	+
A_51_P313566	Lmna	2.360693067	2.305872279	+
A_52_P103628	LOC102637129	2.907123085	2.502511963	+
A_51_P150835	LOC102641619	2.118937512	2.367127523	-
A_55_P2723934	LOC102642530	6.08099851	10.75281668	-
A_55_P2057189	LOC105242475	11.53104012	14.57036311	-
A_51_P200484	Lrp12	2.586313061	2.594796254	-
A_55_P2054967	Lrrc49	2.618684834	2.235853366	-
A_55_P2807240	Lss	2.6967456	2.27505449	+
A_51_P491635	Ly6g6e	4.640270345	4.929639013	+
A_55_P2181738	Lyz1	3.505582253	6.930203776	-
A_51_P321150	Lyz2	2.628956681	3.443517302	-
A_52_P238027	Lyz2	3.288616808	5.566065627	-
A_51_P243514	Macc1	2.883773631	3.406262727	+
A_51_P213030	Macrod1	2.495059337	2.139842785	-
A_66_P119238	Maoa	2.879851764	2.581107081	-
A_55_P1988664	Map3k14	4.610614877	4.568672369	-
A_51_P349495	Mboat1	18.11229721	13.85898705	+
A_51_P490817	Me2	2.076820485	2.285673279	-
A_66_P102500	Meis2	3.179156139	2.968004275	+
A_55_P2067707	Mep1a	7.929287396	11.21099189	-
A_51_P279437	Mfsd2a	2.037150553	2.810430885	+
A_55_P2068265	Mif	2.386717119	2.862589777	+
A_55_P1994947	Mif	2.310068674	2.775971663	+
A_51_P426096	Mmp7	3.454403966	4.156692271	-
A_66_P118835	Mmp7	4.603430019	6.627983973	-
A_55_P2814955	Mpp3	2.911722339	3.207020034	+

A_51_P497039	Mpp3	2.2559183	2.283278827	+
A_55_P2092633	Mptx1	9.52037061	8.430131578	-
A_66_P109060	Mptx2	12.72180682	19.07702419	-
A_51_P355943	Mvd	2.757450348	3.640364521	+
A_55_P2058861	Mvk	2.695575137	2.799299433	+
A_51_P169527	Mvk	2.334508714	2.317709207	+
A_51_P170536	Mycbpap	2.632399301	2.299908889	-
A_66_P121695	Naaladl1	3.85948137	4.749125532	-
A_51_P479230	Nat8	2.333100625	2.268033797	-
A_55_P2910874	Ncald	2.066346514	2.341757379	-
A_55_P2609901	Ncald	2.15472099	2.451283126	-
A_52_P650180	Nipal2	4.228453103	2.207386179	+
A_51_P232708	Npff	9.619099932	12.01028471	-
A_55_P2802986	Oat	5.434147442	5.92776081	-
A_55_P2094916	Ocm	2.427900962	2.522256286	-
A_55_P2073825	Ocm	3.573079689	2.532940374	-
A_66_P115118	Olfr1513	3.025396961	2.59063752	-
A_52_P215176	Opn3	3.687908135	3.082710162	+
A_55_P2019751	Paox	2.575442249	3.124698039	+
A_51_P180613	Paox	2.17170595	2.871579352	+
A_51_P397673	Pcsk9	5.1809386	4.454551486	+
A_55_P2131964	Pdia2	4.370022198	4.169647104	-
A_66_P132039	Pdx1	4.715272245	4.896157196	+
A_66_P127455	Pdzk1	3.047763779	3.692870762	-
A_55_P2011410	Pdzk1	6.274203379	3.875420719	-
A_51_P212491	Pfkfb3	2.482507162	2.343050812	-
A_51_P310896	Pfkl	2.628517586	3.667188431	+
A_55_P1963184	Pgap1	4.50288761	3.339380979	+
A_55_P2081488	Pglyrp1	2.505156408	3.399884544	+
A_51_P195958	Phlda1	3.748918829	2.827178269	+
A_52_P350786	Phlda2	4.024099052	3.793459757	+
A_52_P307938	Pik3r1	2.059231248	2.167000756	-
A_51_P337195	Pipox	4.191320602	3.807576371	-
A_55_P2797212	Pir	3.130639994	3.995185272	+
A_52_P654624	Pisd-ps3	2.012841184	2.016239656	-
A_55_P2499113	Pla2g5	2.400478295	2.580480991	+

A_55_P1997696	Plbd1	2.164863993	2.136043214	-
A_51_P375201	Plk3	2.613179721	2.56246809	+
A_51_P328817	Plk5	3.264451682	2.551174138	-
A_52_P121502	PlIp	2.671153915	2.502759007	+
A_55_P2042606	Pls1	3.340991819	2.94195949	-
A_55_P2088995	Plscr1	2.840518514	2.051581813	+
A_55_P2741134	Pou5f1	7.615856446	7.494338303	-
A_55_P2130555	Prdm11	2.061564982	2.589826725	+
A_55_P2744082	Prelid2	2.562625293	2.267389793	+
A_51_P225793	Prr5l	2.777174993	2.555492517	-
A_51_P477682	Prss12	2.696292822	2.35568299	-
A_51_P429335	Prss16	3.021661809	3.048200157	+
A_55_P2052290	Psat1	2.900987972	2.550194082	+
A_52_P605812	Pthr1	2.617764943	2.505874844	+
A_52_P366462	Pyy	3.277794777	3.302264896	+
A_52_P551476	Raph1	3.215211848	2.203329138	+
A_51_P348433	Rasal1	2.892503243	2.817119111	+
A_51_P329811	Reg1	14.72060296	13.15283033	-
A_51_P267969	Reg3a	15.15667426	14.707921	-
A_55_P2167486	Resp18	2.635498427	2.559781234	-
A_66_P126313	Rhof	2.061405663	2.149279571	+
A_55_P2071329	Rhog	2.474963708	2.064133526	-
A_51_P491987	Ripk3	3.132553265	2.607136305	+
A_52_P249798	Rnase1	2.457332919	3.539894608	-
A_55_P2935946	Rnf150	2.637054301	2.301701543	-
A_55_P2723769	Rnu1a1	2.437034179	2.289436256	-
A_55_P2065991	S100a11	3.30629814	2.417436501	+
A_51_P419226	S100a14	11.9693649	13.22165744	+
A_66_P114627	S100a16	2.785060949	3.480053656	+
A_55_P2148912	S100a16	2.655269692	2.46320632	+
A_51_P108812	S100a5	2.952473654	3.056288636	+
A_51_P281089	S100a6	6.102422136	4.849538992	+
A_51_P129464	Scd2	6.227840766	5.299395124	+
A_55_P2481829	Scmh1	2.08959377	2.4402029	+
A_55_P2030736	Scmh1	2.000028882	2.194674093	+
A_55_P2165414	Serpina1a	2.217734672	2.136513841	-

A_55_P2010301	Serpina1c	2.234012145	2.105657437	-
A_55_P2113857	Serpina1e	2.154759739	2.123352889	-
A_55_P2020203	Sfrp5	3.216057732	3.119074262	-
A_51_P454196	Sh2d4a	2.153112576	2.059710094	+
A_51_P313761	Shmt2	2.089879169	2.295959039	+
A_66_P132493	Siglece	5.692016595	6.688249996	-
A_55_P2022890	Slc12a8	2.19740297	2.015158858	+
A_51_P110759	Slc1a1	2.000219576	2.062334378	-
A_51_P408631	Slc20a1	2.230309338	2.164730234	+
A_51_P211616	Slc27a6	2.723295445	2.793733131	+
A_51_P464738	Slc2a1	3.468860065	3.100025776	+
A_51_P338563	Slc36a1	3.331088572	3.213400689	-
A_51_P253207	Slc51a	2.491216383	2.161246048	-
A_52_P229943	Slc51b	2.306604321	2.07083372	-
A_55_P2101088	Slc5a11	6.295863337	3.93505905	-
A_55_P1965030	Slc5a12	14.14083384	17.31582943	-
A_51_P228971	Slc5a4b	2.947158427	4.27025467	-
A_55_P2883452	Slc7a8	2.436264277	2.565643059	-
A_51_P496569	Slit2	6.551447791	5.52190657	+
A_51_P383140	Slk	2.713692244	2.179499987	+
A_51_P365516	Spink1	2.735011939	2.448728178	-
A_52_P204311	Spry4	2.485672603	2.15788599	+
A_51_P394814	Svep1	4.018884612	5.769449861	-
A_51_P216456	Tac1	2.427324951	2.335482278	+
A_55_P2183597	Tbc1d2	2.252708573	2.20479505	+
A_52_P300451	Tcf23	22.46098429	21.29409628	+
A_52_P949440	Tgfb1i1	2.064649981	2.131217996	-
A_52_P220879	Tgm2	2.440597492	2.386523529	-
A_51_P249989	Tifa	4.903790108	4.864088334	-
A_55_P2011385	Tifa	8.057263504	6.305887059	-
A_51_P371001	Tm4sf4	12.30919837	9.352515326	+
A_55_P1976953	Tmprss9	2.826920818	2.633506417	-
A_51_P131408	Tnfrsf12a	3.204582978	2.728626623	+
A_51_P399305	Tnfrsf19	2.098265216	2.042853476	-
A_55_P2071132	Tnfrsf23	2.068220072	2.630682649	+
A_55_P2010038	Tnfsf9	2.042795506	2.0420478	+

A_51_P333923	Tspan1	2.806785443	3.043284306	+
A_55_P2095019	Ubash3b	9.870001699	13.62069253	-
A_55_P2718015	Ube2f	2.248950619	2.436141769	-
A_55_P1953861	Vstm2l	2.044632905	2.724882603	+
A_52_P561650	Vwa1	3.580946493	3.47477618	-
A_55_P1985950	Xpnpep2	4.571343801	6.34177846	-
A_55_P2016623		3.347497736	3.584007886	+
A_55_P2185359		3.304593979	3.070324947	+
A_55_P2723989		3.298225822	3.032858005	+
A_55_P2017116		3.087465299	2.787446874	+
A_66_P105956		3.031069537	2.765851486	+
A_52_P226489		2.920649099	2.752529846	+
A_55_P2185628		2.784030843	2.65056224	+
A_55_P2088690		2.681012816	2.575126333	+
A_66_P137413		2.59430712	2.552341538	+
A_55_P2026761		2.574206026	2.511816038	+
A_55_P2021455		2.567689954	2.51117332	+
A_55_P2168267		2.54520467	2.494917959	+
A_52_P437084		2.526554604	2.485115941	+
A_55_P1968664		2.449183588	2.474699624	+
A_30_P01026945		2.395362478	2.467246254	+
A_30_P01024970		2.293007973	2.448785479	+
A_55_P2067947		2.261705827	2.299820483	+
A_30_P01029178		2.254595833	2.28214931	+
A_55_P2186929		2.191434744	2.227716742	+
A_30_P01025368		2.173058625	2.208602871	+
A_30_P01027445		2.145084653	2.184139545	+
A_55_P1975837		2.0532757	2.18326885	+
A_30_P01021243		2.034357786	2.18175135	+
A_30_P01029927		2.030812253	2.056626513	+
A_30_P01018414		2.018601419	2.001286501	+
A_55_P2116650		2.06361644	2.094070094	-
A_55_P1954092		2.09814269	2.150812526	-
A_55_P1987406		2.266316438	2.189639411	-
A_30_P01018122		2.372442025	2.339418191	-
A_30_P01024756		2.786319244	2.69747044	-

A_51_P502906	2.861869737	3.443232303	-
A_30_P01021863	2.904238022	3.630721406	-
A_55_P2187235	2.966502065	4.553554035	-
A_66_P108887	4.127366003	5.561688966	-
A_30_P01019373	4.16624269	7.934571365	-
A_52_P379474	6.007348494	8.608221878	-

Appendix 4- A list of genes expressed uniquely in the *Braf*^{LSL-V600E/WT}; *Villin-CreER*^{T0/WT} genotype (Group 2).

A total of 481 genes whose expression is altered by the induction of *V600E Braf*. Expression of these genes is reversed by *Gsk3α/β* mutations in the *Gsk3α*^{S21A/S21A}; *Gsk3β*^{S9A/S9A}; *Braf*^{LSL-V600E/WT}; *Villin-CreER*^{T0/WT} genotype. “+” indicates upregulated genes, whereas “-” indicates downregulated genes.

Agilent ID	Gene Symbol	Fold Change	Regulation
A_55_P2227217	1700123M08Rik	2.41161566	-
A_55_P1970436	2010107G12Rik	2.8679105	+
A_52_P614417	3000002C10Rik	2.11403608	+
A_51_P428316	4930539N22Rik	4.89056111	-
A_55_P2327853	4931431B13Rik	4.75682846	-
A_55_P2286493	4933405E24Rik	2.54912125	-
A_55_P2349148	5830408B19Rik	3.36358566	+
A_55_P1971264	6530403M18Rik	2.09943337	+
A_52_P499028	9130008F23Rik	2.09943337	+
A_55_P2508704	9430091E24Rik	4.85677954	-
A_55_P2470474	9530082P21Rik	2.05622765	+
A_55_P2238059	A730091E23Rik	2.15845647	-
A_52_P671534	Abhd8	2.31337637	-
A_51_P435068	Acadsb	2.96904714	+
A_66_P101407	Acat3	2.14354693	+
A_65_P09709	Acsl3	2.8679105	+
A_55_P2935081	Acss2	3.48220225	-
A_66_P118038	Ada	4.53153554	+
A_51_P430423	Ada	2.73208051	+
A_55_P2025760	Adam9	2.4966611	+
A_55_P2502426	Adh1	2.29739671	+
A_51_P238563	Agpat2	2.1885874	+
A_51_P346165	Agpat4	2.14354693	-
A_51_P323712	Agt	2.1885874	-
A_52_P162509	Ahcyl2	2.3456699	+
A_55_P2153620	Ahnak	2.9896985	-
A_55_P2510197	Airn	3.41053957	-
A_55_P2174743	Akap7	2.4966611	-
A_51_P331288	Akr1b7	2.25011697	-

A_55_P2007196	Aldoa	2.05622765	+
A_51_P423813	Alpi	3.55537072	+
A_51_P132685	Alppl2	3.81055199	+
A_51_P343350	Amn	2.39495741	-
A_51_P481679	Angptl3	2.71320865	+
A_66_P134542	Anln	2.4966611	+
A_55_P2733277	Anxa11	2.0139111	+
A_51_P165342	Anxa2	2.53151319	+
A_55_P2056325	Anxa3	3.22656704	+
A_52_P534355	Anxa7	3.58010028	-
A_55_P2117155	Apoc3	2.8679105	-
A_51_P310629	Apoc3	3.11665832	-
A_55_P2181752	Apol7a	2.05622765	-
A_51_P497724	Apol7a	2.14354693	-
A_52_P527106	Arhgap12	2.15845647	+
A_66_P103456	Arsb	2.31337637	-
A_65_P16786	Ascc2	2.15845647	+
A_55_P2715192	Atp13a4	3.13833639	-
A_55_P2002602	Atp5l	2.02791896	-
A_52_P565847	AU018091	4.65893435	-
A_55_P2509073	B430010I23Rik	2.05622765	+
A_55_P2084611	B4galt6	2.5668518	+
A_55_P2807306	Bambi	2.09943337	-
A_55_P2507986	Bambi-ps1	2.09943337	+
A_51_P121915	BC089597	2.23457428	-
A_51_P158018	Bend5	2.51402675	+
A_52_P340669	Bhlha15	2.05622765	-
A_51_P411926	Bmp8b	2.29739671	+
A_55_P2113633	Bzw1	2.05622765	+
A_51_P110301	C3	3.63007662	-
A_52_P458790	C530008M17Rik	2.23457428	-
A_55_P2021572	C87414	2.02791896	-
A_52_P188261	Camk2d	2.37841423	+
A_55_P2100585	Cass4	3.07375036	-
A_51_P484978	Cblc	2.36198532	+
A_51_P124719	Ccdc93	2.3456699	+

A_52_P18116	Ccl24	2.17346973	-
A_55_P2925449	Ccser1	2.58470566	-
A_55_P2125912	Cct6a	2.15845647	+
A_55_P2004511	Cd300lf	3.03143313	-
A_55_P2101585	Cd55	2.39495741	+
A_51_P388412	Cd55	2.26576777	+
A_66_P109404	Cd55	2.1885874	+
A_55_P2715366	Cd86	2.63901582	+
A_52_P141384	Cdcp1	3.78423059	-
A_51_P450033	Cdk1	2.11403608	+
A_52_P284658	Cdkn2aipnl	2.0139111	+
A_51_P444447	Cebpd	2.0139111	-
A_51_P219970	Cela1	2.12874036	+
A_51_P380587	Cep72	2.0139111	+
A_55_P2120354	Cib2	2.0139111	-
A_55_P2738062	Clasp2	2.02791896	-
A_52_P251450	Cldn2	4.19886673	+
A_66_P109468	Cldn24	4.43827789	-
A_55_P2183453	Cldn4	2.58470566	+
A_55_P2500178	Clic1	2.21913894	+
A_65_P01958	Clpb	2.02791896	+
A_55_P2747563	Cml2	2.17346973	-
A_66_P129600	Commd1	3.36358566	-
A_51_P140731	Cops5	2.02791896	+
A_51_P427674	Cpt1a	2.88785839	+
A_55_P2935306	Cttnbp2nl	2.69446715	-
A_51_P374198	Cxcl16	2.44528056	+
A_51_P485791	Cyp51	2.4794154	+
A_55_P1988113	Cyth2	2.04202425	-
A_55_P1954820	D1Ert622e	2.14354693	+
A_66_P106385	Daf2	2.25011697	+
A_52_P452747	Dao	2.21913894	-
A_55_P2108933	Dao	4.25748073	-
A_51_P326229	Ddx25	4	-
A_51_P491470	Ddx47	2.20381023	+
A_51_P319093	Dgka	2.11403608	+

A_51_P368394	Dnajb8	2.02791896	+
A_55_P2501636	Dnm3	2.96904714	+
A_51_P329818	Dpep3	2.84810039	+
A_51_P120448	Echdc1	2.44528056	+
A_55_P1956418	Efr3b	2	-
A_55_P1989921	Eml2	2	+
A_55_P2087561	Eno1b	2.20381023	+
A_51_P332917	Enpp3	2.58470566	+
A_52_P379277	Enpp3	2.28152743	+
A_52_P630563	Ept1	2.14354693	+
A_51_P204486	Exoc3l4	2.1885874	-
A_51_P174961	F10	3.27160823	-
A_55_P1971889	F3	2.5668518	+
A_65_P20641	Fads2	2.46228883	+
A_51_P431734	Fam185a	2.1885874	+
A_52_P416727	Fam210a	2.0139111	+
A_55_P2430221	Fam35a	2.0139111	-
A_65_P00912	Fam46c	2.32946717	-
A_55_P2626499	Farsb	2.12874036	+
A_52_P588483	Fbln1	2.58470566	-
A_51_P474701	Fbp1	2.67585511	-
A_55_P1965194	Fbxl5	2.25011697	+
A_66_P138027	Fgd6	2.04202425	+
A_51_P399845	Fgf2	3.45814893	-
A_52_P222350	Flnb	2.11403608	+
A_55_P2144556	Flrt3	2.26576777	+
A_66_P122700	Fpgs	2.23457428	+
A_52_P367294	Fsd1l	2.08493152	+
A_55_P2483347	Fut1	2.65737163	-
A_66_P129538	Gale	2.12874036	+
A_55_P1994258	Gapdh	3.01049349	+
A_55_P1965725	Gapdh	2.69446715	+
A_55_P1984284	Gapdh	2.12874036	+
A_55_P1989813	Gcm1	2.4966611	-
A_52_P53144	Gcnt3	2.4966611	+
A_65_P11011	Gcnt3	2.21913894	+

A_55_P2727267	Ggps1	2.9896985	-
A_51_P267700	Gkn3	3.86374532	+
A_55_P2487095	Glyctk	2.07052985	-
A_65_P20683	Gm1070	2.31337637	-
A_66_P130315	Gm11210	2.62078681	-
A_55_P2200054	Gm11266	3.6807506	-
A_55_P2051039	Gm11937	2.02791896	-
A_55_P2737234	Gm11974	3.70635225	-
A_55_P2059323	Gm13315	2.1885874	+
A_55_P2098971	Gm14085	5.24157362	+
A_66_P118249	Gm14137	2.0139111	+
A_55_P2736480	Gm15658	2.53151319	-
A_66_P103164	Gm15764	2.09943337	-
A_66_P114103	Gm19434	3.16016525	-
A_55_P2829137	Gm20684	2.0139111	+
A_65_P07827	Gm2701	3.78423059	-
A_51_P187579	Gm31711	2	+
A_55_P2930354	Gm33586	2.82842712	-
A_55_P2549189	Gm35622	2.63901582	+
A_55_P2730996	Gm38413	2.41161566	-
A_66_P127146	Gm38419	2.15845647	+
A_55_P1992571	Gm41468	2.09943337	-
A_66_P121785	Gm41781	2.67585511	-
A_55_P2749956	Gm4841	2.26576777	-
A_55_P1967533	Gm5069	2.71320865	+
A_55_P2722684	Gm5592	4.28709385	-
A_55_P2322120	Gm5617	4.0840485	+
A_55_P2004721	Gm766	5.77571678	+
A_55_P2108690	Gm8709	2.23457428	+
A_51_P171200	Golm1	2.07052985	+
A_55_P2744563	Gpi1	2.3456699	+
A_52_P141488	Grk5	2.08493152	+
A_52_P46419	Grk6	2.0139111	+
A_55_P2062190	Gstm1	2.21913894	-
A_55_P2094060	Gzma	2.17346973	-
A_55_P1962747	H2-Ab1	2.36198532	-

A_52_P683598	H2-Ab1	2.42838977	-
A_55_P2146560	H2-Ab1	2.63901582	-
A_51_P278868	H2-DMb1	2.39495741	-
A_55_P1984886	Hcst	2	-
A_55_P2106429	Herc2	2.69446715	-
A_55_P2748958	Hhat	2.07052985	-
A_55_P2027999	Hk1	2.37841423	+
A_55_P2109033	Hmgcs2	2.08493152	-
A_55_P2912004	Hmgcs2	2.44528056	-
A_52_P535623	Hook1	2.05622765	+
A_55_P1997936	Hsd17b7	2	+
A_52_P515036	Htati2	2.8679105	+
A_51_P228883	Htati2	2.04202425	+
A_52_P562054	Ick	2.12874036	+
A_51_P467668	Ick	2.08493152	+
A_51_P132978	Idh1	2.12874036	+
A_52_P257502	Igfbp4	2.11403608	-
A_55_P2376423	Igkv4-72	2.65737163	-
A_55_P2825279	Il22ra1	2.37841423	-
A_51_P152550	Iqcg	2.31337637	-
A_52_P518922	Itga1	5.38893431	-
A_51_P269663	Itpr1	2.15845647	-
A_51_P191262	Jsrp1	4.05583792	+
A_52_P642488	Kcnk1	2.1885874	+
A_55_P2745114	Kcnq1	5.06302638	-
A_51_P331805	Kctd15	2.46228883	-
A_55_P2044389	Kif6	3.13833639	-
A_55_P2022074	Klf10	2.4794154	+
A_55_P2004551	Klra1	3.81055199	-
A_55_P2170350	Klra22	3.58010028	-
A_51_P167489	Lama3	2.09943337	+
A_51_P223656	Lamb3	2.62078681	+
A_55_P1967196	Lamb3	2.41161566	+
A_51_P117881	Leap2	3.07375036	-
A_55_P2529154	Lhcgr	2.04202425	-
A_66_P134488	Lif	3.6807506	-

A_51_P334118	Lin7c	2.36198532	+
A_55_P2552889	LOC102643017	2.07052985	-
A_55_P2727165	LOC105243184	3.55537072	+
A_55_P2930128	Lrrc16b	3.13833639	-
A_52_P365342	Lrrn2	3.24900959	-
A_55_P2924612	Lsamp	3.53081199	-
A_51_P296487	Lss	2.4794154	+
A_55_P2015292	Ltc4s	2.77021894	-
A_66_P118567	Lypd6b	4.16986304	-
A_55_P2105843	Mbd1	2.12874036	-
A_55_P2016842	Me1	3.6553258	+
A_55_P2009952	Me1	3.27160823	+
A_51_P376313	Med8	2.04202425	+
A_51_P455997	Meg3	2.08493152	-
A_55_P2736010	Meg3	2.15845647	-
A_55_P2928183	Mgam	2.32946717	-
A_55_P2118916	Mgat4c	2.44528056	+
A_55_P2727629	Mgea5	2.0139111	-
A_55_P2041723	Mid1ip1	2.14354693	+
A_55_P2044282	Mpp6	2.0139111	+
A_51_P289249	Mpzi3	2.04202425	+
A_55_P2180854	Mrgprg	4.46914855	-
A_55_P2077158	Mro	2.17346973	-
A_55_P2739272	Ms4a8a	2.80888975	+
A_66_P104901	Msmo1	2.67585511	+
A_51_P282179	Mtor	2.05622765	+
A_55_P2025687	Muc4	2.58470566	+
A_52_P108346	Myc	2.02791896	+
A_51_P288746	Myo18b	3.94493082	-
A_55_P2130855	Nap111	2.09943337	+
A_52_P443427	Ncoa4	2.37841423	+
A_51_P191649	Ndc80	2.23457428	-
A_66_P108184	Ndfip2	2.02791896	+
A_65_P09473	Neat1	2	+
A_55_P2628192	Nebi	4.50023394	-
A_52_P140005	Nipal1	2.11403608	+

A_55_P2074281	Nr2f1	2.54912125	-
A_55_P2115330	Nrg4	2	-
A_55_P2185900	Nrg4	2.11403608	-
A_52_P297803	Nsdhl	2.4966611	+
A_51_P425696	Nt5c2	2.51402675	+
A_52_P77837	Nt5c3	2.28152743	+
A_55_P2641968	Nt5c3	2.08493152	+
A_52_P574668	Nt5e	3.55537072	+
A_55_P2716786	Nudt5	2.96904714	-
A_55_P2915840	Oit1	2.65737163	+
A_66_P110850	Olfr1385	4.34693945	+
A_66_P116004	Olfr699	3.89061979	-
A_51_P316199	Olfr73	2.21913894	+
A_51_P368894	Onecut1	2.39495741	+
A_55_P2208579	Onecut2	2.08493152	+
A_52_P547795	Opa1	2.12874036	+
A_55_P2718563	Opcml	3.13833639	-
A_66_P108770	Oxct1	2.28152743	+
A_51_P107326	Oxct1	2.15845647	+
A_55_P2039556	Pak6	3.24900959	-
A_66_P102877	Pald1	2.60268371	-
A_52_P37123	Pard6b	2.44528056	+
A_55_P2745124	Park2	3.55537072	-
A_51_P298843	Pcbd2	2.4966611	-
A_55_P2722458	Pcdh15	4.89056111	-
A_52_P452787	Pdcd6ip	2.0139111	+
A_51_P406429	Pdk1	2.3456699	+
A_55_P2118076	Pdzd7	2.80888975	+
A_51_P303397	Pepd	2.08493152	-
A_51_P427530	Pgm1	3.86374532	+
A_65_P09318	Pik3ca	2.02791896	-
A_66_P139646	Pla2g4c	8.81524093	+
A_52_P17207	Pla2g4c	3.50642289	+
A_55_P2121980	Plcb4	2.29739671	-
A_51_P278163	Plcd3	4.46914855	-
A_52_P488437	Plek2	3.53081199	+

A_52_P418644	Plp2	3.78423059	+
A_52_P4598	Pmm1	2.17346973	+
A_55_P1999962	Podn	2.58470566	-
A_55_P2077098	Pof1b	3.27160823	+
A_55_P2727524	Pole2	4.9933222	-
A_55_P2824501	Pou4f1	2.3456699	-
A_51_P106799	Pparg	2.42838977	+
A_51_P224564	Ppm1f	2.53151319	-
A_51_P332652	Pqlc3	2.21913894	+
A_66_P109368	Prex2	4.78991482	-
A_51_P215438	Prodh	2.5668518	-
A_52_P570266	Psemb10	2.0139111	-
A_51_P345367	Psemb8	2	-
A_51_P207988	Ptger4	2.67585511	+
A_52_P571290	Ptms	2.54912125	-
A_66_P110662	Ptn	4.37717481	-
A_66_P119926	Pus7	2.65737163	-
A_51_P209280	Rab31	2.42838977	+
A_55_P1956687	Rab37	2.0139111	-
A_55_P2161923	Rabgap1	3.55537072	-
A_52_P430628	Rabggtb	2.63901582	+
A_51_P115817	Ralgps2	2.07052985	+
A_55_P2035315	Rasgef1b	3.18214594	+
A_52_P574759	Rbpjl	2.32946717	-
A_55_P2898235	Rdh9	2.51402675	-
A_51_P169671	Reg3b	8.45614432	-
A_51_P354126	Reg3g	5.85634278	-
A_52_P343326	Rgp1	2.54912125	+
A_55_P2905246	Rgs12	2.0139111	-
A_66_P107583	Rhox3a	4.34693945	-
A_55_P2000399	Rhox4a	5.0280535	-
A_55_P1975667	Rhox4g	4.62675274	-
A_51_P517672	Rnf152	2.23457428	+
A_51_P148494	Rnft1	2.08493152	+
A_55_P2723745	Rnu1b1	2.05622765	-
A_55_P1987290	Rnu1b6	2.02791896	-

A_51_P166886	Saa2	2.8679105	-
A_52_P198898	Samd5	2.54912125	+
A_51_P212741	Scn2b	2.25011697	-
A_52_P409711	Sec24a	2.0139111	+
A_51_P187602	Serpinb5	4	+
A_66_P138465	Setd1a	3.89061979	+
A_52_P220190	Sf3b1	2.04202425	-
A_55_P2505205	Slc13a1	2.80888975	+
A_55_P2143923	Slc13a2	3.73213197	-
A_55_P2822857	Slc16a12	2.41161566	+
A_55_P2107987	Slc22a13b-ps	3.03143313	-
A_55_P2185362	Slc25a18	2.1885874	-
A_52_P883557	Slc30a10	2.25011697	+
A_51_P279997	Slc4a7	2.67585511	+
A_66_P139208	Slc6a8	2.32946717	+
A_51_P112734	Slc7a8	2.63901582	-
A_55_P2941602	Slco2a1	4.92457765	-
A_51_P423578	Slfn2	2.02791896	-
A_52_P472324	Slpi	3.18214594	-
A_51_P164270	Snrpa1	2.20381023	+
A_55_P2647378	Spag9	4.72397065	-
A_51_P325552	Spert	2.36198532	-
A_55_P2048853	Sprr2a2	3.24900959	+
A_51_P459894	Sprr2b	3.18214594	+
A_51_P491758	Sprr2j-ps	4.05583792	+
A_51_P209261	Sqrdl	2.12874036	+
A_51_P489313	Sri	2.12874036	+
A_55_P2738763	Ssfa2	2.54912125	+
A_55_P2603685	St3gal6	2.5668518	+
A_55_P2740019	St3gal6	2.20381023	+
A_55_P2603690	St3gal6	2.1885874	+
A_55_P2118609	St6galnac1	2.84810039	-
A_51_P236267	St8sia4	2.04202425	-
A_51_P471177	Stra6	2.32946717	-
A_66_P118256	Strn3	2.08493152	+
A_55_P2741163	Swi5	2.08493152	+

A_55_P2370250	Syn3	4.53153554	-
A_55_P2017645	Tap2	2.02791896	-
A_55_P2089565	Tbx22	2.9896985	-
A_52_P161297	Tcea3	2.3456699	-
A_51_P164030	Tcp1	2.4966611	+
A_55_P1968028	Tdgf1	3.50642289	-
A_55_P1994418	Teddm3	4.6913398	+
A_55_P2153990	Tlhc2	2.05622765	+
A_52_P330694	Tle1	2.15845647	+
A_66_P126582	Tmem181a	2	+
A_51_P495485	Tmem55a	3.18214594	-
A_52_P451073	Tnfrsf21	2.20381023	+
A_55_P2018017	Tnfsf10	2.51402675	-
A_55_P2742131	Tom111	2.44528056	+
A_52_P657286	Trim39	2.94853843	-
A_55_P2732428	Trp53rkb	2.32946717	-
A_55_P2043782	Trpm1	2.08493152	-
A_52_P605387	Tsg101	2.08493152	+
A_55_P2724059	Tsga10	2.94853843	+
A_55_P2011061	Tspan12	2.05622765	+
A_55_P2724669	Tspan8	2.09943337	+
A_65_P19832	Ttr	3.24900959	+
A_51_P490023	Tubb2a	2.65737163	+
A_55_P2175245	Tusc3	2.3456699	+
A_55_P2163729	Tvp23a	2.12874036	-
A_52_P463365	Twf1	2.12874036	+
A_55_P1980543	Ube2i	2.39495741	+
A_51_P297105	Ucp2	2.69446715	+
A_52_P90265	Ucp2	2.29739671	+
A_66_P108247	Ucp3	2.15845647	+
A_66_P106021	Usf2	2.36198532	-
A_55_P2491668	Usp2	2.58470566	-
A_65_P19862	Vdr	2.04202425	+
A_55_P2741794	Vegfa	3.13833639	-
A_52_P96552	Vkorc111	2.53151319	+
A_55_P2072150	Vpreb2	4.9588308	-

A_51_P220934	Vstm5	2.15845647	+
A_55_P2844759	Wdr92	2.14354693	-
A_55_P2298029	Whsc111	3.50642289	-
A_66_P139703	Wnt4	2.29739671	-
A_51_P373609	Yars2	2.1885874	+
A_55_P2763719	Zbed4	4.82323131	-
A_55_P2496052	Zfp934	3.34035168	-
A_55_P2054703		5.35171022	+
A_66_P101652		3.91768119	+
A_55_P2021908		3.89061979	+
A_55_P2081137		3.11665832	+
A_55_P2092046		3.09512999	+
A_30_P01019037		3.07375036	+
A_30_P01017441		2.96904714	+
A_55_P2005719		2.96904714	+
A_52_P532370		2.84810039	+
A_55_P2182077		2.84810039	+
A_52_P221024		2.82842712	+
A_66_P106968		2.82842712	+
A_55_P2133680		2.77021894	+
A_55_P2112797		2.71320865	+
A_66_P139927		2.71320865	+
A_30_P01024971		2.65737163	+
A_66_P140076		2.63901582	+
A_66_P117863		2.62078681	+
A_66_P128490		2.62078681	+
A_66_P100016		2.58470566	+
A_55_P1971093		2.5668518	+
A_52_P53507		2.54912125	+
A_55_P2155593		2.53151319	+
A_52_P229210		2.4966611	+
A_52_P272054		2.4794154	+
A_65_P07032		2.4794154	+
A_52_P654437		2.46228883	+
A_66_P136793		2.46228883	+
A_66_P136364		2.44528056	+

A_55_P2001072	2.41161566	+
A_52_P644984	2.39495741	+
A_55_P2156504	2.39495741	+
A_30_P01019015	2.37841423	+
A_55_P1961414	2.37841423	+
A_66_P116378	2.36198532	+
A_66_P116430	2.36198532	+
A_66_P102046	2.3456699	+
A_52_P89683	2.31337637	+
A_55_P2135023	2.31337637	+
A_55_P2167005	2.31337637	+
A_55_P1984070	2.29739671	+
A_52_P395508	2.28152743	+
A_55_P2112701	2.28152743	+
A_66_P107454	2.28152743	+
A_66_P127084	2.28152743	+
A_55_P2108689	2.26576777	+
A_66_P134733	2.26576777	+
A_30_P01031905	2.25011697	+
A_52_P61549	2.25011697	+
A_55_P2060854	2.25011697	+
A_55_P2060938	2.25011697	+
A_66_P126101	2.25011697	+
A_30_P01026822	2.23457428	+
A_52_P92404	2.23457428	+
A_66_P105518	2.23457428	+
A_55_P2139587	2.21913894	+
A_65_P01046	2.21913894	+
A_55_P1975087	2.20381023	+
A_55_P2133679	2.20381023	+
A_65_P08042	2.20381023	+
A_66_P118307	2.20381023	+
A_30_P01020518	2.1885874	+
A_55_P2037424	2.1885874	+
A_55_P2160204	2.1885874	+
A_66_P104393	2.1885874	+

A_55_P2054128	2.15845647	+
A_55_P2067153	2.15845647	+
A_55_P2091247	2.15845647	+
A_55_P2144003	2.15845647	+
A_52_P430427	2.14354693	+
A_55_P1972892	2.14354693	+
A_55_P1992470	2.14354693	+
A_55_P2037689	2.14354693	+
A_55_P1979694	2.12874036	+
A_55_P2013273	2.12874036	+
A_66_P122949	2.12874036	+
A_55_P2069995	2.11403608	+
A_55_P2020080	2.08493152	+
A_30_P01026145	2.05622765	+
A_30_P01032460	2.05622765	+
A_30_P01024929	2.04202425	+
A_55_P2136334	2.04202425	+
A_55_P2021094	2.02791896	+
A_66_P102988	2.0139111	+
A_30_P01020196	2	+
A_51_P152725	2	+
A_30_P01029853	2.04202425	-
A_51_P124315	2.05622765	-
A_30_P01026385	2.08493152	-
A_55_P1974114	2.1885874	-
A_30_P01033068	2.23457428	-
A_30_P01028589	2.28152743	-
A_55_P2040775	2.29739671	-
A_30_P01032372	2.36198532	-
A_55_P2183369	2.42838977	-
A_55_P2088720	2.4794154	-
A_55_P2077522	2.65737163	-
A_66_P119679	2.69446715	-
A_30_P01032404	2.71320865	-
A_55_P1965079	2.82842712	-
A_55_P2151672	2.92817139	-

A_66_P112995	2.92817139	-
A_30_P01020013	2.9896985	-
A_30_P01018083	3.48220225	-
A_30_P01024857	3.48220225	-
A_55_P2173672	3.50642289	-
A_30_P01023602	3.60500185	-
A_30_P01021853	3.86374532	-
A_30_P01030381	3.91768119	-
A_30_P01024471	3.94493082	-
A_55_P2713325	4.0278222	-
A_30_P01028216	4.1410597	-
A_30_P01025695	4.19886673	-
A_30_P01028595	4.22807216	-
A_55_P2726807	4.25748073	-
A_30_P01033661	4.34693945	-
A_30_P01018274	4.46914855	-
A_30_P01022466	4.89056111	-
A_30_P01020171	4.9933222	-
A_30_P01018255	5.20536742	-
A_30_P01031955	5.93809428	-

Appendix 5- List of unique genes expressed in the *Gsk3 α ^{S21A/S21A}*, *Gsk3 β ^{S9A/S9A}*, *Braf^{LSL-V600E/WT}*; *Villin-CreER^{T0/WT}* genotype (Group 3).

A total of 233 genes whose expression is induced as a result of combined V600E Braf induction with the *Gsk3 α/β* mutations.

“+” indicates upregulated genes, whereas “-“ indicates downregulated genes.

Agilent ID	Gene Symbol	Fold Change	Regulation
A_51_P240723	1700022A21Rik	2.234574276	-
A_51_P517608	2010106E10Rik	2.329467173	-
A_52_P155805	2010204K13Rik	2.099433367	+
A_55_P2188374	4930405D01Rik	2.188587403	-
A_55_P2569219	4930459I23Rik	2.713208655	+
A_55_P2230506	4931402H11Rik	2.602683711	-
A_66_P133594	5730416F02Rik	2.694467154	+
A_55_P2728708	5830416P10Rik	2.099433367	+
A_55_P2173576	6330562C20Rik	2.188587403	+
A_66_P107008	8430430B14Rik	2.084931522	+
A_55_P2412319	A830052D11Rik	2.250116969	+
A_51_P116421	Abcc5	2.02791896	+
A_55_P1975140	Acvr1c	2.056227653	-
A_51_P101588	Adamtsl5	2.313376368	+
A_51_P229911	Adcy4	2.281527432	+
A_51_P510418	Aldh1b1	2.02791896	-
A_52_P255304	Amer3	2.848100391	-
A_51_P391159	Ang	3.944930818	-
A_55_P2106489	Ankrd52	2.158456473	+
A_55_P2327027	Ano6	2.281527432	-
A_51_P171999	Apoe	2.808889751	-
A_55_P2736230	Apoe	4.469148552	-
A_52_P239086	Apol10a	7.210003701	-
A_66_P120481	Aqr	2.250116969	-
A_55_P2879860	Arid4b	2.313376368	+
A_52_P56792	Asah2	2.158456473	-
A_52_P436643	Asah2	3.363585661	-
A_55_P2060111	ATP8	2.620786808	-
A_51_P150912	Aurka	2.549121255	+
A_55_P2120254	Avpi1	2.394957409	+

A_55_P2743602	B3glct	2.361985323	+
A_52_P639223	Bche	2.203810232	-
A_52_P64687	Camk2n1	2.265767771	-
A_55_P2087182	Car4	4.34693945	-
A_55_P2809279	Cblb	2.584705661	-
A_51_P392577	Ccbl2	2.02791896	-
A_51_P471362	Ccdc64b	2.056227653	+
A_52_P322141	Ccdc88b	2.219138944	+
A_55_P2009069	Ccrn4l	2.084931522	+
A_55_P1973501	Ceacam16	2.158456473	+
A_51_P228604	Ceacam20	2.732080514	-
A_55_P1972948	Celf5	2.203810232	+
A_51_P443339	Ces2a	2.128740365	-
A_51_P196973	Chaf1a	2.084931522	+
A_55_P2134804	Cinp	2.02791896	+
A_55_P1976224	Ckb	2.250116969	+
A_52_P360112	Clip2	2.099433367	+
A_52_P282058	Col8a1	2.084931522	+
A_51_P494675	Cotl1	2.056227653	+
A_51_P387913	Cox17	2.37841423	-
A_55_P2025038	Cpe	2.234574276	-
A_52_P200121	Cyp2c40	3.160165247	-
A_52_P652059	Cyp2c65	2.428389769	-
A_51_P471126	Cyp2c66	2.602683711	-
A_55_P2728683	Cyp2c69	2.0139111	-
A_52_P204331	D630039A03Rik	2.02791896	-
A_52_P401614	D930048N14Rik	2.042024251	+
A_55_P1959763	Dach1	2.02791896	-
A_55_P2739806	Dcaf10	2.042024251	+
A_55_P1979007	Defa-rs1	5.578974665	-
A_55_P1999108	Defa1	2.0139111	-
A_55_P2068510	Defa1	2.219138944	-
A_55_P1999110	Defa1	2.828427125	-
A_55_P1961408	Defa2	4.377174805	-
A_55_P2104071	Defa23	2.345669898	-
A_52_P476535	Defa23	4.316912946	-

A_55_P2760536	Defa24	2.128740365	-
A_55_P2064913	Defa3	2.808889751	-
A_55_P1961410	Defa3	2.887858391	-
A_66_P107389	Dnah2os	2.732080514	+
A_51_P467110	Dpp4	2.281527432	-
A_52_P362403	Dppa5a	2.37841423	+
A_55_P2122648	Dtymk	2.531513188	+
A_51_P259029	Dusp26	2.173469725	-
A_51_P502614	Dusp6	2.099433367	+
A_51_P114314	Dusp8	2.0139111	+
A_66_P129722	Eci3	2	-
A_55_P2031167	Efna1	2.173469725	+
A_66_P118883	Eif2b5	2.042024251	+
A_55_P2745154	Elk1	2.203810232	+
A_55_P1999653	Enpp7	2.969047141	-
A_55_P2074694	Ephx4	2.496661098	+
A_52_P257625	Esm1	2	+
A_55_P2037454	Etv5	2.219138944	+
A_55_P2033795	Fabp6	2.070529848	+
A_51_P364609	Fads2	2.203810232	+
A_51_P464029	Fads3	2.29739671	+
A_55_P2160910	Faim2	2.584705661	+
A_51_P425824	Fam132a	2.158456473	-
A_55_P2824234	Fam64a	2.265767771	+
A_51_P434758	Fam83e	2.313376368	+
A_55_P2054350	Fbxo44	2.128740365	+
A_51_P130727	Fkbp11	2.584705661	+
A_52_P508991	Fmo1	2	-
A_52_P589568	Foxo6	2.084931522	-
A_51_P440365	Frrs1	2.056227653	+
A_55_P1994275	Gar1	2.234574276	+
A_55_P2500473	Ghr	2.070529848	-
A_55_P2106058	Gm11110	2.056227653	+
A_52_P175679	Gm13023	2.0139111	-
A_55_P1979009	Gm14851	6.190259974	-
A_55_P1954798	Gm15292	3.410539567	-

A_66_P112862	Gm17821	2.188587403	-
A_55_P1995018	Gm21498	4.563054863	-
A_55_P2735930	Gm32880	2.234574276	-
A_55_P1973995	Gm6756	2.928171392	+
A_55_P2484544	Gm7030	2.203810232	-
A_55_P1990205	Gm7849	4.856779538	-
A_52_P94150	Gm8096	2.969047141	+
A_55_P1956160	Gm8909	2.042024251	-
A_66_P101764	Gm9924	2.969047141	-
A_52_P535484	Gvin1	2.203810232	-
A_55_P1978502	H2-Q1	2.345669898	-
A_51_P230269	H2-Q10	2.37841423	+
A_66_P135522	Habp2	2.056227653	-
A_55_P2066230	Hck	2.042024251	-
A_66_P114788	Hoxaas3	2.514026749	+
A_55_P2731026	Ift27	3.758090997	-
A_55_P2008181	Il3ra	2.099433367	+
A_55_P2085295	Inf2	2.188587403	+
A_55_P2803946	Itpril2	2.042024251	-
A_55_P2802751	Kcnn4	2.099433367	+
A_55_P2133027	Kirrel3	2.394957409	+
A_52_P427024	Ldlr	2.234574276	+
A_65_P02173	Ldlr	2.070529848	+
A_66_P131177	LOC102635801	2.158456473	+
A_66_P130576	LOC73899	2.584705661	+
A_55_P2428968	Lrrc2	3.944930818	-
A_55_P2735115	Mettl1	2.070529848	+
A_52_P685999	Mettl7b	2.313376368	-
A_55_P2035872	Mical3	2.143546925	+
A_51_P157976	Mmab	2.313376368	+
A_66_P113268	Mme	2.158456473	-
A_52_P601230	Mro	2.070529848	-
A_51_P286146	Mylk	2.188587403	-
A_55_P2917437	Nceh1	2.070529848	-
A_55_P2039110	ND2	3.073750363	-
A_55_P2132147	ND3	2.281527432	-

A_51_P245525	ND4	2.713208655	-
A_55_P2091350	ND4L	2.770218936	-
A_55_P2050192	ND5	2.732080514	-
A_66_P135870	Nlrp9b	2	-
A_66_P134854	Nlrp9b	2.639015822	-
A_51_P189916	Nol12	2.070529848	+
A_51_P262645	Npc111	2	-
A_55_P2798306	Npl	2.114036081	-
A_51_P265338	Nr0b2	2.042024251	+
A_51_P485756	Nts	5.028053498	-
A_66_P114891	Olfr145	2.531513188	+
A_52_P19606	Osbpl1a	2.070529848	-
A_55_P2087923	Otud3	2.234574276	+
A_55_P2903017	Pdgfc	2.056227653	-
A_55_P2934717	Pfkl	2.173469725	+
A_51_P408732	Phgdh	2.789487333	+
A_55_P2603914	Pi4ka	2.158456473	+
A_51_P256632	Pla2g2a	9.126109727	-
A_51_P451588	Plekhb1	2.203810232	-
A_55_P2119817	Plekhj1	2.056227653	+
A_51_P492410	Pmvk	2.173469725	+
A_55_P2101367	Ppfia3	2.099433367	+
A_51_P514139	Prdm16	2.4794154	+
A_52_P466615	Prkg2	2.37841423	-
A_51_P474169	Proser2	2.566851795	+
A_55_P2889980	Ptpn5	5.775716782	-
A_55_P1955891	Rad51c	2.128740365	-
A_55_P2036942	Rangrf	2.02791896	+
A_52_P257758	Reg4	2.445280555	-
A_66_P129668	Rell1	2.128740365	-
A_51_P319070	Retsat	2.188587403	-
A_55_P2078370	Rgs13	2.411615655	-
A_55_P2028259	Rhbdf2	2.056227653	+
A_66_P133326	Rhd	2.219138944	+
A_51_P338317	Rhoq	2.345669898	-
A_51_P277275	Rit2	2.789487333	+

A_55_P2736734	Rn28s1	15.24220797	-
A_55_P2723748	Rn7sk	2.531513188	-
A_51_P237383	Rnase4	2.411615655	-
A_66_P113490	Sh2b2	2.056227653	-
A_55_P2808493	Ska3	2.056227653	+
A_55_P2806415	Slc15a2	2.867910496	+
A_55_P1959425	Slc16a3	3.271608234	+
A_51_P140751	Slc23a1	3.944930818	-
A_55_P2032445	Slc25a37	2.02791896	-
A_52_P229981	Slc51a	2.042024251	-
A_55_P2032518	Slc5a4a	3.160165247	-
A_65_P20042	Smarca4	2.250116969	-
A_51_P513530	Spag5	2.188587403	+
A_55_P2837304	Sst	2.173469725	-
A_55_P2102350	Stambpl1	2.411615655	+
A_66_P139166	Stmn2	2.329467173	-
A_51_P111554	Sucla2	2.02791896	-
A_66_P132910	Suco	2.329467173	+
A_51_P270741	Syng1	2.428389769	+
A_51_P312952	Tdrd12	2.887858391	+
A_52_P175376	Tfcp2l1	2.234574276	-
A_55_P2797764	Thsd7b	2.694467154	-
A_55_P2739934	Tjap1	2.411615655	+
A_55_P2721797	Tm4sf20	2.37841423	+
A_52_P101399	Tmem130	2.203810232	-
A_65_P11919	Tmem181a	2.099433367	+
A_52_P183524	Tmem86b	2.128740365	-
A_55_P2092085	Tmsb10	2.143546925	+
A_55_P2168990	Tmsb10	2.084931522	+
A_66_P110167	Trim38	2.411615655	-
A_52_P369705	Trim45	2.056227653	-
A_51_P298023	Ugt2a3	2.620786808	-
A_55_P2932738	Upk1b	2.329467173	-
A_55_P2505350	Utp14b	2.099433367	+
A_55_P2085060	Vgf	2.203810232	+
A_55_P2751338	Vip	2	-

A_51_P424532	Vnn1	2.531513188	-
A_51_P390314	Wdfy1	2.042024251	+
A_52_P129443	Wdpcp	2.394957409	+
A_55_P2024155	Zbtb16	2.361985323	-
A_55_P2032695	Zcchc11	2.02791896	-
A_55_P2108397		3.138336392	+
A_55_P2168823		2.770218936	+
A_55_P1958464		2.732080514	+
A_66_P125312		2.620786808	+
A_30_P01027558		2.584705661	+
A_55_P2128229		2.411615655	+
A_30_P01026183		2.37841423	+
A_66_P105891		2.361985323	+
A_30_P01019825		2.188587403	+
A_30_P01023554		2.143546925	+
A_55_P2048498		2.099433367	+
A_30_P01029107		2.042024251	+
A_30_P01018886		2.0139111	-
A_30_P01019185		2.0139111	-
A_52_P459887		2.042024251	-
A_55_P2419854		2.056227653	-
A_66_P109279		2.084931522	-
A_30_P01024192		2.143546925	-
A_51_P435671		2.143546925	-
A_55_P2025655		2.143546925	-
A_30_P01033145		2.203810232	-
A_55_P2117342		2.234574276	-
A_52_P492532		2.265767771	-
A_55_P2124461		2.329467173	-
A_30_P01020128		2.361985323	-
A_55_P2001281		2.37841423	-
A_66_P113466		2.37841423	-
A_66_P105507		2.394957409	-
A_55_P2058040		2.428389769	-
A_66_P134171		2.428389769	-
A_55_P1974014		2.514026749	-

A_55_P2186978	2.584705661	-
A_52_P578436	2.620786808	-
A_55_P2058023	2.67585511	-
A_55_P2722508	2.67585511	-
A_55_P2164443	2.907945035	-
A_52_P58543	2.948538435	-
A_52_P213527	2.989698497	-
A_55_P2075393	3.095129987	-
A_30_P01032670	3.138336392	-
A_66_P133367	3.138336392	-
A_55_P2104076	3.386981249	-
A_55_P2111322	6.680703355	-
A_30_P01026605	8.876555777	-

Appendix 6- A list of genes expressed in both the *Braf*^{L^{SL}-V600E/WT}; *Villin-CreER*^{T0/WT} and *Gsk3α*^{S21A/S21A}; *Gsk3β*^{S9A/S9A}; *Braf*^{L^{SL}-V600E/WT}; *Villin-CreER*^{T0/WT} genotypes (Group 3a).

A total of 13 genes' expression was significantly different between the two genotypes.

“-“ indicates downregulated genes in both genotypes.

Agilent ID	Gene symbol	Fold Change- List1	Fold Change-List2	Regulation
A_66_P134474	Ang3	4.007577464	9.106061323	-
A_52_P98778	Ang4	3.414496232	9.937558961	-
A_55_P2716491	Ang6	3.198153729	7.584071566	-
A_55_P2130024	AY761184	5.5874184	12.86176097	-
A_55_P2044653	Cyp2b10	12.0417853	31.97723654	-
A_51_P467076	Cyp2b9	9.274504684	21.89423648	-
A_55_P2054373	Defa-ps1	5.148445469	11.67485889	-
A_55_P2018863	Defa-rs7	7.517359792	15.17535517	-
A_55_P1969960	Defa25	9.620546471	20.21261398	-
A_55_P1954799	Defa26	5.039017672	14.82352575	-
A_55_P1972868	Gm21498	6.661695841	14.52163068	-
A_55_P2482301	Gm7861	3.599999477	8.433339079	-
A_51_P503757	Iglv1	2.154531621	5.630848749	-

Chapter 9. References

- AMERSI, F., AGUSTIN, M. & KO, C. Y. 2005. Colorectal Cancer: Epidemiology, Risk Factors, and Health Services. *Clinics in Colon and Rectal Surgery*, 18, 133-140.
- ANDREADI, C., CHEUNG, L.-K., GIBLETT, S., PATEL, B., JIN, H., MERCER, K., KAMATA, T., LEE, P., WILLIAMS, A., MCMAHON, M., MARAIS, R. & PRITCHARD, C. 2012. The intermediate-activity (L597V)BRAF mutant acts as an epistatic modifier of oncogenic RAS by enhancing signaling through the RAF/MEK/ERK pathway. *Genes & Development*, 26, 1945-1958.
- ANDREU, P., COLNOT, S., GODARD, C., GAD, S., CHAFEY, P., NIWAKAWAKITA, M., LAURENT-PUIG, P., KAHN, A., ROBINE, S., PERRET, C. & ROMAGNOLO, B. 2005. Crypt-restricted proliferation and commitment to the Paneth cell lineage following Apc loss in the mouse intestine. *Development*, 132, 1443.
- APARICIO, T., SVRCEK, M., ZANAN, A., BEOHOU, E., LAFOREST, A., AFCHAIN, P., MITRY, E., TAIEB, J., DI FIORE, F., GORNET, J. M., THIROT-BIDAULT, A., SOBHANI, I., MALKA, D., LECOMTE, T., LOCHER, C., BONNETAIN, F. & LAURENT-PUIG, P. 2013. Small bowel adenocarcinoma phenotyping, a clinicobiological prognostic study. *British Journal of Cancer*, 109, 3057-3066.
- ATCC. 2019. *A375P human melanoma cells* [Online]. Available: https://www.lgestandards-atcc.org/products/all/CRL-1619.aspx?geo_country=gb-generalinformation [Accessed].
- BARKER, N. & CLEVERS, H. 2006. Mining the Wnt pathway for cancer therapeutics. *Nat Rev Drug Discov*, 5, 997-1014.
- BARKER, N., RIDGWAY, R. A., VAN ES, J. H., VAN DE WETERING, M., BEGTHEL, H., VAN DEN BORN, M., DANENBERG, E., CLARKE, A. R., SANSOM, O. J. & CLEVERS, H. 2008. Crypt stem cells as the cells-of-origin of intestinal cancer. *Nature*, 457, 608.
- BARKER, N., VAN ES, J. H., KUIPERS, J., KUJALA, P., VAN DEN BORN, M., COZIJNSEN, M., HAEGEBARTH, A., KORVING, J., BEGTHEL, H., PETERS, P. J. & CLEVERS, H. 2007. Identification of stem cells in small intestine and colon by marker gene Lgr5. *Nature*, 449, 1003.
- BARNIER, J. V., PAPIN, C., EYCHÈNE, A., LECOQ, O. & CALOTHY, G. 1995. The Mouse B-raf Gene Encodes Multiple Protein Isoforms with Tissue-specific Expression. *Journal of Biological Chemistry*, 270, 23381-23389.

- BATTLE, M. A., BONDOW, B. J., IVERSON, M. A., ADAMS, S. J., JANDACEK, R. J., TSO, P. & DUNCAN, S. A. 2008. GATA4 is essential for jejunal function in mice. *Gastroenterology*, 135, 1676-1686.e1.
- BEAULIEU, J.-M., SOTNIKOVA, T. D., YAO, W.-D., KOCKERITZ, L., WOODGETT, J. R., GAINETDINOV, R. R. & CARON, M. G. 2004. Lithium antagonizes dopamine-dependent behaviors mediated by an AKT/glycogen synthase kinase 3 signaling cascade. *Proceedings of the National Academy of Sciences of the United States of America*, 101, 5099-5104.
- BEAULIEU, J.-M., ZHANG, X., RODRIGUIZ, R. M., SOTNIKOVA, T. D., COOLS, M. J., WETSEL, W. C., GAINETDINOV, R. R. & CARON, M. G. 2008. Role of GSK3 β in behavioral abnormalities induced by serotonin deficiency. *Proceedings of the National Academy of Sciences of the United States of America*, 105, 1333-1338.
- BEN-PORATH, I. & WEINBERG, R. A. 2005. The signals and pathways activating cellular senescence. *The International Journal of Biochemistry & Cell Biology*, 37, 961-976.
- BENNECKE, M., KRIEGL, L., BAJBOUJ, M., RETZLAFF, K., ROBINE, S., JUNG, A., ARKAN, M. C., KIRCHNER, T. & GRETEN, F. R. 2010. Ink4a/Arf and oncogene-induced senescence prevent tumor progression during alternative colorectal tumorigenesis. *Cancer Cell*, 18, 135-146.
- BERSUDSKY, Y., SHALDUBINA, A., KOZLOVSKY, N., WOODGETT, J. R., AGAM, G. & BELMAKER, R. H. 2008. Glycogen synthase kinase-3 β heterozygote knockout mice as a model of findings in postmortem schizophrenia brain or as a model of behaviors mimicking lithium action: negative results. *Behavioural Pharmacology*, 19, 217-224.
- BEUREL, E., GRIECO, S. F. & JOPE, R. S. 2015. Glycogen synthase kinase-3 (GSK3): regulation, actions, and diseases. *Pharmacology & therapeutics*, 0, 114-131.
- BOESPFLUG, A. & THOMAS, L. 2016. Cobimetinib and vemurafenib for the treatment of melanoma. *Expert Opinion on Pharmacotherapy*, 17, 1005-1011.
- BOLLAG, G., TSAI, J., ZHANG, J., ZHANG, C., IBRAHIM, P., NOLOP, K. & HIRTH, P. 2012. Vemurafenib: the first drug approved for BRAF-mutant cancer. *Nature Reviews Drug Discovery*, 11, 873.
- BREULEUX, M. 2007. Role of heregulin in human cancer. *Cellular and Molecular Life Sciences*, 64, 2358-2377.
- C KOZMA, S. & THOMAS, G. 1994. *p70s6k/p85s6k: Mechanism of activation and role in mitogenesis.*

- CAMPISI, J. 2013. Aging, Cellular Senescence, and Cancer. *Annual review of physiology*, 75, 685-705.
- CANCERREASERCHUK. 2016a. *Bowel cancer survival statistics* [Online]. <http://www.cancerresearchuk.org/>: CRUK. Available: <http://www.cancerresearchuk.org/health-professional/cancer-statistics/statistics-by-cancer-type/bowel-cancer/survival> - heading-Three [Accessed 19-9-2017 2017].
- CANCERREASERCHUK. 2016b. *cancer incidence for common cancer* [Online]. Available: <http://www.cancerresearchuk.org/health-professional/cancer-statistics/incidence/common-cancers-compared> - heading-Zero [Accessed 19-09 2017].
- CANCERREASERCHUK. 2016c. *Twenty most common cause of cancer death* [Online]. Available: http://www.cancerresearchuk.org/health-professional/cancer-statistics/mortality/common-cancers-compared?_gac=1.204693924.1505766067.EAlalQobChMlzryC2Mev1glVypPtCh1hdwTjEAAYASAAEgKDEfD BwE&_ga=2.59570030.253065941.1505746033-453566620.1505746033&_gac=1.204693924.1505766067.EAlalQobChMlzryC2Mev1glVypPtCh1hdwTjEAAYASAAEgKDEfD BwE - heading-Zero [Accessed 19-09-2017 2017].
- CARRAGHER, L. A. S., SNELL, K. R., GIBLETT, S. M., ALDRIDGE, V. S. S., PATEL, B., COOK, S. J., WINTON, D. J., MARAIS, R. & PRITCHARD, C. A. 2010. V600EBraf induces gastrointestinal crypt senescence and promotes tumour progression through enhanced CpG methylation of p16INK4a. *EMBO Molecular Medicine*, 2, 458.
- CARULLI, A. J., SAMUELSON, L. C. & SCHNELL, S. 2014. Unraveling intestinal stem cell behavior with models of crypt dynamics. *Integrative biology : quantitative biosciences from nano to macro*, 6, 243-257.
- CAUNT, C. J., SALE, M. J., SMITH, P. D. & COOK, S. J. 2015. MEK1 and MEK2 inhibitors and cancer therapy: the long and winding road. 15, 577.
- CGAN 2012. Comprehensive molecular characterization of human colon and rectal cancer. *Nature*, 487, 330-337.
- CHANG, H.-K., YU, E., KIM, J., BAE, Y. K., JANG, K.-T., JUNG, E. S., YOON, G. S., KIM, J. M., OH, Y.-H., BAE, H.-I., KIM, G. I., JUNG, S. J., GU, M. J., KIM, J. Y., JANG, K. Y., JUN, S.-Y., EOM, D. W., KWON, K. W., KANG, G. H., PARK, J. B., HONG, S., LEE, J. S., PARK, J. Y. & HONG, S.-M. 2010. Adenocarcinoma of the small intestine: a multi-institutional study of 197 surgically resected cases. *Human Pathology*, 41, 1087-1096.
- CHEKULAYEV, V., MADO, K., SHEVCHUK, I., KOIT, A., KALDMA, A., KLEPININ, A., TIMOHHINA, N., TEPP, K., KANDASHVILI, M.,

- OUNPUU, L., HECK, K., TRUU, L., PLANKEN, A., VALVERE, V. & KAAMBRE, T. 2015. Metabolic remodeling in human colorectal cancer and surrounding tissues: alterations in regulation of mitochondrial respiration and metabolic fluxes. *Biochemistry and Biophysics Reports*, 4, 111-125.
- CLARKE, C. N. & KOPETZ, E. S. 2015. BRAF mutant colorectal cancer as a distinct subset of colorectal cancer: clinical characteristics, clinical behavior, and response to targeted therapies. *Journal of Gastrointestinal Oncology*, 6, 660-667.
- CLEVERS, H. & NUSSE, R. 2012. Wnt/ β -Catenin Signaling and Disease. *Cell*, 149, 1192-1205.
- COHEN, P. & FRAME, S. 2001. The renaissance of GSK3. *Nature Reviews Molecular Cell Biology*, 2, 769.
- COLE, A., FRAME, S. & COHEN, P. 2004. Further evidence that the tyrosine phosphorylation of glycogen synthase kinase-3 (GSK3) in mammalian cells is an autophosphorylation event. *Biochemical Journal*, 377, 249-255.
- COSMIC. 2019. *Twenty most frequent mutations in human colorectal carcinoma* [Online]. Available: https://cancer.sanger.ac.uk/cosmic/browse/tissue?hn=carcinoma&in=t&ss=all&n=large_intestine [Accessed].
- COURTOIS-COX, S., JONES, S. L. & CICHOWSKI, K. 2008. Many roads lead to oncogene-induced senescence. *Oncogene*, 27, 2801.
- CROCKETT, S. D., SNOVER, D. C., AHNEN, D. J. & BARON, J. A. 2015. Sessile Serrated Adenomas: An Evidence-Based Guide to Management. *Clinical Gastroenterology and Hepatology*, 13, 11-26.e1.
- CSEH, B., DOMA, E. & BACCARINI, M. 2014. "RAF" neighborhood: Protein-protein interaction in the Raf/Mek/Erk pathway. *Febs Letters*, 588, 2398-2406.
- DABAJA, B. S., SUKI, D., PRO, B., BONNEN, M. & AJANI, J. 2004. Adenocarcinoma of the small bowel. *Cancer*, 101, 518-526.
- DAJANI, R., FRASER, E., ROE, S. M., YOUNG, N., GOOD, V., DALE, T. C. & PEARL, L. H. 2001. Crystal Structure of Glycogen Synthase Kinase 3. *Cell*, 105, 721-732.
- DAVIES, E. J., MARSH DURBAN, V., MENIEL, V., WILLIAMS, G. T. & CLARKE, A. R. 2014. PTEN loss and KRAS activation leads to the formation of serrated adenomas and metastatic carcinoma in the mouse intestine. *The Journal of Pathology*, 233, 27-38.

- DEMIERRE, M.-F., HIGGINS, P. D. R., GRUBER, S. B., HAWK, E. & LIPPMAN, S. M. 2005. Statins and cancer prevention. *Nature Reviews Cancer*, 5, 930.
- DHILLON, A. S., HAGAN, S., RATH, O. & KOLCH, W. 2007. MAP kinase signalling pathways in cancer. *Oncogene*, 26, 3279-3290.
- DI MICCO, R., FUMAGALLI, M., CICALESE, A., PICCININ, S., GASPARINI, P., LUISE, C., SCHURRA, C., GARRE', M., GIOVANNI NUCIFORO, P., BENSIMON, A., MAESTRO, R., GIUSEPPE PELICCI, P. & D'ADDA DI FAGAGNA, F. 2006. Oncogene-induced senescence is a DNA damage response triggered by DNA hyper-replication. *Nature*, 444, 638.
- DING, Y., SU, S., TANG, W., ZHANG, X., CHEN, S., ZHU, G., LIANG, J., WEI, W., GUO, Y., LIU, L., CHEN, Y.-G. & WU, W. 2014. Enrichment of the β -catenin–TCF complex at the S and G2 phases ensures cell survival and cell cycle progression. *Journal of Cell Science*, 127, 4833.
- DO, C., BERTRAND, C., PALASSE, J., DELISLE, M.-B., COHEN-JONATHAN-MOYAL, E. & SEVA, C. 2013. Activation of pro-oncogenic pathways in colorectal hyperplastic polyps. *BMC Cancer*, 13, 531.
- DOBLE, B. & WOODGETT, J. R. 2003. GSK-3: tricks of the trade for a multi-tasking kinase. *Journal of cell science*, 116, 1175-1186.
- DUDLEY, D. T., PANG, L., DECKER, S. J., BRIDGES, A. J. & SALTIEL, A. R. 1995. A synthetic inhibitor of the mitogen-activated protein kinase cascade. *Proceedings of the National Academy of Sciences of the United States of America*, 92, 7686-7689.
- ENSARI, A., BOSMAN, F. T. & OFFERHAUS, G. J. A. 2010. The serrated polyp: getting it right! *Journal of Clinical Pathology*, 63, 665-668.
- EOM, T.-Y. & JOPE, R. S. 2009. Blocked inhibitory serine-phosphorylation of glycogen synthase kinase-3 α/β impairs in vivo neural precursor cell proliferation. *Biological psychiatry*, 66, 494-502.
- EXPASY. 2019a. *HCC364 human lung carcinoma* [Online]. Available: https://web.expasy.org/cellosaurus/CVCL_5134 [Accessed].
- EXPASY. 2019b. *RKO human colon carcinoma* [Online]. Available: https://web.expasy.org/cellosaurus/CVCL_HE17 [Accessed].
- FAGIANI, E. & CHRISTOFORI, G. 2013. Angiopoietins in angiogenesis. *Cancer Letters*, 328, 18-26.
- FAVATA, M. F., HORIUCHI, K. Y., MANOS, E. J., DAULERIO, A. J., STRADLEY, D. A., FEESER, W. S., VAN DYK, D. E., PITTS, W. J., EARL, R. A., HOBBS, F., COPELAND, R. A., MAGOLDA, R. L., SCHERLE, P. A. & TRZASKOS, J. M. 1998. Identification of a Novel

- Inhibitor of Mitogen-activated Protein Kinase Kinase. *Journal of Biological Chemistry*, 273, 18623-18632.
- FEARON, E. R. 2011. Molecular Genetics of Colorectal Cancer. *Annual Review of Pathology: Mechanisms of Disease*, 6, 479-507.
- FEARON, E. R. & VOGELSTEIN, B. 1990. A genetic model for colorectal tumorigenesis. *Cell*, 61, 759-767.
- FERRETTA, A., MAIDA, I., GUIDA, S., AZZARITI, A., PORCELLI, L., TOMMASI, S., ZANNA, P., COCCO, T., GUIDA, M. & GUIDA, G. 2016. New insight into the role of metabolic reprogramming in melanoma cells harboring BRAF mutations. *Biochimica et Biophysica Acta (BBA) - Molecular Cell Research*, 1863, 2710-2718.
- FLEMING, M., RAVULA, S., TATISHCHEV, S. F. & WANG, H. L. 2012. Colorectal carcinoma: Pathologic aspects. *Journal of Gastrointestinal Oncology*, 3, 153-173.
- FRAME, S. & COHEN, P. 2001. GSK3 takes centre stage more than 20 years after its discovery. *Biochemical Journal*, 359, 1-16.
- FREY, M. R. & BRENT POLK, D. 2013. ErbB receptors and their growth factor ligands in pediatric intestinal inflammation. *Pediatric Research*, 75, 127.
- GARNETT, M. J. & MARAIS, R. 2004. Guilty as charged. *Cancer Cell*, 6, 313-319.
- GERBER, D. E. & CHOY, H. 2010. Cetuximab in combination therapy: from bench to clinic. *Cancer and Metastasis Reviews*, 29, 171-180.
- GOMEZ, D., DE ROSA, A., ADDISON, A., BROOKS, A., MALIK, H. Z. & CAMERON, I. C. 2013. Cetuximab therapy in the treatment of metastatic colorectal cancer: The future frontier? *International Journal of Surgery*, 11, 507-513.
- GÓMEZ-SINTES, R., HERNÁNDEZ, F., LUCAS, J. J. & AVILA, J. 2011. GSK-3 Mouse Models to Study Neuronal Apoptosis and Neurodegeneration. *Frontiers in Molecular Neuroscience*, 4, 45.
- GUERRA, C., MIJIMOLLE, N., DHAWAHIR, A., DUBUS, P., BARRADAS, M., SERRANO, M., CAMPUZANO, V. & BARBACID, M. 2003. Tumor induction by an endogenous *K-ras* oncogene is highly dependent on cellular context. *Cancer Cell*, 4, 111-120.
- GUINNEY, J., DIENSTMANN, R., WANG, X., DE REYNIÈS, A., SCHLICKER, A., SONESON, C., MARISA, L., ROEPMAN, P., NYAMUNDANDA, G., ANGELINO, P., BOT, B. M., MORRIS, J. S., SIMON, I. M., GERSTER, S., FESSLER, E., DE SOUSA E MELO, F., MISSIAGLIA, E., RAMAY, H., BARRAS, D., HOMICKO, K., MARU, D., MANYAM, G. C., BROOM,

- B., BOIGE, V., PEREZ-VILLAMIL, B., LADERAS, T., SALAZAR, R., GRAY, J. W., HANAHAH, D., TABERNERO, J., BERNARDS, R., FRIEND, S. H., LAURENT-PUIG, P., MEDEMA, J. P., SADANANDAM, A., WESSELS, L., DELORENZI, M., KOPETZ, S., VERMEULEN, L. & TEJPAR, S. 2015. The Consensus Molecular Subtypes of Colorectal Cancer. *Nature medicine*, 21, 1350-1356.
- HAGGAR, F. A. & BOUSHEY, R. P. 2009. Colorectal Cancer Epidemiology: Incidence, Mortality, Survival, and Risk Factors. *Clinics in Colon and Rectal Surgery*, 22, 191-197.
- HALING, JACOB R., SUDHAMSU, J., YEN, I., SIDERIS, S., SANDOVAL, W., PHUNG, W., BRAVO, BRANDON J., GIANNETTI, ANTHONY M., PECK, A., MASSELOT, A., MORALES, T., SMITH, D., BRANDHUBER, BARBARA J., HYMOWITZ, SARAH G. & MALEK, S. 2014. Structure of the BRAF-MEK Complex Reveals a Kinase Activity Independent Role for BRAF in MAPK Signaling. *Cancer Cell*, 26, 402-413.
- HANKS, S. K. & HUNTER, T. 1995. Protein kinases 6. The eukaryotic protein kinase superfamily: kinase (catalytic) domain structure and classification. *The FASEB Journal*, 9, 576-96.
- HEY, F., GIBLETT, S., FORREST, S., HERBERT, C. & PRITCHARD, C. 2016. Phosphorylations of Serines 21/9 in Glycogen Synthase Kinase 3 α/β Are Not Required for Cell Lineage Commitment or WNT Signaling in the Normal Mouse Intestine. *PLoS ONE*, 11, e0156877.
- HEYER, J., YANG, K., LIPKIN, M., EDELMANN, W. & KUCHERLAPATI, R. 1999. Mouse models for colorectal cancer. *Oncogene*, 18, 5325-33.
- HINDLEY, A. & KOLCH, W. 2002. Extracellular signal regulated kinase (ERK)/mitogen activated protein kinase (MAPK)-independent functions of Raf kinases. *Journal of Cell Science*, 115, 1575.
- HOEFLICH, K. P., LUO, J., RUBIE, E. A., TSAO, M.-S., JIN, O. & WOODGETT, J. R. 2000. Requirement for glycogen synthase kinase-3 β in cell survival and NF- κ B activation. *Nature*, 406, 86.
- HUNG, K. E., MARICEVICH, M. A., RICHARD, L. G., CHEN, W. Y., RICHARDSON, M. P., KUNIN, A., BRONSON, R. T., MAHMOOD, U. & KUCHERLAPATI, R. 2010. Development of a mouse model for sporadic and metastatic colon tumors and its use in assessing drug treatment. *Proceedings of the National Academy of Sciences of the United States of America*, 107, 1565-1570.
- IRELAND, H., KEMP, R., HOUGHTON, C., HOWARD, L., CLARKE, A. R., SANSOM, O. J. & WINTON, D. J. 2004. Inducible cre-mediated control of gene expression in the murine gastrointestinal tract: effect of loss of β -catenin. *Gastroenterology*, 126, 1236-1246.

- JACKSON, E. L., WILLIS, N., MERCER, K., BRONSON, R. T., CROWLEY, D., MONTOYA, R., JACKS, T. & TUVESON, D. A. 2001. Analysis of lung tumor initiation and progression using conditional expression of oncogenic K-ras. *Genes & Development*, 15, 3243-3248.
- JACKSTADT, R. & SANSOM, O. J. 2016. Mouse models of intestinal cancer. *The Journal of Pathology*, 238, 141-151.
- JANKU, F., WHELER, J. J., NAING, A., FALCHOOK, G. S., HONG, D. S., STEPANEK, V. M., FU, S., PIHA-PAUL, S. A., LEE, J. J., LUTHRA, R., TSIMBERIDOU, A. M. & KURZROCK, R. 2013. PIK3CA mutation H1047R is associated with response to PI3K/AKT/mTOR signaling pathway inhibitors in early phase clinical trials. *Cancer research*, 73, 276-284.
- JANSSEN, K. P., MARJOU, F. E., PINTO, D., SASTRE, X., ROUILLARD, D., FOUQUET, C., SOUSSI, T., LOUVARD, D. & ROBINE, S. 2002. Targeted expression of oncogenic K-ras in intestinal epithelium causes spontaneous tumorigenesis in mice. *Gastroenterology*, 123, 492-504.
- JASS, J. R. 2007. Classification of colorectal cancer based on correlation of clinical, morphological and molecular features. *Histopathology*, 50, 113-130.
- JOHNSON, R. L. & FLEET, J. C. 2013. Animal Models of Colorectal Cancer. *Cancer metastasis reviews*, 32, 39-61.
- JONKER, D. J., O'CALLAGHAN, C. J., KARAPETIS, C. S., ZALCBERG, J. R., TU, D., AU, H.-J., BERRY, S. R., KRAHN, M., PRICE, T., SIMES, R. J., TEBBUTT, N. C., VAN HAZEL, G., WIERZBICKI, R., LANGER, C. & MOORE, M. J. 2007. Cetuximab for the Treatment of Colorectal Cancer. *New England Journal of Medicine*, 357, 2040-2048.
- KAIDANOVICH-BEILIN, O., LIPINA, T. V., TAKAO, K., VAN EEDE, M., HATTORI, S., LALIBERTÉ, C., KHAN, M., OKAMOTO, K., CHAMBERS, J. W., FLETCHER, P. J., MACAULAY, K., DOBLE, B. W., HENKELMAN, M., MIYAKAWA, T., RODER, J. & WOODGETT, J. R. 2009. Abnormalities in brain structure and behavior in GSK-3alpha mutant mice. *Molecular Brain*, 2, 35-35.
- KAIDANOVICH-BEILIN, O. & WOODGETT, J. R. 2011. GSK-3: Functional Insights from Cell Biology and Animal Models. *Frontiers in Molecular Neuroscience*, 4, 40.
- KANG, H.-B., FAN, J., LIN, R., ELF, S., JI, Q., ZHAO, L., JIN, L., SEO, J. H., SHAN, C., ARBISER, J. L., COHEN, C., BRAT, D., MIZIORKO, H. M., KIM, E., ABDEL-WAHAB, O., MERGHOUB, T., FRÖHLING, S., SCHOLL, C., TAMAYO, P., BARBIE, D. A., ZHOU, L., POLLACK, B. P., FISHER, K., KUDCHADKAR, R. R., LAWSON, D. H., SICA, G., ROSSI, M., LONIAL, S., KHOURY, H. J., KHURI, F. R., LEE, B. H., BOGGON, T.

- J., HE, C., KANG, S. & CHEN, J. 2015. Metabolic rewiring by oncogenic BRAF V600E links ketogenesis pathway to BRAF-MEK1 signaling. *Molecular cell*, 59, 345-358.
- KARIM, B. O. & HUSO, D. L. 2013. Mouse models for colorectal cancer. *American Journal of Cancer Research*, 3, 240-250.
- KEMP, C. J., DONEHOWER, L. A., BRADLEY, A. & BALMAIN, A. 1993. Reduction of p53 gene dosage does not increase initiation or promotion but enhances malignant progression of chemically induced skin tumors. *Cell*, 74, 813-822.
- KERKELA, R., KOCKERITZ, L., MACAULAY, K., ZHOU, J., DOBLE, B. W., BEAHM, C., GREYTAK, S., WOULFE, K., TRIVEDI, C. M., WOODGETT, J. R., EPSTEIN, J. A., FORCE, T. & HUGGINS, G. S. 2008. Deletion of GSK-3 β in mice leads to hypertrophic cardiomyopathy secondary to cardiomyoblast hyperproliferation. *The Journal of Clinical Investigation*, 118, 3609-3618.
- KLAUS, A. & BIRCHMEIER, W. 2008. Wnt signalling and its impact on development and cancer. *Nat Rev Cancer*, 8, 387-398.
- KO, H. M., HARPAZ, N., MCBRIDE, R. B., CUI, M., YE, F., ZHANG, D., ULLMAN, T. A. & POLYDORIDES, A. D. 2015. Serrated colorectal polyps in inflammatory bowel disease. *Mod Pathol*, 28, 1584-1593.
- KOMIYA, Y. & HABAS, R. 2008. Wnt signal transduction pathways. *Organogenesis*, 4, 68-75.
- KONG, Y., CUI, H., RAMKUMAR, C. & ZHANG, H. 2011. Regulation of Senescence in Cancer and Aging. *Journal of Aging Research*, 2011, 963172.
- KOPETZ, S., DESAI, J., CHAN, E., HECHT, J. R., O'DWYER, P. J., LEE, R. J., NOLOP, K. B. & SALTZ, L. 2010. PLX4032 in metastatic colorectal cancer patients with mutant BRAF tumors. *Journal of Clinical Oncology*, 28, 3534-3534.
- KOTARBA, G., KRZYWINSKA, E., GRABOWSKA, A. I., TARACHA, A. & WILANOWSKI, T. 2018. TFCP2/TFCP2L1/UBP1 transcription factors in cancer. *Cancer Letters*, 420, 72-79.
- KRIEGL, L., NEUMANN, J., VIETH, M., GRETEN, F. R., REU, S., JUNG, A. & KIRCHNER, T. 2011. Up and downregulation of p16Ink4a expression in BRAF-mutated polyps/adenomas indicates a senescence barrier in the serrated route to colon cancer. *Modern Pathology*, 24, 1015.
- KUILMAN, T., MICHALOGLOU, C., MOOI, W. J. & PEEPER, D. S. 2010. The essence of senescence. *Genes & Development*, 24, 2463-2479.

- KUMAR, P., MUNNANGI, P., CHOWDARY, K. V. S. R., SHAH, V. J., SHINDE, S. R., KOLLI, N. R., HALEHALLI, R. R., NAGARAJARAM, H. A. & MADDIKA, S. 2017. A Human Tyrosine Phosphatase Interactome Mapped by Proteomic Profiling. *Journal of Proteome Research*, 16, 2789-2801.
- LAMONT, B. J., VISINONI, S., FAM, B. C., KEBEDE, M., WEINRICH, B., PAPAPOSTOLOU, S., MASSINET, H., PROIETTO, J., FAVALORO, J. & ANDRIKOPOULOS, S. 2006. Expression of Human Fructose-1,6-Bisphosphatase in the Liver of Transgenic Mice Results in Increased Glycerol Gluconeogenesis. *Endocrinology*, 147, 2764-2772.
- LAVOIE, H. & THERRIEN, M. 2015. Regulation of RAF protein kinases in ERK signalling. *Nat Rev Mol Cell Biol*, 16, 281-298.
- LEE, B. H., TAYLOR, M. G., ROBINET, P., SMITH, J. D., SCHWEITZER, J., SEHAYEK, E., FALZARANO, S. M., MAGI-GALLUZZI, C., KLEIN, E. A. & TING, A. H. 2013. Dysregulation of cholesterol homeostasis in human prostate cancer through loss of ABCA1. *Cancer research*, 73, 1211-1218.
- LUO, F., BROOKS, D. G., YE, H., HAMOUDI, R., POULOGIANNIS, G., PATEK, C. E., WINTON, D. J. & ARENDS, M. J. 2007. Conditional expression of mutated K-ras accelerates intestinal tumorigenesis in Msh2-deficient mice. *Oncogene*, 26, 4415-4427.
- MA, J., CHEN, M., WANG, J., XIA, H. H. X., ZHU, S., LIANG, Y., GU, Q., QIAO, L., DAI, Y., ZOU, B., LI, Z., ZHANG, Y., LAN, H. & WONG, B. C. Y. 2008. Pancreatic duodenal homeobox-1 (PDX1) functions as a tumor suppressor in gastric cancer. *Carcinogenesis*, 29, 1327-1333.
- MACDONALD, B. T., TAMAI, K. & HE, X. 2009. Wnt/ β -catenin signaling: components, mechanisms, and diseases. *Developmental cell*, 17, 9-26.
- MACFARLANE, A. J., MCENTEE, M. F. & STOVER, P. J. 2014. Azoxymethane-induced colon carcinogenesis in mice occurs independently of de novo thymidylate synthesis capacity. *The Journal of nutrition*, 144, 419-424.
- MADISON, B. B., DUNBAR, L., QIAO, X. T., BRAUNSTEIN, K., BRAUNSTEIN, E. & GUMUCIO, D. L. 2002. cis Elements of the Villin Gene Control Expression in Restricted Domains of the Vertical (Crypt) and Horizontal (Duodenum, Cecum) Axes of the Intestine. *Journal of Biological Chemistry*, 277, 33275-33283.
- MAH, A. T., YAN, K. S. & KUO, C. J. 2016. Wnt pathway regulation of intestinal stem cells. *The Journal of Physiology*, 594, 4837-4847.
- MÄKINEN, M. J. 2007. Colorectal serrated adenocarcinoma. *Histopathology*, 50, 131-150.

- MAO, M., FENG, T., MARIADASON, J. M., TSAO, C. C., LEMOS, R., DAYYANI, F., NANDA, V. G. Y., JIANG, Z.-Q., WISTUBA, I. I., TANG, X. M., BORNMAN, W. G., BOLLAG, G., MILLS, G. B., POWIS, G., DESAI, J., GALLICK, G. E., DAVIES, M. A. & KOPETZ, S. 2013. Resistance to BRAF inhibition in BRAF-mutant colon cancer can be overcome with PI3K inhibition or demethylating agents. *Clinical cancer research : an official journal of the American Association for Cancer Research*, 19, 657-667.
- MARGOLIS, B. & SKOLNIK, E. Y. 1994. Activation of Ras by receptor tyrosine kinases. *Journal of the American Society of Nephrology*, 5, 1288-99.
- MARLEY, A. R. & NAN, H. 2016. Epidemiology of colorectal cancer. *International Journal of Molecular Epidemiology and Genetics*, 7, 105-114.
- MARTINS, S. F., AMORIM, R., VIANA-PEREIRA, M., PINHEIRO, C., COSTA, R. F. A., SILVA, P., COUTO, C., ALVES, S., FERNANDES, S., VILAÇA, S., FALCÃO, J., MARQUES, H., PARDAL, F., RODRIGUES, M., PRETO, A., REIS, R. M., LONGATTO-FILHO, A. & BALTAZAR, F. 2016. Significance of glycolytic metabolism-related protein expression in colorectal cancer, lymph node and hepatic metastasis. *BMC Cancer*, 16, 535.
- MCCAIN, J. 2013. The MAPK (ERK) Pathway: Investigational Combinations for the Treatment Of BRAF-Mutated Metastatic Melanoma. *Pharmacy and Therapeutics*, 38, 96-108.
- MCCART, A. E., VICKARYOUS, N. K. & SILVER, A. 2008. Apc mice: Models, modifiers and mutants. *Pathology - Research and Practice*, 204, 479-490.
- MCCUBREY, J. A., DAVIS, N. M., ABRAMS, S. L., MONTALTO, G., CERVELLO, M., BASECKE, J., LIBRA, M., NICOLETTI, F., COCCO, L., MARTELLI, A. M. & STEELMAN, L. S. 2014. Diverse roles of GSK-3: Tumor promoter–tumor suppressor, target in cancer therapy. *Advances in Biological Regulation*, 54, 176-196.
- MCCUBREY, J. A., STEELMAN, L. S., CHAPPELL, W. H., ABRAMS, S. L., WONG, E. W. T., CHANG, F., LEHMANN, B., TERRIAN, D. M., MILELLA, M., TAFURI, A., STIVALA, F., LIBRA, M., BASECKE, J., EVANGELISTI, C., MARTELLI, A. M. & FRANKLIN, R. A. 2007. ROLES OF THE RAF/MEK/ERK PATHWAY IN CELL GROWTH, MALIGNANT TRANSFORMATION AND DRUG RESISTANCE. *Biochimica et biophysica acta*, 1773, 1263-1284.
- MCMANUS, E. J., SAKAMOTO, K., ARMIT, L. J., RONALDSON, L., SHPIRO, N., MARQUEZ, R. & ALESSI, D. R. 2005. Role that phosphorylation of GSK3 plays in insulin and Wnt signalling defined by knockin analysis. *The EMBO Journal*, 24, 1571-1583.

- MEDINA, M. & WANDOSELL, F. 2011. Deconstructing GSK-3: The Fine Regulation of Its Activity. *International Journal of Alzheimer's Disease*, 2011, 479249.
- MERCER, K., GIBLETT, S., GREEN, S., LLOYD, D., DIAS, S. D., PLUMB, M., MARAIS, R. & PRITCHARD, C. 2005. Expression of Endogenous Oncogenic (V600E)B-raf Induces Proliferation and Developmental Defects in Mice and Transformation of Primary Fibroblasts. *Cancer research*, 65, 11493-11500.
- MERCER, K. E. & PRITCHARD, C. A. 2003. Raf proteins and cancer: B-Raf is identified as a mutational target. *Biochimica et Biophysica Acta (BBA) - Reviews on Cancer*, 1653, 25-40.
- MESSINA, S., FRATI, L., LEONETTI, C., ZUCHEGNA, C., DI ZAZZO, E., CALOGERO, A. & PORCELLINI, A. 2011. Dual-specificity phosphatase DUSP6 has tumor-promoting properties in human glioblastomas. *Oncogene*, 30, 3813.
- MOTOSHIMA, H., GOLDSTEIN, B. J., IGATA, M. & ARAKI, E. 2006. AMPK and cell proliferation – AMPK as a therapeutic target for atherosclerosis and cancer. *The Journal of Physiology*, 574, 63-71.
- MÜLLER, M. F., IBRAHIM, A. E. K. & ARENDS, M. J. 2016. Molecular pathological classification of colorectal cancer. *Virchows Archiv*, 469, 125-134.
- MUÑOZ, J. J., TÁRREGA, C., BLANCO-APARICIO, C. & PULIDO, R. 2003. Differential interaction of the tyrosine phosphatases PTP-SL, STEP and HePTP with the mitogen-activated protein kinases ERK1/2 and p38alpha is determined by a kinase specificity sequence and influenced by reducing agents. *Biochemical Journal*, 372, 193-201.
- MUÑOZ-ESPÍN, D. & SERRANO, M. 2014. Cellular senescence: from physiology to pathology. *Nature Reviews Molecular Cell Biology*, 15, 482.
- NIEHRS, C. 2012. The complex world of WNT receptor signalling. *Nat Rev Mol Cell Biol*, 13, 767-779.
- O'BRIEN, W. T., HARPER, A. D., JOVÉ, F., WOODGETT, J. R., MARETTO, S., PICCOLO, S. & KLEIN, P. S. 2004. Glycogen Synthase Kinase-3β Haploinsufficiency Mimics the Behavioral and Molecular Effects of Lithium. *The Journal of neuroscience : the official journal of the Society for Neuroscience*, 24, 6791-6798.
- OHTANI, N., YAMAKOSHI, K., TAKAHASHI, A. & HARA, E. 2004. The p16INK4a-RB pathway: molecular link between cellular senescence and tumor suppression. *The Journal of Medical Investigation*, 51, 146-153.

- OLD, W. M., SHABB, J. B., HOUEL, S., WANG, H., COUTS, K. L., YEN, C.-Y., LITMAN, E. S., CROY, C. H., MEYER-ARENDT, K., MIRANDA, J. G., BROWN, R. A., WITZE, E. S., SCHWEPPE, R. E., RESING, K. A. & AHN, N. G. 2009. Functional Proteomics Identifies Targets of Phosphorylation by B-Raf Signaling in Melanoma. *Molecular cell*, 34, 115-131.
- PANDEY, M. K. & DEGRADO, T. R. 2016. Glycogen Synthase Kinase-3 (GSK-3)-Targeted Therapy and Imaging. *Theranostics*, 6, 571-593.
- PARMENTER, T. J., KLEINSCHMIDT, M., KINROSS, K. M., BOND, S. T., LI, J., KAADIGE, M. R., RAO, A., SHEPPARD, K. E., HUGO, W., PUPO, G. M., PEARSON, R. B., MCGEE, S. L., LONG, G. V., SCOLYER, R. A., RIZOS, H., LO, R. S., CULLINANE, C., AYER, D. E., RIBAS, A., JOHNSTONE, R. W., HICKS, R. J. & MCARTHUR, G. A. 2014. Response of BRAF mutant melanoma to BRAF inhibition is mediated by a network of transcriptional regulators of glycolysis. *Cancer discovery*, 4, 423-433.
- PARRY, L., YOUNG, M., EL MARJOU, F. & CLARKE, A. R. 2013. Evidence for a Crucial Role of Paneth Cells in Mediating the Intestinal Response to Injury. *Stem Cells (Dayton, Ohio)*, 31, 776-785.
- PAUL, S., NAIRN, A. C., WANG, P. & LOMBROSO, P. J. 2002. NMDA-mediated activation of the tyrosine phosphatase STEP regulates the duration of ERK signaling. *Nature Neuroscience*, 6, 34.
- PEARSON, G., ROBINSON, F., BEERS GIBSON, T., XU, B.-E., KARANDIKAR, M., BERMAN, K. & COBB, M. H. 2001. Mitogen-Activated Protein (MAP) Kinase Pathways: Regulation and Physiological Functions*. *Endocrine Reviews*, 22, 153-183.
- PEREZ-COSTAS, E., GANDY, J. C., MELENDEZ-FERRO, M., ROBERTS, R. C. & BIJUR, G. N. 2010. Light and Electron Microscopy Study of Glycogen Synthase Kinase-3 β in the Mouse Brain. *PLoS ONE*, 5, e8911.
- PINO, M. S. & CHUNG, D. C. 2010. THE CHROMOSOMAL INSTABILITY PATHWAY IN COLON CANCER. *Gastroenterology*, 138, 2059-2072.
- PRAHALLAD, A., SUN, C., HUANG, S., DI NICOLANTONIO, F., SALAZAR, R., ZECCHIN, D., BEIJERSBERGEN, R. L., BARDELLI, A. & BERNARDS, R. 2012. Unresponsiveness of colon cancer to BRAF(V600E) inhibition through feedback activation of EGFR. *Nature*, 483, 100-103.
- PRATILAS, C. A., TAYLOR, B. S., YE, Q., VIALE, A., SANDER, C., SOLIT, D. B. & ROSEN, N. 2009. (V600E)BRAF is associated with disabled feedback inhibition of RAF-MEK signaling and elevated transcriptional output of the pathway. *Proceedings of the National Academy of Sciences of the United States of America*, 106, 4519-4524.

- PRITCHARD, C., CARRAGHER, L., ALDRIDGE, V., GIBLETT, S., JIN, H., FOSTER, C., ANDREADI, C. & KAMATA, T. 2007. Mouse models for BRAF-induced cancers. *Biochemical Society transactions*, 35, 1329-1333.
- QIAN, Y. & CHEN, X. 2010. Tumor suppression by p53: making cells senescent. *Histology and histopathology*, 25, 515-526.
- QIAN, Y. & CHEN, X. 2013. Senescence Regulation by the p53 Protein Family. *Methods in molecular biology (Clifton, N.J.)*, 965, 37-61.
- QIU, D., YE, S., RUIZ, B., ZHOU, X., LIU, D., ZHANG, Q. & YING, Q.-L. 2015. Klf2 and Tfcp2l1, Two Wnt/ β -Catenin Targets, Act Synergistically to Induce and Maintain Naive Pluripotency. *Stem Cell Reports*, 5, 314-322.
- RAD, R., CADIÑANOS, J., RAD, L., VARELA, I., STRONG, A., KRIEGL, L., CONSTANTINO-CASAS, F., ESER, S., HIEBER, M., SEIDLER, B., PRICE, S., FRAGA, MARIO F., CALVANESE, V., HOFFMAN, G., PONSTINGL, H., SCHNEIDER, G., YUSA, K., GROVE, C., SCHMID, ROLAND M., WANG, W., VASSILIOU, G., KIRCHNER, T., MCDERMOTT, U., LIU, P., SAUR, D. & BRADLEY, A. 2013. A Genetic Progression Model of BrafV600E-Induced Intestinal Tumorigenesis Reveals Targets for Therapeutic Intervention. *Cancer Cell*, 24, 15-29.
- RAHMAN, M. A., SALAJEGHEH, A., SMITH, R. A. & LAM, A. K. Y. 2013. B-Raf mutation: A key player in molecular biology of cancer. *Experimental and Molecular Pathology*, 95, 336-342.
- RAYESS, H., WANG, M. B. & SRIVATSAN, E. S. 2012. Cellular senescence and tumor suppressor gene p16. *International Journal of Cancer. Journal International du Cancer*, 130, 1715-1725.
- ROBERTS, P. J. & DER, C. J. 2007. Targeting the Raf-MEK-ERK mitogen-activated protein kinase cascade for the treatment of cancer. *Oncogene*, 26, 3291-3310.
- ROSKOSKI, R. 2010. RAF protein-serine/threonine kinases: Structure and regulation. *Biochemical and Biophysical Research Communications*, 399, 313-317.
- SANSOM, O. J., MENIEL, V. S., MUNCAN, V., PHESSÉ, T. J., WILKINS, J. A., REED, K. R., VASS, J. K., ATHINEOS, D., CLEVERS, H. & CLARKE, A. R. 2007. Myc deletion rescues Apc deficiency in the small intestine. *Nature*, 446, 676.
- SANSOM, O. J., REED, K. R., HAYES, A. J., IRELAND, H., BRINKMANN, H., NEWTON, I. P., BATLLE, E., SIMON-ASSMANN, P., CLEVERS, H., NATHKE, I. S., CLARKE, A. R. & WINTON, D. J. 2004. Loss of Apc in vivo immediately perturbs Wnt signaling, differentiation, and migration. *Genes & Development*, 18, 1385-1390.

- SATOH, K., YACHIDA, S., SUGIMOTO, M., OSHIMA, M., NAKAGAWA, T., AKAMOTO, S., TABATA, S., SAITOH, K., KATO, K., SATO, S., IGARASHI, K., AIZAWA, Y., KAJINO-SAKAMOTO, R., KOJIMA, Y., FUJISHITA, T., ENOMOTO, A., HIRAYAMA, A., ISHIKAWA, T., TAKETO, M. M., KUSHIDA, Y., HABA, R., OKANO, K., TOMITA, M., SUZUKI, Y., FUKUDA, S., AOKI, M. & SOGA, T. 2017. Global metabolic reprogramming of colorectal cancer occurs at adenoma stage and is induced by MYC. *Proceedings of the National Academy of Sciences of the United States of America*, 114, E7697-E7706.
- SCHWENK, F., BARON, U. & RAJEWSKY, K. 1995. A cre-transgenic mouse strain for the ubiquitous deletion of loxP-flanked gene segments including deletion in germ cells. *Nucleic Acids Research*, 23, 5080-5081.
- SEOANE, M., COSTOYA, J. A. & ARCE, V. M. 2017. Uncoupling Oncogene-Induced Senescence (OIS) and DNA Damage Response (DDR) triggered by DNA hyper-replication: lessons from primary mouse embryo astrocytes (MEA). *Scientific Reports*, 7, 12991.
- SHIBATA, H., TOYAMA, K., SHIOYA, H., ITO, M., HIROTA, M., HASEGAWA, S., MATSUMOTO, H., TAKANO, H., AKIYAMA, T., TOYOSHIMA, K., KANAMARU, R., KANEGAE, Y., SAITO, I., NAKAMURA, Y., SHIBA, K. & NODA, T. 1997. Rapid Colorectal Adenoma Formation Initiated by Conditional Targeting of the Apc Gene. *Science*, 278, 120-123.
- SILVA, D. D., AUSINA, P., ALENCAR, E. M., COELHO, W. S., ZANCAN, P. & SOLA-PENNA, M. 2012. Metformin reverses hexokinase and phosphofructokinase downregulation and intracellular distribution in the heart of diabetic mice. *IUBMB Life*, 64, 766-774.
- SINGH, S., ARCAROLI, J., THOMPSON, D. C., MESSERSMITH, W. & VASILIOU, V. 2015. Acetaldehyde and Retinaldehyde-Metabolizing Enzymes in Colon and Pancreatic cancers. *Advances in experimental medicine and biology*, 815, 281-294.
- SMITH, B. & LAND, H. 2012. Anti-cancer activity of the cholesterol exporter ABCA1 gene. *Cell reports*, 2, 580-590.
- SNOVER, D. C. 2011. Update on the serrated pathway to colorectal carcinoma. *Human Pathology*, 42, 1-10.
- SOH, D., DONG, D., GUO, Y. & WONG, L. 2010. Consistency, comprehensiveness, and compatibility of pathway databases. *BMC Bioinformatics*, 11, 449.
- SOTGIA, F., MARTINEZ-OUTSCHOORN, U. E., PAVLIDES, S., HOWELL, A., PESTELL, R. G. & LISANTI, M. P. 2011. Understanding the Warburg effect and the prognostic value of stromal caveolin-1 as a marker of a lethal tumor microenvironment. *Breast Cancer Research : BCR*, 13, 213-213.

- STANFORDUNIVERSITY. 2017. *WNT target genes* [Online]. Available: http://web.stanford.edu/group/nusselab/cgi-bin/wnt/target_genes [Accessed].
- SUN, C., WANG, L., HUANG, S., HEYNEN, G. J. J. E., PRAHALLAD, A., ROBERT, C., HAANEN, J., BLANK, C., WESSELING, J., WILLEMS, S. M., ZECCHIN, D., HOBOR, S., BAJPE, P. K., LIEFTINK, C., MATEUS, C., VAGNER, S., GRERNRUM, W., HOFLAND, I., SCHLICKER, A., WESSELS, L. F. A., BEIJERSBERGEN, R. L., BARDELLI, A., DI NICOLANTONIO, F., EGGERMONT, A. M. M. & BERNARDS, R. 2014. Reversible and adaptive resistance to BRAF(V600E) inhibition in melanoma. *Nature*, 508, 118.
- SUR, S., PAGLIARINI, R., BUNZ, F., RAGO, C., DIAZ, L. A., KINZLER, K. W., VOGELSTEIN, B. & PAPADOPOULOS, N. 2009. A panel of isogenic human cancer cells suggests a therapeutic approach for cancers with inactivated p53. *Proceedings of the National Academy of Sciences*, 106, 3964.
- TAKAHASHI, A., OHTANI, N. & HARA, E. 2007. Irreversibility of cellular senescence: dual roles of p16(INK4a)/Rb-pathway in cell cycle control. *Cell Division*, 2, 10-10.
- TAKAHASHI-YANAGA, F. 2013. Activator or inhibitor? GSK-3 as a new drug target. *Biochemical Pharmacology*, 86, 191-199.
- TSAI, J.-H., LIAU, J.-Y., LIN, Y.-L., LIN, L.-I., CHENG, Y.-C., CHENG, M.-L. & JENG, Y.-M. 2014. Traditional serrated adenoma has two pathways of neoplastic progression that are distinct from the sessile serrated pathway of colorectal carcinogenesis. *Mod Pathol*, 27, 1375-1385.
- WALTERS, J. R., HOWARD, A., RUMBLE, H. E., PRATHALINGAM, S. R., SHAW-SMITH, C. J. & LEGON, S. 1997. Differences in expression of homeobox transcription factors in proximal and distal human small intestine. *Gastroenterology*, 113, 472-477.
- WAN, P. T. C., GARNETT, M. J., ROE, S. M., LEE, S., NICULESCU-DUVAZ, D., GOOD, V. M., PROJECT, C. G., JONES, C. M., MARSHALL, C. J., SPRINGER, C. J., BARFORD, D. & MARAIS, R. 2004. Mechanism of Activation of the RAF-ERK Signaling Pathway by Oncogenic Mutations of B-RAF. *Cell*, 116, 855-867.
- WELLBROCK, C., KARASARIDES, M. & MARAIS, R. 2004. The RAF proteins take centre stage. *Nat Rev Mol Cell Biol*, 5, 875-885.
- WEN, F. & LI, Q. 2016. Treatment dilemmas of cetuximab combined with chemotherapy for metastatic colorectal cancer. *World Journal of Gastroenterology*, 22, 5332-5341.

- WHITE, S. H., WIMLEY, W. C. & SELSTED, M. E. 1995. Structure, function, and membrane integration of defensins. *Current Opinion in Structural Biology*, 5, 521-527.
- WU, D. & PAN, W. 2010. GSK3: a multifaceted kinase in Wnt signaling. *Trends in biochemical sciences*, 35, 161-168.
- WU, P.-K. & PARK, J.-I. 2015. MEK1/2 Inhibitors: Molecular Activity and Resistance Mechanisms. *Seminars in oncology*, 42, 849-862.
- XIA, S., LIN, R., JIN, L., ZHAO, L., KANG, H.-B., PAN, Y., LIU, S., QIAN, G., QIAN, Z., KONSTANTAKOU, E., ZHANG, B., DONG, J.-T., CHUNG, Y. R., ABDEL-WAHAB, O., MERGHOU, T., ZHOU, L., KUDCHADKAR, R. R., LAWSON, D. H., KHOURY, H. J., KHURI, F. R., BOISE, L. H., LONIAL, S., LEE, B. H., POLLACK, B. P., ARBISER, J. L., FAN, J., LEI, Q.-Y. & CHEN, J. 2017. Prevention of dietary fat-fueled ketogenesis attenuates BRAF V600E tumor growth. *Cell metabolism*, 25, 358-373.
- YOSEF, R., PILPEL, N., PAPISMADOV, N., GAL, H., OVADYA, Y., VADAI, E., MILLER, S., PORAT, Z., BEN-DOR, S. & KRIZHANOVSKY, V. 2017. p21 maintains senescent cell viability under persistent DNA damage response by restraining JNK and caspase signaling. *The EMBO Journal*, 36, 2280-2295.
- YOUNG, M., ORDONEZ, L. & CLARKE, A. R. 2013. What are the best routes to effectively model human colorectal cancer? *Molecular Oncology*, 7, 178-189.
- YUEH, A. E., PAYNE, S. N., LEYSTRA, A. A., VAN DE HEY, D. R., FOLEY, T. M., PASCH, C. A., CLIPSON, L., MATKOWSKYJ, K. A. & DEMING, D. A. 2016. Colon Cancer Tumorigenesis Initiated by the H1047R Mutant PI3K. *PLOS ONE*, 11, e0148730.
- YUN, J., RAGO, C., CHEONG, I., PAGLIARINI, R., ANGENENDT, P., RAJAGOPALAN, H., SCHMIDT, K., WILLSON, J. K. V., MARKOWITZ, S., ZHOU, S., DIAZ, L. A., VELCULESCU, V. E., LENGAUER, C., KINZLER, K. W., VOGELSTEIN, B. & PAPADOPOULOS, N. 2009. Glucose Deprivation Contributes to the Development of KRAS Pathway Mutations in Tumor Cells. *Science*, 325, 1555.
- ZHAN, T., RINDTORFF, N. & BOUTROS, M. 2017. Wnt signaling in cancer. *Oncogene*, 36, 1461-1473.
- ZHANG, W. & LIU, H. T. 2002. MAPK signal pathways in the regulation of cell proliferation in mammalian cells. *Cell Res*, 12, 9-18.
- ZOU, H., HARRINGTON, J. J., SUGUMAR, A., KLATT, K. K., SMYRK, T. C. & AHLQUIST, D. A. 2007. Detection of Colorectal Disease by Stool

Defensin Assay: An Exploratory Study. *Clinical Gastroenterology and Hepatology*, 5, 865-868.